UNIVERSIDAD DE MÁLAGA
Facultad de Ciencias
Departamento de Ingeniería Química

TESIS DOCTORAL

PREPARACIÓN DE FIBRAS SUBMICROMÉTRICAS DE BASE CARBONOSA PARA APLICACIONES ENERGÉTICAS Y MEDIOAMBIENTALES

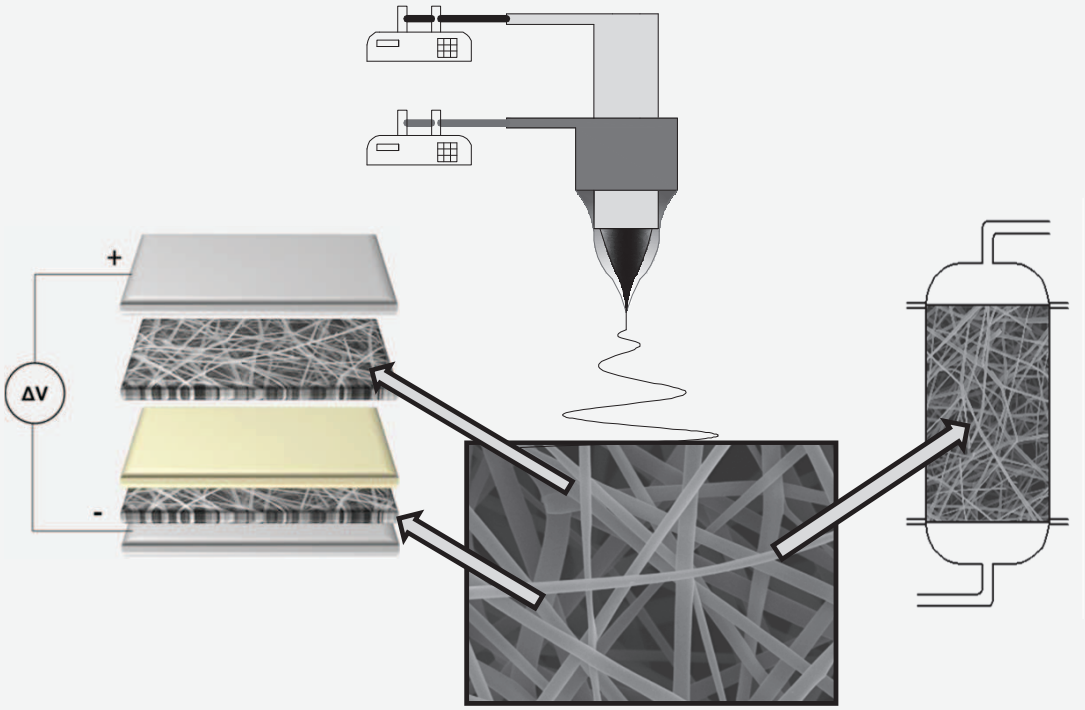

Francisco José García Mateos

Directores:
Dr. D. Tomás Cordero Alcántara
Dr. D. José Rodríguez Mirasol

Málaga, 2017

UNIVERSIDAD DE MÁLAGA

FACULTAD DE CIENCIAS

DEPARTAMENTO DE INGENIERÍA QUÍMICA

TESIS DOCTORAL

PREPARACIÓN DE FIBRAS SUBMICROMÉTRICAS DE BASE CARBONOSA PARA APLICACIONES ENERGÉTICAS Y MEDIOAMBIENTALES

Autor: Francisco José García Mateos

Directores: Prof. Dr. D. Tomás Cordero Alcántara

Prof. Dr. D. José Rodríguez Mirasol

Programa de Doctorado: Química Avanzada. Preparación y Caracterización de Materiales

Málaga, Mayo 2017

AUTOR: Francisco José García Mateos

http://orcid.org/0000-0001-6474-9430

EDITA: Publicaciones y Divulgación Científica. Universidad de Málaga

D. TOMÁS CORDERO ALCÁNTARA, Catedrático de Ingeniería Química de la Universidad de Málaga,

D. JOSÉ RODRÍGUEZ MIRASOL, Catedrático de Ingeniería Química de la Universidad de Málaga,

CERTIFICAN: Que el trabajo de investigación recogido en la presente Memoria ha sido realizado bajo su dirección en el Departamento de Ingeniería Química de la Universidad de Málaga por el Ingeniero D. Francisco José García Mateos, y reúne, a su juicio, contenido científico suficiente y las condiciones necesarias para ser presentado y defendido ante el Tribunal correspondiente para optar al Grado de Doctor en la Universidad de Málaga.

Málaga, Mayo de 2017

Fdo.: Dr. D. Tomás Cordero Alcántara

Fdo.: Dr. D. José Rodríguez Mirasol

A mi familia

Overview

The preparation of carbon fibers from Alcell lignin, which is an available, renewable and cheap biopolymer, has been studied by the electrospinning technique. Porous carbon fibers are relevant materials for many functional applications of industrial and technological interest. Specially, they receive great attention in catalysis, adsorption, gas storage and/or separation processes, electrochemical devices for energy storage and conversion, etc. Regarding the obtainment of advanced properties, the preparation of carbon fibers by a simple and versatile technique, such as electrospinning, entails an advantageous and promising approach. It solves the most important problems associated to conventional melt-extrusion, since it allows the preparation of continuous fibers with considerably smaller diameters (micro- and submicro-scale) at room temperature, directly in a single step without the aid of blending polymeric additives and/or chemical treatments. Also, by the electrospinning technique, it is possible to incorporate the metal precursor (Pt in our case) and therefore the preparation of Alcell fibers with metal content in one step.

In this technique, the pumping of the conductive solution towards the spinning needle is subjected to an external electric field. Under suitable conditions a jet of fluid is formed from the capillary tip, producing the fibers solidification in a metallic collector.

All fibers prepared in this work have been produced by using co-axial electrospinning devices, which renders a higher stability of the ejecting area of the device (the Taylor cone), reflected in continuous production of fibers with high length-to-diameter ratios and smooth surfaces.

The addition of H_3PO_4 to the initial solution has allowed the preparation of carbon fibers with a large variety of porosity and chemical properties. In addition, H_3PO_4 allows the preparation of carbon fibers by other routes and reduces the preparation time by 60 times with respect to pure carbon fibers (from Alcell lignin without phosphoric acid).

This Ph. D. thesis is divided into 9 chapters. The first and second ones, introduction and experimental methods, respectively, have been written in Spanish, whereas the rest of the thesis is presented in English language. The data provided in Chapters 3 to 8 is adapted from already published, accepted or submitted papers. Those

chapters are devoted to the preparation of lignin-based carbon fibers, phosphorus-containing carbon fibers and platinum doped carbon fibers for applications as phenol adsorption, isopropanol decomposition, alcohol electro-oxidation and energy storage devices. The final chapter collects a small insight into the remaining and future work coming as a result of this thesis.

Agradecimientos

Quizás esta pequeña e importante parte de la Tesis Doctoral sea la parte más complicada y, a la vez, más fácil de redactar. Es complicada porque en este punto, un doctorando comienza a pensar en todas las personas que han formado parte de la tesis e intenta buscar las palabras apropiadas para explicar los sentimientos que se producen durante la redacción de estos agradecimientos. Pero como he dicho, también resulta muy fácil, ya que he tenido la suerte de contar con personas, dentro y fuera del trabajo, que me han hecho llevar la Tesis de la mejor forma posible.

En primer lugar, me gustaría agradecer a mis directores, los profesores Tomás Cordero Alcántara y José Rodríguez Mirasol, por la confianza que habéis depositado en mí desde el primer día que llegué al laboratorio y el trato que he recibido por vuestra parte. Gracias por estar disponibles en cualquier momento, gracias por los consejos que he recibido, gracias por las largas horas de discusión, gracia por hacerlo todo más fácil.

Gracias a los profesores Luis Cotoruelo y Olga Guerrero por los consejos recibidos durante el desarrollo de la Tesis Doctoral, y gracias a los doctores que han pasado por esta gran familia. Gracias a María José Valero por su trabajo y constancia, ver personas como tú nos anima a seguir trabajando duro. Gracias a Raúl Berenguer por tus consejos y la gran ayuda que he recibido por tu parte para la realización de esta Tesis. Como no, agradecer a Ramiro Ruiz, un fenómeno. Gracias a ti me encuentro hoy escribiendo los agradecimientos de esta Tesis Doctoral, gracias por tratar a un Ingeniero Industrial que pisaba por primera vez un laboratorio de Ingeniería Química con la suficiente delicadeza y paciencia para que no saliese corriendo. Gracias por tu apoyo, confianza y consejos desde que me dirigiste el proyecto fin de carrera hasta hoy. Y para terminar, y por eso no menos importante, gracias a Nani Rosas. Gracias por tus consejos, tus cabreos, tus interminables conversaciones, tu implicación con los que estamos en el laboratorio, y gracias por luchar y defender siempre a los que estamos en escalones inferiores. He aprendido, y me queda por aprender mucho de ti. Gracias jefa.

A mis compañeros de Tesis, Aurora, Elisa, Paul, Juanjo, Jose, Imane, Mpho, Rafael y ahora Javi. Gracias por hacer que las horas de laboratorio sean más llevaderas y gracias por la felicidad que mostráis al trabajar. Eli, al final lo hemos conseguido. Agradecer también a otro compañero de Tesis, que aunque esté más hacia el norte, se deja caer de

vez en cuando para visitarnos. Gracias Tomás Jr, por tu ayuda y por compartir tus conocimientos conmigo, parte de esta Tesis es tuya también.

Gracias a los proyectandos que he tenido la suerte de dirigir. A Javi y mis tres Marías, María Lourdes, María Olaya y María Elizabeth por la alegría que le habéis dado al laboratorio, y por trabajar, y hacerme trabajar duro. A Hugo por ayudarme a realizar los experimentos de adsorción presentados en esta Tesis. Gracias también a Miguel Ángel y Miguelito por hacer más llevadero el tiempo en el laboratorio. Os debo una comida.

Gracias a los técnicos del SCAI. Gracias a María Dolores Marqués, técnico de sólidos porosos, por ser la mejor en su trabajo, por sus consejos y por sus caramelos. Gracias al equipo que compone el servicio de microscopia, Goyo, Adolfo y David, es una gozada ir a utilizar vuestros servicios y poder disfrutar. Gracias a Valle (XPS), Laura (DRX), Augusto (Análisis elemental) y Cristina (Raman).

También me gustaría agradecer a los Profesores de la Universidad de Alicante, Emilia Morallón y Diego Cazorla Amorós por el trato recibido durante mi corta estancia en Alicante. Gracias a los miembros del grupo de Materiales Carbonosos y Medio Ambiente y al grupo de Electrocatálisis y Electroquímica de Polimeros de la Universidad de Alicante por tratarme como un miembro más del grupo desde el momento en que llegué.

Gracias a mi familia, por la confianza que han depositado en mí. Gracias a mis padres que han hecho todo lo posible para que hoy pueda finalizar esta Tesis Doctoral. Gracias a mi hermana Inma, Atanasio, Celia y a mis suegros por el apoyo mostrado durante todo este tiempo.

Quizás requiere un especial agradecimiento mi mujer Vicky, gracias por soportar todos estos años las horas interminables de laboratorio, gracias por ayudarme, por tu apoyo y por ser mi amiga. Sabes que parte del trabajo que he realizado aquí ha sido gracias a ti.

En el campo de los agradecimientos institucionales quiero agradecer al MINECO la concesión de contratos de investigación con cargo a los proyectos CTQ-2012-36408 y CTQ-2015-68654-R. Gracias al Departamento de Ingeniería Química de la Universidad de Málaga por la total disponibilidad de sus instalaciones para la realización de la Tesis Doctoral. Gracias Pedro y María José.

CONTENTS

NOTATION

a	empirical parameter (s^{-1})
A_{BET}	specific surface area by Brunauer, Emett, Teller method ($m^2 \cdot g^{-1}$)
Ac	Acetone
AC	Activated carbon
A_{DR}	Dubinin Radushkevich surface area ($m^2 \cdot g^{-1}$)
AF	As spun lignin fibers
At	external area ($m^2 \cdot g^{-1}$)
B	time constant (s^{-1})
b	empirical parameter ($m^2 \cdot s^{-1}$)
c	empirical parameter (s)
C	outlet concentration ($mg \cdot L^{-1}$)
C_0	initial concentration ($mg \cdot L^{-1}$)
C_b	phenol bed concentration ($mol \cdot m^{-3}$)
C_e	equilibrium concentration ($mg \cdot L^{-1}$)
Ceff	Coulombic efficience
C_f	concentration in the fiber external surface ($mol \cdot m^{-3}$)
CFHPt	Carbon fibers with high Pt content
CF-I	Interconected carbon fibers
CF-IA	Interconected gasified carbon fibers
CF-L	Linear carbon fibers
CFLPt	Carbon fibers with low Pt content
CFs	Carbon Fibers
Cg	Gravimetric capacitance ($F\ g^{-1}$)
Ci	inlet concentration ($mg \cdot L^{-1}$)
CNFs	Carbon nano fibers
CNTs	Carbon nano tubes
Ct	concentration at time t ($mg \cdot L^{-1}$)
CV	Ciclic voltametry
d	empirical parameter (s)
D_e	effective internal diffusion coefficient ($m^2 \cdot s^{-1}$)
D_l	molecular diffusivity of the solute in water ($m^2 \cdot s^{-1}$)
DMFC	Direct methanol fuel cell
DRX	X Ray difraction
Ds	surface diffusion coefficient ($m^2 \cdot s^{-1}$)

DSC	Diferential scanning calorimetry
Dz	axial dispersion coefficient ($m^2 \cdot s^{-1}$)
E	Energy
Ea	Activation energy
E_{eff}	Energy efficiente
*E*g	Specific energy
EHD	Electrohydraulic forces
EIS	Electrochemistry impedance spectroscopy
EOR	Ethanol oxidation reaction
ESR	Equivalent serie resistance
F_{olPA}	Isopropanol molar flow rate
GCD	Galvanostatic charge discharge
HER	hydrogen evolution reaction
HR	Heating rate
I	Current (A)
I_b	current density in the reverse scan
I_f	current density in the forward scan
Ir_{drop}	Ohmic drop
j	Current density
k_f	external film mass-transfer coefficient ($m \cdot s^{-1}$)
k_i	intraparticle mass transfer (s^{-1})
K_L	equilibrium constant of Langmuir equation ($L \cdot mg^{-1}$)
K_{L0}	pre-exponential factor in Langmuir equation ($L \cdot mg^{-1}$)
L_b	bed length (cm)
LLP	lower limit potential
MOR	Methanol oxygen reaction
N	number of transfer units
N_S	diffusion molar flux ($mol \cdot m^{-2} \cdot s^{-1}$)
P	Power
PAS	As spun phosphorus lignin fibers
PCF	Phosphorus carbon fibers
PCFHPt	Phosphorus carbon fibers with high Pt content
PCFLPt	Phosphorus carbon fibers with low Pt content
PEMFC	proton exchange membrane fuel cells
PEO	poly(ethylene oxide)

PET	ethylene terephthalate
P_g	Specific power
P_{olPA}	Isopropanol partial pressure
PP	Propilene
PSF	phoshporus Stabilized lignin fibers
Q	flow rate ($mL \cdot min^{-1}$)
q|Cf	adsorbed concentration at the solid external surface
q_{cal}	calculated adsorption capacity from models at C/Ci = 1 ($mg \cdot g^{-1}$)
q_e	adsorption capacity at equilibrium ($mg \cdot g^{-1}$)
q_{exp}	experimental adsorption capacity at C/Ci = 0.99 ($mg \cdot g^{-1}$)
q_i	adsorption capacity at Ci concentration ($mg \cdot g^{-1}$)
q_L ($mg \cdot g^{-1}$)	maximum adsorption capacity at equilibrium of Langmuir equation
q_m	empirical parameter ($mg \cdot g^{-1}$)
q_t	adsorption capacity at time t ($mg \cdot g^{-1}$)
R	gases constant (8.31 $J \cdot mol^{-1} \cdot K^{-1}$)
R^2	determination coefficient
R_b	bed radius
R_{cell}	Cell resistance
R_f	fiber size (mm)
R_S	separation factor
SEM	Scanning electron microscope
SF	Stabilized lignin fibers
STP	estándar temperature pressure
T	throughput parameter
t	time (min)
T_c	Cristalization temperature
TEM	Transmision electron microscope
TG	Thermogravimetric
T_g	Glass transition temperature
T_m	melting temperature
TPD	Temperature desorption programmed
TT	Thermal treatment
u	superficial liquid velocity ($m \cdot s^{-1}$)
ULP	upper limit potential

V	Voltage
V_b	molar volume of solute at the normal boiling point ($cm^3 \cdot mol^{-1}$)
V_{DR}	Dubinin Radushkevich narrow micropore volume ($cm^3 \cdot g^{-1}$)
V_{mes}	mesopore volume from the N_2 isotherm ($cm^3 \cdot g^{-1}$)
V_t	micropore volume from the N_2 isotherm ($cm^3 \cdot g^{-1}$)
V_{tot}	total pore volume from the N_2 isotherm ($cm^3 \cdot g^{-1}$)
vz	axial velocity ($m \cdot s^{-1}$)
w	adsorbent dose ($g \cdot L^{-1}$)
W	mass of activated carbon (mg)
X	Conversion
XEDS	X-ray energy dispersive spectroscopy
XPS	X Ray spectroscopy
z	axial position in bed

Greeks characters

ε_b	bed porosity
ε_f	fiber porosity
μ_l	fluid dynamic viscosity (cP)
η	yield
ρ_b	bed density ($kg \cdot m^{-3}$)
ρ_l	fluid density ($kg \cdot m^{-3}$)
ρ_f	fiber density ($kg \cdot m^{-3}$)

0. OBJECTIVES

The main objective of this doctoral thesis is the valorization of lignocellulosic residues, as Alcell lignin, for the preparation and characterization of carbonaceous fibers by electrospinning and their use in applications of interest for chemical engineering. One of the objectives is the preparation of carbon fibers from lignin in a simple, fast and cheap way. For this reason, the incorporation of H_3PO_4 seems to be a solution to avoid the long preparation times, and allows the preparation of carbon fibers with a high variety of porous and chemical properties.

Consequently, this thesis reports the use of electrospinning in the preparation, as well as the characterization and tests the different carbon fibers in applications of:

- ✓ Porous carbon fibers for liquid phase adsorption,
- ✓ Porous carbon fibers for catalytic application, and
- ✓ The preparation of novel carbon electrodes for electrochemical application as supercapacitors and fuel cells.

Chapter 1

Introducción

1.0. Abstract

This chapter has provided an overview of the methods to prepare carbon fibers and the carbon fibers types. The properties of Alcell® lignin as raw material have been described. The activated carbon methods have been elucidated and the advantages of the use of lignocellulosic materials as raw material for activated carbon have been listed. The electrospinning technique is explained, indicating the importance of the parameters that govern the fibers spinning. This chapter also contains a small introduction to adsorption and catalyst process, being focused on the phenol adsorption and alcohol decomposition, respectively. Finally a description for the use of carbon materials as electrodes for fuel cells and for energy storage has been realized.

1.1.Biopolímeros

Los polímeros son macromoléculas formadas por la unión de enlaces covalentes de uno o más monómeros. La producción de polímeros sintéticos se realiza, principalmente, a partir del petróleo, por lo que la aparición del concepto de biopolímero o bioplástico ha surgido del interés para disminuir la emisión de gases de efecto invernadero y el uso de productos químicos a partir de fuentes renovables [1,2]. Los biopolímeros son polímeros derivados de recursos naturales renovables o bien polímeros biodegradables. Según su fuente de obtención los biopolímeros se pueden clasificar de la siguiente forma:

- ✓ Biopolímeros extraídos directamente de la biomasa como puede ser el almidón o la celulosa y en menor cantidad la lignina. También se han conseguido biopolímeros a partir de proteínas de fuente animal como la gelatina y de origen vegetal (proteína de soja o gluten). Algunos de estos biopolímeros pueden procesarse utilizando tecnologías convencionales de procesado plástico.
- ✓ Los microorganismos también pueden ser de utilidad en esta búsqueda de alternativas. La celulosa bacteriana, un polímero obtenido por fermentación con microorganismos, o los polihidroxialcanoatos, biopolímeros que algunos microorganismos acumulan como reserva de carbono y energía cuando hay limitaciones nutricionales en el medio donde viven, tienen aplicaciones como envases de larga y corta duración, implantes utilizados en medicina y productos de higiene.

- ✓ Biopolímeros obtenidos a partir de monómeros derivados de biomasa. Es el caso del ácido poliláctico, obtenido generalmente a partir de almidón de maíz, y otros biopoliésteres.

1.2. Lignina

La lignina es, junto con la celulosa y la hemicelulosa, uno de los constituyentes básicos de las plantas, materiales vegetales y madera. Junto a la celulosa y la hemicelulosa conforma la pared celular de las plantas, cementando las fibras de celulosa y proporcionando rigidez y flexibilidad a las mismas en una disposición regulada a nivel nano-estructural. Además desempeña unas labores fundamentales en el transporte interno de agua, nutrientes y metabolitos. El contenido en lignina de las plantas es variable, incluso dentro de una misma especie, pero se puede considerar que los materiales lignocelulósicos están compuestos por aproximadamente un 25 % de este polímero natural. Esto convierte a la lignina como el segundo polímero más abundante de la naturaleza después de la celulosa. La lignina puede considerarse una red polimérica tridimensional al azar formada por unidades de fenilpropano unidas entre sí en diferentes posiciones, Figura 1.1.. Estas unidades son acopladas al azar en distintas partes de la pared celular, donde se lleva a cabo la polimerización. La lignina posee un gran contenido de núcleos aromáticos, lo cual debería favorecer un mejor ordenamiento tras tratamiento térmico frente a otros polímeros naturales como la celulosa [3].

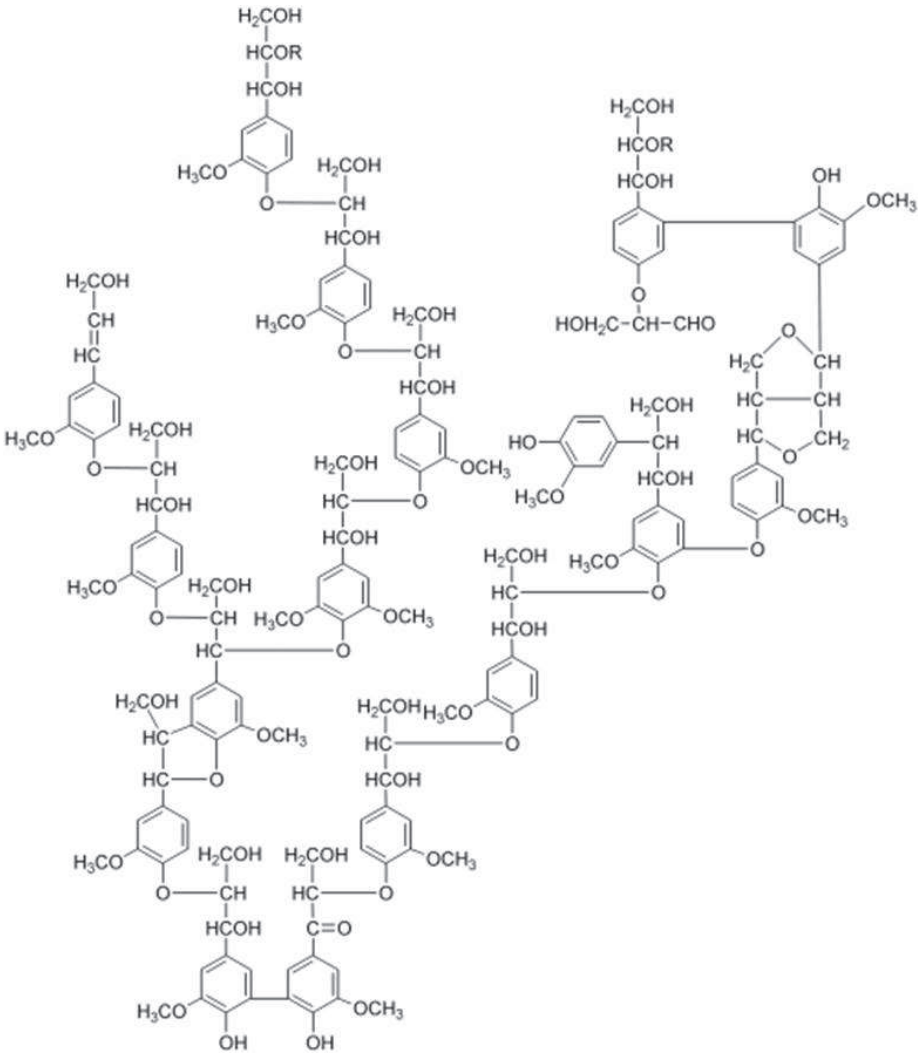

Figura 1.1. Estructura de la lignina propuesta por Alder [4].

La lignina es el principal co-producto de la industria de la pulpa de celulosa. El procedimiento químico más usado por la industria papelera para la separación de la lignina es el proceso a sulfato. Como consecuencia de la digestión de la madera se obtiene la pasta de celulosa y una lejía negra o lejía kraft en la que se encuentra disuelta la lignina. Las lejías negras se reutilizan, previa evaporación, en los sistemas de recuperación de las materias y energía de la planta. De esta forma, el calor generado en el quemado de la lejía se utiliza para la evaporación previa de la misma y su transformación en energía eléctrica. Este procedimiento dota a la lignina de un alto contenido en cenizas y sales, por lo que su combustión, además de proporcionar energía para la planta, también recupera las sales usadas durante el proceso. Otra vía para obtener lignina es el proceso Alcell®, el cual confiere un alto grado de pureza al material, librándolo de casi toda la materia inorgánica.

El bajo coste y la alta disponibilidad de la lignina, cuya producción anual mundial, según datos del "International Lignin Institute", se estima en torno a 50 millones de toneladas [5]. La gran producción de lignina, hace atractivo su uso como precursor de materiales carbonosos, gracias a que tiene un elevado contenido en carbono (básicamente como grupos aromáticos).

En nuestro grupo de investigación (TERMA, UMA) se viene estudiando desde hace tiempo el aprovechamiento de la lignina vía tratamientos termoquímicos. Así, por carbonización se han obtenido materiales que tratados a altas temperaturas producen materiales carbonosos altamente ordenados [6]. Por gasificación parcial de los carbonizados se pueden obtener carbones activos [7] al igual que por pirólisis catalizada de la lignina con $ZnCl_2$ y H_3PO_4. [8,9] También se ha empleado como precursor para la obtención de tamices moleculares de carbón por tratamiento a altas temperaturas o por deposición controlada de carbono pirolítico [10,11] y, más recientemente, como precursor de nanofibras de carbono por la técnica de electrohilado [12-14].

1.3. El carbón activo.

Se conoce como carbón activo a todo material carbonoso que, una vez sometido a un proceso de activación presenta una elevada porosidad y, por lo tanto, una gran superficie interna. Su principal característica es una elevada capacidad de adsorción. Por lo general, una carbonización no es suficiente para obtener una estructura muy porosa y es necesario activarlo. Los carbones activos se clasifican desde el punto de vista comercial según su textura o forma y pueden ser: granular, si el tamaño de partícula está comprendido entre 150 μm y 5 mm, y en polvo, si el tamaño de partícula es menor de 150 μm.

Cualquier material orgánico que posea altas proporciones de carbono es apropiado para la preparación de carbones activos. Actualmente existen numerosos precursores para la preparación de carbón activo, siendo la madera, residuos forestales, tipos de biomasa, turba, lignito y otros carbones minerales los más usados industrialmente. Las propiedades del carbón activo están directamente relacionadas con la naturaleza de la materia prima, el proceso de activación y las condiciones de preparación. Por tanto, es muy importante seleccionar la materia prima en base a las características que se quieran obtener, con un mínimo contenido en impurezas. También debe tenerse en cuenta el coste y la disponibilidad de la materia prima, así como la

facilidad de transportarla. Por todos estos factores, sólo se utilizan unos cuantos materiales para su producción a nivel comercial.

Existe una gran importancia en la obtención de carbones activos a partir de residuos lignocelulósicos [6,8,15-18]. Al preparar carbones activos a partir de residuos biomásicos se está realizando una gestión medioambiental, ya que se realiza una gestión de ese residuo y además se incrementa su valor añadido.

1.3.1. Preparación de carbón activo.

Actualmente se utilizan dos métodos para la preparación de carbones activos, la activación física y la activación química. La Figura 1.2. presenta un esquema simplificado de estas dos vías de preparación de carbón activo, cuyos pasos se describen a continuación:

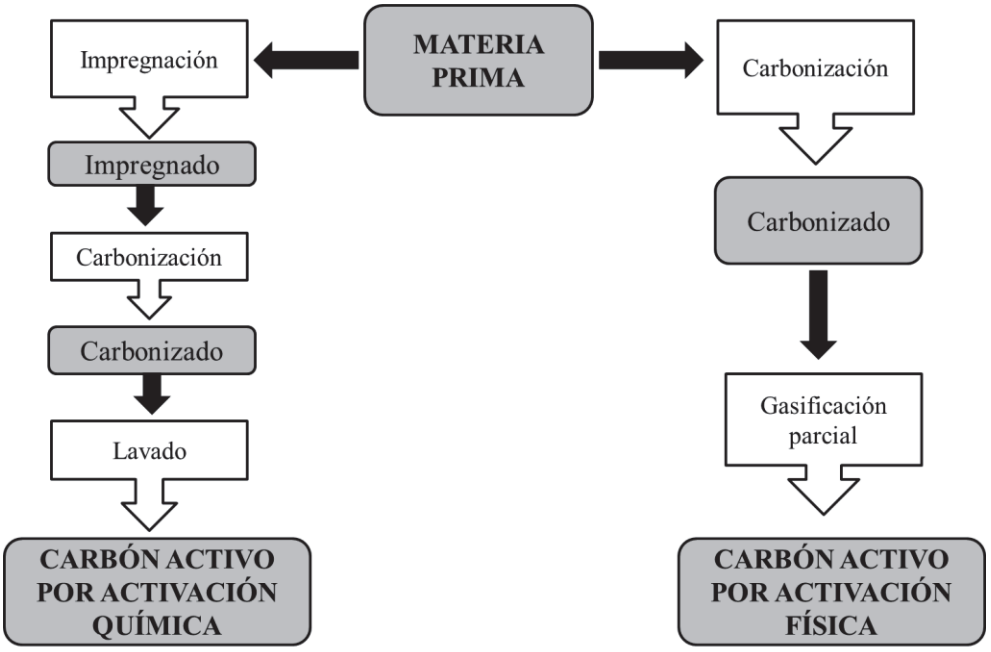

Figura 1.2 Esquema representativo de las etapas de los métodos de preparación de carbón activo.

La activación física consta fundamentalmente de dos etapas: carbonización y activación. En la etapa de carbonización la materia prima se somete a temperaturas comprendidas entre 800 y 1000 ºC en una atmósfera inerte para eliminar los heteroátomos unidos al carbono por descomposición pirolítica, de forma que el residuo se enriquece en carbono. Se produce un reordenamiento de los átomos de carbono, pero no se produce un desarrollo significativo de la porosidad, para lo que es necesaria la etapa de activación.

La activación consiste en una gasificación parcial con un agente oxidante como aire, CO_2, vapor de agua, O_2 o una mezcla de ellos. La gasificación parcial es una reacción heterogénea gas-sólido en la que la conversión del carbón no es total y, por lo tanto, resulta un sólido poroso. En condiciones de reacción en las que existe control químico, el agente oxidante penetra en la estructura interna del carbonizado y, mediante una serie de reacciones, elimina parte de los átomos de carbono, produciéndose de esta forma un ensanchamiento de los poros existentes, así como la generación de otros nuevos.

En la activación química, la materia prima se hace reaccionar con un agente activante químico que orienta la descomposición térmica hacia la deshidratación generalizada de la biomasa, el reordenamiento y la repolimerización de la estructura carbonada. En general, durante la activación química se evita la formación de alquitranes y se obtienen rendimientos mayores que en la activación física [19]. Las etapas implicadas en el proceso de activación química son: impregnación de la materia prima con el agente activante, tratamiento térmico en atmósfera inerte entre 350 y 900 ºC, siendo en esta etapa donde se produce el desarrollo de la porosidad. Finalmente los materiales carbonosos se lavan para la eliminación del agente activante ocluido en la porosidad.

Los parámetros fundamentales que controlan el proceso de activación química y el producto obtenido son: la relación de impregnación, la temperatura de activación y el tiempo de residencia. Los valores de estos parámetros van a tener una influencia notable en la estructura final del carbón activo obtenido.

Existen numerosos compuestos que pueden usarse como agentes activantes. Sin embargo, los más utilizados industrialmente, a lo largo de la historia son: *Cloruro de zinc ($ZnCl_2$):* la temperatura óptima se encuentra entre 450-550ºC, *Ácido fosfórico (H_3PO_4)*: en este caso, el rango de temperatura óptima se encuentra entre 350-500 ºC, *Hidróxido de potasio (KOH):* el empleo de este KOH supone temperaturas de activación superiores, que pueden llegar a los 900 ºC, aunque generalmente no superan los 700-750 ºC. La característica común de estos agentes es su acción deshidratante, que orienta la descomposición pirolítica hacia una menor formación de alquitranes y aumenta el rendimiento en sólido [20-22].

1.4. Fibras

Por estructura fibrosa se entiende una forma maciza o hueca que es continua en una dimensión. Las fibras de origen vegetal provenientes del lino, el algodón o el cáñamo, y de origen animal, como la lana o la seda fueron las primeras fibras usadas por el hombre, siendo destinadas al hilado de textiles.

Las primeras patentes para producir fibras de celulosa, conocidas como rayón, aparecen en el siglo XIX. El siguiente gran avance vino de la mano del descubrimiento de los polímeros sintéticos en los años treinta del siglo XX. Hasta ese momento, las fibras se obtenían a partir de polímeros naturales como la mencionada celulosa. Con la llegada del nylon, producido por polimerización de la caprolactama, las principales materias primas para la fabricación de fibras pasan a ser los derivados del petróleo.

Hoy en día las fibras son preparadas a partir de diversos polímeros, las de mayor importancia son las fibras textiles, aunque las novedosas aplicaciones de las fibras de carbono las convierten en productos muy atractivos y de alto valor añadido. La producción de fibras se realiza mediante diversas técnicas que se enumeran a continuación.

1.4.1. Producción de fibras por extrusión

El método más usado para la producción de fibras es el hilado. Este procedimiento consta de las siguientes etapas de preparación:

- Disolución o fundido del precursor deseado.
- Extrusión de la mezcla en una hiladora.
- En la preparación de fibras de carbono es necesario un proceso de estabilización de las fibras precursoras mediante un tratamiento oxidativo con disoluciones ácidas o estabilización térmica, lo cual conlleva mayor tiempo de la preparación de las fibras y modifica la termoplasticidad de la fibra, evitando que esta se funda en la etapa siguiente. Para completar la etapa de preparación de fibras de carbono es necesario una etapa de carbonización, la cual se realiza a elevadas temperaturas y en atmósfera inerte.

Mediante el proceso de extrusión se obtienen fibras con un diámetro final de hasta 10 μm.

1.4.2. Producción de fibras por otros métodos mecánicos

Otros métodos mecánicos usados para la preparación de fibras son los siguientes:

1.4.2.1Hilado de bicomponentes

Esta técnica es una variante de la producción de fibras por extrusión con la variante de que se utilizan varios materiales. Gracias a los avances tecnológicos en los sistemas de hilado es posible preparar fibras con distintas estructuras y morfologías, e incluso preparar fibras con materiales distintos en corteza y núcleo. Las aplicaciones de estas conformaciones permiten, por ejemplo, retirar a posteriori uno de los componentes para obtener una fibra de menor tamaño o de aspecto segmentado.

1.4.2.2. Soplado fundido

Este proceso usa flujos de aire de alta velocidad para atenuar los filamentos que se producen de materiales poliméricos o materiales fundidos [23]. Las fibras así obtenidas no son ordenadas y alcanzan tamaños alrededor de 3 μm, habiéndose registrado tamaños entre los 0.1 y los 15 μm. Aunque su módulo de Young no suele ser elevado, los textiles así obtenidos tienen una elevada opacidad, y su reducido tamaño hace que gocen de una elevada área específica externa, posibilitando su uso en adsorbentes y en aislantes.

1.4.3. Producción de fibras de reducido tamaño por métodos químicos

Además de los métodos basados en extrusión o inyección, existen métodos químicos para producir nanofibras. El principal problema que se encuentra a la hora de usar estos métodos es la baja velocidad de producción que poseen y el elevado precio de las fibras así producidas. Entre estos métodos se encuentran el autoensamblaje y el nanomoldeo. El *autoensamblaje* consiste en la correcta disposición de las moléculas que componen las fibras. Las moléculas se disponen en estructuras ordenadas por interacciones de tipo no covalente. Se han producido nanotubos de pared múltiple de anchuras de pared por debajo de los 500 nm usando esta vía [24]. En el *nanomoldeo* se utiliza un material como molde o negativo de carácter nanoestructurado [25]. El material precursor, que ha estar en estado líquido o gaseso, es infiltrado en la red porosa del molde. Para conseguir un correcto mojado de los poros del molde, es necesario que la química superficial del molde y del disolvente sean parecidas. La temperatura, el pH

y las condiciones de trabajo han de ser cuidadosamente escogidas para evitar el colapso del molde. Finalmente, el molde se elimina mediante lavado y permanece la fibra nanoestructurada.

1.4.4. Tipos de fibras atendiendo a su composición

Además de las fibras orgánicas, como las de carbono para refuerzo en materiales compuestos o las poliméricas del sector textil, es posible la preparación en forma de fibra de materiales inorgánicos, siendo el caso más aplicado comercialmente el del óxido de silicio, del que se producen las fibras ópticas utilizadas en telecomunicaciones y las fibras de vidrio usadas como refuerzo. En cuanto a la aplicación de fibras en ingeniería química, las fibras de carbono activado son las que presentan mayor uso.

Las fibras de carbono son un material de elevada importancia tecnológica y económica. Estos materiales se distinguen por su morfología fibrosa y un alto contenido en carbono, superior al 90% en peso. Sus propiedades químicas, mecánicas y eléctricas las hacen idóneas para multitud de aplicaciones avanzadas en campos tan dispares como la industria aeroespacial, la catálisis heterogénea o el material deportivo. Desde que se ideara un método de preparación de fibras de carbono a partir de la carbonización de filamentos de bambú (celulosa) a finales del siglo XIX, han aparecido una amplia gama de materiales carbonosos que son susceptibles de ser usados como precursores de estas fibras. En la década de los sesenta, la Union Carbide ideó un método en el que se usaba rayón (celulosa purificada) para obtener fibras de alto módulo de Young. Más adelante hizo su aparición el poliacrilonitrilo (PAN), precursor más utilizado en la actualidad debido a las excelentes propiedades mecánicas de las fibras de carbono obtenidas. Sin embargo, la preparación de estas fibras de carbono tiene un elevado coste. El uso de breas de petróleo o resinas fenólicas como materias primas para la preparación de fibras de carbono abarata el coste, pero empeora sus propiedades. En las últimas dos décadas se ha investigado el uso de breas como precursores [26,27]. También se investiga en este campo el uso de fuentes renovables o recicladas de carbón [28]. Según el método de preparación que se haya seguido, el precursor utilizado, así como las propiedades obtenidas, las fibras comerciales se clasifican en:

- ✓ ***Fibras de carbono de altas prestaciones.*** Preparadas a partir de breas de mesofase (ultra-alto módulo) o poliacrilonitrilo (alto módulo). Se necesitan tratamientos térmicos adicionales a 2000-3000 ºC para su preparación. Se

utilizan en la industria aeroespacial, material deportivo, refuerzo en los materiales compuestos, etc.

- ✓ ***Fibras de carbono conductoras/grafíticas.*** Se preparan a partir de fibras de carbono, siempre que sean grafitizables, con un tratamiento térmico entre 2400-3000 ºC produciendo excelentes propiedades conductoras.
- ✓ ***Fibras de carbono de uso general***. Se preparan a partir de breas de carbón y petróleo y resinas fenólicas. Entre ellas se cuentan las fibras de carbono activadas y las fibras de carbono crecidas en fase vapor. Las fibras de carbono activadas se distinguen por su elevada área superficial y distribución de tamaño de poros muy uniforme. Las fibras de carbono crecidas en fase vapor se obtienen mediante un proceso catalítico de depósito químico en fase vapor.

1.5. Electrospinning

Electrospinning o electrohilado es una técnica de producción de fibras derivada de la aplicación de fuerzas electrohidrodinámicas (EHD) a un líquido conductor. La preparación de fibras se limita a materiales poliméricos, pero esta técnica permite preparar fibras a partir de cualquier material en disolución o mezcla fundida gracias a la correcta elección de disolventes y de la configuración del equipo de electrohilado.

Las fibras preparadas mediante electrohilado, presentan la característica de poseer un reducido tamaño, siendo posible alcanzar diámetros de decenas de nanómetros a partir de precursores de mayor tamaño y gran disponibilidad.

Tras el redescubrimiento de la técnica, en los años 90, el electrohilado ha despertado un interés creciente en la comunidad científica. Aquí se pretende presentar la técnica y describir los apartados que tienen un mayor grado de implicación en el trabajo desarrollado en esta tesis doctoral. Para obtener una panorámica más concreta sobre los aspectos más importantes del electrohilado sería recomendable acudir a algunas de las revisiones bibliográficas más destacadas, como aquellas sobre aplicaciones [29-31], configuraciones del equipo [32], materiales electrohilables [33], la escalabilidad y la recolección de fibras [34], la descripción y modelado de las fuerzas EHD que hacen posible la técnica [35] y otras muchas sobre el estado del arte, disponibles en la literatura científica.

1.5.1. Historia

El electrospinning tal y como es estudiado hoy día aparece por primera vez en una patente de Anton Formhals en la década de los 30 del siglo pasado, donde se menciona que la acción de un campo eléctrico sobre una disolución conductora permite producir hilos de reducido tamaño.

Para el uso del electrospinning de forma comercial, habría que esperar hasta la década de los ochenta en el mundo occidental, cuando la compañía Donaldson comienza a producir masivamente fibras electrohiladas como componente adsorbente de sus filtros. A pesar de la versatilidad de esta técnica, fue ignorada por la comunidad científica hasta los años 90, momento en que, con los trabajos del grupo de Reneker [36], Rutledge [37] o de Loscertales [38] el electrospinning fue revalorizado como una fuente potencial de fibras continuas de reducido tamaño y de una vasta variedad de compuestos poliméricos y precursores cerámicos.

1.5.2. Descripción de la técnica

En el electrospinning, un uso preciso de las fuerzas electrostáticas es necesario para abordar la producción de fibras submicrométricas. Se puede definir el electrospinning como un proceso en el que una disolución de un polímero, un sol o una mezcla fundida, todas ellas conductoras, son hiladas en fibras de pequeño diámetro usando un campo eléctrico de elevado potencial. Las ventajas más evidentes de esta técnica son su simplicidad y flexibilidad.

1.5.2.1. Equipo básico

A pesar de la complejidad de las interacciones físicas, químicas y eléctricas que rigen en este proceso, el montaje del aparato usado para electrohilado es sencillo, Figura 1.3. El equipo está compuesto por una fuente eléctrica de alto voltaje, que se usa para cargar eléctricamente una disolución de precursor de fibra que es bombeada hacia la boquilla de la hiladora, normalmente una aguja metálica. En frente de la jeringa y a una distancia de no más de un metro, se coloca un colector metálico cargado eléctricamente con polaridad inversa a la de la disolución de precursor.

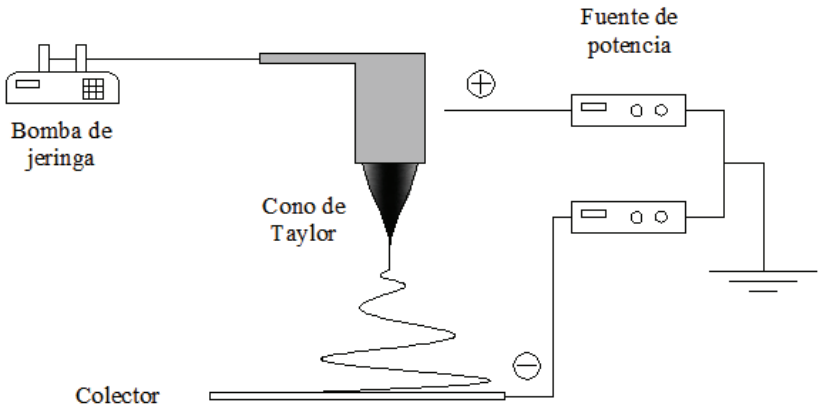

Figura 1.3. Equipo básico de electrospinning.

1.5.2.2. Cono de Taylor

La disolución del precursor del material al que queremos dotar de forma fibrosa se bombea desde la jeringa hasta la aguja. Una gota de la disolución aparece en la punta de la aguja de la hiladora donde la fuente de alto voltaje, conectada a la misma, induce la carga de la disolución. En ella, el equilibrio de fuerzas viscosas, de tensión superficial y eléctricas de repulsión entre cargas en la superficie de la gota causan que ésta se deforme, adoptando forma cónica denominada cono de Taylor, en la Figura 1.4. se muestra el cono de Taylor para una disolución de lignina y etanol. Más allá de una determinada carga crítica de la disolución, este cono se vuelve inestable, venciendo las fuerzas eléctricas a las de tensión superficial, produciéndose la eyección de líquido desde el cono hacia el colector. La estabilidad de este cono es crítica si se quiere mantener el proceso de electrospinning en funcionamiento durante un tiempo prolongado.

Figura 1.4. Cono de Taylor compuesto de una disolución de lignina Alcell y etanol.

1.5.2.3. Eyección del chorro

El chorro emitido del cono del cono de Taylor está cargado, y la acción del campo eléctrico entre la aguja y el colector hace que se acelere en sentido aguja-colector. En este sistema, para una disolución de una conductividad dada, el flujo impuesto de líquido en la bomba de jeringa y el potencial de campo eléctrico dictarán la dinámica de eyección de ese chorro a través de la resultante intensidad de corriente, siendo posible escoger unos valores de estos parámetros que mantengan estable el sistema durante un largo periodo de tiempo [35]. Además, de ellos dependerá el grosor del chorro, estrechamente relacionado con el tamaño final de la fibra.

1.5.2.4. Inestabilidades

En el vuelo del chorro hacia el colector, alguna de las fuerzas que están actuando simultáneamente sobre el filamento de fluido se impondrá, causando la aparición de las llamadas inestabilidades, responsables de cambios en la trayectoria, forma e incluso estabilidad del chorro. Se ha de considerar que, para conseguir mantener el electrospinning operativo se debe mantener el chorro continuo y el disolvente utilizado se debe evaporar en ese vuelo, obteniendo un filamento sólido que se recogerá en el colector. El estudio de las inestabilidades es, por lo tanto, primordial para poder favorecer la acción de aquellas que nos interesen, y suprimir otras que pongan en peligro la estabilidad del sistema.

- ✓ ***Inestabilidades de Rayleigh y variceal***. Deforman el chorro de forma axisimétrica, lo que quiere decir que causan ensanchamiento y estrechamiento radiales a lo largo de la longitud del chorro. Son causadas por la tensión superficial del líquido, y si se le da el tiempo suficiente, causa la rotura del chorro en gotas, obteniéndose el aerosol característico de la técnica de electrospray [39].
- ✓ ***Inestabilidad de latigueo***. Consiste en una oscilación lateral del chorro causada por la repulsión resultante entre los iones [40]. El perímetro que alcanza este latigueo radialmente va incrementándose según el chorro avanza hacia el colector, cubriendo un volumen con forma de cono invertido. El modelo propuesto por Reneker et al. [41] demuestra que esa elongación es responsable del estrechamiento del chorro, por lo que la aparición de esta inestabilidad se hace muy importante.

- ✓ ***Inestabilidad de multichorro***. En ella el chorro se divide en varios filamentos de menor tamaño debido al exceso de densidad de carga superficial.

1.5.2.5. Recolección de la fibra

Cuando las fibras impactan sobre el colector, van acumulándose una sobre otra formando una película de fibras enmarañadas. Estas fibras pueden ser recogidas en forma de membrana, la más habitual de las conformaciones en las que se presentan las nanofibras electrohiladas. En el caso de querer obtener fibras con la misma orientación, es posible aplicar varias estrategias. La más habitual es el uso de un tambor rotatorio como colector [42]. También se pueden usar colectores con formas tan variadas como puntas [43], barras paralelas o cables conductores para dirigir la recolección de la fibra en una orientación preferencial.

1.5.3. Variables de operación

Los principales parámetros que controlan la estabilidad del proceso de electrospinning son aquellos que participan en las fuerzas eléctricas, de tensión superficial y viscoelásticas puestas en juego en este sistema. Estos parámetros se reparten en dos grupos; los pertenecientes a la disolución a hilar y los que corresponden al equipo de electrospinning.

Los parámetros del equipo que más influyen en la formación de la fibra son:

- ✓ ***Voltaje***. El voltaje es responsable de la carga eléctrica del fluido. Será necesario un valor mínimo de voltaje para iniciar la eyección del chorro, mientras que un valor demasiado alto llevará a la aparición de la inestabilidad de multichorro. El aumento del voltaje aplicado conlleva una velocidad de deposición de fibra más alta por una mayor transferencia de masa desde la punta de la aguja [44] y una disminución del tamaño de fibra.
- ✓ ***Distancia aguja- colector***. Afecta a la estructura y morfología de las fibras electrohiladas. Mayores distancias favorecen la eliminación de la inestabilidad variceal, pero se hace necesario un mayor voltaje para mantener la fuerza del campo eléctrico.
- ✓ ***Velocidad de bombeo de la disolución***. Aunque favorece la producción de más cantidad de fibra, un mayor bombeo de líquido a la aguja lleva a mayores diámetros de fibra.

Por otro lado, los parámetros de la disolución de mayor importancia son:

- ✓ ***Concentración del precursor***. La concentración de la disolución es un parámetro de gran importancia porque afecta a la viscosidad y a la tensión superficial. Un valor bajo de concentración favorece la aparición de electrospray y un valor alto puede imposibilitar el hilado de la fibra. Normalmente, el diámetro de la fibra aumenta al hacerlo la concentración de la disolución.
- ✓ ***Conductividad de la disolución***. La disponibilidad de iones cargados en la disolución es un requisito indispensable para hacer electrohilable una disolución. Una mayor conductividad permite incrementar la capacidad de carga del líquido, incrementando el efecto del campo eléctrico. Baumgarden et al [45] demostraron que el radio del chorro varía inversamente con la raíz cúbica de la conductividad eléctrica de la disolución. En cuanto a las inestabilidades, el aumento de la conductividad conlleva la supresión de la inestabilidad variceal, produciendo fibras de superficies más regulares.
- ✓ ***Volatilidad del disolvente.*** La importancia de esta propiedad es obvia, al determinar el tiempo necesario de vuelo para que el disolvente se evapore del chorro. Por otro lado, si el disolvente es muy volátil puede aparecer la solidificación del chorro antes de que se inicie la inestabilidad de latigueo, produciendo fibras demasiado gruesas al no haberse producido la elongación por el latigueo. Incluso puede ocurrir la solidificación del cono de Taylor, deteniéndose el proceso [46]. Aunque la volatilidad es una propiedad de la disolución, es posible modificar su efecto actuando sobre el ambiente en el que se lleva a cabo el electrospinning; por ejemplo, la humedad ambiental afecta a la hidrólisis de fibras de alcóxidos, y un control de la misma puede usarse para modificar la velocidad de solidificación de esas fibras.

1.5.4. Electrospinning co- y tri-axial

En 2002, los fundadores de Yflow publicaron en Science un método para generar conos de Taylor compuestos a partir del bombeo simultáneo de dos líquidos a través de dos agujas concéntricas. Esto permitía encapsular un líquido en otro siempre que fueran inmiscibles [38]. En la Figura 1.5a. se muestra la instalación correspondiente a la configuración co-axial. En él, se han duplicado las bombas y se ha añadido una

segunda aguja concéntrica a la boquilla de hilado, sin necesidad de variar el montaje usado para tal fin

Este sistema de electrospinning puede ser usado para producir nanocápsulas de líquidos inmiscibles e hilar líquidos inmiscibles, tal y como se ha descrito en el párrafo anterior. También se pueden obtener fibras compuestas con distinta composición entre el interior y la superficie y fibras huecas extrayendo el líquido bombeado por la aguja interna, temas a los que se dedican dos de los capítulos de esta tesis. Otra variable a la configuración co-axial es la disposición tri-axial cuyo esquema se muestra en la Figura 1.5b. El funcionamiento es análogo al explicado anteriormente.

En cuanto a las variables de operación en el eletrospinning co-axial, además de los parámetros descritos con anterioridad, aparecen tres nuevas variables:

- La tensión superficial entre ambos líquidos, los cuales no son miscibles, es grande, y debe ser reducida al mínimo para obtener un cono de Taylor estable. Se suele conseguir añadiendo surfactantes u otros aditivos que sean miscibles en ambos líquidos.
- La viscosidad de ambos líquidos debe ser suficientemente elevada como para que el movimiento impuesto por el líquido de arrastre o conductor se transmita hacia el otro líquido gracias al rozamiento en la interfase, venciendo además las fuerzas de tensión superficial que podrían acabar con el cono de Taylor compuesto.
- Por último, los cocientes de velocidad de bombeo externo e interno son controlados para evitar la aparición de un modo de goteo o la desaparición de la capa de líquido externo, que podría verse arrastrada en gotas disueltas en el elevado flujo bombeado por la aguja interna.

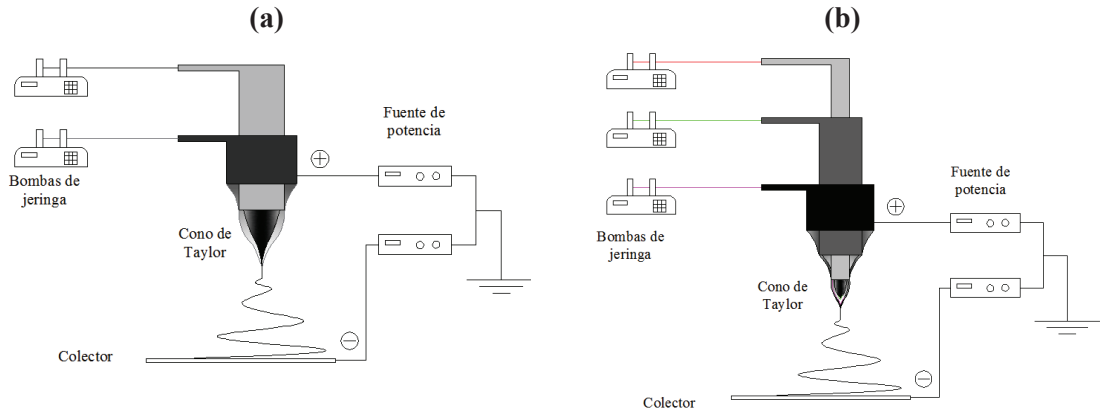

Figura 1.5. Montaje de instalación co-axial (a) y tri-axial (b).

1.6. Aplicaciones de las fibras

Los materiales en forma de fibra pueden ser usados en multitud de aplicaciones. En los últimos años se ha observado un enorme aumento en las publicaciones donde se muestran las ventajas de las fibras debido a su pequeño tamaño y a las propiedades de los materiales obtenidos.

El área de mayor aplicación de las fibras es la biomedicina. Gracias a la gran versatilidad que proporciona la técnica de electrospining, es posible electrohilar disoluciones de polímeros sintéticos que sean biocompatibles con el cuerpo humano que puedan ser usados para la producción de tejidos, donde las fibras ayudarían como soporte para el crecimiento de las células [47,48]. Otra aplicación importante en este campo es la dosificación de medicamentos, donde el material electrohilado serviría para el encapsulamiento de medicamentos pudiéndose liberar en la zona a tratar mediante un estímulo adecuado [49-51].

La aplicación de fibras en la separación de aguas, usadas como filtros, es otro de los campos en los que estos materiales están cobrando importancia. Esta fue la primera aplicación en la que se usaron fibras electrohiladas. Con ellas, es posible filtrar partículas de tamaño submicrométicо [52] con la ventaja de causar bajas pérdidas de presión, así las membranas adquieren gran importancia en el campo de la separación de aguas y, además, dependiendo del precursor utilizado estas membranas pueden estar cargadas eléctricamente ejerciendo de filtros electrostáticos [53].

Los materiales semiconductores como los óxidos de titanio, estaño, wolframio, molibdeno y otros pueden ser usados como sensores, ya que poseen la capacidad de detectar concentraciones de gases en el nivel de traza [54]. Al ser electrohilados, la elevada área específica junto con su elevada conductividad hacen de estos materiales productos idóneos para preparar nanosensores. Cuando el gas contaminante a analizar se adsorbe en una nanofibra de un metal semiconductor, la resistividad de este se ve alterada, produciendo un cambio de voltaje que puede ser relacionado con la presencia del gas.

1.7. Aplicaciones de las fibras de carbón en ingeniería química.

Numerosas son las aplicaciones de las fibras de carbono, entre ellas cabe destacar su uso como refuerzos en materiales compuestos. La presente tesis doctoral está dedicada a la preparación de fibras de carbono con propiedades funcionales para ser usadas en aplicaciones de ingeniería química, tales como la adsorción, catálisis, electrocatálisis y almacenamiento de energía. Gracias a la versatilidad de la técnica de electrospinning se han preparado materiales carbonosos en forma fibrilar con distintas propiedades texturales y químicas que hacen apropiado su uso para las distintas aplicaciones tratadas.

1.7.1. Adsorción.

La adsorción es una de las operaciones de separación más importantes en la industria química. Mediante la adsorción, el adsorbente (sólido poroso) de elevada superficie específica se pone en contacto con una corriente gaseosa o líquida en la que se encuentra un adsorbato. Las moléculas del adsorbato se adsorberán en la superficie del adsorbente mediante interacciones de naturaleza física o química, purificando, de esta forma, la corriente de gas o líquido tratada. Entre los aspectos positivos de la adsorción como método de tratamiento de aguas residuales cabe señalar: su capacidad para trabajar eficazmente a concentraciones bajas de contaminante, su flexibilidad frente a las variaciones de caudal y concentración, sus moderadas necesidades de espacio, la facilidad de automatización, la posibilidad de regenerar el adsorbente y la posibilidad de recuperar sustancias retenidas cuando ello resulte de interés económico. Entre los aspectos negativos hay que señalar que el coste de operación suele ser comparativamente alto y, por esta razón, su empleo queda restringido, en general, a los

casos de necesidad o a otros en que convenga reutilizar las aguas tratadas o, como se ha indicado, recuperar algún producto de las mismas.

El adsorbente más frecuente es el carbón activo, aunque a veces se emplean la alúmina, el gel de sílice o los tamices moleculares.

En la presente tesis doctoral se ha estudiado la adsorción de fenol sobre fibras de carbono activadas. El fenol es un compuesto orgánico aromático que posee un anillo bencénico en su estructura el cual le proporciona una alta estabilidad y reactividad química. En 2012, la producción mundial de este compuesto aromático fue de 8,9 millones de toneladas. La farmacéutica APAC fue líder indiscutible del mundo en la producción de fenol, representando más del 41% (por encima de 3,7 millones de toneladas) de la producción global. En este mismo año, China, EE.UU., Japón, Taiwán y Corea del Sur fueron los cinco principales países de fabricación de fenol con una producción de más de 5,5 millones de toneladas en volumen. En 2015, la capacidad de producción anual mundial de fenol aumentó a 10 millones de toneladas. La industria siderúrgica, conjuntamente con la petrolífera, son las mayores generadores de estos residuos fenólicos. En la industria siderúrgica, las aguas de coquería y la de alto horno son las que presentan mayor toxicidad.

El fenol y sus derivados, incluso a bajas concentraciones, proporciona al agua un olor y sabor característico. La toxicidad de los fenoles en estos efluentes se debe tanto a su carácter nocivo, como al elevado consumo de oxígeno durante su degradación. Estos compuestos se caracterizan por ser muy poco biodegradables; el tiempo de vida media de descomposición está entre 2 y 72 días [55]. Otro aspecto a tener en cuenta en relación con la elevada toxicidad del fenol es la irritabilidad que causa en ojos, membranas mucosas y piel, producción de convulsiones por simple absorción, afección al hígado, sistema nervioso y a los riñones, y su absorción por la piel, que puede llegar a ser mortal [56].

1.7.2. Catálisis

Los catalizadores juegan un papel muy importante en los procesos industriales, permitiendo producir más cantidad de producto con menor requerimiento de energía [57,58]. Se distingue dentro de ella la catálisis homogénea y la heterogénea, que hace

referencia a si el catalizador se encuentra en la misma o en distinta fase que los reactivos, respectivamente.

En la catálisis heterogénea el catalizador se compone normalmente de fase activa y soporte, que suele ser un material inerte, estable química, mecánica y térmicamente, de elevada área superficial específica y estructura porosa desarrollada [57,59]. De la interacción soporte-fase activa dependerá que se consiga una elevada dispersión del catalizador sobre la superficie [60,61]. Problemas de transferencia de materia en la película en torno a la partícula o de difusión en la partícula de catalizador producirían un bajo aprovechamiento del catalizador [62,63]. La conformación del catalizador puede determinar la pérdida de presión en el reactor. El uso de fibras como catalizadores y/o soporte de catalizadores puede reducir los problemas derivados de la transferencia de masa y problemas de difusión, así como producir menores pérdidas de carga en los reactores.

La gran variedad de grupos superficiales oxigenados presentes en los carbones activos hacen que estos materiales posean buenas propiedades catalíticas. Las ventajas de la utilización de carbón activo en catálisis heterogénea son varias. En primer lugar, la estructura del carbón es resistente a medios ácidos y básicos, siendo esta estable a elevadas temperaturas. Existe la posibilidad de controlar la estructura porosa y la química superficial de los catalizadores, pudiendo prepararse una larga variedad de estos, y además el coste de estos materiales es menor que el de otros soportes como son la alúmina o la sílice.

En esta Tesis Doctoral se caracterizan las propiedades ácidas y/o básicas de catalizadores de fibras de carbono mediante la descomposición de isopropanol en catálisis heterogénea.

La descomposición de isopropanol se ha estudiado principalmente para caracterizar las propiedades ácido-básicas de los catalizadores. La mayoría de los autores concluyen que el isopropanol se deshidrata sobre los sitios ácidos del catalizador para producir propileno y sobre los sitios básicos se deshidrogena para producir acetona [64].

1.7.3. Pilas de combustible

Las pilas de combustible tienen un funcionamiento similar al de las baterías y tienen la capacidad de transformar la energía química en eléctrica. En las baterías, los reactivos se encuentran almacenados internamente, por ello, una vez que se agotan la batería deja de funcionar. Por el contrario, en una celda de combustible las especies activas son suministradas externamente y su funcionamiento se mantendrá mientras se suministre combustible [65]. Una de las principales ventajas de las baterías y las pilas de combustible es la elevada densidad de energía. Las pilas de combustible juegan un papel esencial en la economía del hidrógeno, ya que otra de sus particularidades es hacer posible el uso de hidrógeno como combustible, originando agua como producto. El funcionamiento de estas pilas se fundamenta en una reacción global de combustión, de ahí su nombre, producto de la suma de dos reacciones individuales: i) la reacción de oxidación del combustible, en el ánodo; ii) la reacción de reducción de oxígeno (ORR, por sus siglas en inglés), en el cátodo [66].

La Figura 1.6 presenta un esquema de una celda de combustible junto con sus reactivos (combustible y oxidante) y sus productos. Una celda de combustible, está constituida básicamente por: i) un ánodo o electrodo negativo donde ocurre la reacción de oxidación del combustible, ii) un cátodo en el que se lleva a cabo la reducción del oxidante y iii) un electrolito que permite la transferencia de los iones entre los compartimentos anódico y catódico, cerrando así el circuito eléctrico de la celda.

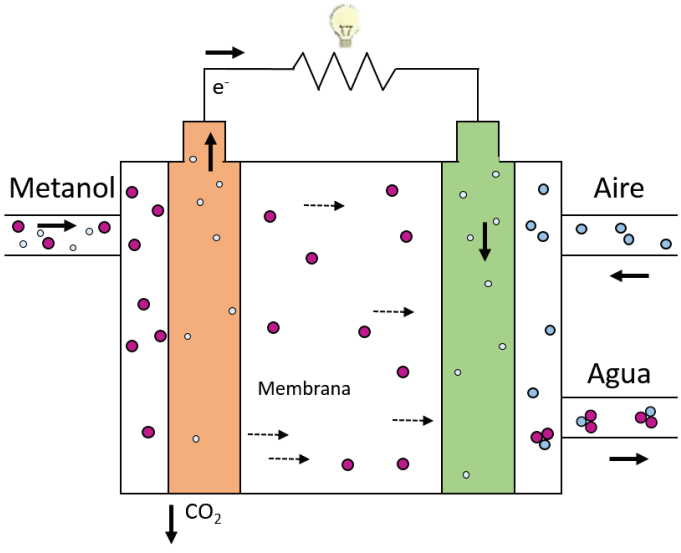

Figura 1.6. Esquema de una celda de combustible de electrólito alimentada con metanol. Adaptado de [67]

Las pilas de combustible se pueden clasificar en función del combustible elegido, así como del electrolito empleado, que determina la temperatura de operación y las reacciones que ocurrirán en los electrodos. En la actualidad, la mayoría de los prototipos emplea hidrógeno como combustible. Sin embargo, es posible emplear otros combustibles, sobre todo alcoholes y otros hidrocarburos. Destaca entre ellos el metanol, mientras que otros reactivos como el ácido fórmico, el formaldehído, el etanol y el etilenglicol, son empleados bajo condiciones muy específicas.

Por tanto, los dos prototipos más estudiados son aquellos que emplean el hidrógeno, en condiciones de baja temperatura y con electrolito polimérico, y el metanol como combustibles, siendo denominados pila de combustible de membrana polimérica y pila de metanol directa (PEMFC y DMFC).

Como combustible, el metanol ofrece varias ventajas sobre el hidrógeno, incluyendo la facilidad de transporte, el almacenamiento y de alta densidad de energía. Presenta también una aplicabilidad adecuada a bajas temperaturas y se puede obtener a partir de gas de síntesis mediante rutas sostenibles, aunque presenta los inconvenientes de ser inflamable y tóxico. La reacción de oxidación de metanol (MOR) se produce en el ánodo de las DMFC. El platino es el candidato más prometedor entre los metales puros para su aplicación en DMFC. Este metal es quien tiene la actividad catalítica más alta, sin embargo, las superficies de Pt puro son envenenadas por el monóxido de carbono, un subproducto de la oxidación de metanol a temperatura ambiente [68].

Los electrocatalizadores de platino muestran gran actividad para los ambientes ácidos de las DMFC. Sin embargo, el CO puede adsorberse fuertemente en la superficie del ánodo de Pt empleado en celdas de combustible [69,70], causando el bloqueo de sitios activos y provocando gran disminución en el rendimiento del electrodo.

Por otro lado, existe la desventaja de la oxidación electroquímica en los soportes carbonosos. Este hecho es conocido desde hace tiempo [71], sin embargo, la relación con la degradación en celdas de combustible no ha sido muy estudiada. La oxidación electroquímica del material carbonoso se produce en un mecanismo de dos pasos, siendo el primero la formación de óxidos superficiales, seguido por el desprendimiento de CO_2. Esta gasificación del soporte se convierte en una reacción que compite con la oxidación del metanol, reduciendo la eficiencia y poniendo en compromiso la

estabilidad estructural del catalizador. El problema de la oxidación electroquímica del carbón puede ser solucionado preparando materiales carbonosos más resistentes. En nuestro grupo de investigación, se ha demostrado que la preparación de carbones activos con H_3PO_4 produce carbones activos con mayor resistencia a la oxidación, tanto en fase gaseosa y electrolítica [72,73].

Por otro lado, se han realizado estudios en diferentes nanoestructuras de carbono como soportes catalíticos en celdas de combustible [74], lo cual ha mostrado que la interacción del precursor de platino con el material soporte varía según las heterogeneidades de la superficie y las características, originando partículas de Pt con diferentes tamaños, parámetros de red y morfología [75-77]. En la presente tesis se estudia un método novedoso para la preparación de fibras de carbono con distintos contenidos de Pt mediante electrospinning. Gracias a esta técnica es posible la obtención de electrocatalizadores con partículas de Pt muy bien distribuidas y con reducido tamaño.

1.7.4. Supercondensadores

El término de supercondensador o condensador electroquímico hace referencia a los sistemas de almacenamiento de energía compuestos por dos electrodos de elevada porosidad separados por una membrana porosa y en contacto con un electrolito. En esta configuración, la adsorción de los iones se realiza en un electrodo que es denominado ánodo o positivo, y sobre el cátodo o negativo se realiza la adsorción de los aniones. De esta forma, la mayor parte de la energía es acumulada por adsorción de los iones del electrolito en la interfase electrodo/electrolito, conocida como la doble capa eléctrica.

Estos sistemas se caracterizan porque, su respuesta a cambios impuestos en el potencial entre electrodos es rápida, lo que se traduce en una potencia elevada. Sin embargo, la mayor disponibilidad de área en los condensadores electroquímicos se traduce en densidades energéticas varios órdenes de magnitud superiores que la de los condensadores tradicionales. El material más utilizado como electrodo es el carbón activo, que combina estabilidad térmica y química, bajo precio y buena conductividad eléctrica con las mayores superficies específicas [78]. En esta Tesis doctoral se han preparado electrodos carbonosos a partir de lignina para ser utilizados como electrodo positivo y negativo de los supercondensadores. El uso de las fibras de carbono como electrodos posee la ventaja de que no es necesario añadir ningún aglomerante, el cual

reduce la porosidad de los electrodos, ni ningún promotor de la conductividad. Además, estos electrodos carbonosos flexibles presentaron excelentes propiedades en supercondensadores con elevadas velocidad de carga y descarga [14].

La vida media del supercondensador es muy elevada, pudiendo acumular hasta cientos de miles de ciclos de carga y descarga sin sufrir pérdidas notorias de su capacidad de almacenamiento y de conductividad [78]. Otra de sus ventajas es que los tiempos de carga son bajos, pudiéndose completar en cuestión de segundos.

Los dos parámetros más importantes en un condensador electroquímico son la energía (*E*) y la potencia específica (*P*). La energía acumulada en el condensador depende de del potencial aplicado (*V*) y de la capacidad (*C*), y se puede calcular usando la siguiente ecuación:

$$dW = V \cdot dQ \;\rightarrow W = E = \int_0^Q V \cdot dQ = \int_0^Q \frac{Q}{C} \cdot dQ = \frac{1}{2} \cdot C \cdot V^2$$

donde *Q* es la carga eléctrica y *W* es el trabajo del proceso

La potencia máxima que puede suministrar el condensador está limitada por la resistencia equivalente en serie, *ESR*, de la celda. Esta potencia se puede calcular atendiendo a la siguiente ecuación:

$$P = \frac{V^2}{4 \cdot ESR}$$

La resistencia equivalente en serie de un condensador engloba la resistencia del material que se usa como electrodo, la resistencia entre el electrodo y el colector de corriente y la resistencia iónica, relacionada con la difusividad de los iones que se desplazan en la red porosa y a través de la membrana situada entre los electrodos [79].

1.8. Referencias

[1] J.C. Philp, R.J. Ritchie,K. Guy, K. Trends Biotechnol., 31 (2) (2013) 65-67.

[2] B.E. DiGregorio. Chem Biol., 16 (1) (2009) 1-2.

[3]. J. Bedia. Tesis Doctoral, Universidad de Málaga, Málaga, 2008; capítulo 1: 7-9.

[4] E. Adler. Wood Sci. Technol. 11 (1977) 169-218.

[5] http://www.ili-lignin.com

[6] J. Rodríguez-Mirasol, T. Cordero, J.J. Rodríguez. Carbon 34 (1996) 43-52.

[7] J. Rodríguez-Mirasol. Tesis Doctoral, Universidad de Málaga, Málaga, 1991.

[8] E. González Serrano, T. Cordero, J. Rodríguez-Mirasol, J.J. Rodríguez. Ind Eng Chem Res. 36 (1997) 4832-4838.

[9] E. Gonzalez-Serrano, T. Cordero, J. Rodriguez-Mirasol, L. Cotoruelo, J.J. Rodríguez. Water Research. 38 (2004) 3043–3050.

[10] C. Pedrero, T. Cordero, J. Rodríguez-Mirasol, J.J. Rodríguez. Carbon'99, Charleston, SC ,1999.

[11] J.M. Rosas, J. Bedia, J. Rodríguez-Mirasol, T. Cordero. Carbon. 42 (2004) 1285-1290.

[12] M. Lallave, J. Bedia, R. Ruiz-Rosas, J. Rodríguez-Mirasol, T. Cordero, J.C. Otero, M. Marquez, A. Barrero, I.G. Loscertales. Adv. Mater. 19 (2007) 4292–4296.

[13] R. Ruiz-Rosas, J. Bedia, M. Lallave, I.G. Loscertales, A. Barrero, J. Rodríguez-Mirasol, T. Cordero. Carbon. 48(3) (2010) 696-705.

[14] R. Berenguer, F.J. García-Mateos, R. Ruiz-Rosas, D. Cazorla-Amorós, E. Moralón, J. Rodríguez-Mirasol, T. Cordero. Green Chem. 18 (2016) 1506-1515.

[15] F. Rodríguez-Reinoso, M. Molina-Sabio. Carbon 30 (1992) 1111-1118.

[16] J.C. Gonzalez, M.T. Gonzalez, M. Molina-Sabio, F. Rodriguez-Reinoso, A. Sepulveda-Escribano. Carbon. 33 (1995) 1175-1177.

[17] J.M. Rosas, J. Bedia, J. Rodríguez-Mirasol, T. Cordero. Fuel Proccess. Technol. 91 (2010) 1345-1354.

[19] M Jagtoyen, F Derbyshire. Carbon. 36 (1998) 1085-1087.

[20] J.V. Ibarra, R. Moliner, J.M. Palacios. Fuel 70 (1991) 727-732.

[21] M.R. Khan, R.G. Jenkins. Fuel. 68 (1989) 1336-1339.

[22] V. Verheyen, M. Jagtoyen, F. Derbyshire. Prep Pap Am Chem Soc., Div Fuel Chem 38 (1993) 400-407.

[23] M. Zhang, A.A. Ogale, Carbon. 69 (2014) 626–629.

[24] A. Huczko. Appl. Phys. A, 70 (2000) 365-376.

[25] J.C. Hulteen, C.R. Martin. J. Mater. Chem. 7 (1997) 1075-1087.

[26] J. Alcañiz Monge., D. Cazorla-Amorós., A. Linares-Solano, A. Oya, A. Sakamoto, K. Hoshi. Carbon 35 (1997) 1079-1087.

[27] I. Mochida, S.-H. Yoon, N. Takano, F. Forti, Y. Korai, K. Yokogawa. Carbon. 34 (1996) 941-956.

[28] W.M. Qiao, M. Huda, Y. Song, S.-H. Yoon, Y. Korai., I. Mochida. Energy & Fuels. 19 (2005) 2576-2582.

[29] R.S. Barhate, S. Ramakrishna. J. Membrane Science. 296 (2007) 1-8.

[30] S. Agarwal, J.H. Wendorff, A. Greiner. Adv. Mater. 21 (2009) 3343-3351.

[31] B. Ding, M. Wang, J. Yu, Gang Sun. Sensors. 9 (2009) 1609-1624.

[32] S. Park, K. Park, H. Yoon, J. Son, T. Min, G. Kim. Polym Int., 56 (2007) 1361-1366.

[33] W. Sigmund, J. Yuh, H. Park, V. Maneeratana, G. Pyrgiotakis, A. Daga, J. Taylor, J. C. Nino. J. Am. Ceram. Soc. 89 (2006) 395-407.

[34] A.K. Moghe, B.S. Gupta. Polymer Reviews. 48 (2008) 353-377.

[35] G.C. Rutledge, S.V. Fridrikh. Advanced Drug Delivery Reviews. 59 (2007) 1384-1391.

[36] J. Doshi, D. Reneker. J. Electrostatics. 35 (1995) 151-160.

[37] Y.M. Shin, M.M. Hohman, M.P. Brenner, G.C. Rutledge. Appl Phys Lett. 78 (2001)1149-1151.

[38] I.G. Loscertales, A. Barrero, I. Guerrero, R. Cortijo, M. Marquez, A.M. Gañán-Calvo. Science 295-c (2002) 1695-1698.

[39] O.A. Basaran. AIChE Journal. 48 (2002) 1842-1846.

[40] A.L. Yarin, S. Koombhongse, D.H. Reneker. J. Appl. Phys. 89 (2001) 3018-3026.

[41] D.H. Reneker, A.L. Yarin, H. Fong, S. Koombhongse. J. Appl. Phys. 87 (2000) 4531-4547.

[42] B. Ding, H.Y. Kim, S.C. Lee, D.R. Lee, K.J.Choi. Fiber. Polym. 3 (2002) 73-79.

[43] B. Sundaray, V. Subramanian, T.S. Natarajan, R.Z. Xiang, C.C. Chang, W.S. Fann. Appl. Phys. Lett. 84 (2004) 1222–1224.

[44] T. Subbiah, G.S. Bhat, S. Parameswaran, S.S. Ramkumar. J Appl Polymer Sci. 96 (2005) 557-569.

[45] P.K. Baumgarten. J colloid Interface Sci. 36 (1971) 71-79.

[46] S. Ramakrishna, K. Fujihara, W.-E. Teo, T.-C. Lum, Z. Ma. World Scientific Publishing Co. Pte. Ltd. 2005, ISBN 981-256-415-2.

[47] Y.K. Luu, K. Kim, B.S. Hsiao, B. Chu, M. Hadjiargyrou. J. Control. Release. 89 (2003) 341–353.

[48] H. Yoshimoto, Y.M. Shin, H. Terai, J.P. Vacanti. Biomaterials. 24 (2003) 2077–2082.

[49] K. Kim, Y.K. Luu, C. Chang, D. Fang, B.S. Hsiao, B. Chu, M. Hadjiargyrou. J Control Release. 98 (2004) 47-56.

[50] X. Xu, X. Chen, X. Xu, T. Lu, X. Wang, L. Yang, X. Jing. J Control Release. 114 (2006) 307-316.

[51] S.Y. Chew, J. Wen, E.K. Yim, K.W. Leong. Biomacromolecules. 6 (2005) 2017-2024.

[52] K.M. Sawicka, P. Gouma. J. Nanopart. Res. 8 (2006) 769–781.

[53] S.A. Angadjivand, M.G. Schwartz, P.D. Eitzman, M.E. Jones. 2002. US patent 6,375,886

[54] R.L.V. Wal, G.M. Berger, M.J. Kulis, G.W. Hunter, J.C. Xu, L. Evans. Sensors. 9 (2009) 7866-7902.

[55] N. Masqué, E. Pocurrull, R.M. Marcé, F. Borrull. Analyst, 47 (1993) 176-182.

[56] P. Zhang, D. Littlejohn. Analyst, 118 (1993) 1065-1071.

[57] M.A. Vannice. “Kinetics of Catalytic Reactions” Springer-Verlag, NY, 2005.

[58] R. L. Burwell, Jr. Chemtech 17 (1987) 586.

[59] M. Boudart and G. Djega-Mariadassou. Kinetics of Heterogeneous Catalytic Reactions, Princeton University Press, Princeton, NJ, 1984.

[60] B.C. Gates. Chem. Rev. 95 (1995) 511-522.

[61] J. Guzman, B.C. Gates. Dalton Trans. 17 (2003) 3303-3318.

[62] E.W. Thiele. Ind. Eng. Chem. 31 (1939) 916.

[63] J. J. Carberry, ‘‘Chemical and Catalytic Reaction Engineering’’, McGraw-Hill, NY, 1976.

[64] DC Tomczak, JL Allen, KR Poeppelmeier. J Catal 146 (1994) 155-165

[65] D. Linden, T. B. Reddy, Handbook of Batteries, McGraw-Hill, 1984.

[66] E. Frackowiak, F. Béguin, Carbon 40 (2002) 1775–1787.

[67] L. Carrette, K. a Friedrich, U. Stimming, Fuel Cells. 1 (2001) 5–39.

[68] E. Antolini, T. Lopes, E. R. Gonzalez, J. Alloys Compd. 461 (2008) 253–262.

[69] S. Wasmus, a. Küver, J. Electroanal. Chem. 461 (1999) 14–31.

[70] T. J. Schmidt, M. Noeske, H. A. Gasteiger, R. J. Behm, P. Britz, W. Brijoux, H. Bönnemann, Langmuir 13 (1997) 2591–2595.

[71] K. Kinoshita, J. Bett, Carbon 11 (1973) 237–247.

[72] J.M. Rosas, R. Ruiz-Rosas, J. Rodríguez-Mirasol, T. Cordero. Carbon. 50 (2012) 1523-1537.

[73] R. Berenguer, R. Ruiz-Rosas, A. Gallardo, D. Cazorla-Amorós, E. Morallón, H. Nishihara, T. Kyotani, J. Rodríguez-Mirasol, T. Cordero. Carbon. 95 (2015) 681-689.

[74] D. Mirabile Gattia, M. V. Antisari, L. Giorgi, R. Marazzi, E. Piscopiello, A. Montone, S. Bellitto, S. Licoccia, E. Traversa, J. Power Sources 194 (2009) 243–251.

[75] A. Pebler, J. Electrochem. Soc. 133 (1986) 133, 9–17.

[76] M. Carmo, V. A. Paganin, J. M. Rosolen, E. R. Gonzalez, J. Power Sources 142 (2005) 169–176.

[77] P. Ehrburger, P. L. Walker, J. Catal. 55 (1978) 63–70.

[78] A.G. Pandolfo, A.F. Hollenkamp. Journal of Power Sources 157 (2006) 11-27.

[79] Conway, B.E. (Ed.) (1999). Electrochemical Supercapacitors. New York: Kluwer Academic.

Chapter 2

Metodología experimental

2.1. Preparación de fibras de carbón.

2.1.1. Electrohilado

Para la preparación de las fibras de carbono se ha usado como materia prima Lignina Alcell®. Se han preparado distintas disoluciones de lignina/etanol y H_3PO_4/lignina/etanol con las concentraciones apropiadas para obtener una viscosidad idónea para el electrohilado. En el caso de la preparación de fibras de lignina las concentraciones en peso usadas de lignina/etanol han sido de 1/1[1,2], cuando la disolución inicial se ha impregnado con ácido fosfórico las concentraciones másicas usadas de H_3PO_4/lignina/etanol han sido de n/1/1, siendo n = 0.1 y 0.3 dependiendo del material a preparar. También se han preparado fibras de lignina con Pt, para ello diferentes concentraciones másicas del precursor de platino (acetil acetonato de Pt) se han añadido a la solución inicial con y sin presencia de H_3PO_4.

Para el electrohilado de las fibras de lignina se ha utilizado la configuración co-axial del electrospining mostrado en la Figura 2.1. En todos los casos se ha usado etanol como disolvente por la aguja exterior para evitar la solidificación del chorro. En el caso de la preparación de fibras de lignina y fibras de lignina con ácido fosfórico en su menor relación de impregnación (0.1), se ha bombeado la disolución con un flujo de 1 $mL \cdot h^{-1}$ por la aguja interna, mientras que el caudal de disolvente ha sido de 0.1 $mL \cdot h^{-1}$. Para la preparación de fibras de lignina con una relación de impregnación inicial de H_3PO_4 de 0.3, son necesarios mayores caudales para la formación el cono de Taylor y un hilado estable, siendo el caudal de disolución por la aguja interna de 3 $mL \cdot h^{-1}$ y de etanol por la aguja externa de 0.3 $mL \cdot h^{-1}$. La diferencia de potencial aplicado entre la aguja y el colector ha variado entre 14 y 24 kV.

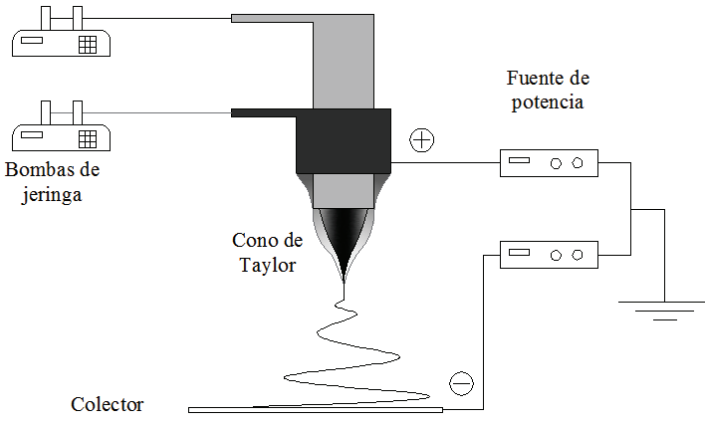

Figura 2.1. Configuración co-axial del equipo de electrospinning

2.1.2. Estabilización de fibras de lignina.

La estabilización de las fibras de lignina se ha llevado a cabo en la instalación mostrada en la Figura 2.2. que consta de los siguientes elementos:

- ✓ ***Botella de nitrógeno o aire****:* Proporciona el gas que mantiene la atmósfera inerte u oxidante dentro del horno donde se encuentra la muestra.
- ✓ ***Medidor de flujo másico****:* Es un elemento transductor de señal (caudal-señal eléctrica). Se ubica a la salida del controlador de presión de los gases. El medidor usado es de la marca BROOKS, modelo 5850 TR.
- ✓ ***Controlador de flujo másico****:* Permite controlar el flujo de gas que se introduce en el sistema para mantener la atmósfera inerte. Este dispositivo junto con el medidor de flujo másico permite fijar el caudal de gas usado en los experimentos. El controlador usado es de la marca GOOSEN, modelo 5878.
- ✓ ***Horno****:* El horno utilizado es de tipo tubular horizontal. Permite obtener temperaturas de hasta 1000 ºC a las que se llega con un programa de calentamiento variable. El horno utilizado es de la casa CARBOLITE FURNACES, modelo CFT 12/75, de 75 mm. de diámetro y 750 mm. de longitud.

La estabilización de las fibras de lignina sin presencia de H_3PO_4 se ha realizado en atmósfera oxidante (aire 150 $cm^3 \cdot min^{-1}$). Para este tipo de materiales es necesario una velocidad de calentamiento muy baja para evitar la fusión de las fibras en la etapa de estabilización y/o carbonización. En este caso la velocidad de calentamiento ha sido 0.08 $ºC \cdot min^{-1}$ desde temperatura ambiente hasta 200 ºC, manteniendo la temperatura final durante 80 horas. Por el contrario, las fibras de lignina con presencia de ácido fosfórico se han estabilizado en atmósfera de aire y nitrógeno (150 $cm^3 \cdot min^{-1}$) usando velocidades de calentamiento entre 0.08 y 4 $ºC \cdot min^{-1}$, con temperaturas finales que han variado entre 100 y 250 ºC, manteniendo las temperaturas de estabilización entre 1 y 6 horas.

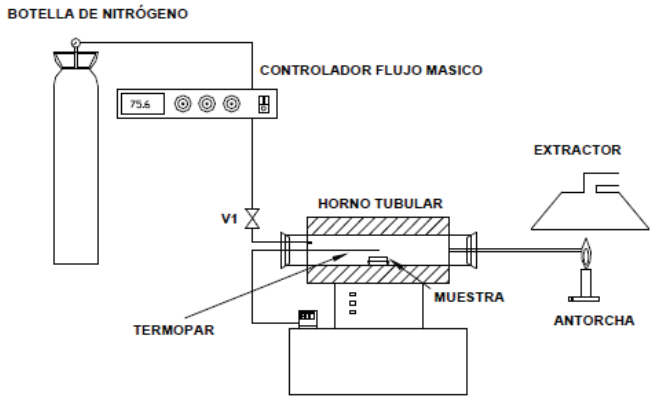

Figura 2.2. Instalación para la estabilización y carbonización de fibras de lignina

2.1.3. Carbonización de las fibras estabilizadas

Las fibras estabilizadas se han introducido en un horno tubular como el mostrado en la Figura 2.2. Se ha utilizado una velocidad de calentamiento de 10 ºC·min^{-1} hasta alcanzar la temperatura de carbonización, la cual ha variado entre 500 y 900 ºC. Una vez terminado el proceso de carbonización se ha mantenido el flujo de atmósfera inerte mientras disminuye la temperatura.

2.1.4. Lavado y secado

En el caso de la preparación de fibras de carbono con H_3PO_4 es necesario realizar un proceso de lavado para extraer el agente activante que se encuentra ocluyendo los poros y de esta forma liberar la estructura porosa del carbón. El lavado se realiza con agua destilada a 60 ºC en un sistema de filtración a vacío hasta pH constante. Una vez filtrada la muestra, el sólido resultante, se seca en estufa durante 24 horas a 80 ºC, obteniéndose el carbón seco.

2.1.5. Tratamientos térmicos.

Se han realizado tratamientos térmicos sobre las fibras de carbono preparadas a 900 ºC. Para estos tratamientos se ha utilizado un horno vertical de la casa FORNS HOBERSAL (temperatura máxima 1750 ºC). Los tratamientos térmicos se han realizado a una velocidad de calentamieno de 5 ºC·min^{-1} desde temperatura ambiente hasta temperaturas de 1200 o 1600 ºC, manteniendo la temperatura final durante 1 hora.

2.2. Caracterización de las fibras de carbono

2.2.1. Análisis elemental y cenizas

El análisis elemental proporciona el contenido total de carbono, hidrógeno, nitrógeno, azufre y oxígeno (por diferencia del total de muestra seca, descontadas las cenizas), de las muestras.

Los análisis elementales se han realizado en un analizador elemental LECO® CHNS-932, en el cual se introduce la muestra seca previamente pesada y empaquetada en un contenedor de estaño/aluminio, a una temperatura de aproximadamente 1000 ºC en atmósfera de oxígeno puro y las cantidades de CO_2, SO_2 y H_2O se cuantifican mediante sensores de infrarrojos y el N_2 mediante un catarómetro.

Para el cálculo de las cenizas se ha empleado un horno de tipo mufla. Se deposita la muestra (aproximadamente 1 g) en un crisol, que se introduce en la mufla, aumentando la temperatura hasta 650 ºC. Se mantiene a esta temperatura hasta pesada constante, tal y como establece la norma ASTM 2866-83.

2.2.2. Estructura porosa

La estructura porosa de las muestras se ha caracterizado mediante adsorción-desorción de N_2 a -196 ºC y adsorción de CO_2 a 0 ºC en un equipo ASAP 2020 de la casa Micromeritics. Las muestras han sido previamente desgasificadas durante al menos 8 horas a una temperatura de 150 ºC.

A partir de las isotermas de adsorción-desorción de N_2, se ha calculado el área aparente (A_{BET}) mediante la aplicación de la ecuación BET [3], el volumen de microporo (V_t) y el área externa (A_t) se han determinado empleando el método t [4] y el volumen de mesoporo (V_{mes}) se ha calculado como la diferencia entre el volumen de nitrógeno adsorbido a la presión relativa de 0.95 (V_{tot}) y el volumen de microporo (V_t) [5]. Por otro lado, el área de microporo estrecho (A_{DR}) y el volumen de microporo estrecho (V_{DR}) se han obtenido mediante la aplicación del método de Dubinin-Radushkevich [6] aplicado a las isotermas de adsorción de CO_2.

Además, se ha utilizado la técnica de análisis de porosimetría de mercurio para completar la caracterización de la estructura porosa. Para llevar a cabo esta técnica se ha utilizado un equipo AUTOPORE IV de la casa comercial Micromeritics®. Ésta técnica

se basa en la intrusión de mercurio en una estructura porosa bajo presiones controladas rigurosamente para la obtención de la porosidad de la muestra y valores de densidades aparentes.

2.2.3. Química superficial

La química superficial se analizó mediante análisis de espectroscopía fotoelectrónica de rayos X (XPS), difracción de Rayos X (DRX) y desorción térmica programada (DTP).

2.2.3.1. Espectroscopia fotoelectrónica de Rayos X (XPS).

Los análisis de XPS se han llevado a cabo usando un espectrofotómetro modelo 5700C de la casa Physical Electronics® con radiación MgKα de 1253.6 eV. Para el análisis de los espectros de alta resolución del XPS, la posición del pico del C1s fue establecida en 284.5 eV y usada como referencia para posicionar los demás picos del espectro [7,8]. Los espectros de alta resolución se deconvolucionaron usando curvas Gaussiana-Lorentziana.

Una vez obtenido el espectro de baja resolución e identificados los elementos que corresponden a cada uno de los picos, se obtienen los espectros de alta resolución o picos de cada elemento, gracias a los cuales pueden visualizarse con claridad los estados de oxidación de los distintos elementos de la muestra, así como el tipo de enlace que forma con otros elementos presentes en la superficie.

2.2.3.2. Difracción de Rayos X (DRX)

Los datos de difracción de rayos-X se adquirieron usando un difractómetro Philips X´Pert PRO MPD. El sistema óptico de este equipo consta de un monocromador primario del tipo Johansson con un cristal de Ge (111), que proporciona una radiación estrictamente monocromática CuKα (λ = 1.5406 Å). Las rendijas de divergencia y antidivergencia se fijaron a ½º y se utilizaron rendijas Soller (haz incidente y difractado) de 0.04 rad. El sistema de detección consiste en un X´Celerator RTMS (Real Time Multiple Strip) constituido por 128 detectores de Si colocados en línea, con la longitud activa al máximo.

Las medidas se realizaron desde 2θ = 5º a 80º durante 37 min, con un tamaño de paso de 0.017º. La radiación incidente fue de 45 kV y 40 mA. Las medidas se realizaron en un portamuestras giratorio de zero-background.

2.2.3.3. Desorción térmica programada (DTP)

Los experimentos de DTP se han realizado empleando un reactor de cuarzo tubular situado en el interior de un horno eléctrico. Las muestras (aproximadamente 70 mg) se introdujeron en el interior del reactor y se calentaron desde temperatura ambiente hasta 1000 ºC a una velocidad de calentamiento de 10 ºC·min^{-1} en un flujo de helio (200 cm^3 STP·min^{-1}). Las cantidades de CO y CO_2 desorbidas se monitorizaron con analizadores de gases mediante infrarrojos no dispersivos (NDIR, Siemens® ULTRAMAT 22) y las cantidades desorbidas de otros gases con un espectrómetro de masas de Pfeiffer Vacuum® modelo ThermoStar MSC ‑ 200.

2.2.3.4. Acidez superficial

La adsorción de moléculas básicas, tales como la piridina, se usa frecuentemente para analizar la acidez de sólidos. La piridina interactúa con los sitios ácidos debido a que poseen un par de electrones no compartidos en el átomo de nitrógeno que pueden ser donados a un sitio ácido de Lewis aunque también puede aceptar un protón de un sitio ácido de Brönsted.

Los análisis se han realizado en un sistema termogravimétrico como el que se muestra en la Figura 2.3. Para ello, se han utilizado entre 10-15 mg de catalizador, el cual se ha desgasificado a 150 ºC durante 1 hora en atmósfera inerte. Posteriormente se procede a la adsorción de piridina a 120 ºC durante un tiempo no inferior a 1 hora hasta obtener una pesada constante que indique que el catalizador se ha saturado de piridina. Se realiza una desorción a la temperatura de adsorción de piridina (120 ºC) en atmósfera inerte, donde se lleva a cabo la desorción de la piridina adsorbida físicamente. Finalmente, la cantidad final de piridina quimisorbida sobre el catalizador nos proporcionará información sobre la acidez superficial del mismo.

2.2.4. Análisis termogravimétricos (TG)

Los análisis se han realizado colocando aproximadamente 15 mg de la muestra en un crisol, que se mantiene suspendido por un hilo de cuarzo. La temperatura se ha

aumentado a razón de 10 ºC·min^{-1} desde temperatura ambiente hasta 900 ºC, usando un flujo de aire de 150 cm^3 STP·min^{-1}. Para la realización de los experimentos termogravimétricos se ha usado un equipo de termobalanza estanco (Figura 2.3). Este equipo consiste en un sistema modular de la casa CI ELECTRONICS.

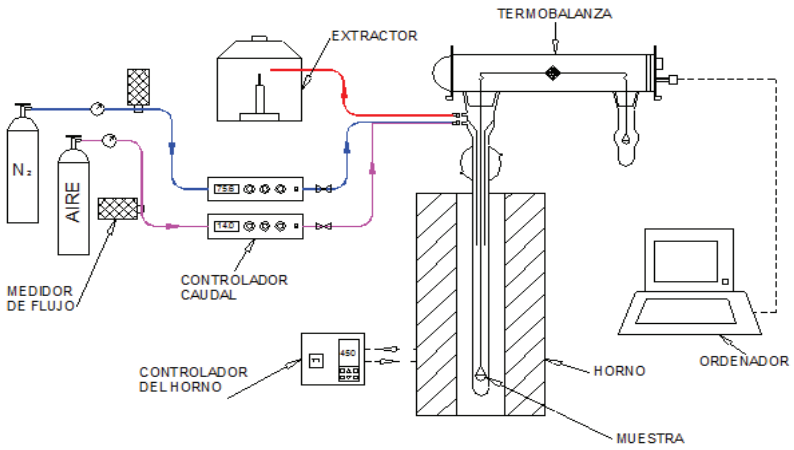

Figura 2.3. Instalación utilizada en el análisis termogravimétrico.

2.2.5. Calorimetría diferencial de barrido (DSC)

La calorimetría diferencia de barrido se ha realizado en un calorímetro diferencial de barrido de METTLER TOLEDO modelo DSC 1. La celda de medida está formada por un horno de plata modelo 400W que opera ente RT-700 ºC, con una velocidad de calentamiento máxima de 100 ºC·min^{-1}, y un sensor cerámico modelo HSS8 formado por 120 termopares de Au-Au/Pd. El equipo incorpora además un sistema de enfriamiento mediante N_2 líquido que permite bajar la temperatura de operación mínima a los -150 ºC. Como gas protector se utiliza un flujo continuo de N_2 de 20 mL·min^{-1}. Los ensayos se realizaron en crisoles de Al_2O_3 de 70 µl en el intervalo de temperaturas 30-250 ºC, con un flujo de aire o nitrógeno de 50 mL·min^{-1} y una velocidad de calentamiento de 2 ºC·min^{-1}. Se han utilizado masas de muestra comprendidas entre 5 y 10 mg.

2.2.6. Morfología superficial

La morfología superficial se ha examinado mediante microscopia electrónica de barrido, SEM (Scanning Electron Microscopy). El microscopio electrónico empleado es

un modelo JSM 6490L de la casa comercial JEOL® trabajando a un elevado voltaje de entre 20 y 25 kV.

Para analizar la estructura de algunas de las muestra se ha utilizado microscopía de transmisión electrónica, TEM (Transmission Electron Microscopy). El TEM empleado es el modelo CM200 de la casa comercial Philips®, trabajando con un voltaje de aceleración de 200 kV y una resolución < 0.2 nm.

2.3. Equipos e instalaciones utilizados para la adsorción de fenol.

La adsorción de fenol sobre las fibras de carbono activadas se ha realizado a temperaturas comprendidas entre 15 y 35 ºC. La instalación mostrada en la Figura 2.4. se ha utilizado para realizar el estudio termodinámico y el estudio en columna de adsorción. El estudio cinético se ha llevado a cabo en la instalación presente en la Figura 2.5. En estas instalaciones se utiliza un refrigerador y un tectrón de la casa comercial JP SELECTA para mantener la temperatura deseada. El UV-Vis utilizado es de la casa comercial VARIANT, y las bombas peristálticas utilizadas son de la casa comercial WATSON MARLOW.

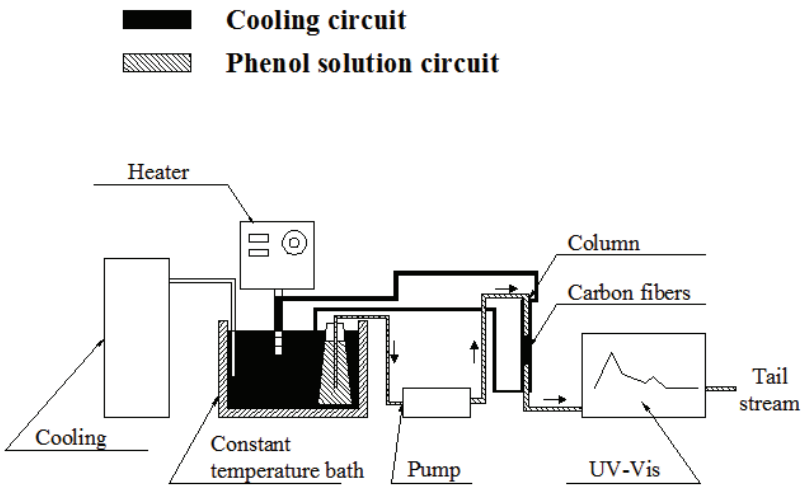

Figura 2.4. Instalación utilizada para estudio termodinámico y estudio de adsorción en columna

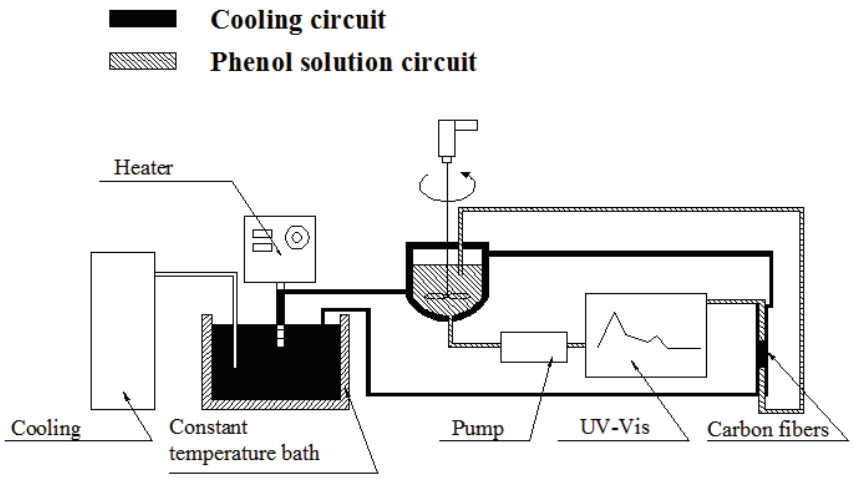

Figura 2.5. Instalación utilizada para estudio cinético de adsorción.

2.4. Equipos para la descomposición de alcoholes

Para la realización de los experimentos de descomposición de alcoholes se ha empleado una instalación como la que se esquematiza en la Figura 2.6 y que consta de los siguientes elementos:

- ✓ ***Botellas de gases y medidores de flujo másico***. Elementos transductores de señal (caudalseñal eléctrica). Se ubican a la salida de las botellas de gases. El medidor usado es de la marca BROOKS, modelo 5850 TR.
- ✓ ***Controlador de flujo másico***. Este dispositivo junto con los medidores de flujo másico permite fijar el caudal de gas usado en los experimentos. El controlador usado es de la marca GOOSEN, modelo 5878.
- ✓ ***Cable térmico*****,** mediante el cual se calefactan las conducciones de entrada y salida del reactor para evitar que se produzca condensación de reactivos o productos en las paredes de estas conducciones.
- ✓ ***Reactor***, tubo de cuarzo de 4mm de diámetro interior y una longitud de unos 40 cm, en el interior del cual de deposita el catalizador y en el que se realiza la reacción.
- ✓ ***Horno***, para elevar la temperatura en el interior de reactor.
- ✓ ***Termopar***, para poder medir y controlar la temperatura en el interior de reactor. Controlador del horno, compara la temperatura del termopar con la temperatura programada y actúa en consecuencia.

- ✓ ***Jeringas de inyección*** (Cole-Parmer® 74900-00,-05 Syringe Pump), para introducir el Metanol/Etanol/Agua en el sistema.
- ✓ ***Analizadores de gases***, para poder seguir la evolución de los reactivos y de los productos de reacción. Se emplearon un espectrómetro de masas y un cromatógrafo de gases. El espectrómetro de masas es de la casa Pfeiffer Vacuum® modelo OmniStar. El cromatógrafo de gases es de la marca Agilent modelo 490 micro-GC, y está equipado con las columnas PPQ, 5A molsieve y Wax. El método de análisis online diseñado permite la toma de datos cada 3 minutos.

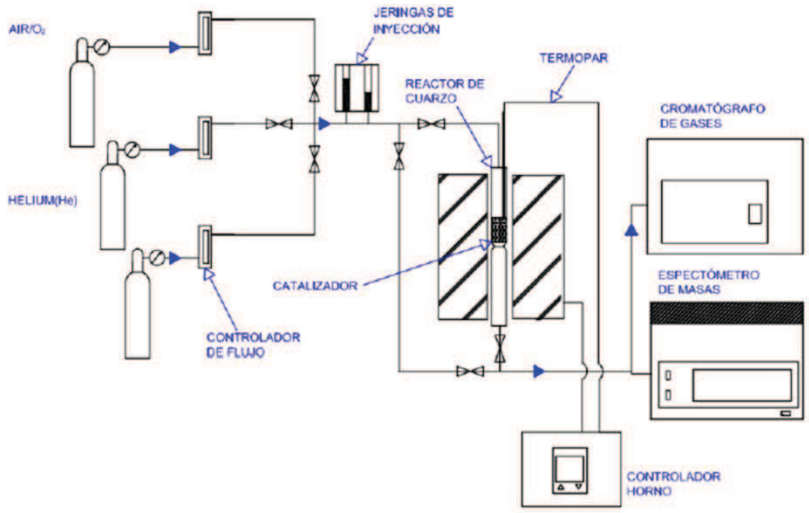

Figura 2.6. Instalación utilizada para la descomposición de isopropanol

2.5. Equipos para caracterización de pilas de combustible

Se ha utilizado una celda electroquímica de tres electrodos como la mostrada en la Figura 2.7. Esta celda está compuesta de un electrodo de trabajo, formado por los electrodos carbonosos y un colector de corriente adecuado (carbón vítreo); un contraelectrodo inerte (hilo de platino); y un electrodo de referencia de Ag/AgCl inmerso en una disolución de KCl 3 M y separado del electrolito de trabajo (H_2SO_4 0.5 M) mediante un capilar Luggin. Antes de iniciar la medición, el electrolito es saturado con N_2 durante 15 minutos para eliminar el O_2 presente; a su vez, se mantiene una atmósfera inerte en la celda durante todo el desarrollo del experimento. Todas las mediciones electroquímicas se han realizado en un potenciostato-galvanostato modelo VSP de la marca BioLogic.

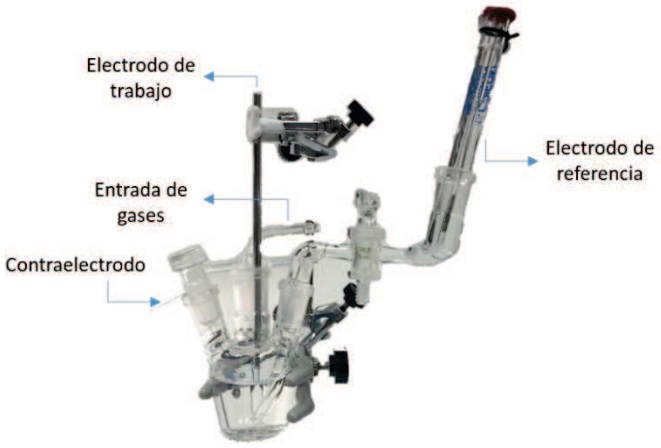

Figura 2.7. Celda electroquímica de tres electrodos.

2.6. Supercondensadores

Las mediciones electroquímicas se han realizado en H_2SO_4 1M, utilizando, para las celdas de tres electrodos, un potenciostato Autolab PGSTAT302 equipado con un módulo FRA para espectroscopía de impedancia electroquímica (EIS), voltametría cíclica (CV) y mediciones de descarga de carga galvanostatica (GCD). Los experimentos de descarga de carga galvanostatica y pruebas de durabilidad en celdas de dos electrodos se han realizado en un equipo Arbin SCTS. Se ha utilizado un sistema Swagelock de teflón en forma de T equipado con colectores de oro y electrodo de referencia Ag/AgCl 3M KCl. Para evaluar el rendimiento de la celda se cortaron piezas de fibra de carbón de forma redonda con una superficie de 0.196 cm^2. Como separador se ha utilizado una pieza redonda de membrana de nylon (tamaño de poro: 0.45 μm, 7 mm de diámetro). Los electrodos se secaron a 80ºC bajo vacío durante 2 horas antes de su peso y después se mojaron en el electrolito durante 1 h antes del montaje de la celda y las mediciones electroquímicas.

2.7. Referencias

[1] M. Lallave, J. Bedia, R. Ruiz-Rosas, J. Rodríguez-Mirasol, T. Cordero, J.C. Otero, M. Marquez, A. Barrero, I.G. Loscertales. Adv. Mater. 19 (2007) 4292–4296.

[2] R. Ruiz-Rosas, J. Bedia, M. Lallave, I.G. Loscertales, A. Barrero, J. Rodríguez-Mirasol, T. Cordero. Carbon. 48(3) (2010) 696-705.

[3] S. Brunauer, P.H. Emmett, E. Teller. J Amer Chem Soc. 60 (1938) 309-319.

[4] B.C. Lippens, J.H. de Boer. J Catal. 4 (1965) 319-323.

[5] F. Rodríguez-Reinoso, M. Molina-Sabio, M.T. González. Carbon. 33 (1995) 15-23.

[6] M.M. Dubinin, E.D. Zaverina, L.V. Radushkevich. J. Phys. Chem. (URSS) 21 (1947) 1351-1362.

[7] S. Biniak, G. Szymanski, J. Siedlewski, A. Swiatkowski. Carbon 35 (1997) 1799-1810.

[8] E. Desimoni, G.I. Casella, A. Morone, A.M. Salvi. Surf Interface Anal. 15 (1990) 627-634.

Chapter 3

Phosphorus functionalization for the rapid preparation of highly nanoporous submicron-diameter carbon fibers by electrospinning of lignin solution

3.0. Abstract

The modification of chemical properties of abundant and sustainable polymeric precursors, like lignin, and the control of their thermochemical reactions will be crucial for the development of a next-generation of functional carbon fibers (CFs) with novel and advanced properties. This chapter presents a fast and versatile method to prepare high added value CFs from lignin. It involves the production of submicron-sized P-functionalized lignin fibers by electrospinning of lignin/H_3PO_4 solutions. The phosphorus functionalities enable to shorten the conventional stabilization process to avoid fiber fusion from more than 80 h to only 2 h or even to stabilize them in inert atmosphere. Moreover, they promote the chemical activation of lignin fibers and greatly increase their oxidation resistance, avoiding their complete combustion during carbonization under low concentration of O_2 at temperatures as high as 900 ºC. The resulting CFs gather different interesting properties, such as sub-micron diameters ($\leq$ 1 μm), large surface area (~2000 $m^2 \cdot g^{-1}$), relatively high performance in relation to their mechanical properties for functional applications and a rich variety of uniformly-distributed O and P surface functionalities, which make them very attractive for heterogeneous catalysis, adsorption and electrochemical applications.

3.1. Introduction

Porous carbon fibers (CFs) are relevant materials for many functional applications of industrial and technological interest [1-4]. Especially, they receive great attention in catalysis, adsorption, gas storage and/or separation processes, electrochemical devices for energy storage and conversion, etc [1-4]. In spite of such potential applicability, the real and feasible wider utilization of porous CFs demands a reduction of their production costs and/or the development of unique properties or crucial advantages to improve their present competitiveness and performance [5,6].

With respect to cost, there is an increased interest and remarkable scientific efforts are currently being focused, even for functional applications, on the replacement of more expensive petroleum-based precursors or different synthetic polymers, and their associated processing, by a cheaper and sustainable manufacture from renewable and low-cost polymeric precursors [5,6]. The development of CFs with novel and useful properties from lignin has received special attention [5-13], given that it is the second most abundant polymer in nature,. In addition, the development of high-value co-

products from lignocellulosic biomass-derived industries, such as biorefineries and pulp and paper mills, could suppose a significant opportunity to minimize their related costs and environmental impacts [7,8].

Regarding the obtain of advanced properties, the preparation of CFs by means of a simple and versatile technique, such as electrospinning, entails an advantageous and promising approach [14,15]. It solves the most important problems associated to conventional melt-extrusion, since it allows the preparation of continuous fibers with considerably smaller diameters (micro- and submicro-scale) at room temperature, directly in a single step. In this sense, we previously presented the preparation of CFs by electrospinning of Alcell® lignin without the aid of blending polymeric additives and/or chemical (purification, modification) treatments, thus, considerably reducing the manufacture complexity, time and costs [9,10].

After decade-long investigation, however, lignin-based CFs exhibiting competitive performance or unique properties for specific applications are challenging. This usually makes necessary the utilization of additional activation and/or functionalization post-treatments that, apart from slowing down, making complex and raising the costs of the process, may compromise the fibrous structure [11-13]. On the other hand, the production of fibrous carbon materials from lignin is greatly limited by the need of a long oxidative stabilization treatment (more than 3 days), given that lignin shows a glass transition temperature (Tg) far below the temperature required for carbonization/activation [9,10,16]. In this sense, to develop a next-generation of lignin-based CFs, with novel and advanced properties as well as faster production, the design of strategies to control both structural and chemical properties of lignin polymer as well as its thermochemical reactivity will be crucial.

In this chapter, it is presented a new method to prepare low-cost lignin-based CFs in a remarkably short time. The method involves the electrospinning of lignin/H_3PO_4 solutions into submicro-sized P-functionalized lignin fibers that can be stabilized at much faster heating rates (up to 60 times) in less than 2 h, and under a wider variety of atmospheres. Next, the method entails the functionalized fibers to undergo a high development of porosity directly during their carbonization at high temperatures by different activation mechanisms acting together. Interestingly, the stabilized phosphorus-lignin fibers, apart from being chemical activated during the

carbonization step, can be activated at temperatures as high as 900 ºC under a low concentration of O_2, obtaining in this case an extra activation due to the partial gasification of the produced carbonzaceous fibers. As a result, the obtained CFs gather a unique combination of textural and chemical properties, i.e. a well-developed microporosity and high surface area (around 2000 $m^2 \cdot g^{-1}$) in very fine fibers (mainly 400 nm-1 μm diameter), together with a rich variety of P and O surface functionalities. In addition, the P-functionalization enhances the oxidation resistance and acidity of these CFs. All these properties have been found very attractive for their potential application in heterogeneous catalysis, adsorption and electrochemistry.

3.2. Materials and methods.

3.2.1. Preparation of electrospun-functionalized carbon fibers (P-CFs).

Pure lignin fibers were prepared by electrospinning of Alcell® lignin-ethanol solutions [9,10]. For the H_3PO_4/lignin fibers, spinnable H_3PO_4(85 wt %)/lignin/ethanol solutions (0.3/1/1 weight ratios) were used [17]. Solutions were heated at 60 ºC and shaken at 200 rpm during 12 h, obtaining a viscosity (350 – 450 cPs) suitable for electrospinning. The lignin solution flow rate was 3 $cm^3 \cdot h^{-1}$ for the inner capillary tip, whereas pure ethanol was fed at 0.3 $cm^3\ h^{-1}$ by the outermost one. The tip-to-collector distance was 30 cm and the electrical potential difference was 24 kV (the collector was at -12 kV and the tips at +12 kV). Thermo- stabilization and carbonization were carried out in a horizontal tubular furnace (150 cm^3 gas(STM)$\cdot min^{-1}$) under different conditions described in the text and figures. Particularly, the effect of heating variables during stabilization, and that of the atmosphere used in the stabilization and carbonization steps have been studied. Finally, some of the resulting carbonized fibers were analyzed by different techniques.

For comparison purposes, equivalent powdery carbon materials were also prepared from lignin powder without the electrospinning step. For such a purpose, H_3PO_4 (85 wt %)/lignin/ ethanol solutions (n/1/1 weight ratios, with n = 0; 0.3; and also 0.8), identical to those used for electrospinning, were dried for 24 h at 60 ºC. Next, the stabilization and carbonization conditions were similar to those utilized for the fibers. The P-containing carbonized fibers and powders were washed with hot distilled water to remove weakly-anchored P species, and dried overnight at 80 ºC prior to characterization.

The as-spun, stabilized and carbonized fibers are referred to as AF, SF and CF for the pure lignin fibers, respectively. In the case of the preparation of carbon fibers by chemical activation with H_3PO_4 (impregnation ratio of 0.3), the fibers are referred to as PAF, PSF and PCF. In the case of stabilized fibers, the heating rate (0.08; 1 or 3 ºC·min^{-1}) or the particular use of N_2 atmosphere is also reflected in the nomenclature. For carbonized fibers, the stabilization conditions (without P: 0.08 ºC·min^{-1} up to 200 ºC + 60 h at 200 ºC; with P: 1 ºC·min^{-1} up to 200 ºC + 1 h at 200 ºC) are not specified and only the particular use of N_2 atmosphere for stabilization (N_2-PCF) or the oxidizing one for carbonization (PCF-3%O_2) are considered in the nomenclature. The carbonized lignin powders are designated as AC (in reference to conventional activated carbons (ACs)), followed by a number (n) indicating the aforementioned H_3PO_4 weight ratio (n = 0; 03 for 0.3 or 08 for 0.8) in the H_3PO_4/lignin/ethanol (n/1/1) solutions.

3.2.2. Characterization of activated carbon fibers.

SEM and TEM images were obtained by a JEOL JSM-6490LV microscope (at 25 kV voltage) and a Philips CM200 microscope (at an accelerating voltage of 200 kV), respectively. Raman spectra were recorded with a RENISHAW micro-Raman system using an Ar+ laser at 514 nm as the excitation source with a spectral resolution of 2 cm^{-1}. The textural properties were characterized by physical adsorption of gases (N_2 at -196 ºC and CO_2 at 0 ºC) in a Micromeritics ASAP2020. Samples were previously outgassed for 8 h at 150 ºC under vacuum. The mechanical properties were measured as non-aligned multi-fiber carbon meshes, in a DEBEN Microstest (2KN Tensile). TPD experiments were performed in a tubular vertical furnace and the amounts of CO and CO_2 evolving groups were monitored by NDIR analyzers (Siemens; ULTRAMAT 22 model). XPS data were registered by a 5700C model Physical Electronics apparatus with Mg Kα radiation (1253.6 eV). For the analysis of XPS peaks, the maximum signal eas set at 284.5 eV. The fitting of the XPS peaks was done by least squares using Gaussian–Lorentzian peak shapes. For thermogravimetric analysis (TG), a CI Electronics MK2 balance and samples between 10 and 15 mg were used.

The catalytic decomposition of 2-propanol was studied in a fixed bed reactor as previously reported [18], with 70 mg of CFs, a 2-propanol partial pressure of 0.018 atm in inert atmosphere and a space time of 0.055 g s μmol^{-1}. The concentrations of 2-propanol and products were analyzed by on line gas chromatography (490 micro-GC

equipped with PPQ, 5A molsieve and Wax columns, Agilent). γ-Al_2O_3 (Puralox 150/200 from Sasol) was used as a reference acid catalyst. The electrochemical characterization was carried out in a standard three-electrode cell in different electrolytes by using a Pt wire as counter electrode and a Ag/AgCl/Cl–(sat.) electrode as the reference one (Electrochemical Analyzer 600D Series, CH Instrument Inc.). To be used as binderless electrodes, the CFs were manually compressed in between two stainless steel meshes (current collectors).

3.3. Result and discussion

3.3.1. Preparation of electrospun phosphorus-functionalized carbon fibers (P-CFs).

Phosphoric acid-containing lignin fibers were prepared by electrospinning of H_3PO_4/lignin/ethanol (0.3/1/1 wt ratio) solutions in ethanol. The as-spun H_3PO_4/lignin fibers show diameters ranging from 400 nm to 3 μm (PAF in Figure 3.1), mostly ≤ 1 μm. Since the presence of H_3PO_4 increases the viscosity and electrical conductivity of the lignin/ethanol solutions, promoting whipping instability [14,15], more curly fibers were observed when compared with H_3PO_4-free ones (AF and PAF in Figure 3.1).

The electrospun fibers were subjected to a thermo-oxidative stabilization step prior to carbonization in order to increase the glass transition temperature of lignin and thus prevent fibers from partial or total fusion. The heat-treatment was carried out under air atmosphere (150 $cm^3(STP)\cdot min^{-1}$) and different heating rates up to 200 ºC, and this temperature was kept for different times. As shown in Figure 3.1, in the absence of H_3PO_4 the stabilization must be necessary slow (0.08 $ºC\cdot min^{-1}$ to 200 ºC + 60 h at 200 ºC) (SF-0.08) to maintain a high glass transition temperature, preventing fibers from fusion [16]. Hence, faster heating rates such as 1 $ºC\cdot min^{-1}$ produce complete fusion of pure lignin fibers (SF-1 in Figure 3.1). By contrast, and apart from a conventional long stabilizations process (PSF-0.08 in Figure 3.1), the presence of H_3PO_4 allows using heating rates as high as 1-3 $ºCmin^{-1}$ without producing partial fusion or swelling of the fibers (PSF-1 and PSF-3 in Figure 3.1). Thus, electrospun H_3PO_4/lignin fibers can be stabilized in only 1 h and 45 min, whereas the pure lignin fibers ones require more than 80 h, what entails a remarkable time reduction (50-60 times) of the thermostabilization treatment.

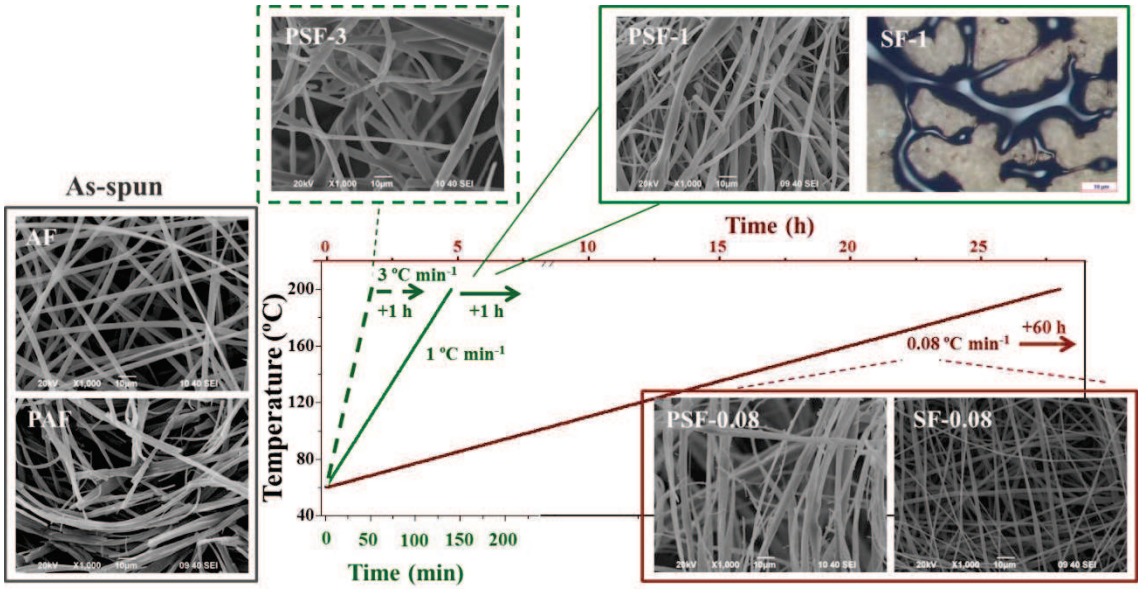

Figure 3.1. Effect of the heating rate (HR) on the morphology (SEM images) of the air-stabilized lignin fibers with (PSF-HR) and without (SF-HR) H_3PO_4. The Figure also shows the images of the corresponding as-spun fibers (PAF and AF, respectively).

Furthermore, the stabilized fibers showed similar diameter to the as-spun ones and the incorporation of H_3PO_4 increased the stabilization yields from 76 for SF-0.08 to 83 wt % for PSF-0.08.

Table 3.1 shows the weight surface concentration obtained from XPS analysis for lignin-based fibers, where an increase in the oxygen content after stabilization is observed for both prepared fibers. The increase in the oxygen content after stabilization step is expected to be low due to the high oxygen content of the raw lignin.

Table 3.1. Weight surface concentration by XPS of as spun and stabilized lignin fibers

Samples	Weight surface concentration by XPS (%)		
	C	O	P
AF	73.4	26.6	--
SF	68.0	32.0	--
PAF	64.5	28.2	7.3
PSF	64.1	29.5	6.4

Figure 3.2 shows the O1s, C1s and P2p spectra of as spun and stabilized lignin fibers without and with phosphoric acid. In the case of as spun lignin fibers, a band centered at about 532.6 eV can be observed in the O1s spectrum,

corresponding to oxygen as in C-OH and C-O-C bonds (Figures 3.2 b and d). However, the band is more intense and narrower for the phosphoric acid-containing lignin fibers (PAF in Figure 3.2 d), which can be ascribed to the presence of oxygen in C-O-P bonds, as in phosphate and polyphosphates surface groups [19]. Stabilization of the lignin fibers caused a significant modification of the profiles for the O1s and C1s spectra (SF in Figure 3.2 a and b), widening the O1s band at lower binding energies, at about 531 eV (Figure 3.2 b), as a consequence of formation of oxygen as in C=O bond. In the case of P-containing lignin fibers, the stabilization process did not produce such a notable change on these profiles, leading only to a slight reduction of the band observed at 532.6 eV and to the appearance of a small tail at 530.9 eV (Figure 3.2 d), which can be associated to oxygen as in C=O bond or even as in P=O one. For the case of stabilization of lignin fibers, a noticeable band (or a shoulder of the C-C band located at 284.5 eV) can be observed in the C1s spectrum from approximately 287.5 to 290.8 eV (Figure 3.2 a), which indicates the presence of C=O and/or O-C=O bonds. However, this small band at 288.2 eV is not clearly observed after stabilization of P-containing lignin fibers (Figure 3.2 c), suggesting that the small tail of the O1s spectrum for this sample, at about 530.9 eV, may correspond to P=O bond instead of C=O one. In this sense, Figure 3.2 e presents the P2p spectra for PAF and PSF that show a band with a main peak at a binding energy around 134 eV, characteristic of pentavalent tetracoordinated phosphorus, as in phosphates and/or polyphosphates [20-25]. A slightly shift of this band to lower binding energy and a small reduction of the band area can be appreciated after stabilization of the P-containing lignin fibers (PSF in Figure 3.2 e), which evidences slight modifications of the state of P in the lignin structure after the stabilization treatment, producing some phosphorus in a more reduced state as in C-PO bonds, as a consequence of dehydration and cross-linking reactions.

These results are in agreement with other studies. The increase in the oxygen content during oxidative stabilization of lignin fibers is related to the incorporation of mainly carbonyl and carboxylic surface structures at low temperature, that can be incorporated into anhydride and ester groups [9,10,16], generating cross-links within the lignin fibers structure. In the case of phosphorus containing lignin fibers, the increase of oxygen content after stabilization is lower

than that observed for the pure lignin fibers (Table 3.1). Figure 3.3 and 3.4 show the lignin structure propose by Adler [26] and this structure after reaction with H_3PO_4, respectively. The incorporation of H_3PO_4 to the initial lignin solution produce more oxidized spun lignin fibers (PAF), but of the whole lignin fiber matrix in this case, due to the reaction of phosphoric acid with the dissolved lignin, generating phosphate (and/or polyphosphate) esters throughout the structure of lignin fibers [21,25]. These phosphate groups have been found to be very active for surface carbon oxidation, even at room temperature [19,22] and thus seems to be the responsible for the production of cross-linking reactions that are, in this case, very active and effective in increasing the glass transition temperature of the lignin fibers, reducing the time needed for the stabilization step and improving this process. On the contrary, the oxidative stabilization of the lignin fibers in the absence of phosphoric acid takes place on the surface of the fibers and, in this case, oxygen has to diffuse to the inner part, the core, of the lignin fiber matrix to form cross-linkage that favour higher glass transition temperatures to prevent fibers from fusion during the carbonization/activation process, which is only possible with much slower heating rates.

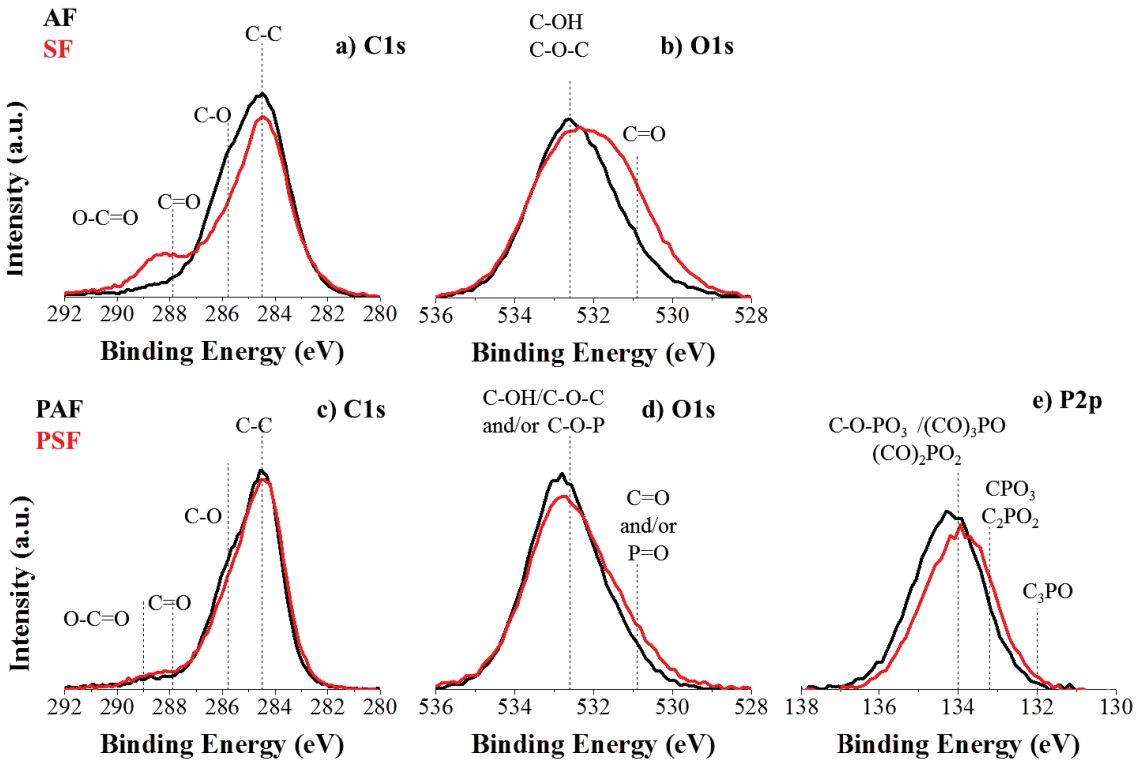

Figure 3.2. XPS spectra of C(1s), O(1s) and P(2p) core-levels of as-spun and stabilized fibers under oxidizing atmosphere. (a, b) pure lignin fibers, (c – f) phosphorus lignin fibers.

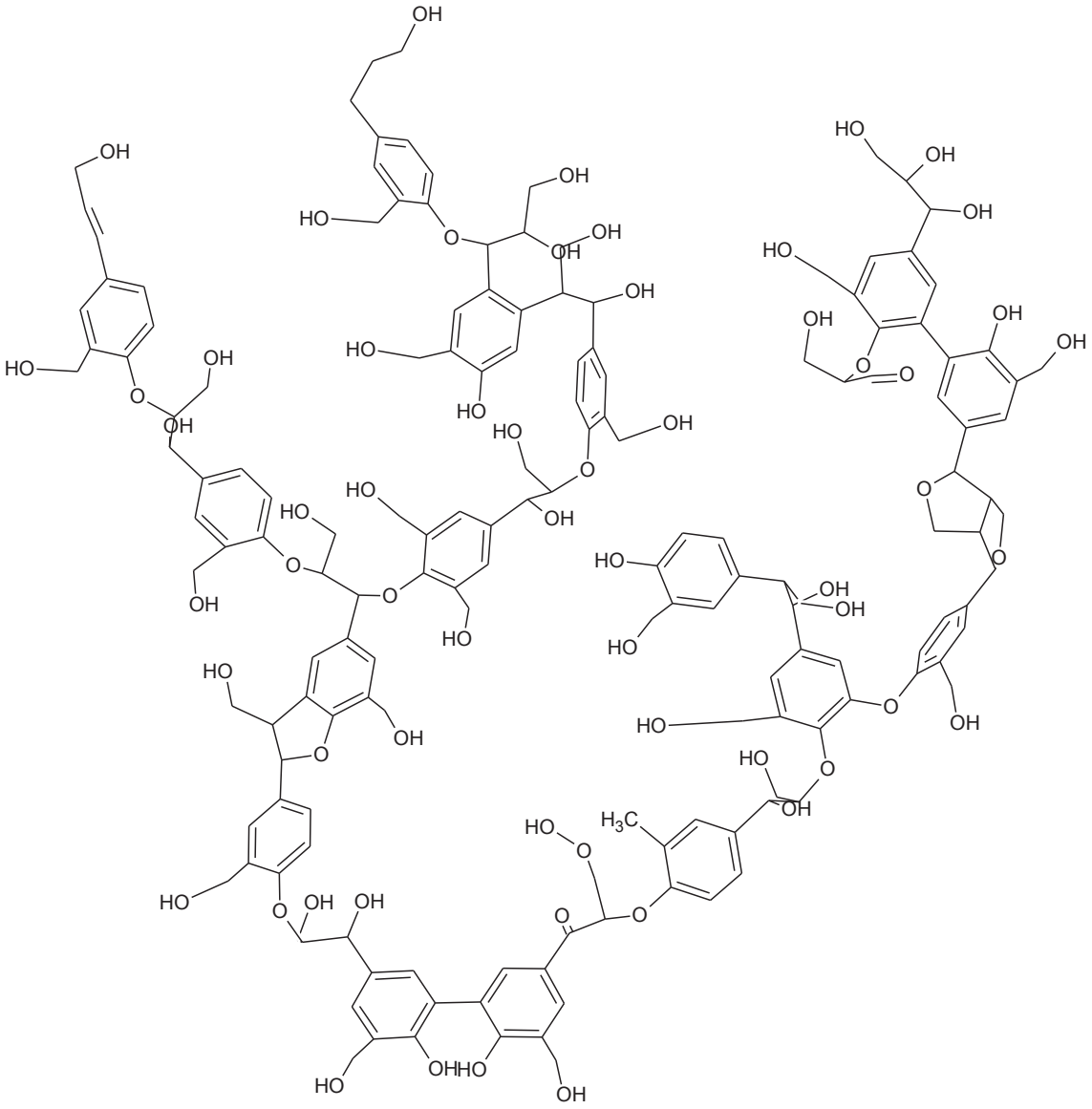

Figure 3.3. Alcell lignin structure proposed by Adler [26]

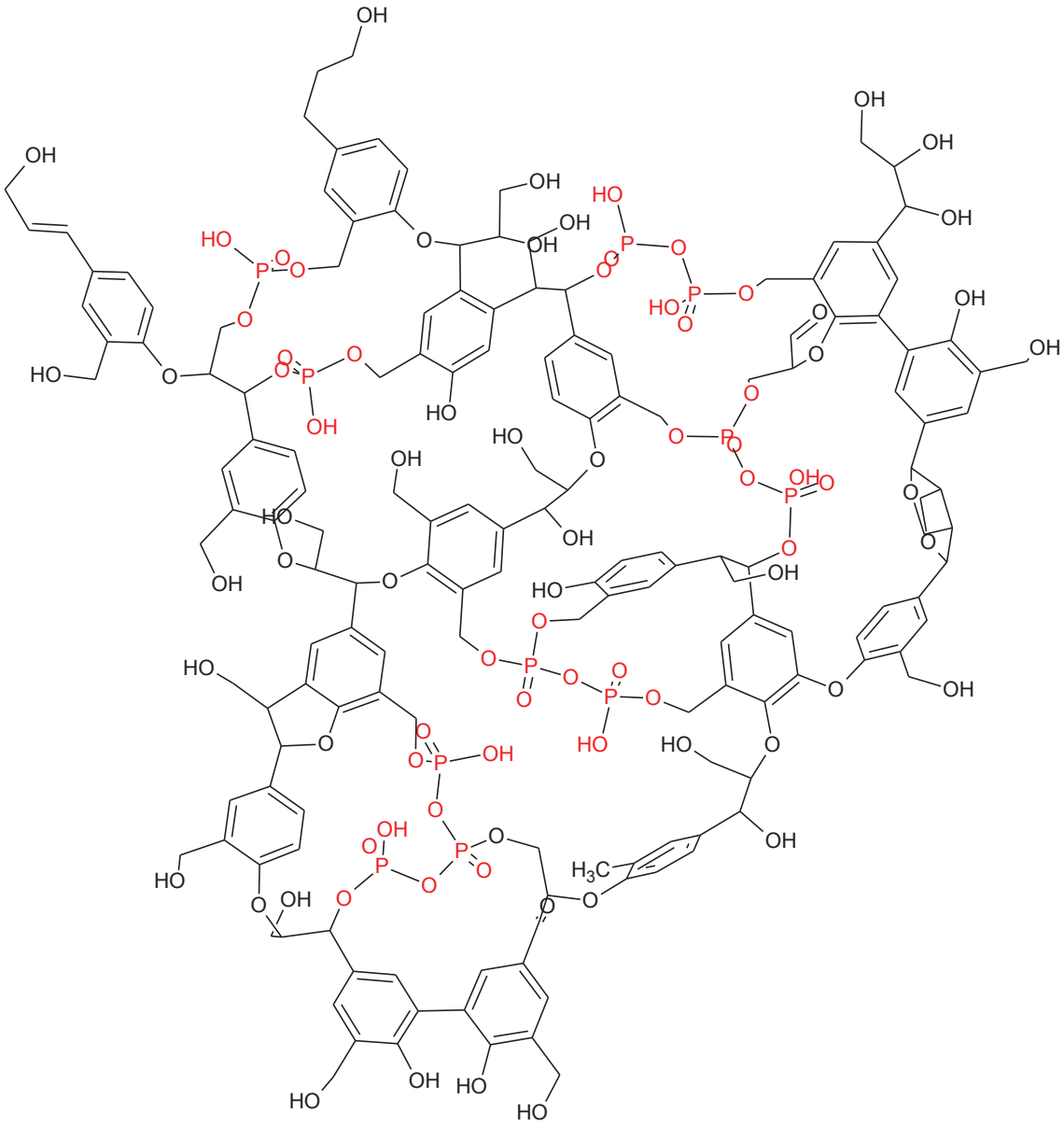

Figure 3.4. Alcell lignin structure after reaction with H_3PO_4.

The presence of stable phosphate and/or polyphosphate esters allows also the stabilization of electrospun lignin fibers even under inert (N_2) conditions at fast heating rates, given that these P species generate by themselves cross-links within the lignin fibers structure, without the need to incorporate oxygen surface groups from the gas phase.

The stabilized materials were heat-treated at 10 ºC·min^{-1} up to 900 ºC under inert (N_2) or oxidizing (3 vol % O_2 in N_2) atmospheres. The influence of P-functionalization and the atmosphere on weight loss during carbonization was studied by thermogravimetric analysis (Figure 3.5a). In agreement with our previous works, stabilized pure lignin fibers can be carbonized under inert conditions with a 37 % yield (SF-N_2 in Figure 3.5a) (27 % total yield, considering stabilization + carbonization) [9,10]. On the other hand, the presence of P species in the stabilized lignin fibers increases the carbonization yield up to 48 % (40 % total yield) (PSF-N_2), by favoring the restriction of tars formation during the carbonization process and dehydration reactions produces at high carbonization temperatures, increasing the carbon content [25,27] Regarding the oxidadtion or combustion behaviour, while pure lignin fibers suffer from total combustion at 700 ºC in an atmosphere of 3% of O_2 (SF-3%O_2), a 18 % of the initial lignin weight remains as carbon fibers when phosphorus is present after heating up to 900 ºC (15 % total yield) (PSF-3%O_2). Thus, CFs can be produced at 900 ºC even in an oxidative atmosphere (O_2 3%v), due to the presence of phosphorus surfaces groups that are incorporated when the precursor has been dissolved in ethanol with H_3PO_4, which are responsible for the high oxidation resistance of stabilized lignin and carbonized fibers [19,25,27].

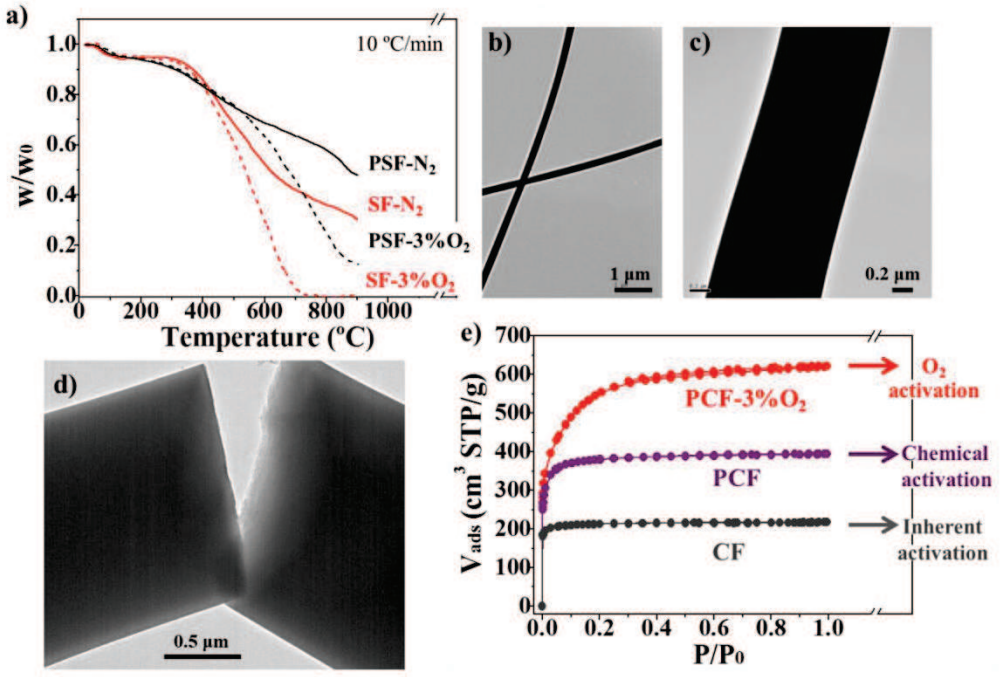

Figure 3.5. (a) Weight-loss of air-thermostabilized lignin fibers (SF and PSF correspond to SF-0.08 and PSF-1 samples, respectively) during heating up to 900 ºC under inert (N_2) or oxidizing (3 vol % O_2) conditions. (b,c,d) Different TEM images of PCF sample; and (e) N_2 adsorption-desorption isotherms (-196 ºC) of various carbonized fibers.

As a consequence of such versatile methodology due to the presence of phosphorus groups in the lignin structure, the thermal processing of as-spun into lignin-based CFs can be carried out through not only the conventional 2 steps-route, stabilization (air) + carbonization (N_2) (route a, Scheme 1), but also under 2 new combinations (routes b and c, Scheme 1), as well as directly in a single step under inert (route d, Scheme 1) or oxidizing atmosphere (route e, Scheme 1). This allows to produce CFs with a wider variety of properties and, in the case of a single step (route e, Scheme 1), in only 2 h 40 min (total thermal processing).

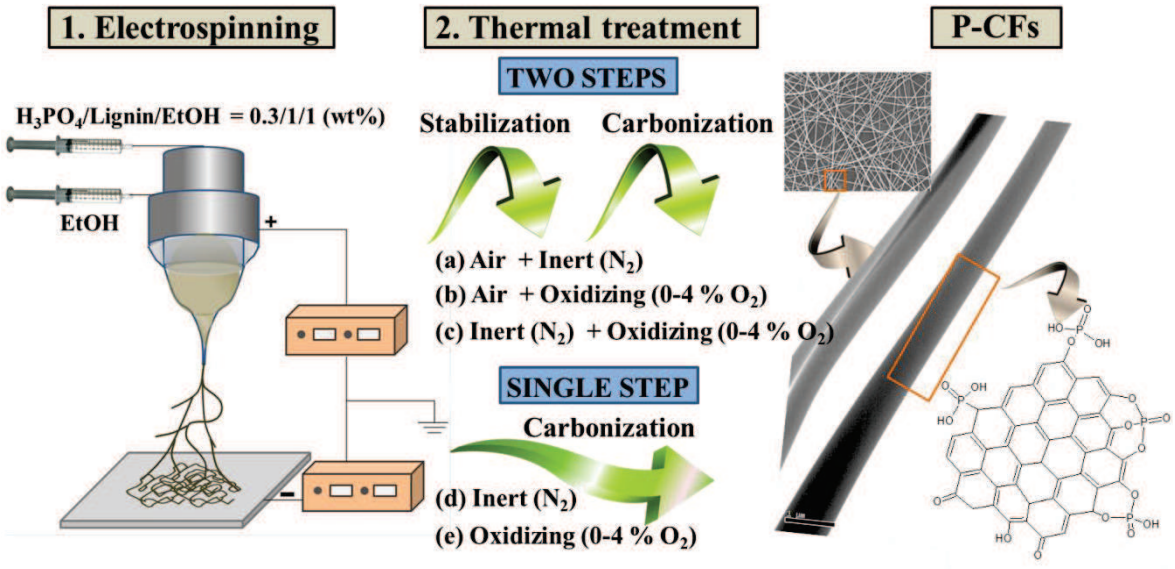

Scheme 1. Scheme of the overall preparation procedure of P-CFs representing the two- and single-step thermal routes.

3.3.2. Textural properties.

The P-CFs display quite similar diameters to those of the as-spun and stabilized ones, mainly ranging between 400 nm (Figure 3.5b) to 1 μm (Figure 3.5c), and an apparently smooth surface with no microscopic defects, even at ending zones (Figure 3.5d). Textural characterization points out that the carbonization of pure lignin fibers (CF) produces a well-defined microporous structure, as deduced by the type-I shape of the N_2 adsorption isotherm (Figure 3.5e), and a high specific surface area of around 850 $m^2 \cdot g^{-1}$ (Table 3.2). In particular, the higher CO_2-mircopore volume, if we compared it with that derived from the adsorption of nitrogen ($V_{DR}(CO_2) > V_t\ (N_2)$) indicates the presence of narrow micropores (diameters below 0.7 nm). This large development of microporosity is has alredy been ascribed to the high oxygen content of

lignin [9,10], which may be a key factor during devolatilization in the carbonization process, namely, the oxygen-driven inherent activation of lignin fibers. The carbonization of phosphorus electro-spun fibers (PCF) results in CFs with a substantially higher surface area (ca. 1450 $m^2 \cdot g^{-1}$) and microporosity, with a higher proportion of wider micropores ($V_t(N_2) > V_{DR}(CO_2)$) (see Table 3.2). These effects on the porous texture may be attributed to the H_3PO_4-chemical activation process upon heating [25,27-30]. On the other hand, when phosphorus-lignin fibers have been stabilized under N_2 atmosphere (N_2-PCF) (see Table 3.2) no effect on the activation of the lignin fibers has been shown, which suggests that oxygen incorporation during air stabilization seems to be of paramount importance for the chemical activation contributions. It has been reported that the phosphate- and/or polyphosphate-carbon structures may favour oxygen spill-over [19,31,32] by adsorption of molecular oxygen on the P surface complexes and migration of activated oxygen species from these P groups to de carbonaceous matrix. After the oxidative stabilization step, this activated oxygen in the fiber carbonaceous matrix may partially gasify the structure of the fibers during the carbonization process, developing a larger porosity and surface area in the final carbon fiber than if no oxygen is used during the stabilization process.

Apart from the chemical activation effect, the carbonization of stabilized P-functionalized fibers under an O_2-containing atmosphere up to temperatures as high as 900 ºC (Figure 3.5a) further provokes a larger porosity development (PCF-3%O_2 in Figure 3.5e and Table 3.2). This O_2 activation at high temperatures produces carbonized materials with apparent surface areas of ca. 2000 $m^2 \cdot g^{-1}$ (3 times that of the pure CFs), accompanied by a microporosity widening and the generation of mesopores (around a 10 % of total pore volume) (see Table 3.2). It has been reported that stable C-O-P surface groups decompose to C'-P surface groups at temperatures higer than 700-750 ºC, with formation of gaseous CO (C' represents a new surface carbon site), and that in the presence of molecular oxygen this C'-P surface groups are (re)oxidized to C'-O-P, where the P-surface groups act as inhibitors for the surface carbon gasification at temperatures lower than 700-750 ºC (enhancing the oxidation resistance of the carbon fiber) and as a selective gasification agent or catalyst at temperatures higher than 700-750 ºC (production of surface C''-P and gaseous C'O and again (re)oxidation to C'''-O-P) [19].

Table 3.2. Porous structure parameters (calculated as reported elsewhere[10]) and mass surface composition for lignin-based carbon powders (ACs) and fibers (CFs).

	N_2 adsorption				**CO_2 adsorption**		**XPS mass surface concentration**		
Sample	A_{BET}[a] m^2g^{-1}	A_t[b] m^2g^{-1}	V_t[c] cm^3g^{-1}	V_{meso}[d] cm^3g^{-1}	A_{DR}[e] m^2g^{-1}	V_{DR}[f] cm^3g^{-1}	C %wt	O %wt	P %wt
AC0	86	0.4	0.033	0.005	514	0.206	92.1	7.9	0.0
AC03	719	6	0.282	0.009	825	0.331	87.4	10.2	2.4
AC08	1177	18	0.507	0.002	844	0.338	87.8	9.4	2.8
CF	850	7	0.329	0.006	1001	0.401	96.3	3.7	0.0
PCF	1448	25	0.580	0.009	1027	0.412	90.8	7.9	1.3
N_2-PCF	869	6	0.342	0.005	675	0.271	90.3	6.2	3.4
PCF-3%O_2	2000	112	0.849	0.107	1021	0.409	81.2	16.0	2.8

[a] A_{BET} is the apparent surface area. [b] A_t is the external surface area. [c] V_t is the micropore volume. [d] V_{meso} is the mesopore volume. [e] A_{DR} is the narrow micropore surface area. [f] V_{DR} is the narrow micropore volume.

The robustness of the CFs is an important property even for functional applications. The degree of structural ordering in the P-CFs was followed by Raman spectroscopy. In spite of the higher porosity of these P-CFs, the quite similar spectroscopic features obtained for PCF and PCF-3%O_2 samples compared to that of CF (prepared from pure lignin) (Figure 3.6 and Table 3.3) suggests that the P functionalities may induced or promote certain structural ordering [33,34].

The Raman spectra of the CFs (Figure 3.6) show two main broad and overlapping bands, at about 1350 and 1600 cm^{-1}, the former being associated to the E_{2g} vibration mode of the ideal graphitic lattice (G band), and the later characteristic for disordered carbon (D band) [9,10,35,36].

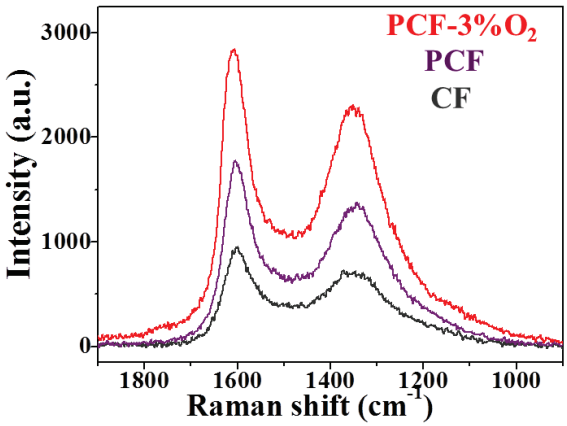

Figure 3.6. Raman spectra of various lignin-based

These spectra were deconvoluted as reported so far [10,36], and the spectral parameters are collected in Table 3.3. The Raman shift (ν) of G band, the full width at half maximum (Δν) of D and G bands and the intensity ratio (I_D/I_G) of the fibers carbonized at 900 ºC under inert atmosphere are independent of the P functionalization. Nevertheless, the noticeable narrowing of D band could point out a lower contribution of structural disorder in P-CFs. On the contrary, the shift of G band towards larger wavenumbers, as well as the increase in G band width and the I_D/I_G ratio observed for the highly porous P-CFs (PCF-3%O_2) are all Raman features characteristic of a less ordered structure [35,36]. This is in accordance with their much more developed microporosity (see Table 3.1).

Table 3.3. Raman parameters determined from the deconvolution of first-order Raman spectra of different lignin-based CFs.

Samples	ν_G [cm^{-1}]	$\Delta\nu_G$ [cm^{-1}]	$\Delta\nu_D$ [cm^{-1}]	I_D/I_G
CF	1599	67.3	182.8	0.87
PCF	1600	67.3	153.9	0.88
N_2-PCF	1600	57.7	153.9	0.89
PCF-3%O_2	1607	71.6	144.3	0.94

As a result, the hereby reported submicron-diameter microporous P-CFs exhibit a remarkable flexibility. Mechanical properties are also of great importance even for functional application carbon fibers. Tensile strength values of 250-300 MPa

and Young's modulus values of 2-4 GPa have been obtained for carbon fibers prepared in this work. In spite of these values are lower than those repoted for non-porous carbon fibers obtained from kraft lignin [37,38] for structural applicantions, the small carbon fibers diameters obtained by electrospinning of lignin solution make the materials thus prepared more mechanically resistant than other carbon fibers preparaed by lignin or other lignocelullosic precuersor. In this sense Dallmeyer et al. [39] found that the inter-fiber bonding improve the mechanical properties of the carbon fibers, reporting tensile strength and Young's modulus values of 75Mpa and 4 GPa, respectively, for bonding fibers carbonized at 1000 ºC with a relatively poor development of porosity (BET surface area of 400 m^2 g^{-1}). On the other hand, Uraki et al. [40] studied the effect of the surface area on the tensile strength of carbon fibers obtained from softwood acetic acid lignin. They found a decrease in tensile strength value from 150 to 100 MPa when the carbonized fibers were activated under steam flow for different times, obtaining BET surfaces areas from 370 to 1930 m^2 g^{-1}. It is noteworthy to highlight that, these mechanical properties are not sufficient for structural applications. However, they are unusually high in such porous materials of small diameter and enough suitable for functional application such as in adsorbents, catalysis, electrodes, etc.

3.3.3. Chemical properties.

As shown in Table 3.2, the in-corporation of P to the lignin-based CFs increases the surface oxygen content from 4 wt % for CF to 8 wt % for PCF and from 6.2 wt% for N_2-PCF to 16 wt % for PCF-3%O_2 when carbonization is carried out under inert or oxidizing atmosphere, respectively. On the other hand, the amount of surface phosphorus on the P-CFs was found to vary around 1.5 - 3.5 wt % P (Table 3.2).

The nature and relative contribution of the different O and P functionalities on P-CFs was further investigated from the XPS spectra and TPD profiles (Figure 3.7). The C(1s) region of XPS spectra was deconvoluted into 4 contributions (see an example in Figure 3.7a). Apart from a main contribution due to the aromatic -C-C- bonds formed upon carbonization, the P-CFs present a remarkable contribution of single-bonded -C-O- and/or -C-P- species (285.8 eV), as well as some -C=O and –COOH and/or –COOR species (at 287.9 and 289 eV, respective-ly) [41]. On the other hand, the XPS-P(2p) spectrum of P-CFs (Figure 3.7b) shows a broad band centered at ca. 133 eV,

characteristic of strongly-attached P-species in activated carbons prepared at high temperatures [25,27,28-30]. This spectrum can be deconvoluted into 3 doublets corresponding to 3 different surface groups of P functionalities: polyphosphates and/or phosphates (referred to as –C–O–P– species: $(CO)_3PO$, $(CO)_2PO_2$ and $(CO)PO_3$)) at 134.0 eV; –C–P–O– species ($C–PO_3$ and/or $C_2–PO_2$ groups) at 133.2 eV; and the major contribution, $–C_3PO$ groups, at 132.3 eV.

From TPD profiles (Figure 3.7c) it can be clearly discerned that the amount of CO-evolving groups in highly activated P-CFs is considerably much higher than that of CO_2-evolving ones (CO/CO_2 ratio = 7.3). In particular, the CO profile is characterized by a sharp rise from 500 ºC and two discernible contributions with maxima at ca. 700 ºC and 850 ºC. Considering that anhydride groups evolve as CO and CO_2 and the low overall evolution of CO_2-evolving groups, including anhydrides, the first CO contribution (500–900 ºC) may mainly correspond to phenol and ether groups [42]. The second one (above 700 ºC) is mainly associated to the decomposition of phosphorus groups of high thermal stability (–C–O–P– and/or –C–P–O– species) formed during the activation process [25,28-30], although the contribution of quinone and carbonyl groups should not be ruled out [42]. This higher content in phenols, ethers and –C–O–P– and –C–P–O– species greatly agrees with the functionalities distribution observed by XPS (Figure 3.7a and 3.7b) and it is also found in other less oxidized samples (PCF and N_2-PCF) (Figures not shown). CFs without P present a much lower evolution of CO and CO_2. The profiles for these two gases indicate that these sample mainly contain quinone- and/or carbonyl-like surface groups evolving as CO above 700 ºC (Figure 3.7c) [42], i.e., a poor surface chemistry characteristic of carbon materials prepared at high temperatures under inert atmosphere.

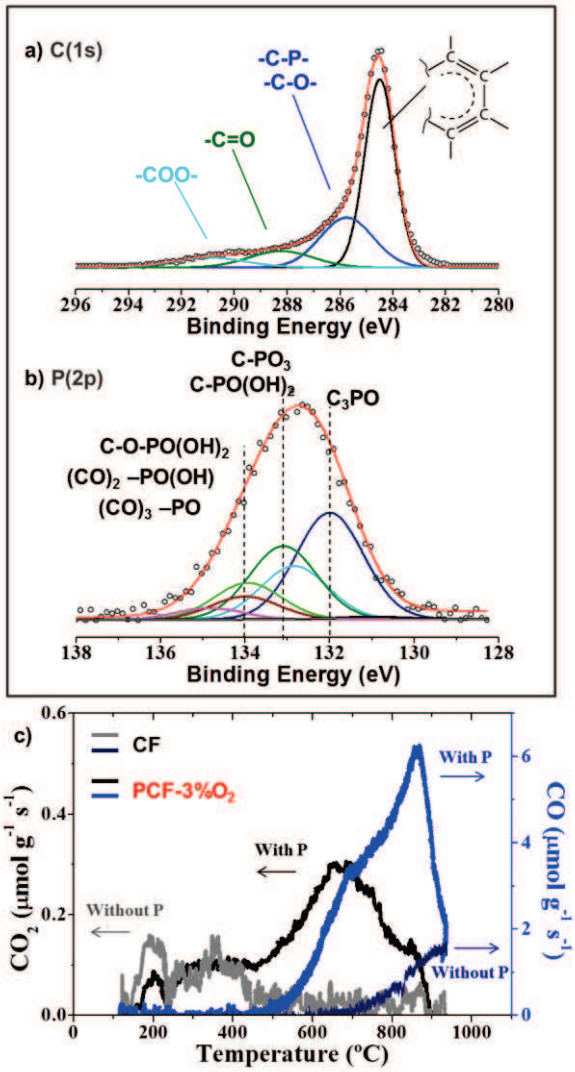

Figure 3.7. (a) C(1s) and (b) P(2p) XPS deconvoluted spectra of PCF-3%O_2 fibers; (c) CO_2 and CO evolution during TPD experiments of CFs with and without P.

The distribution of phosphorus species on the prepared P-CFs was analyzed by X-ray energy dispersive spectroscopy (XEDS) (Figure 3.8). CFs without P display a negligible blank P signal (Figure 3.8a for CF). However, in general, the much higher intensity and density of P signals on the selected area, together with the increased and constant intensity of P signals across the width of P-CFs (Figure 3.8b for PCF), indicate that the phosphorus functionalities are uniformly distributed throughout these P-CFs.

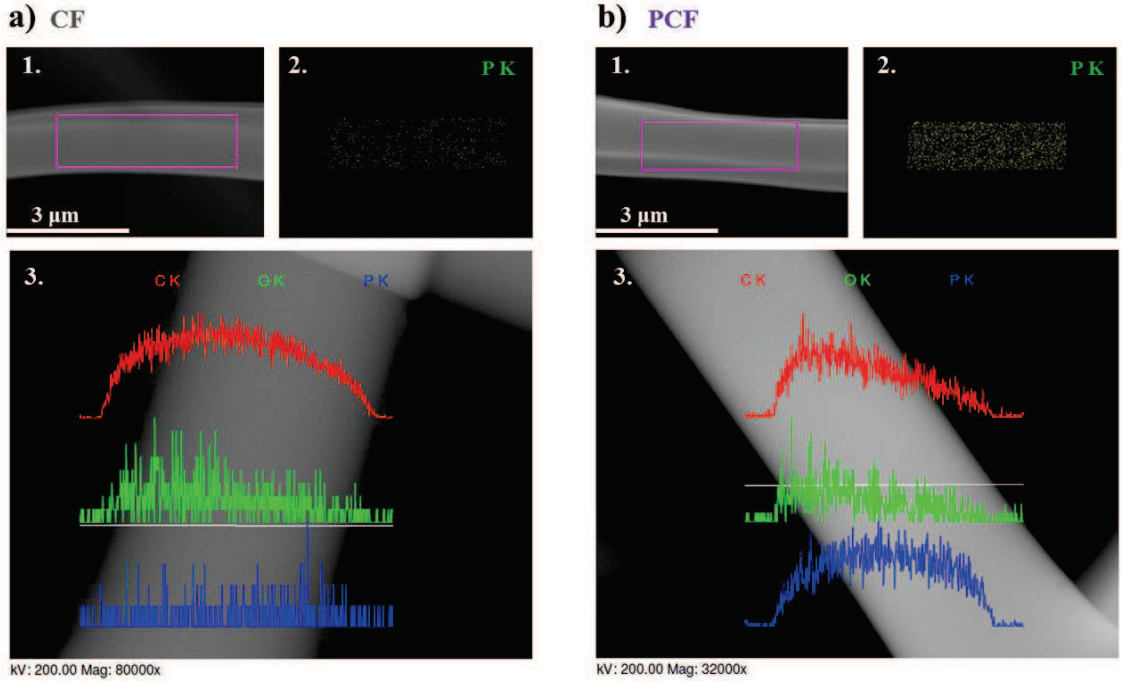

Figure 3.8. Two (1,2) and one (3) dimensional distributions of P and other species (O, C) on different lignin-based CFs, as determined by XEDS.

3.3.4. Phosphorus functionalization: the key for the unique production procedure and advanced properties.

The functionalization of submicron lignin fibers with phosphorus species plays a decisive role in the length reduction and versatility of the hereby reported new method for production of functional CFs. The most interesting effects of P can be highlighted as follows:

1. The promotion of stabilization is tremendously advantageous to shorten the CFs production time. This is simply achieved by adding a small amount of H_3PO_4, which reacts with lignin to generate –C-O-P phosphate (and/or phlyphosphate) esters groups. Previous strategies on optimizing the stabilization of fibers from lignin or other biopolymers have been focused on new extraction routes, physical and/or chemical modification treatments and/or the incorporation of polymer additives [38,43-45], what usually entails more complex and expensive procedures. Other approaches were based on stabilizers or precursors completely different to H_3PO_4 or lignin, respectively [46,47].
2. Highly-activated and -functionalized CFs can be directly prepared, without additional impregnation/drying and/or post-functionalization steps. In order to

achieve very high specific surface areas (2000 $m^2 \cdot g^{-1}$) and a large amount of functional groups, conventional CFs would necessarily require of additional chemical (NaOH, KOH, H_3PO_4, $ZnCl_2$, etc.) and/or physical (CO_2 or steam water at 800-900 ºC) activation processes [1,11-13,48,49], and liquid- or gas-phase oxidation post-treatments [33].

3. The extent of the H_3PO_4-chemical activation process in the electrospun lignin fibers has been found extraordinarily enlarged, since the P-CFs (PCF), which are prepared from electrospun with a H_3PO_4/lignin wt ratio value of = 0.3/1 (after ethanol evaporation) show greater porosity development and higher surface area than those observed for lignin-based powders activated carbons (ACs) prepared by chemical activation of Alcell lignin with H_3PO_4 with impregnation ratio values (wt H_3PO_4/wt lignin) of 0.3/1 and 0.8/1 (AC03 and AC08, respectively) (Table 3.2). In agreement with this result, considerably much higher activating agent contents (from 10 to 20 times) are usually necessary to produce the chemical activation degree observed for the P-CFs reported in the present work [1,28-30,48,49]. The observed enlarged activation in P-CFs is attributed to the uniform distribution of the reactant phosphorus species through the entire fibers matrix, with a structure easily accessible (narrow diameter and high outer surface area) to the reactant atmosphere, uniquely produced by the electrospinning method.

3.3.5. Advanced properties for specific applications.

The benefits of the aforementioned textural and chemical properties of P-CFs were analyzed for practical application. Firstly, it is well-known that the large surface-to-volume ratio and endless form of fibrous structures promote excellent mass transfer characteristics, low pressure drop, ease of handling and reduced inter-particle boundaries that, compared to other morphologies (powder, granular, pellet, etc.), offer several advantages for catalytic reactions, adsorption and separation processes, electrochemical applications, etc [1-4].

1. ***In catalysis***. The catalytic behavior of the differ-ent CFs was analyzed for the 2-propanol decomposition reaction. This is a test reaction for the evaluation of the acid and base properties of heterogeneous catalysts [50-52]. It is generally accepted that the reaction conversion increases with the surface acidity (or

basicity) of the catalyst and that 2-propanol mainly dehydrates to propylene (PP) over acid sites, whereas it decomposes through dehydrogenation over basic sites, yielding acetone (Ac).

Figure 3.9a represents the 2-propanol conversion as a function of temperature over various lignin-based CFs with and without P used as catalysts. The conversion increases with the reaction temperature for all the catalysts. In particular, whereas pure lignin-based CF (CF) shows total conversion at 600 ºC, the CFs catalysts with surface phosphorus groups exhibit conversions of 100 % between 300 and 370 ºC and their activity increases with the phosphorus surface content (N_2-PCF ≈ PCF-3%O_2 > PCF). The selectivity of P-CFs towards the production of PP increases rapidly with temperature, so that it is higher than 90 % above 200 ºC (Figure 3.9b). On the contrary, the selectivity of the CFs markedly changes in the absence of surface phosphorus functionalities (CF) and a high selectivity towards Ac (70%) is obtained even at conversions of 15 % (415 ºC). In this case, although the selectivity to PP gradually increases upon raising the temperature, it reaches no more than 70 % for total conversions at 600 ºC. The high conversions and selectivities to PP found for the P-CFs maybe attributed to the presence of Brönsted acid sites of surface P groups [50-52], highlighting their acidic character. On the contrary, the production of acetone is indicative of the presence of basic sites on CFs without phosphorus.

The catalytic performance of the lignin-based P-CFs was compared to that of commercial γ-Al_2O_3 (powder), which is among the most studied acid catalysts. The P functionalized carbon fibers (P-CFs) present almost comparable catalytic activity for 2-propanol dehydration (Figure 3.9a), as well as similar selectivity towards PP (Figure 3.9b) to that of γ-Al_2O_3 catalyst. Nevertheless, it is necessary to increase the temperature at least 30 ºC to get the same conversion. This is in agreement with previous studies on the acidity of carbon catalysts [50], which indicate that the acid strength of P-containing carbons is weaker than that of alumina. It is well known that this weaker acidity of P-CFs, however, may be advantageous from the stability point of view, since a too strong acid character like that of the conventional catalyst causes a more severe deactivation and shorter lifetimes by coke deposition [53]. Therefore, the reported P-CFs seem to

be very attractive for acid catalysis application from both environmental and economic point of views.

On the other hand, beside surface acidigy, a high oxidation resistance is also a required property of carbon materials for their potential use as catalysts and catalyst supports in several reactions involving oxygen [1,2,27-30,50-52]. Thus the thermal stability of the catalysts under oxygen atmosphere becomes crucial. Figure 3.9c shows the non-isothermal air oxidation profiles of lignin-based CFs with and without P. Although CFs without P show a remarkable oxidation resistance themselves, they start to lose weight (oxidize) slowly from 350-400 ºC to 500ºC, temperature at which they quickly combust. The P-CFs, however, do not suffer from any weight-loss until 525-550 ºC, showing an increased oxidation resistance induced by the high thermal stability of the P surface groups in presence of molecular oxygen, already reported in the literature [25,27].

2. ***Adsorption and electrochemical application***. Because of their high surface area and versatile physic-chemical properties, porous carbons constitute the most efficient and broadly used materials as adsorbents [54-58] or electrodes in multiple electrochemical applications [59-63].

   The high microporosity and specific surface area of the P-CFs (Table 3.2) are so far well-recognized and -demonstrated suitable properties to provoke high adsorption capacities in multiple processes and applications [54-56]. However, unlike other carbons, the advanced textural properties in this case have been developed directly during carbonization, without additional impregnation or post-activation steps. On the other hand, the fine diameter ($\leq$ 1 μm) of these fibers [55,56], together with their network of mesopores and wider micropores (Table 3.2) may enormously enhance the accessibility and fast diffusion of molecules to the inner microporous structure [57,58]. The benefits of these properties were confirmed for the adsorption of phenol in aqueous solutions, obtaining adsorption capacities of around 180 mgg^{-1} P-CFs (at 25 ºC and 25 $mg \cdot L^{-1}$). These values are higher than those found, at the same adsorption conditions, for ACs prepared by conventional physical [64] and chemical [65] activation.

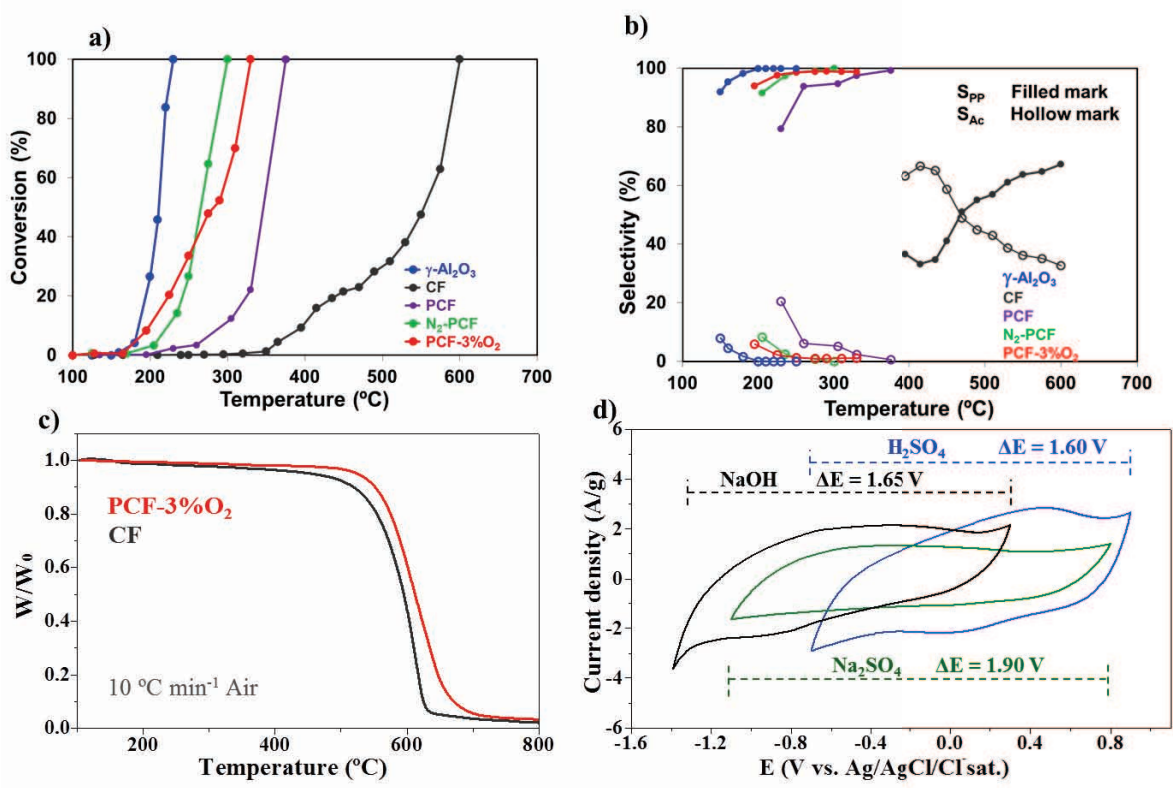

Figure 3.9. (a) Evolution of 2-propanol (2-PrOH) conversion and (b) selectivity for propylene (SPP) and acetone (SAc) with temperature (P2-PrOH = 0.018 atm in He; Space time (W/F)2-PrOH= 0.055 g s μmol^{-1}). (c) Non-isothermal oxidation profiles in air. (d) Steady-state voltammograms of P-CFs in different electrolytes (concentration = 0.5 M; scan rate = 10 mV s^{-1}).

For their application as electrode materials, carbons are generally required to show a high conductivity and surface area, as well as adequate chemical and electrochemical stability in different electrolytes. The basic electrochemical features of the P-CFs were tested, directly as binderless electrodes, by conventional cyclic voltammetry in a three-electrode cell. The straight shape and large current densities observed in the voltammograms of the self-standing P-CFs (Figure 3.9d) clearly reflect their suitable conductivity and great potentiality for electrochemical applications. The high conductivity of P-CFs is in agreement with their ordered structure observed by Raman (see Figure 3.6).

Another feature of upmost importance is the electro-chemical stability. It is related to the range of electrode potentials (potential window (ΔE)) at which neither the electrode nor the electrolyte suffer from electrochemical decomposition. The former mainly occurs by electro-oxidation [66], which greatly declines the performance and durability of carbon electrodes in multiple

electrochemical applications. On the other hand, the electrolyte decomposition by electro-oxidation and -reduction are the most important side reactions that reduce the current efficiency of multiple electrochemical processes. Hence, the preparation of carbon materials showing high overpotentials for these three electrochemical processes becomes decisive for their feasible utilization as electrodes and electrocatalyst supports in multiple applications.

As observed in Figure 3.9d, the P-CFs (see as an example the PCF fibers) show no oxidation currents up to 0.90 V, 0.30 V or 0.80 V in the acid, basic or neutral electrolytes, respectively. This points out that the P-CFs present an extraordinary electro-oxidation resistance, i.e. they can operate safely up to very high potentials, stressing their potential application in supercapacitors, fuel cells, (bio)sensors, electrosynthesis, etc [60-62]. On the other hand, on the negative side the P-CFs start to display reduction currents at very low potentials (below -0.7 V, -1.35 V or -1.1 V in the acid, basic or neutral electrolytes, respectively), at which the electrochemical H storage and/or H_2 evolution occurs [67,68]. Such a low electro-activity for these processes is advantageous for cathodic reactions of industrial and environmental interest, like the electro-reduction of CO_2, dechlorination of pollutants, electrosynthesis of organics, etc [69-71]. The observed enhanced electro-oxidation resistance [72] and low potentials for the electrolyte decomposition [73] have been unequivocally attributed to the presence of surface P functionalities in carbons, a unique characteristic of the hereby reported P-CFs.

As a consequence, the P-CFs exhibit wide stability potential windows: ΔE = 1.60 V, 1.65 V or 1.90 V in H_2SO_4, NaOH and Na_2SO_4, respectively, which are probably among the widest ever reported for aqueous electrolytes (ΔE values for porous carbons are usually around 1.00 V). Such a high electrochemical stability induced by P functionalities has been found beneficial for energy storage in supercapacitors [73,74]. Moreover, the high surface area and microporosity of P-CFs, together with their small diameter and the presence of mesopores, are well-known properties of carbons for an optimum ion adsorption and fast diffusion, respectively, for this application [62,75]. Although a detailed study is not the aim of the present work, the energy density of these materials in a supercapacitor (SC) device can be predicted from the equation

$E = 0.5 \cdot CV^2$; where C is the cell capacitance and V is the operating voltage. Considering that in a symmetric SC (2-electrodes cell) the maximum capacitance is a fourth of that calculated by using a 3-electrode cell (from the voltammograms of Figure 3.9d, these values are around 150-200 $F \cdot g^{-1}$) and that the operating voltage can be optimized to approach the aforementioned stability potential windows (1.90-1.60 V), symmetric SCs using P-CFs (PCF) electrodes could potentially display energy densities of 15-20 $W \cdot h \cdot kg^{-1}$. These energy densities are 2-5 times higher than those shown by commercial activated carbons in organic electrolytes and similar to those of hybrid Li-ion capacitors. Hence, taking into account the excellent performance of lignin-based CFs (without any functionalization) as electrodes for supercapacitors [75], the obtained P-CFs, which exhibit considerably better stability and larger surface area, constitute promising low-cost electrode candidates for energy storage.

3.4. Conclusions.

A new versatile route to prepare advanced functional CFs in remarkably short time, from an abundant and renewable polymer like lignin, has been reported. The route implies the electrospinning of H_3PO_4/lignin solutions to produce submicron-diameter P-functionalized lignin fibers, in which the phosphorus functionalities produce unique effects on their thermal processing. First, the P functionalization remarkably promotes the stabilization of lignin fibers, reducing the time for the process up to 60 times under air atmosphere or enabling it under inert conditions without suffering from fusion. Second, the uniform distribution and easy accessibility of P functionalities in these thin fibers result in an unusually enlarged chemical activation with only a small concentration of H_3PO_4. Third, the P functionalities extraordinarily enhance the oxidation resistance of the CFs, avoiding their complete combustion during carbonization under low concentration of O_2 at very high temperatures (900 ºC), despite their small diameter. Under these conditions the P-CFs can experience partial gasification to produce further activation.

All these effects permit to diversify (under a wider range of conditions) and simplify (to fewer steps) the preparation process of lignin-based CFs, as well as to enormously reduce the time for their thermal processing from more than 80 h, as conventionally, to less than 3 h. At the same time, the reported P-CFs exhibit a unique

combination of advanced structural properties (high surface areas of around 2000 $m^2 \cdot g^{-1}$, diameters in the submicron scale and acceptable structural order) and a rich variety of phosphorus and oxygen functionalities that considerably enhance their oxidation resistance, surface acidity and electrochemical stability. The benefits of all these properties have been demonstrated, by using generalized tests and standard techniques. As a result, these P-CFs seem to be very interesting in catalysis, adsorption and electrochemical applications.

3.5. References.

[1] A. Linares-Solano, D. Cazorla-Amorós. Handbook of Advanced Ceramics (Ed.: S. Somiya) Academic Press: Elsevier Inc., 2013. pp. 155-169.

[2] Y. Matatov-Meytal, M. Sheintuch. Appl. Catal. A Gen. 231 (2002) 1-16.

[3] V. Thavasi, G. Singh, S. Ramakrishna. Energy Environ. Sci. 1 (2008) 205-221.

[4] S. Agarwal, A. Greiner, F.H. Wendorff. Prog. Polym. Sci. 38 (2013) 963-991.

[5] D.A. Baker, T.G. Rials. J. Appl. Polym. Sci. 130 (2013) 713-728.

[6] E. Frank, L.M. Steudle, D. Ingildeev, J.M. Spörl, M.R. Buchmeiser. Angew. Chem. Int. Ed. 53 (2014) 5262-5298.

[7] A. J. Ragauskas, G. T. Beckham, M. J. Biddy, R. Chandra, F. Chen, M.F. Davis, B.H. Davison, R.A. Dixon, P. Gilna, M. Keller, P. Langan, A.K. Naskar, J.N. Saddler, T.J. Tschaplinski, G.A. Tuskan, C.E. Wyman. Science 344 (2014) 1246843.

[8] J.M. Rosas, R. Berenguer, M.J. Valero-Romero, J. Rodríguez-Mirasol, T. Cordero. Front. Mater. 1:29 (2014) 1-17.

[9] M. Lallave, J. Bedia, R. Ruiz-Rosas, J. Rodríguez-Mirasol, T. Cordero, J.C. Otero, M. Márquez, A. Barrero, I.G. Loscertales. Adv. Mater. 19 (2007) 4292-4296.

[10] R. Ruiz-Rosas, J. Bedia, M. Lallave, I.G. Loscertales, A. Barrero, J. Rodríguez-Mirasol, T. Cordero. Carbon48 (2010) 696-705.

[11] S. Kubo, Y. Uraki, Y. Sano. Carbon. 36 (1998) 1119-1124.

[12] Q. Shen, T. Zhang,W.X. Zhang, S. Chen, M. Mezgebe. J. Appl. Polym. Sci. 121 (2011) 989-994.

[13] J. Lin, S. Kubo, T. Yamada, K. Koda, Y. Uraki. BioResources. 7 (2010) 5634-5646.

[14] S. Ramakrishna, K. Fujihara, W.-E. Teo, T. Yong, Z. Ma, R. Ramaseshan. Mater. Today 9 (2006) 40-50.

[15] A. Greiner, J.H. Wendorff. Angew. Chem. Int. Ed. 46 (2007) 5670-5703.

[16] J.L. Braun, K. Holtman, J.F. Kadla. Carbon. 43 (2005) 385-394.

[17] F.J. García Mateos, T. Cordero-Lanzac, R. Berenguer, E. Morallón, D. Cazorla-Amorós, J. Rodríguez-Mirasol, T. Cordero. Appl. Catal. B Environ. 211 (2017) 18-30.

[18] J. Bedia, J.M. Rosas, D. Vera, J. Rodríguez-Mirasol, T. Cordero. Catal. Today 158 (2010) 89-96

[19] M.J. Valero-Romero, F.J. García-Mateos, J. Rodríguez-Mirasol, T. Cordero. Fuel Process. Technol. 157 (2017) 116-126.

[20] X. Wu, L.R. Radovic. Carbon. 44 (2006) 141-151.

[21] M. Jagtoyen, F. Derbyshire. Carbon. 36 (1998) 1085-1097.

[22] A.M. Puziy, O.I. Poddubnaya, A. Martinez-Alonso, F. Suárez-García, J.M.D. Tascon. Carbon. 43 (2005) 2857-2868.

[23] R. Fu, L. Liu, W. Huang, P. Sun. J. Appl Polymer Sci. 57 (2002) 2253-2264.

[24] A.M. Puziy, O.I. Poddubnaya, A.M. Ziatdinov. Appl Surf Sci (252 (2006) 8036-8038.

[25] J.M. Rosas, J. Bedia, J. Rodríguez-Mirasol, T. Cordero. Fuel 88 (2009) 19-26.

[26] E. Adler. Wood Sci. Technol. 11 (1977) 169-218.

[27] J.M. Rosas, R. Ruiz-Rosas, J. Rodríguez-Mirasol, T. Cordero. Carbon 50 (2012) 1523-1537.

[28] J.M. Rosas, J. Bedia, J. Rodríguez-Mirasol, T. Cordero. Ind. Eng. Chem. Res. 47 (2008) 1288-1296.

[29] J. Bedia, R. Ruiz-Rosas, J. Rodríguez-Mirasol, T. Cordero. AIChE 56 (2010) 1557-1568.

[30] J. Bedia, R. Barrionuevo, J. Rodríguez-Mirasol, T. Cordero. Appl. Catal. B: Env. 103 (2011) 302-310.

[31] L.T. Weng, P. Ruiz, B. Delmon. Stud. Surf. Sci. Catal. 72 (1992) 399-413.

[32] G. Mul, J.P.A. Neeft, F. Kapteijn, J.A. Moulijn. Carbon. 36 (1998) 1269-1276.

[33] X. Yan, Y. Liu, X. Fan, X. Jia, Y. Yu, X. Yang. J. Power Sources 248 (2014) 745-751.

[34] Z. Zhou, K. Liu, C. Lai, L. Zhang, J. Li, H. Hou, D.H. Reneker, H. Fong. Polym. 51 (2010) 2360-2367.

[35] J. Rodríguez-Mirasol, T. Cordero, J.J. Rodríguez. Carbon 34 (1996) 43-52.

[36] A. Sadezky, H. Muckenhuber, H. Grothe, R. Niessner, U. Poschl. Carbon 43 (2005) 1731-1742.

[37] J.F. Kadla, S. Kubo, R.A. Venditti, R.D. Gilbert, A.L. Cornpere, W. Griffith. Carbon., 40 (2002) 2913-2920.

[38] S. Kubo, J.F. Kadla. J. Polym. Environ. 13 (2005) 97-105.

[39] I. Dallmeyer, L.T. Lin, Y. Li, K. Ko, J.F. Kadla. Macromol. Mater. Eng. 299 (2014) 540-551.

[40] Y. Uraki, A. Nakatani, S. Kubo, Y. Sano. J. Wood Sci. 47 (2001) 465-469.

[41] H.P. Bohem. Carbon 40 (2002) 145-149.

[42] J.L. Figueiredo, M.F.R. Pereira, M.M.A. Freitas, J.J.M. Orfao. Carbon 37 (1999) 1379-1389.

[43] S. Hu, Y.-L. Hsieh. J. Mater. Chem. A 1 (2013) 11279-11288.

[44] W. Qin, J.F. Kadla. J. Appl. Polym. Sci. 126 (2012) E203-E213.

[45] E. Sjöholm, G. Gellerstedt, R. Drougge, I. Norberg. WO 2013/112100 A1, 2013.

[46] A. Poeppel, E. Frank. EP 2644758 A1, 2013.

[47] E.C. Chenevey, R.M. Kimmel. US 4002426 A, 1977.

[48] H. Sakurai, M. Kitahara, M. Hirata, T. Sawaki. EP 1666649 A1, 2006.

[49] A. Linares-Solano, M.A. Lillo-Ródenas, J.P. Marco-Lozar, M. Kunowsky, A.J. Romero-Anaya. Int. J. Ener. Environ. Econ. 20 (2012) 59-91.

[50] J. Bedia, J.M. Rosas, D. Vera, J. Rodríguez-Mirasol, T. Cordero. Catal. Today 158 (2010) 89-96.

[51] J. Bedia, J.M. Rosas, J. Márquez, J. Rodríguez-Mirasol, T. Cordero. Carbon 47 (2009) 286-294.

[52] J. Bedia, R. Ruiz-Rosas, J. Rodríguez-Mirasol, T. Cordero. J. Catal. 271 (2010) 33.

[53] A.G. Gayubo, A. Alonso, B. Valle, A.T. Aguayo, J. Bilbao. Appl. Catal. B: Environ. 97 (2010) 299-306.

[54] C. Moreno-Castilla. Carbon 42 (2004) 83-94.

[55] J.L. Shmidt, A.V. Pimenov, A.I. Lieberman, H.Y. Cheh. Sep. Sci. Technol. 32 (1997) 2105-2114.

[56] M. Li, Y. Luo, R.C. Wu, H.Y. Liang, S.F. Wang. Advanced Materials Research 356-360 (2012) 1524-1527.

[57] C.-T. Hsieh, H. Teng. Carbon 38 (2000) 863-869.

[58] A.M. Redding, F.S. Cannon. Water Res. 56 (2014) 214-224.

[59] K. Kinoshita Carbon: Electrochemical and Physicochemical Properties, Wiley: New York, 1988.

[60] B.C.H. Steele, A. Heinzel. Nature 414 (2001) 345-352.

[61] A.P.F. Turner. Chem. Soc. Rev. 42 (2013) 3184-3196.

[62] P. Simon, Y. Gogotsi. Nat. Mater. 7 (2008) 845-854.

[63] J.M. Tarascon, M. Armand. Nature 414 (2014) 359-367.

[64] N. Tancredi, N. Medero, F. Möller, J. Píriz, C. Plada, T. Cordero. J. Colloid Interface Sci. 279 (2004) 357-363.

[65] E. González-Serrano, T. Cordero, J. Rodríguez-Mirasol, L. Cotoruelo, J.J. Rodríguez. Water Res. 38 (2004) 3043-3050.

[66] R. Berenguer, H. Nishihara, H. Itoi, T. Ishii, E. Morallón, D. Cazorla-Amorós, T. Kyotani. Carbon 54 (2013) 94-104.

[67] K. Jurewicz, E. Frackowiak, F. Béguin. Appl. Phys. A 78 (2004) 981-987.

[68] S. Leyva-García, E. Morallón, D. Cazorla-Amorós, F. Béguin, D. Lozano-Castelló. Carbon 69 (2014) 401-408.

[69] C. Costentin, M. Robert, J.M. Savéant. Chem. Soc. Rev. 42 (2013) 2423-2436.

[70] I.F. Cheng, Q. Fernando, N. Korte. Environ. Sci. Technol. 31 (1997) 1074-1078.

[71] Y. Sang, B. Wang, Q. Wang, G. Zhao, P. Guo. Sci. Rep. 4 (2014) 6321.

[72] R. Berenguer, R. Ruiz-Rosas, A. Gallardo, D. Cazorla-Amorós, E. Morallón, H. Nishihara, T. Kyotani, J. Rodríguez-Mirasol, T. Cordero. Carbon 95 (2015) 681-689.

[73] C.C. Huang, T. Sun, D. Hulicova-Jurcakova. ChemSusChem 6 (2013) 2330-2339.

[74] D. Hulicova-Jurcakova, A.M. Puziy, O.I. Poddubnaya, F. Suárez-García, J.M.D. Tascón, G.Q. Lu. J. Am. Chem. Soc. 131 (2009) 5026-5027.

[75] R. Berenguer, F.J. García-Mateos, R. Ruiz-Rosas, D. Cazorla-Amorós, E. Morallón, J. Rodríguez-Mirasol, T. Cordero. Green Chem. 18 (2016) 1506.

Chapter 4

Influence of H_3PO_4 on the stabilization and activation of lignin fibers prepared by electrospinning. Optimization of thermo-stabilization conditions

4.0. Abstract

Phosphorus functionalization of lignin has been recently proposed to overcome the long thermostabilization treatment required for the production lignin-based carbon fibers (CFs). In this chapter, the influence of phosphoric acid in the stabilization and carbonization of electrospun lignin fibers, as well as in the morphology and physicochemical properties of the resulting fibrous carbon materials has been thoroughly analyzed. Particularly, the effect of gas atmosphere, temperature, time and heating rate on the stabilization of electrospun H_3PO_4/lignin fibers has been studied. Results show that the presence of H_3PO_4 allows to increase the heating rate from 0.08 up to 3 ºC·min^{-1} while reducing the needed oxidative stabilization temperature and time to 150 ºC for 1 h, respectively, without fusion. Moreover, the effect of H_3PO_4 is so prominent that it promotes the stabilization of lignin fibers even under inert conditions. XPS and DSC characterization reveal that, independently of the stabilization atmosphere, H_3PO_4 itself induces the needed crosslinking reactions by forming stable phosphates with lignin chains that greatly increase the glass transition, crystallization and melting temperatures of lignin fibers. Next, upon carbonization the presence of these phosphates causes the development of microporosity by chemical activation, obtaining carbon fibers with high specific surface area (up to 1700 $m^2 \cdot g^{-1}$), the functionalization of the resulting CFs with P species, as well as an increase in the manufacture yields.

4.1. Introduction

Lignin is the second most abundant polymer in nature, accounting for 30% of all non-fossil organic carbon on Earth [1]. This makes lignin a feasible sustainable carbon source to substitute non-renewable precursors for the production of several chemicals and products [1,2]. On the other hand, lignin is worldwide produced, between 40 and 50 million tons per year, mostly as non-commercialized waste product, from paper industry and biorefineries [3]. Hence, the development of products with added-value or novel and useful properties from this abundant polymeric precursor is expected to cause great impact in multiple technological areas [1,2,4-6], as well as significant environmental and economic benefits to lignocellulosic biomass-derived industries [1,3,7].

Accordingly, intense research on lignin valorization is being carried out from multidisciplinary areas [5-7]. Among different alternatives, the production of carbon

materials by thermochemical conversion of lignin has received a growing interest in last two decades [4,6]. Specifically, the replacement of petroleum-based precursors, like PAN and pitch, for the production of low-cost carbon fibers (CFs) for both structural and functional applications, is currently a hot topic in the research community and the industry [7-16]. On the other hand, CFs manufacturers and providers are also concentrated on reducing the specific energy consumption of the manufacturing process [17].

Lignin is a thermosetting polymer with a glass transition temperature (Tg) far below the temperatures required for carbonization. As a consequence, it requires a stabilization pre-treatment to prevent softening and fusion [18,19]. Oxidative thermostabilization in air is a simple method that, through crosslinking reactions, enables to keep the Tg of the material above the process temperature, rendering it infusible [18,19]. In order to do that, however, the stabilization heat treatment necessarily has to be carried at very slow rate [18], greatly limiting the overall production of lignin-based CFs. On the other hand, the experimental conditions of the thermostabilization treatment greatly affect the final, structural, chemical and mechanical properties of the resulting CFs [8,9,19], so that their optimization becomes crucial. Hence, new synthesis methods and stabilization strategies need to be developed to reduce the long time and high energy consumption of the process and designing improved carbonized products.

In this sense, whereas several strategies have been aimed to improve the stabilization of fossil-derived precursors, much fewer approaches have been addressed to optimize and shorten the procedure with lignin fibers [20-27]. Essentially, the proposed strategies have been focused on (i) the design of new extraction/purification routes to obtain lignins with higher glass transition temperature (Tg) [20,21]; (ii) physical and/or chemical modification treatments [13,22,23]; (iii) the incorporation of polymer additives, like poly(ethylene terephthalate) (PET) [24] or poly(ethylene oxide) (PEO) [25,26]; and/or the addition of an stabilizer [27]. Nevertheless, all these treatments entail more complex and expensive procedures.

By contrast, a simple and straightforward method to promote the stabilization of lignin fibers by functionalization with phosphorus has been proposed [28,29]. The method involves the preparation of lignin fibers with ultrathin diameter, i.e. highly

accessible surface, and uniformly distributed H_3PO_4 molecules, uniquely achieved by electrospinning of H_3PO_4/lignin solutions. It was found that the phosphorus functionalities enable to shorten the conventional stabilization process from more than 80 h to less than 2 h or even to stabilize the fibers in inert atmosphere. Furthermore, they promote their chemical activation, obtaining novel CFs with an unprecedented combination of submicron-diameter, large surface area, high acidity and high oxidation and electro-oxidation resistance; properties that were found very attractive for adsorption, heterogeneous catalysis and electrochemical applications. On the other hand, regarding the specific energy consumption of the manufacturing process, the proposed method not only reduces the length of heating during stabilization, but also it benefits from the electrospinning technique, which, unlike conventional melt extrusion, enables operating at room temperature without any added plasticizer [14,15].

Despite the significance of the method, however, neither the mechanism nor the optimization of stabilization induced by the phosphorus have been investigated yet. In this chapter, the influence of phosphoric acid in the stabilization and subsequent carbonization of electrospun H_3PO_4/lignin fibers has been thoroughly analyzed. Particularly, the effect of the stabilization temperature, time, gas atmosphere and heating rate on the production yields and physicochemical properties of the stabilized and carbonized fibers has been studied by multiple techniques to find the optimum stabilization conditions. Furthermore, the detailed characterization is combined with thermal analysis to deepen into the stabilization mechanism.

4.2. Experimental section

4.2.1. Materials

Alcell® lignin (Repap Technologies Inc.), obtained as a sulfur-free, fine, brown powder, was used as precursor. The composition of this lignin (dry-ash-free basic) was determined by CHNS/O elemental analysis (PerkinElmer® 2400C Instruments) as: 65.9 wt% C; 6.3 wt% H; 0.2 wt% N; 0.00 wt% S; and 27.6 wt% O (calculated by difference), while the ash content was 0.00 wt%. Aqueous phosphoric acid (85 wt%) was used for the functionalization of lignin and ethanol (p. a. Merck) was used as solvent.

4.2.2. Electrospinning

Phosphorus-functionalized lignin fibers were prepared by co-axial electrospinning of H_3PO_4/lignin /ethanol solutions (0.3/1/1 weight ratios), as reported before [28,29]. For comparison, lignin fibers without P were also prepared by using lignin/ethanol solutions (1/1 weight ratios) [14,15]. The tip-to-collector distance was 30 cm in both cases and the electrical potential difference was 24 kV and 12 kV, respectively. In the presence of H_3PO_4, the lignin solution was flowed at 3 $cm^3 \cdot h^{-1}$ for the inner spinneret, and pure ethanol was fed at 0.3 $cm^3 \cdot h^{-1}$ by the outermost one. On the other hand, for the preparation of pure lignin fibers, the flow rates were 1 $mL \cdot h^{-1}$ and 0.1 $mL \cdot h^{-1}$, respectively. The as-spun fibers without or with H_3PO_4 are referred to as *AF* or *PAF*, respectively.

4.2.3. Stabilization and carbonization

The thermostabilization and carbonization of the electrospun fibers were carried out in a horizontal tubular furnace. The thermostabilization was generally performed under air atmosphere (200 $cm^3(STP) \cdot min^{-1}$) at different heating rates (*HR*): 0.08, 1.00, 2.00 and 3.00 ºC·min^{-1}; up to different temperatures (*T*): 100, 150, 200 and 250 ºC; and keeping this final temperature for different times (*t*): 1, 6 and 50 h. Additionally, some experiments were also conducted under N_2 gas (200 $cm^3(STP) \cdot min^{-1}$) to study the influence of the thermostabilization atmosphere. All the stabilized fibers were carbonized at 10 ºC·min^{-1} up to 900 ºC under inert (N_2) atmosphere (150 $cm^3(STP) \cdot min^{-1}$).

The stabilized and carbonized fibers without phosphorus species are referred to as *SF* and *CF*, respectively. In the case of chemical activation with phosphoric acid, the nomenclature used is *PSF* and *PCF* for the stabilized and carbonized fibers, respectively. In addition, this nomenclature is followed by three numbers reflecting the experimental conditions used for stabilization (*HR*, *T* and *t*); i.e. series *SF-HR-T-t* and *CF-HR-T-t*, and *PSF-HR-T-t* and *PCF-HR-T-t* respectively. Particularly, the name of the fibers thermostabilized under inert conditions also includes *(N_2)* at the end.

4.2.4. Characterization

The electrospun and thermostabilized fibers were characterized as prepared. In the case of phosphorus carbonized fibers, the samples were washed with hot distilled

water, to remove weakly-anchorage P species, and dried overnight at 80 ºC prior characterization.

The morphology of the different fibers was followed by scanning electron microscopy (SEM) by means of a JSM 6490LV JEOL microscope working at 25 kV voltage.

The surface chemistry of the samples was characterized by X-ray photoelectron spectroscopy (XPS), by using a 5700C model Physical Electronics apparatus with Mg Kα radiation (1253.6 eV). For the analysis of the XPS peaks, the C1s peak position was set at 284.5 eV and used as reference to locate the other peaks.

The textural properties of carbonized fibers were characterized by N_2 adsorption–desorption at -196 ºC and CO_2 adsorption at 0 ºC, in a Micromeritics ASAP2020 apparatus, after samples out-gassing at 150 ºC under vacuum for 8 h. The apparent surface areas (A_{BET}) were calculated using the Brunauer–Emmett–Teller (BET) method using the N_2 adsorption data in the relative pressure range of 0.01~0.08 [30]. The total pore volumes (V_{tot} (0.995)) were calculated from the N_2 adsorption amount at $P/P_0 = 0.995$. The micropore volume (V_t) and the external surface area (A_t) were calculated using the t-method. The narrowest microporosity (V_{DR} and A_{DR}) (pore size smaller than 0.7 nm) was assessed using the expression of the Dubinin–Radushkevich from CO_2-adsorption isotherm.

Heat flow change upon heating of the as-spun lignin and H_3PO_4/lignin fibers was measured by Differential Scanning Calorimetry (DSC), using a DSC 1 thermal analyzer (METTLER TOLEDO).. Samples (5 – 9 mg) were heated on Al_2O_3 crucibles from 30 to 250 ºC under N_2 or air flow (50 mL min^{-1}) at 2 ºC min^{-1}. The glass transition (Tg), crystallization (Tc) and melting (Tm) temperatures were recorded as the midpoint temperature of the corresponding heat flow transitions.

4.3. Results and Discussion

The electrospinning of pure [14,15] and phosphoric acid-containing [28,29] lignin fibers was previously reported. SEM characterization (Figure 4.1a,d) revealed that both kind of as-spun fibers display diameters ranging mainly from 400 nm to 1 μm, although the presence of H_3PO_4 resulted in more curly fibers with a slightly wider diameter distribution (diameters up to 3 μm) [28,29].

Next, the as-pun fibers were submitted to different thermostabilization treatments under a wide variety of experimental conditions. A detailed analysis of the influence of H_3PO_4 and the stabilization conditions on the physicochemical properties of the resulting stabilized materials, as well as those subsequently obtained by carbonization, is presented in the following sections.

4.3.1. Thermo-oxidative stabilization

4.3.1.1. Effect/optimization of stabilization gas atmosphere

The stabilization of lignin fibers with and without H_3PO_4 was studied under air or N_2 atmosphere. It is known that stabilization of pure lignin fibers have to be carried out at lower heating rate in oxidizing atmosphere to prevent the fusion of lignin fibers (Figure 4.1b) [14,15,18]. In presence of inert atmosphere a complete fibers fusion is produced, even at low heating rates (Figure 4.1c), indicating that the stabilization of lignin fibers necessarily requires oxidation to increase the glass transition temperature and prevent fusion [18]. The use of H_3PO_4 in the initial solution, as it was observed in Chapter 3, allows the faster stabilization of lignin fiber under oxidizing or inert or atmosphere (Figure 4.1e and 4.1f) due to the formation of phosphate esters in the lignin structure. This extraordinary effect opens the way for a fast and simplified manufacture of CFs by using only one atmosphere.

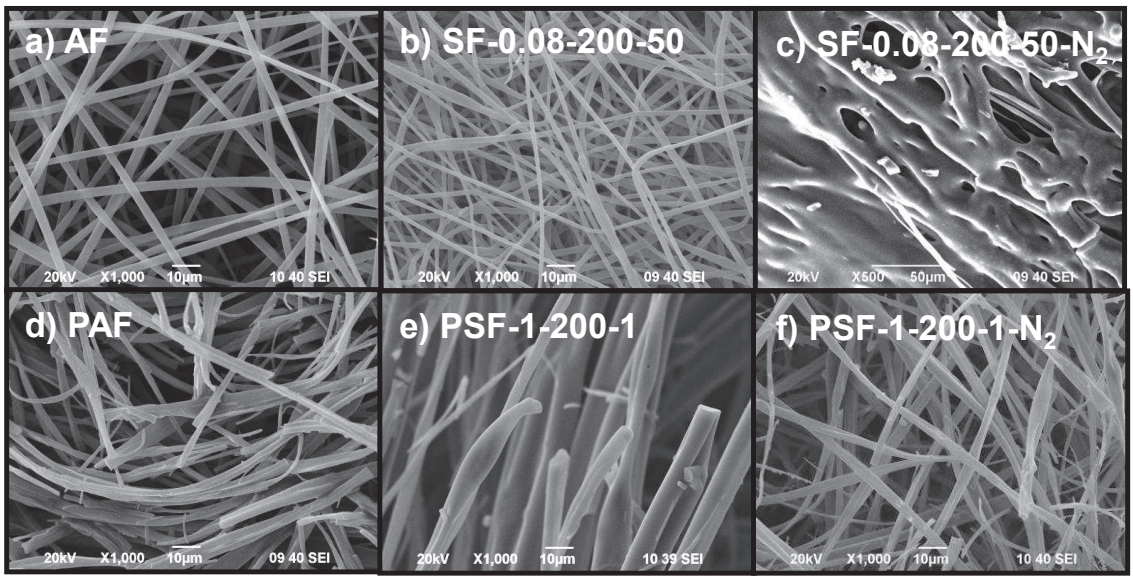

Figure 4.1. SEM images of as spun, stabilized lignin fibers under air and inert atmosphere. Pure lignin fibers (a-c), phosphorus-containing lignin fibers (d-f)

The stabilization yields and the analysis of surface chemical composition are shown in Table 4.1. The results reveal that, in the absence of H_3PO_4, the stabilization under inert conditions (SF-0.08-200-50(N_2) sample) reduces the oxygen content in the as-spun fibers (AF) to the half (ca. 16 wt%O). On the contrary, the stabilized H_3PO_4/lignin fibers under inert atmosphere (PSF-1-200-1(N_2)) show practically the same chemical composition to that of as-spun ones (PAF) and fibers stabilized under air atmosphere (PSF-1-200-1).

Table 4.1. Stabilization yields and weight surface composition by XPS of as spun and stabilized fibres.

Sample	Stabilization yield (%)	Mass surface composition by XPS (wt%)		
		C	O	P
AF	–	73.4	26.6	---
SF-0.08-200-50	76	68.0	32.0	---
SF-0.08-200-50(N_2)	74	83.6	16.4	---
PAF	--	64.5	28.3	7.2
PSF-1-200-1	83	64.1	29.5	6.4
PSF-1-200-1(N_2)	82	63.4	28.3	8.3

The mechanism of thermo-oxidative thermostabilization of lignin has been studied by different authors [15,18,31-35]. The observed weight-losses in stabilization steps have been attributed to condensation and dehydration reactions during cross-linking reactions, the evaporation of occluded ethanol, and the release of some oxygen groups (as CO and CO_2) [15,18,33]. On the other hand, it is generally accepted that at temperatures below 250 ºC, the oxidation of lignin results in an apparent increase in oxygen content [18,33], although this oxygen gain is low since lignin presents an already oxidized structure. Hence, the larger mass loss observed when lignin is treated in N_2 atmosphere may be explained considering that under these conditions only volatilization occurs [36], whereas under air atmosphere the heat-treatment of fibers produces volatilization together with oxygen uptake (mass gain), therefore, showing a lower net mass loss. Lower stabilization yield are observed for pure lignin fibers, in these cases the higher stabilization times produce an increase in the cross linking reactions and on the surface oxidation.

Figures 4.2a and 4.2b show the C(1s) and O(1s) core-level XPS spectra, respectively, of the as-spun lignin fibers (AF), the fibers subjected to thermostabilization heat-treatment under air (SF-0.08-200-50) or N_2 atmosphere (SF-0.08-200-50-N_2). The C(1s) spectrum of as-spun fibers (Figure 4.2a) is composed of two overlapped main contributions at 284.5 eV and 286.0 eV which correspond to C=C/C–C and C–O (C-OH and C-O-C) groups, respectively [14,37]. The presence of these oxygen functionalities agree with the quite symmetric O(1s) spectrum (Figure 4.2b) centered at ca 532.6 eV, associated to oxygen (*) in C-O*H, RO-C=O* and -R-O*-R- groups [15,37]. These spectra features well fit with the molecular structure of lignin and its main (p-hydrophenyl (H), guaiacyl (G), and syringyl (S)) units, with a varying degree of methoxylation [38,39].

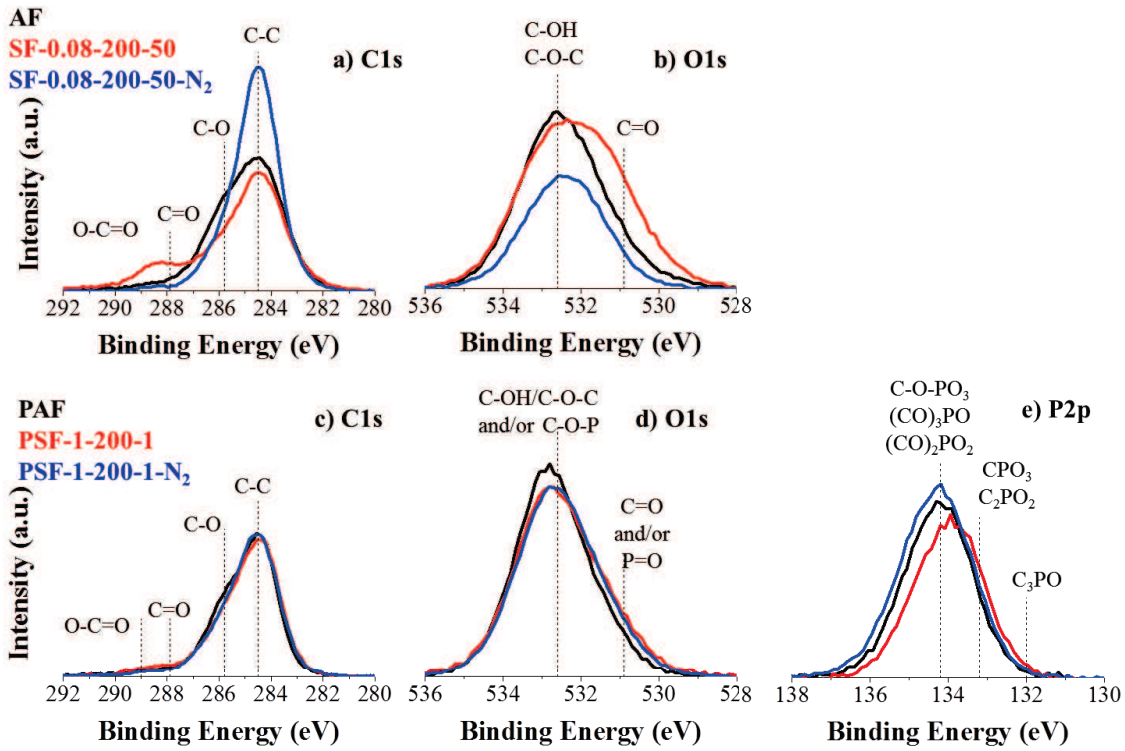

Figure 4.2. XPS spectra of C(1s), O(1s) and P(2p) core-levels of as-spun and stabilized fibers under oxidizing or inert atmosphere.

After stabilization in air, the C(1s) of SF-0.08-200-50 spectrum shows a relative decrease in the intensity of C–O contribution (286.0 eV) and the appearance of a new band centered at ca. 288.4 eV with a small tail near 290.0 eV (Figure 4.2a). This spectral feature can be attributed to the formation of –C=O (287.6 eV) and –O–C=O

(at 289 eV) bonds in carbonyl or anhydride, ester and/or carboxylic groups, respectively, these groups are generated after cross linking reaction [15,18,37]. This change is in agreement with the O(1s) broadening towards lower binding energies (530.9 eV in Figure 4.2b), where the carbonyl groups are increased after stabilization. By contrast, the spectrum of fibers stabilized in N_2 (SF-0.08-200-50-N_2) involves the decrease in the intensity of C–O contribution (286.0 eV) in C(1s) spectrum (Figure 4.2a) and that of the whole O(1s) spectrum (Figure 4.2b). These results confirm that the heat treatment of lignin fibers in N_2 atmosphere only produces the release (volatilization) of oxygen functional groups, without oxidation or crosslinking reactions, avoiding any possibility of stabilization, and subsequent production of CFs, under these conditions.

XPS characterization for phosphorus containing fibers (Figures 4.2c - 4.2e) reveals slight but meaningful differences between the surface chemistry of the different as-spun fibers. Compared to the pure fibers (AF), the H_3PO_4/lignin fibers (PAF) show a lower relative intensity but better defined contribution at 286.0 eV in C(1s) spectrum, together with an increase at 532.6 eV of the O(1s) spectrum. These changes may involve a relative increase in C-O-P species due to the presence of H_3PO_4. In this sense, PAF fibers show a symmetric band in the P(2p) spectrum (Figure 4.2e) centered at 134.2 eV, which exactly corresponds with the binding energy reported for C-O-P species in C-O-PO_3,$(C\text{-}O)_2PO_2$ or $(C\text{-}O)_3PO$ groups [40-43]. These results suggest that H_3PO_4 may react with the oxygen functionalities of lignin (C-OH) to form different phosphates and/or polyphosphates. Paying attention to the stabilization atmosphere, slight differences have been found, having practically identical composition to those of as-spun phosphorus fibers. A slight decrease at 532.6 eV in O1s spectra is found due to the release of C-O-C and C-OH groups. A higher increase in carbonyls groups is observed when O1s spectra of SF-0.08-200-50 and PSF-1-200-1 are compared. In this case, the long stabilization of pure lignin fibers (more than 80 hours) favors the carbonyl groups generation. These groups have been found the responsible to avoid the fiber fusion in carbonization step [14,15,18], but when H_3PO_4 is added to the initial solution, phosphates esters generated are enough to prevent the fibers fusion. Furthermore, the P(2p) bands of both stabilized fibers are centered approximately at the same binding energy to that of PAF (Figure 4.2e), although the spectrum of fibers stabilized in air (PSF) is slightly shifted towards lower binding energies, producing

some phosphorus in a more reduced state as in C-PO bonds, as a consequence of dehydration and cross-linking reactions.

Differential scanning calorimetry (DSC) was used to study the influence of phosphorus functionalities in the thermal behavior of the electrospun lignin fibers. This technique can quantitatively analyze both physical transitions and chemical reactions.

The particularly interesting but complex thermal behavior of lignin, including Alcell® lignin, has been previously studied [44-47]. It is well known that these thermal properties remarkably depend on the history of the sample (extraction/purification treatments, storage temperature and storage time, heating and/or cooling treatments, etc.). In this sense, the thermal behavior of the electrospun lignin fibers is expected to be greatly influenced by the experimental steps followed for their production (the procedure for the preparation of the ethanolic solution and the electrospinning process) and, therefore, somehow different to that of the pristine Alcell® lignin powder.

Figure 4.3 depicts the DSC thermograms of the as-spun pure and H_3PO_4-containing lignin fibers under different atmospheres. As it can be observed, independently of the presence of H_3PO_4 or the used atmosphere, the thermograms show two-three clear subsequent heat-exchange processes that are attributed to characteristic physical transitions on plastic polymeric materials, namely, glass transition, crystallization and melting [48,49]. The corresponding glass transition temperature (Tg), crystallization temperature (Tc) and melting temperature (Tm) were recorded as the midpoint temperature of the corresponding heat flow transitions and are collected in Table 4.2.

Independently of the used atmosphere, the glass transition of both the as-spun H_3PO_4–free and H_3PO_4–containing lignin fibers occur at low temperatures, ranging between 57-63 ºC (Table 4.2). These Tg values are lower compared to those reported for Organosolv lignins (between 90-130 ºC) in literature [45-47], highlighting the importance of the stabilization treatment to produce lignin-based CFs. Nevertheless, some clear effects of H_3PO_4 and the atmosphere on this process can be observed: (i) the Tg values of both type of lignin fibers in air atmosphere are higher than in inert conditions; (ii) differences are higher for the fibers without H_3PO_4; (iii) in air atmosphere lignin fibers show a higher Tg than lignin/H_3PO_4; (iv) in the presence of

H_3PO_4 the glass transition is accompanied by a considerably higher heat exchange and enthalpy relaxation [49-50].

After glass transition, further heating induces crystallization of the different lignin fibers (Figure 4.3). This process is assigned to the rearrangement/ordering of polymer chains and, as observed in the Figure 4.3, it is strongly influenced by the introduction of H_3PO_4 in the fibers. In particular, the presence of H_3PO_4 hinders this structural transition in both air and N_2 atmospheres, so that the lignin fibers need to achieve considerably higher temperatures (around extra 60 ºC) to experience it (Table 4.2). Moreover, the heat release associated to this process is, like in the case of glass transition, much higher when H_3PO_4 is incorporated in the fibers. On the other hand, the influence of atmosphere in this process seems to be negligible for both lignin and lignin/H_3PO_4 fibers.

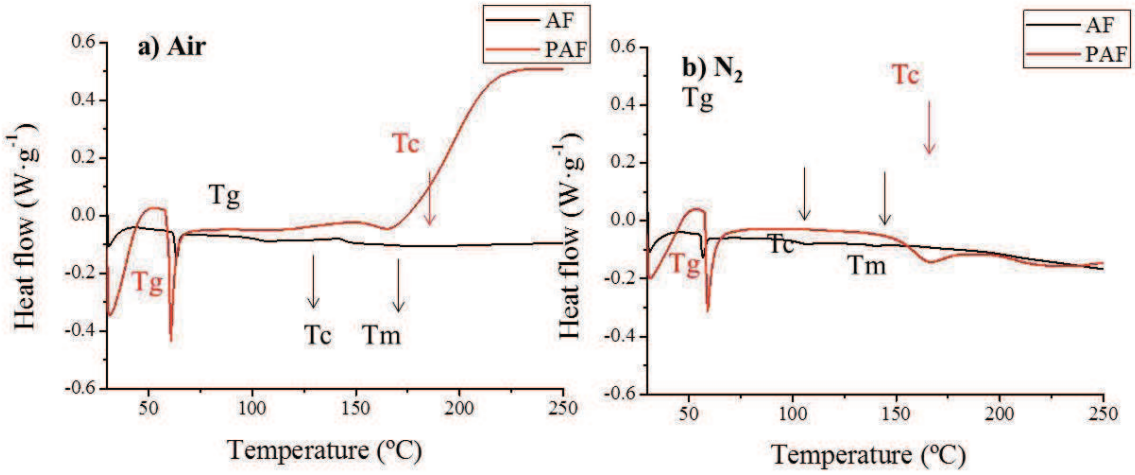

Figure 4.3. DSC of as-spun lignin (AF) and lignin/H_3PO_4 (PAF) fibers under (a) air or (b) N_2 atmosphere (HR = 2 ºC·min^{-1}).

Table 4.2. Glass transition (Tg), crystallization (Tc) and melting (Tm) temperatures calculated from DSC measurements and heat flows (integral).

Sample	Tg (ºC)	Integral (J/g)	Tc (ºC)	Integral (J/g)	Tm (ºC)	Integral (J/g)
AF-air	63.13	-5.39	107.43	-2.64	141.67	4.26
AF-N_2	56.63	-5.22	107.27	-1.56	140	-0.49
PAF-air	60.67	-49.86	167	-6.1	--	--
PAF-N_2	59.07	-35.30	165.80	-45.16	--	--

Finally, the DSC curves of pure lignin fibers show a third heat exchange process after crystallization, which has been attributed to polymer melting. In the case of fibers

stabilized in air, the process occurs at ca. 142 ºC and is found endothermic; while in inert conditions it is observed as an exothermic process at practically the same temperature (ca. 140 ºC). By contrast, the presence of H_3PO_4 seems to suppress (at least below 250 ºC) or to delay (at higher temperatures) the melting transition.

4.3.1.2. Effect of stabilization temperature and time

The electrospun phosphoric-containing lignin fibers (PAF) were subjected to thermo-oxidative stabilization under air atmosphere at different temperatures and for different times. For this study, the used heating rate was 1 ºC·min^{-1}, which was found to produce complete fusion of lignin fibers in the absence of H_3PO_4. The SEM images of the as spun and stabilized phosphorus-containing fibers are shown in Figure 4.4. As it can be observed, the fibers stabilized under the wide variety of tested conditions (Figures 4.4b-i) retain the same curly morphology and diameter, without swelling or partial fusion, to those of the as-spun materials. This reflects the outstanding capability of H_3PO_4 to promote the stabilization of lignin fibers.

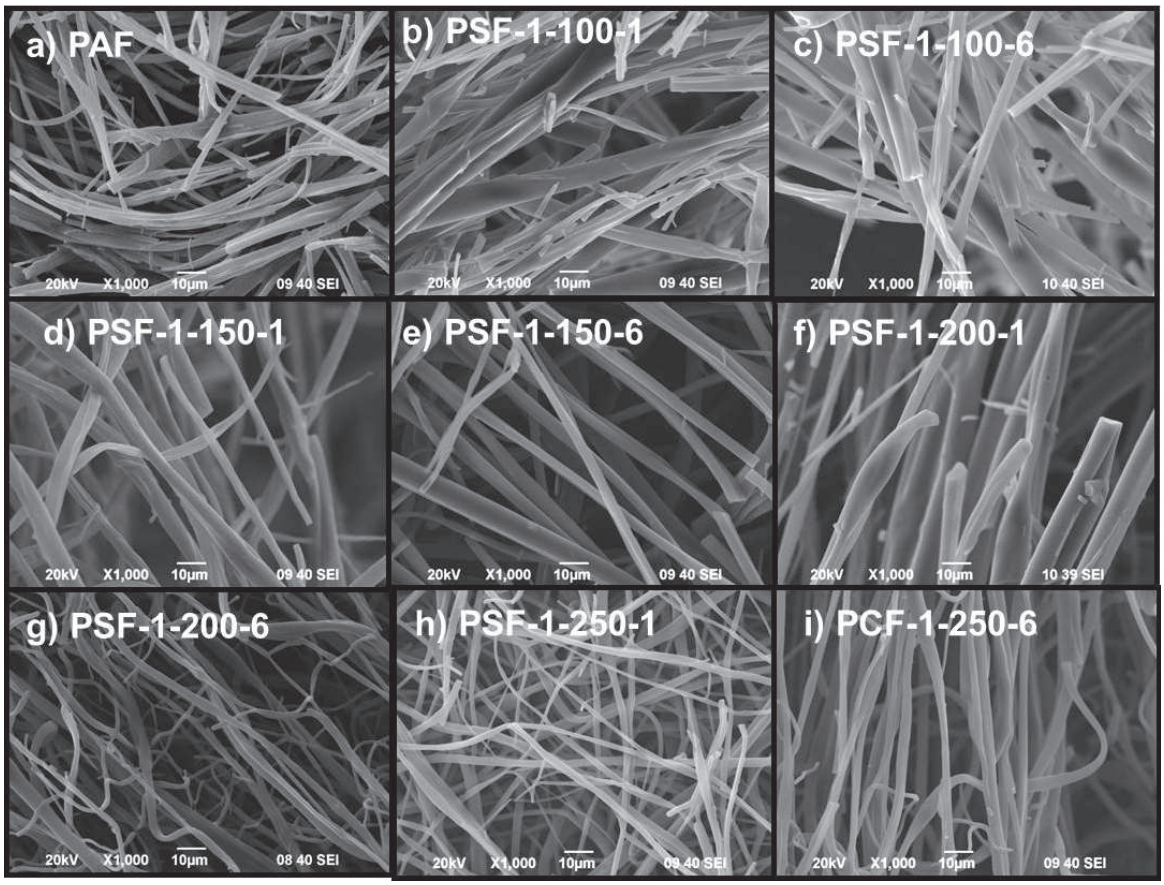

Figure 4.4. SEM images of H_3PO_4/lignin fibers as spun (a) and stabilized at 1 ºC·min^{-1} in air atmosphere under various conditions of temperature and time (b-i)

Table 4.3 collects the stabilization yields of H_3PO_4/lignin fibers at all the studied conditions. As it can be observed in Figure 4.5, the stabilization yields decrease with the temperature for a given treatment time (1 or 6 h); as well as by prolonging the treatment time at a given temperature. It is known that in the fibers stabilization step, dehydration, condensation, cross-linking and eliminations reaction are carried out [51-53]. Thus, higher stabilization temperatures (at same heating rate) and, specially, higher stabilization times lead to longer reactions and greater changes in lignin structure.

Table 4.3. Yields of stabilization treatments based on the mass of as-spun and stabilized fibers, respectively; and mass surface concentration (wt%) of different elements in the stabilized fibers determined by XPS. Effect of stabilization temperature and time.

Sample	Stabilization yield (%)	Mass surface concentration by XPS (%)		
		C	O	P
PAF	–	63.9	29.6	6.5
PSF-1-100-1	98.0	62.0	29.0	9.0
PSF-1-100-6	95.0	58.4	33.1	8.5
PSF-1-150-1	92.0	65.2	27.9	6.9
PSF-1-150-6	89.7	64.6	29.2	6.2
PSF-1-200-1	85.0	64.1	29.5	6.4
PSF-1-200-6	80.0	61.8	31.3	6.9
PSF-1-250-1	76.5	56.8	36.1	7.1
PSF-1-250-6	68.0	57.8	34.9	7.3

Table 4.3 also includes the surface mass composition of the as-spun and stabilized fibers. Comparing with the as-spun fibers (PAF), the stabilization treatment at 100 ºC for 1 h produces almost no change on the surface oxygen content, while a 3 wt%O increase is observed when the treatment is prolonged for 6 h. This seems to indicate that neither significant thermochemical reactions nor volatilization may occur under such a low temperature and short treatment. On the other hand, this net oxygen gain after the treatment at 100 ºC (6 h) may be assigned to some surface oxidation and the lignin dehydration produced when it is in contact with H_3PO_4.

Above 100 ºC, the surface oxygen content first decreases with temperature to a minimum value of ca. 28 wt%O at 150 ºC, and it subsequently increases up to ca.

35 wt%O for the treatment at 250 ºC. In Figure 4.5 is also included the oxygen carbon ratio (O1s/C1s), this ratio increase after a minimum obtained at 150 ºC. Similar behavior has been found in pitch fibers stabilization [51]. As it can be seen in Figure 4.6, the increase in oxygen content (or oxygen/carbon ratio) is related to the generation of carbonyls groups after stabilization step.

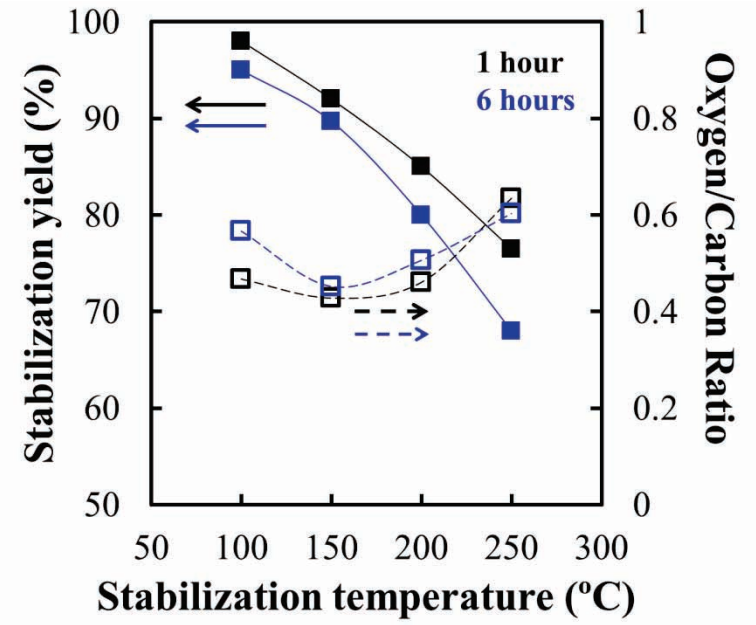

Figure 4.5. Effect of stabilization temperature and time on stabilization yield and O1s/C1s ratio

Figure 4.6 presents the C(1s), O(1s) and P(2p) spectra of air-stabilized H_3PO_4/lignin fibers as a function of the stabilization temperature and time. As it can be observed, above 150 ºC the rise in temperature gradually increases the proportion of C=O and –O–C=O contributions (between 287-289 eV and 530-533 eV in C(1s) and O(1s) spectra, respectively) for both 1 h (Figures 4.6a and 4.6b) and 6 h (Figures 4.6d and 4.6e) treatments, being the increase of carbonyls groups higher at longer stabilization times. As we discussed before, an increase in the stabilization time produce a longer stabilization steps, being more effective the generation of these groups types.

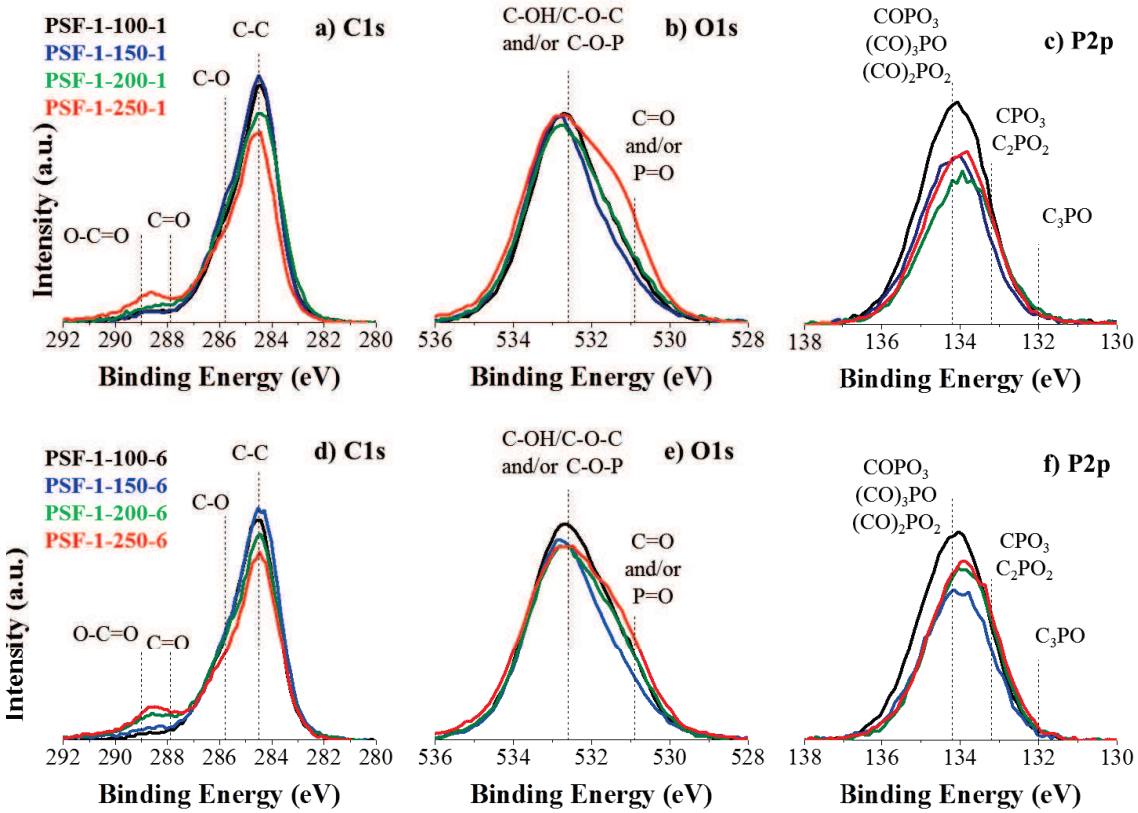

Figure 4.6. C(1s), O(1s) and P(2p) XPS spectra of air-stabilized lignin/H_3PO_4 fibers. Effect of stabilization temperature and time.

In parallel to the observed oxidation, the utilization of stronger oxidizing conditions produces a slight but progressive shift of the center of P(2p) band towards lower binding energies (Figures 4.6c and 4.6f). Although the P mainly exists like C-O-P species (the band is always centered close to 134 eV), this shift in P(2p) band may point out the generation of other less oxidized P species, like C-P-O groups [37-40].

The results reported in this work indicate that the phosphate esters (C-O-P) groups generated by reaction of lignin structure with H_3PO_4 are highly stable so that they can protect carbon atoms from oxidation. The changes on XPS spectra observed in Figure 4.6 suggest that under strong oxidizing conditions, stable -C-O-P-like species could react with O_2 molecules and transfer some oxygen atoms to neighboring carbon sites.

4.3.1.3. Effect of thermostabilization heating rates.

Figure 4.7 shows the SEM images of H_3PO_4/lignin fibers stabilized in air conditions at different heating rates up to 150 ºC and 1 h. In this figure is observed that H_3PO_4/lignin fibers can be stabilized without swelling or partial fusion at heating rates as high as 3 ºC min^{-1}. Similar results were found independently of the final temperature or treatment times of stabilization, at least in the range 150-250 ºC or 1-6 h, respectively. However, regardless of the final temperature and treatment times, swelling and partial fusion of lignin fibers occurred during stabilization when heated at or above 4 ºC min^{-1} (Figure 4.7d).

The influence of heating rate on the air-stabilization yields of H_3PO_4/lignin fibers can be analyzed from the data in Table 4.4. As it can be observed, the stabilization yields of samples heated in the range of 1-3 ºC min^{-1} are quite similar (around 92 %) and relatively high, being indicative of a slight weight loss. High and similar yields achieved at faster heating rates (between 1-3 ºC min^{-1} up to 150 ºC) may be a consequence of the overall shorter heat-treatments and length of thermochemical reactions under these conditions. This is in agreement with previous studies on Kraft lignin powders [18], which reported very little mass loss and a small influence of heating rate (in the range 0.11-1 ºC·min^{-1}) below 190 ºC, but a marked and increasing loss above this temperature, with the rising temperature and lower heating rates. However, the influence of heating rate becomes more important if the compared values are much more different and/or when working up to higher temperatures. Thus, for example, the yield obtained for a slow stabilization at 0.08 ºC·min^{-1} up to 200 ºC (+ 50 h) (around 83 %) is lower than heating at 1 ºC·min^{-1} up to the same temperature (+ 1 h) (around 85-88 %). Meanwhile, comparison at slow heating rates indicates that the stabilization yields of H_3PO_4/lignin fibers (83 %) are higher than in the absence of H_3PO_4 (77 %).

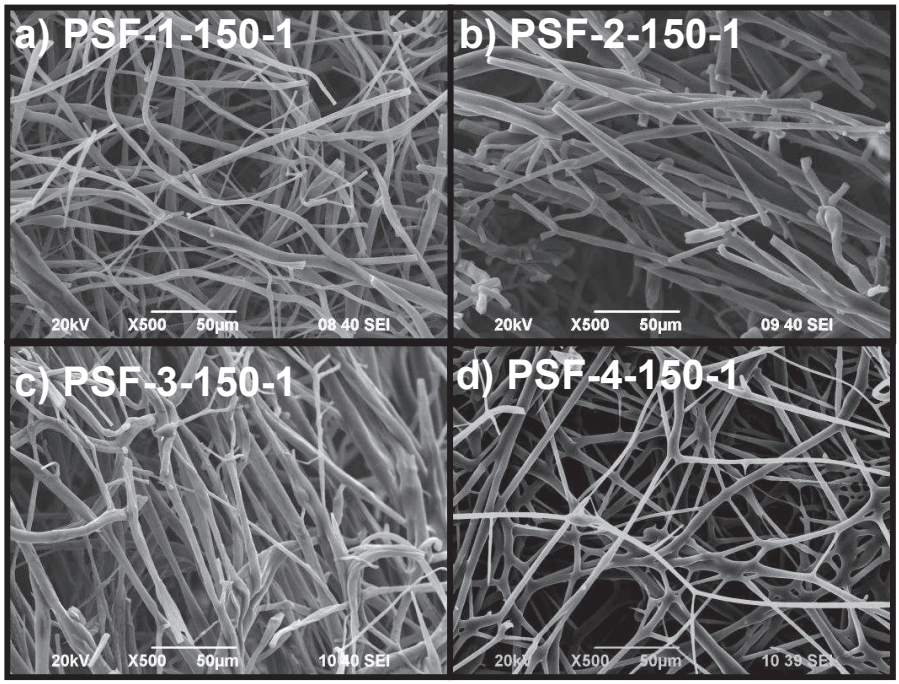

Figure 4.7. SEM images of H_3PO_4/lignin fibers (a-c,g) stabilized under air atmosphere at different heating rates (HR = 1, 2, 3 and 4 ºC·min^{-1}), (d-f) the carbonized product of (a-c), (h) stabilized under N_2 atmosphere (HR = 1 ºC·min^{-1}) and (i) the carbonized product of (h). General stabilization conditions T = 150 ºC, t = 1 h.

Surface chemical composition of stabilized fibers is quite similar (Table 4.4). Figure 4.8 shows the C(1s), O(1s) and P(2p) XPS spectra of stabilized fibers at different heating rates, where no differences are appreciated by varying the heating rate. From these results it can be inferred that, despite the fibers are successfully stabilized and thermochemical reactions occur upon the fast heat-treatment, the phosphate (C-O-P) groups present in the as-spun PAF fibers seem to prevent the fibers fusion, even at 3 ºC min-^{1}, and stabilization mechanism, in H_3PO_4/lignin fibers, is not determited by oxidation cross linking reactions.

Table 4.4. Stabilization yields and mass surface concentration (wt%) in the stabilized and carbonized fibers determined by XPS. Effect of stabilization heating rate.

Sample	Stabilization yiedl (%)	Mass surface composition by XPS (%)		
		C	O	P
PSF-1-150-1	92.0	65.2	27.9	6.9
PSF-2-150-1	92.3	64.2	27.9	7.9
PSF-3-150-1	92.1	66.6	26.2	7.2

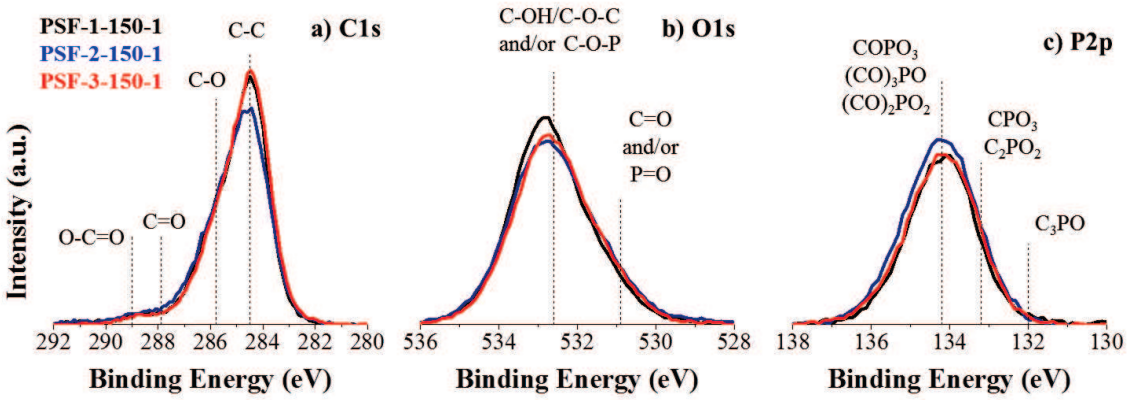

Figure 4.8. C(1s), O(1s) and P(2p) XPS spectra of air-stabilized lignin/H_3PO_4 fibers. Effect of heating rate.

4.3.2. Carbonization step

4.3.2.1. Effect of stabilization temperature and time on carbonized fibers.

Figure 4.9 shows the SEM images of carbonized fibers (pure lignin carbon fibers (a) and effect of time and stabilization time on phosphorus carbonized fibers (b-i)).When the stabilization is carried out at the lowest tested temperature (100 ºC) and shortest tested time (1 h), however, the fibers suffered from swelling and partial fusion upon subsequent carbonization (Figure 4.9b), causing fiber interconnection at contact points. This indicates that these conditions were not enough suitable to stabilize the fibers. Nevertheless, by extending the treatment time at 100 ºC, for example, up to 6 h, the fibers did not experience swelling or fusion upon carbonization (Figure 4.9c). Furthermore, above 100 ºC the stabilization promoted by H_3PO_4 was effective to prevent the carbonized fibers from fusion within the whole range of studied temperatures and times (see for example the fibers carbonized after stabilization at the highest tested temperature and time in Figure 4.9i). Hence, the incorporation of H_3PO_4 enables the preparation of ultrathin lignin-based carbon fibers that can be stabilized from 100 ºC for 6 h to 250 ºC for 6 h.

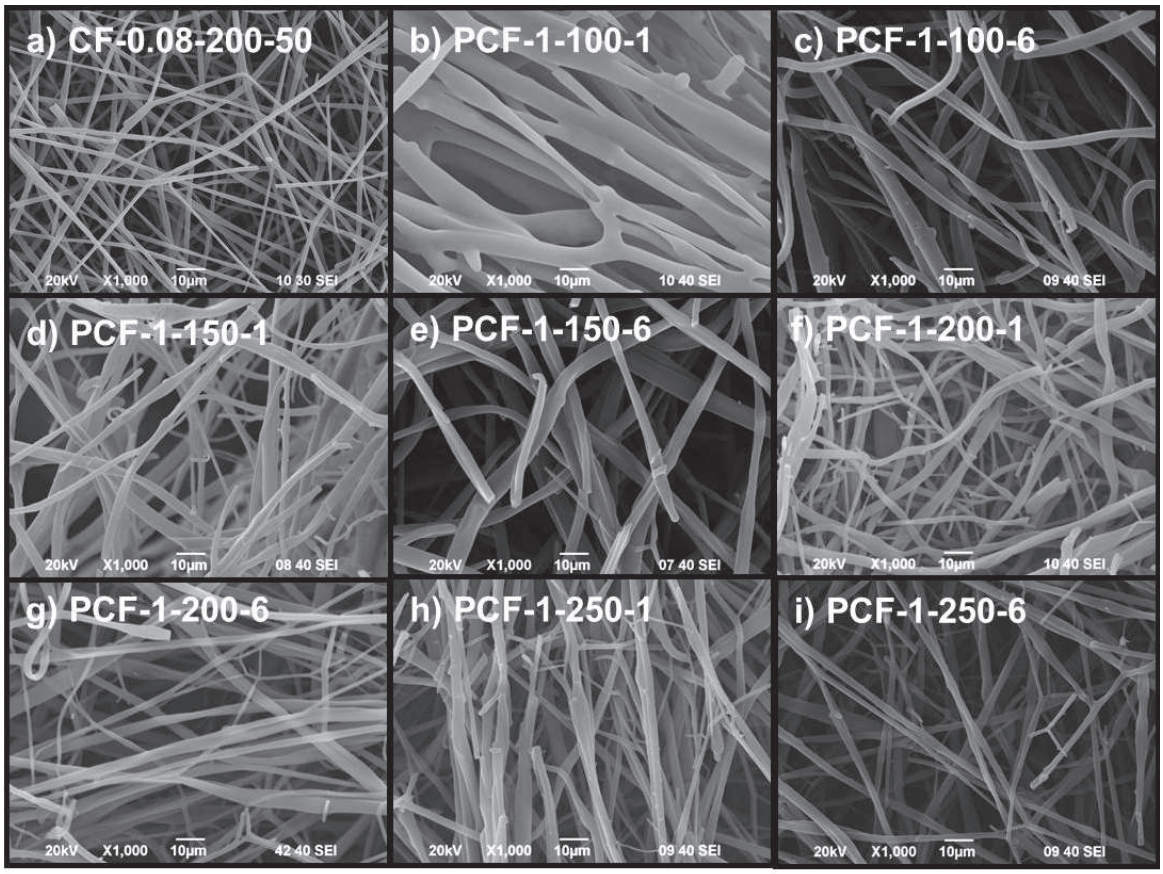

Figure 4.9. SEM images carbonized fibres. Pure carbon lignin fibers (a) and H_3PO_4/carbon fibers stabilized at 1 ºC·min^{-1} in air atmosphere under various conditions of temperature and time

Stabilization conditions and, therefore, the different composition of the stabilized fibers affect the composition changes and the carbonization yields, which range between 30 to 36 % (Table 4.5). Carbonization yield decays as the oxygen content in the stabilized fibers increases (see Table 4.3 for stabilized fibers), and therefore, at higher oxygen-loss (ΔO) during carbonization step (Figure 4.10a). The higher oxygen content on stabilized fibers may produce a slight gasification when temperature is increase in carbonization step, obtaining lower carbonization yields.

The textural properties of the carbonized fibers were analyzed by physical adsorption of gases. Regardless of the different stabilization conditions, all the carbonized fibers exhibit Type I N_2-adsorption isotherms (Figure 4.10b), characteristic of microporous materials [54]. Table 4.5 also summarizes the main textural properties calculated from N_2 and CO_2 adsorption isotherms. As it can be observed, the carbonized fibers present high micropore volume (V_t), ranging between 0.4 - 0.7 cm^3·g^{-1}.

Concerning the microporosity, the high values of $V_{DR}(CO_2)$ reveal the formation of a large amount of narrow micropores (d < 0.7 nm), around 70-80 % of total micropore volume, which practically is not influenced by the different stabilization conditions.

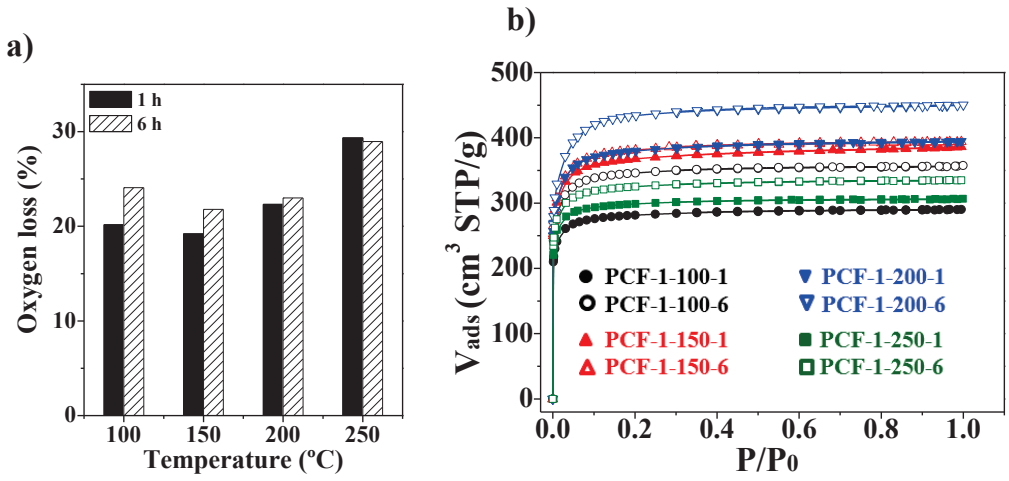

Figure 4.10. a) Oxygen-loss during carbonization of H_3PO_4/lignin fibers. HR = 1 ºC·min^{-1}; Air atmosphere. b) N_2 adsorption-desorption isotherms at -196 ºC of carbonized lignin/H_3PO_4 fibers. Effect of stabilization temperature and time.

The high microporosity of the carbonized fibers gives rise to large specific surface areas (A_{BET}) between 1200 and 1600 m^2·g^{-1} (Table 4.5). This surface area must be easily accessible, as deduced from the high values of external surface area (A_t), between 17 - 30 m^2·g^{-1}, assigned to the narrow diameter of the electrospun fibers and the presence of mesopores. The values of V_t, A_{BET}, and A_t increase with the stabilization temperature and time, reaching a maximum for the treatment at 200 ºC for 6 h. When the stabilization is carried out under these conditions, the specific surface area and micropore volume are the double of those of lignin fibers prepared without H_3PO_4 (Table 4.5). Accordingly, the addition of H_3PO_4 to the initial solution not only enables to perform the stabilization treatment at lower temperatures and considerably shorter times, but also to produce carbonized fibers with remarkably higher textural properties.

Table 4.5. Carbonization yield and textural properties of carbonized fibers. Effect of the stabilization temperature and time.

Sample	Carb. yield (%)	N_2 Isotherm				CO_2 Isotherm	
		A_{BET} ($m^2 \cdot g^{-1}$)	At ($m^2 \cdot g^{-1}$)	Vt ($cm^3 \cdot g^{-1}$)	V_{tot} ($cm^3 \cdot g^{-1}$)	A_{DR} ($m^2 \cdot g^{-1}$)	V_{DR} ($cm^3 \cdot g^{-1}$)
CF-0.08-200-50	30.3	851	8	0.329	0.337	1002	0.402
PCF-1-100-1	35.8	1093	17	0.433	0.448	890	0.357
PCF-1-100-6	34.5	1321	17	0.536	0.551	1031	0.413
PCF-1-150-1	32.8	1403	33	0.563	0.597	1068	0.428
PCF-1-150-6	32.0	1454	21	0.589	0.609	1046	0.419
PCF-1-200-1	33.0	1448	25	0.586	0.610	1027	0.412
PCF-1-200-6	31.5	1626	26	0.671	0.697	1081	0.433
PCF-1-250-1	29.4	1179	12	0.463	0.474	1046	0.419
PCF-1-250-6	29.2	1262	17	0.503	0.518	1007	0.403

Table 4.6 shows the mass surface composition of carbonized fibers after stabilization at different temperatures and time. Independently of the stabilization conditions, the carbonization step causes a remarkable reduction in both the oxygen and phosphorus surface contents down to 6-9 wtO% and 1.6-2.2 wt%P, respectively. Figure 4.11 shows the C1s, O1s and P2p spectra of carbonized fibers (effect on the temperature and time stabilization). The O1s spectra of phosphorus-carbon fibers show a high contribution of C-OH, C-O-C and/or C-O-P linkages at 532.6 eV and at lower binding energies 530.9 eV characteristic of C=O and P=O groups. The P2p spectra show a band with a main peak at a binding energy of 133.7 eV, which is characteristic of phosphates and/or polyphosphates groups [55,56]. Wu and Radovic assigned the peak at a binding energy about 134 eV to C-O-P bonds [57], such as C-O-PO_3, $(C\text{-}O)_2PO_2$ and $(C\text{-}O)_3PO$ groups. A binding energy of about 133.2 eV is characteristic of C-P bonding as in C-PO_3 groups [14] and/or C_2PO_2 groups. Lower value of binding energies at 132.0 and 131.0 eV can be associated to C_3PO [57-59] and C_3P groups [60], respectively. For carbon fibers that has been stabilized at 250 ºC for 6 hours (PCF-1-250-6), the P2p spectrum is shifted at lower bindings energies toward more reduced phosphorus, what may be related to the higher oxygen-loss during carbonization.

Table 4.6. Mass surface composition of carbonized fibers after stabilization at different temperatures and times.

Sample	Mass surface composition by XPS (wt%)		
	C	O	P
CF-0.08-200-50	96.0	4.0	---
PCF-1-100-1	88.8	8.9	1.7
PCF-1-100-6	88.3	9.0	1.6
PCF-1-150-1	88.3	8.3	1.9
PCF-1-150-6	91.1	5.9	2.2
PCF-1-200-1	90.7	6.7	2.0
PCF-1-200-6	89.3	8.1	2.0
PCF-1-250-1	88.6	6.7	1.9
PCF-1-250-6	91.7	6.1	1.8

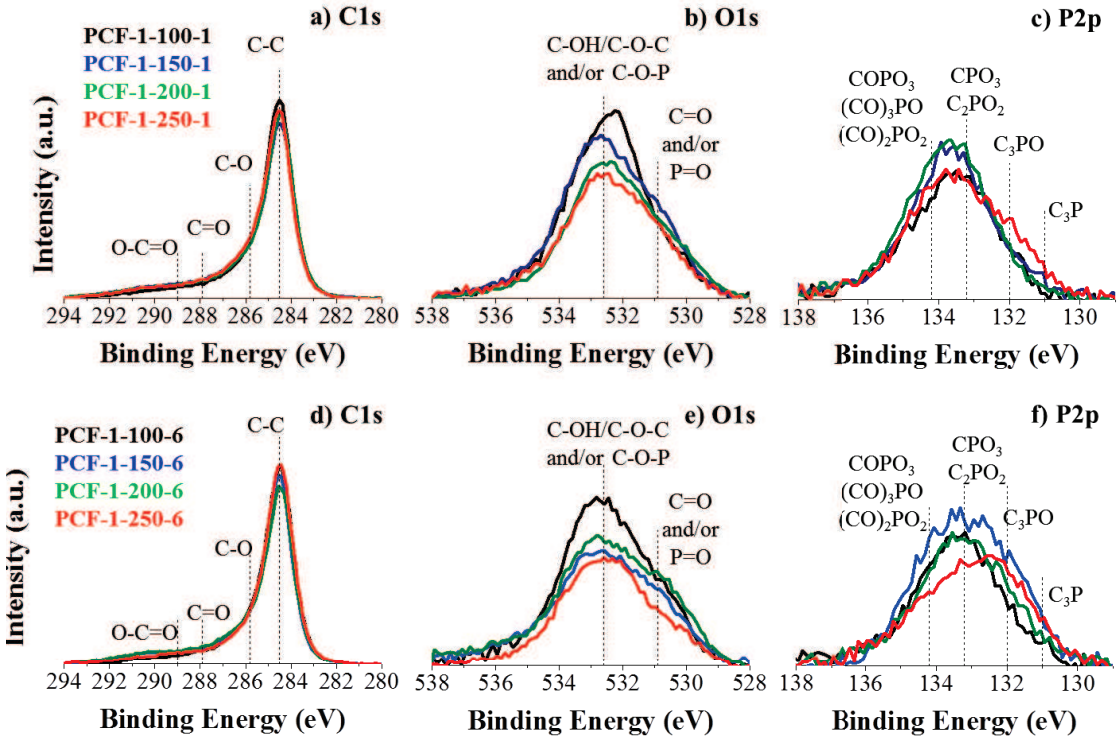

Figure 4.11. C(1s), O(1s) and P(2p) XPS spectra of phosphorus-containing carbon fibers. Effect of stabilization temperature and time.

4.3.2.2. Effect of thermostabilization heating rate and gas atmosphere on carbonized fibers

Figure 4.12 shows SEM images of carbonized fibers that have been stabilized at different heating rates and gas atmospheres. They demonstrate that the H_3PO_4/lignin fibers stabilized at lower temperatures and faster heating rates (Figure 4.12a-c) can be carbonized without presenting fibers fusion. Moreover, carbonization of stabilized lignin fiber under inert atmospheres retains the initial morphology. This indicates that the introduction of H_3PO_4 permits to successfully prepared carbon fibers that have been stabilized at a low temperature and fast heating rate, in anoxic conditions.

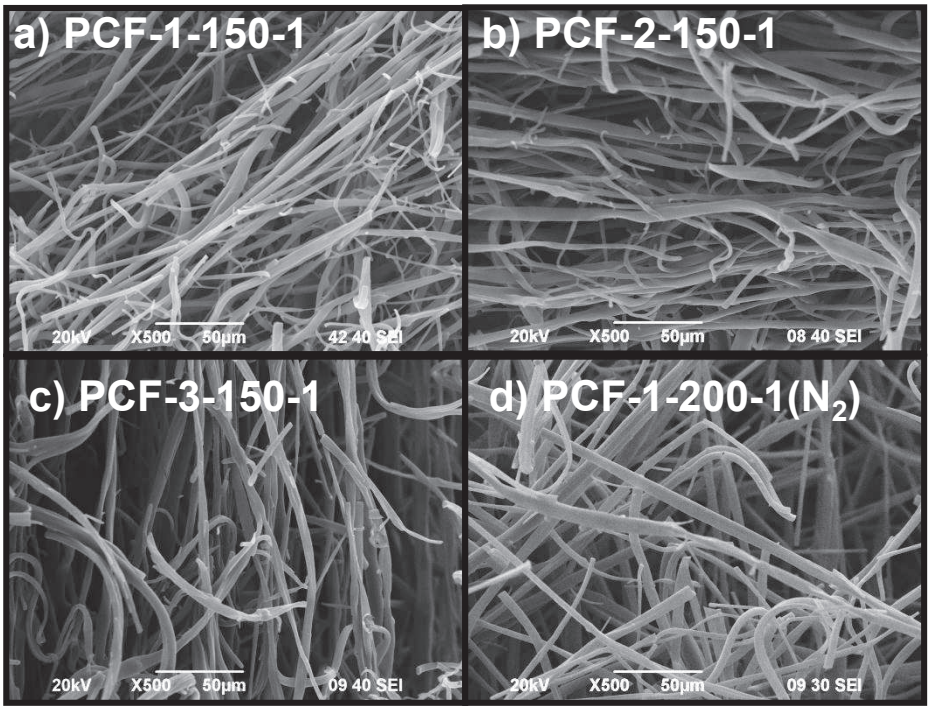

Figure 4.12. SEM images of carbonized fibers. Effect of stabilization heating rate (a-c) and gas atmosphere (d).

With regard to the carbonization yields, the influence of the different fast stabilization heating rates (HRs) (1-3 ºC·min^{-1}) seems to be also small (Table 4.7). A higher carbonization yield is obtained for carbon fibers stabilized under N_2 atmosphere; this result could be in accordance with the lowest oxygen-loss in carbonization step.

Table 4.7. Effect of the stabilization temperature and time on the textural properties of the carbonized fibers. Effect of heating rate and gas atmosphere.

	Samples	Carb yield (%)	N_2 Isotherm				CO_2 Isotherm	
			A_{BET} ($m^2 \cdot g^{-1}$)	A_t ($m^2 \cdot g^{-1}$)	Vt ($cm^3 \cdot g^{-1}$)	V_{tot} ($cm^3 \cdot g^{-1}$)	A_{DR} ($m^2 \cdot g^{-1}$)	V_{DR} ($cm^3 \cdot g^{-1}$)
	CF-0.08-200-50	30.3	851	8	0.329	0.337	1002	0.402
Heating rate	PCF-1-150-1	32.8	1403	33	0.563	0.597	1068	0.428
Heating rate	PCF-2-150-1	31.2	1476	30	0.597	0.625	1048	0.420
Heating rate	PCF-3-150-1	31.8	1429	22	0.574	0.596	969	0.388
N_2	PCF-1-200-1(N_2)	42.2	869	6	0.342	0.360	675	0.271

In addition, the N_2 adsorption-desorption isotherms (Figure 4.13a) and textural parameters (Table 4.7) of the carbonized products are practically identical and the surface chemical composition of carbonized fibers is quite similar (Table 4.8). This negligible effect of HR under these fast stabilization conditions enables the production of CFs with the same attractive properties (in terms of porosity, surface area and surface chemistry) to those found for the fibers stabilized at 1 ºC·min^{-1}, but at triple rate (or with enhanced properties and at 43 times faster respect to the conventional process without H_3PO_4). Regarding textural properties, the H_3PO_4/lignin fibers stabilized under inert conditions do not develop as high microporosity as in the case of oxidizing atmosphere (Table 4.7). By contrast, they display almost identical N_2 adsorption-desorption isotherm (Figure 4.13b) and textural parameters (Table 4.7) than the fibers without H_3PO_4 stabilized in air (CF-0.08-200-50). Accordingly, by the right choice of the stabilization atmosphere, the proposed method (electrospinning of H_3PO_4/lignin fibers) enables the preparation of CFs with the same textural properties to those obtained from pure lignin, but in much shorter time and with a considerably higher degree of functionalization.

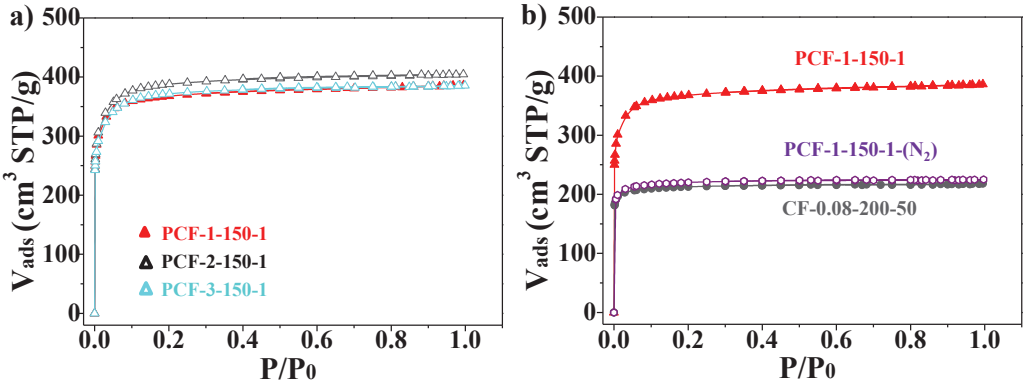

Figure 4.13. N_2 adsorption-desorption isotherms at -196 ºC of carbonized lignin/H_3PO_4 fibers stabilized under different conditions: (a) Effect of stabilization heating rate (T = 150 ºC, t = 1 h, air atmosphere); (b). Effect of stabilization atmosphere

Table 4.8. Mass surface concentration (wt%) of carbonized fibers determined by XPS. Effect of stabilization heating rate and atmosphere.

Sample		Mass surface composition by XPS (wt%)		
		C	O	P
	CF-0.08-200-36	96.01	3.99	---
Heating rate	PCF-1-150-1	88.3	8.3	1.9
	PCF-2-150-1	90.2	7.0	1.7
	PCF-3-150-1	91.7	5.9	1.8
Atmosphere	PCF-1-200-1(N_2)	90.1	6.5	3.4

Figure 4.14 shows the C1s, O1s and P2p spectra of carbonized fibers (effect on heating rate and gas atmosphere in stabilization step). Similar results have been obtained at different stabilization heating rates. After carbonization, the H_3PO_4/lignin fibers stabilized in inert atmosphere retain a larger amount of phosphorus but similar/lower oxygen than those conventionally stabilized in air. Furthermore, phosphorus species are presented as the most reduce ones, increasing the contribution of C-P-O and C_3PO groups.

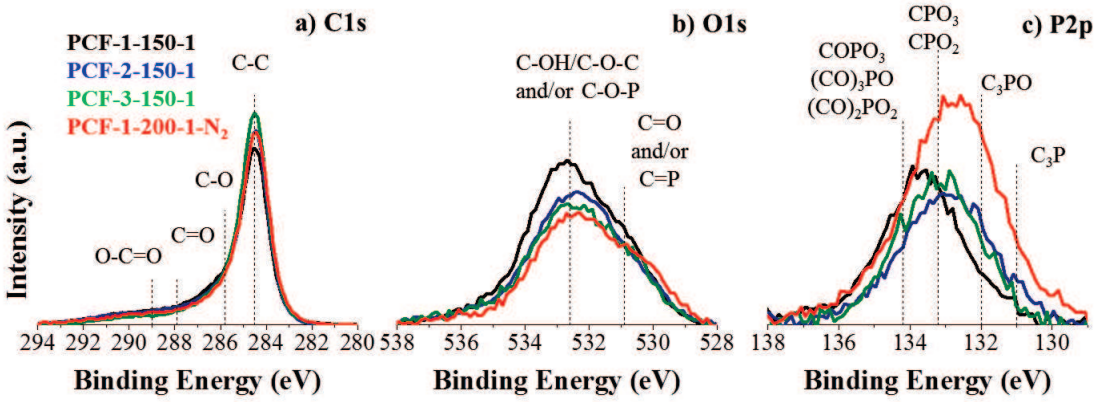

Figure 4.14. C(1s), O(1s) and P(2p) XPS spectra of phosphorus-containing carbon fibers. Effect of stabilization heating rate and atmosphere

Considering that the oxidation of lignin in air atmosphere is essential for the stabilization of pure lignin fibers, the inhibition of oxidation together with the promoted stabilization caused by phosphorus species in H_3PO_4/lignin fibers infers that their stabilization mechanism may be different. This is in line with the promoted stabilization found even under inert conditions. Instead, the formation of phosphate structures observed in this work is proposed as the predominant stabilization mechanism in H_3PO_4/lignin fibers. In this sense, the generation of phosphates (-C-O-P- bonds), which are formed in the reaction of H_3PO_4 with oxygen functionalities of lignin, may inherently suppose crosslinking reactions between lignin molecules and chains. Comparing Alcell lignin structure with the Alcell lignin structure after H_3PO_4 impregnation (see Figures 3.3 and 3.4 in Chapter 3), each molecule of H_3PO_4 may be capable of forming up to three phosphate ester bonds, thus explaining the high stabilization power of H_3PO_4 independently of the stabilization atmosphere. Nevertheless, a high enough temperature and/or long enough treatment time (at least 100 ºC for 6 h and/or HRs lower than 4 ºC·min^{-1}) may be necessary to induce enough crosslinking to permit the successful stabilization of H_3PO_4/lignin.

4.5. Conclusions

The influence of H_3PO_4 on the preparation of carbon fibers by electrospinning of Alcell lignin has been studied. The addition of H_3PO_4 to the initial solution allows the stabilization of phosphorus-lignin fibers, without fusion, in shorter times than when the fibers are stabilized without the presence of H_3PO_4, thus, the incorporation of H_3PO_4

allows faster stabilization heating rates (up to 3 ºC·min^{-1}), as well as shorter stabilization times (1 hour). The incorporation of H_3PO_4 and the formation of C-O-P groups (phosphates esters) will accelerate the cross-linking reactions in the lignin material, consequently favoring the stabilization step in the presence or absence of oxygen. An increase in oxygen content has been observed at higher temperatures and stabilization times. The carbonization step produced the development of microporosity by chemical activation with H_3PO_4, finding the highest surface area when the fibers are stabilized at 200 ºC and 6 h (1700 m^2·g^{-1}), the functionalization of the resulting CFs with P species, as well as an increase in the manufacture yields.

4.6. References

[1] N. Smolarski. Paris: Frost & Sullivan,15 (2012).

[2] J. H. Lora, W. G. Glasser. J. Polymers Environ. 10 (2002) 39-48.

[3] The International Lignin Institute, ILI. http://www.ili-lignin.com/

[4] J. M. Rosas, R. Berenguer, M. J. Valero-Romero, J. Rodríguez-Mirasol, T. Cordero, Front. Mater. 1 (2014) 1-17.

[5] A. J. Ragauskas, G. T. Beckham, M. J. Biddy, R. Chandra, F. Chen, M. F. Davis, B. H. Davison, R. A. Dixon, P. Gilna, M. Keller, P. Langan, A. K. Naskar, J. N. Saddler, T. J. Tschaplinski, G. A. Tuskan, C. E. Wyman. Science 344 (2014) 1246843.

[6] J. J. Rodríguez, T. Cordero, J. Rodríguez-Mirasol. Edition: Biofuels and Biorefineries; Eds. Z. Fang and R. L. Smith Jr; Springer, (2016). 217-262.

[7] D. A. Baker, T. G. Rials. J. Appl. Polym. Sci. 130 (2013) 713-728.

[8] E. Frank, L. M. Steudle, D. Ingildeev, J. M. Spörl, M. R. Buchmeiser. Angew. Chem. Int. Ed. Engl. 53 (2014) 5262-5298.

[9] A. Linares-Solano, D. Cazorla-Amorós. In Handbook of Advanced Ceramics; Somiya, S., Ed.; Academic Press: Elsevier Inc., 2013. p. 155-169.

[10] S. Kubo, Y. Uraki, Y. Sano. Carbon 36 (1998) 1119-1124.

[11] S. Kubo, T. Yoshida, J. F. Kadla, J. Wood Chem. Technol. 27 (2007) 257.

[12] Q. Sheng, T. Zhang, W.-X. Zhang, S. Chen, M. Mezgebe. J. Appl. Polym. Sci. 121 (2011) 989-994.

[13] J. Lin, S. Kubo, T. Yamada, K. Koda, Y. Uraki. BioResources 7 (2010) 5634-5646.

[14] M. Lallave, J. Bedia, R. Ruiz-Rosas, J. Rodríguez-Mirasol, T. Cordero, J. C. Otero, M. Márquez, A. Barrero, I. G. Loscertales, Adv. Mater. 19 (2007) 4292-4296.

[15] R. Ruiz-Rosas, J. Bedia, M. Lallave, I. G. Loscertales, A. Barrero, J. Rodríguez-Mirasol, T. Cordero. Carbon 48 (2010) 696-705.

[16] A. A. Ogale, M. Zhang, J. Jin. J. Appl. Polym. Sci. 133 (2016) 43794.

[17] Sustainability key to development of carbon fiber, 5 February 2016, http://www.materialstoday.com/carbon-fiber/news/sustainability-key-to-development-of-carbon-fiber/

[18] J. L. Braun, K. M. Holtman, J. F. Kadla. Carbon 43 (2005) 385-394.

[19] D. L. Chung. Buttherworth-Heinemann, New York, 1994

[20] E. Sjöholm, G. Gellerstedt, R. Drougge, I. Norberg (Innventia AB).. WO 2013/112100A1, 2013.

[21] O. Hosseinaei, D. P. Harper, J. J. Bozell, T. G. Rials. ACS Sustainable Chem. Eng. 4 (10) (2016) 5785–5798

[22] W. Qin, J. F. Kadla. J. Appl. Polym. Sci. 126 (2012) 203–212.

[23] Q. Sun, R. Khunsupat, K. Akato, J. Tao, N. Labbé, N. C. Gallego, J. J. Bozell, T. G. Rials, G. A. Tuskan T. J. Tschaplinski A. K. Naskar, Y. Puf, A. J. Ragauskas. Green Chem., 18 (2016) 5015-5024.

[24] S. Kubo and J. F. Kadla. J. Polym. Environ. 13(2) (2005) 97-105.

[25] S. Hu, Y.-L. Hsieh. J. Mater. Chem. A 1 (2013) 11279-11288.

[26] I. Dallmeyer, L. T. Lin, Y. Li, F. Ko, J. F. Kadla. Macromol. Mater. Eng. 298 (2013) 1–12

[27] A. Poeppel, E. Frank (Honda R&D Europe (Deutschland) GmbH. EP 2644758A1, 2013;

[28] R. Berenguer, J. Fornells, F.J. García-Mateos, M.O. Guerrero-Pérez, J. Rodríguez-Mirasol, T. Cordero. Catalysis Today 277 (2016) 266–273.

[29] F.J. García Mateos, T. Cordero-Lanzac, R. Berenguer, E. Morallón, D. Cazorla-Amorós, J. Rodríguez-Mirasol, T. Cordero. Appl. Catal. B Environ. 211 (2017) 18-30.

[30] J. Rouquerol, P. Llewellyn, F. Rouquerol. Studies in Surface Science and Catalyst. 160 (2007) 49-56.

[31] I. Brodin, M. Ernstsson, G. Gellerstedt, E. Sjöholm. Holzforschung, 66 (2012) 141–147.

[32] M. Foston , G. A. Nunnery, X. Meng, Q. Sun, F. S. Baker, A. Ragauskas. Carbon 52 (2013) 65 –73.

[33] Y. Li, D. Cui, Y. Tong, L. Xu. Int. J. Biol. Macromolec. 62 (2013) 663– 669.

[34] A. Beste, F.F: Reax. J. Phys. Chem. A 118 (2014) 803−814.

[35] A. Beste, F.F. Reax. Energy Fuels 28 (2014) 7007−7013.

[36] J. Rönnols, H. Schweinebarth, A. Jacobs, J. S. Stevanic, A.-M. Olsson, A. Reimann, F. Aldaeus. Biorefinery 30 (2015) 550-561.

[37] Z.R. Yue, W. Jiang, L. Wang, S.D. Gardner, C.U. Pittman Jr. Carbon 37 (1999) 1785–1796.

[38] P. Karhunen, P. Rummakko, J. Sipilä, G. Brunow, I. Kilpeläinen. Tetrahedron Lett. 36 (1995) 4501–4504.

[39] L. P. Christopher, B. Yao, Y. Ji. Front. Energy Res., 2 (2014) article 12, 1-13.

[40] J.M. Rosas; J. Bedia; J. Rodríguez-Mirasol; T. Cordero. Ind. Eng. Chem. Res. 47 (2008) 1288-1296.

[41] J.M. Rosas J. Bedia; J. Rodríguez-Mirasol; T. Cordero. Fuel 88 (2009) 19-26.

[42] J.M. Rosas; R. Ruiz-Rosas, J. Rodríguez-Mirasol, T. Cordero. Carbon 50 (2012) 1523-1537.

[43] J. Bedia; R. Barrionuevo; J. Rodríguez-Mirasol; T. Cordero. Appl. Catal. B: Env. 103 (2011) 302-310.

[44] S. Sen, S. Patil, D. S. Argyropoulos. Green Chem., 17 (2015) 4862-4887.

[45] G.W. Schmidl. Ph. D. Dissertation, University of Florida, Gainesville, FL, 1992.

[46] W.G. Glasser, R.K. Jain. Holzforschung 47 (1993) 225–233.

[47] A. Tejado, C. Peña, J. Labidi, J.M. Echeverria, I. Mondragon. Bioresource Technology 98 (2007) 1655–1663.

[48] A. Gregorova. Ed. A. A. Elkordy, InTech, 2013.

[49] Thermal Analysis of Polymers - Mettler Toledo Selected Applications

[50] Y. Liu , B. Bhandari, W. Zhou. J. Agric. Food Chem. 54 (2006) 5701–5717.

[51] T. Matsumoto, I. Mochida. Carbon, 30(7) (1992) 1041-6

[52] J. Drbohlav, W.T.K. Stevenson. Carbon, 33(5) (1995) 693-711.

[53] C.Q.Yang, J.R. Simms. Carbon, 31(3) (1993) 451-9.

[54] K. S. W. Sing, D. H. Everett, R. A. W. Haul, L. Moscou, R. A. Pierotti, J. Rouquérol, T. Siemieniewska. Pure Appl. Chem. 57 (1985) 603-619.

[55] A.M. Puziy, O.I. Poddubnaya, A. Martinez-Alonso, F. Suarez-García, J.M.D. Tascón, Carbon, 43 (2005) 2857-2868.

[56] A.M. Puziy, O.I. Poddubnaya, A.M. Ziatdinow, Appl. Surf. Sci. 252 (2006) 8036-8038.

[57] X. Wu, L.R. Radovic, Carbon. 44 (2006) 141–151.

[58] J. Bedia, R. Ruiz-Rosas, J. Rodríguez-Mirasol, T. Cordero. J. Catal. 271 (2010) 33-42.

[59] J.F. Moulder, W.F. Stickle, P.E. Sobol, K.D. Bomben, Handbook of X-ray Photoelectron Spectroscopy, 1995.

[60] J. Bedia, J.M. Rosas, D. Vera, J. Rodríguez-Mirasol, T. Cordero. Catal. Today 158 (2010) 89-96.

Chapter 5

Modeling the dynamic adsorption of phenol on activated carbon fibers using batch parameters

5.0. Abstract

The remediation of phenol has been studied in the 0.3-75 $mg \cdot L^{-1}$ concentration range using as adsorbent two biomass-derived activated carbon fibers prepared by electrospinning of Alcell lignin solutions. Phenol uptakes of ca. 250 and 200 $mg \cdot g^{-1}$ over the activated carbons fibers have been obtained at the highest studied concentration (75 $mg \cdot L^{-1}$), with the adsorption isotherms being fairly explained by the Langmuir model. The application of Reichemberg and the Vermeulen equations to the batch kinetics experiments allowed to estimate heterogeneous (reflecting the dependence of diffusion with the surface coverage of phenol) diffusion coefficients. A series of rapid small-scale column tests were carried out to determine the breakthrough curves under different operational conditions (temperature, phenol inlet concentration, flow rate, bed length). The suitability of the proposed adsorbent for phenol remediation was proven by the high phenol adsorption capacity along with the small height of the mass transfer zone of the columns. In this study, it has been demonstrated that, thanks to the use of the heterogeneous diffusion coefficient, the proposed mathematical approach for the numerical solution to the mass balance of the column provides a reliable description of the breakthrough profiles and the design parameters. Regeneration studies have been carried out at 25 ºC. Phenol adsorption is mainly produced in the micropores of the activated carbon fibers, being difficult to remove all phenol adsorbed at the desorption temperature studied. To obtain a high regeneration grade, desorption at higher temperatures have been carried out.

5.1. Introduction

Activated carbons are the most important commercial adsorbents. Their high surface area together with their surface chemical structure allows them to be used in a wide variety of industrial applications, some of the most important dealing with the environmental field and particularly with water purification and industrial wastewater cleaning [1,2]. In these applications adsorption with activated carbon is most commonly oriented toward the removal of species which are recognized as toxic pollutants.

Phenol and its derivatives represent an important group of refractory organic compounds present in a variety of industrial wastewaters, as refineries, pharmaceutical, petrochemicals, etc, because they are used as intermediates in the synthesis of dyes,

pesticides, explosives, insecticides, etc. Phenol worldwide production is estimated at 10 millions of tons.

Studies on adsorption of phenol and phenol derivatives with activated carbons have been reported in the literature [3–7], although the adsorption process on ultra-thin carbon fibers has not been reported yet.

The adsorption in fixed beds columns with activated carbon is one of the most efficient advanced methods to remove organic micropollutants from aqueous effluents. For envisaging their viability, it is critical to develop models and experimental procedures that could be used for accurately describing the dynamics of the pollutant adsorption and desorption under a variety of operating conditions from lab scale measurements. One of the most interesting approaches for this aim is the use of the rapid small-scale column tests (RSSCT) [8,9], which enables the design of fixed-bed activated carbon adsorbers in lab-scale that fairly reproduces the behavior of full-scale adsorbers [10]. Even so, most of the laboratories are equipped for the determination of the thermodynamic and kinetic adsorption parameters using batch experiments, and the development of analytical tools for obtaining information of adsorbent performance in batch studies that is valuable for designing fixed-bed adsorbers is still necessary. Thus, the adsorption equilibrium and kinetics for each specific contaminant must be determined, being related to the chemical surface and the porous structure of the activated carbon used as adsorbent. On the one hand, the porous structure of the adsorbent must provide a high and reachable specific surface area where the pollutant could be potentially adsorbed, but the surface chemistry of the carbon should be at least compatible with the adsorption of the pollutant in terms of polarity, acidity, aromatic degree, which can even enhance the affinity of the adsorbate for the carbon surface if adequately tuned [11-13]. On the other hand, it is necessary to use adsorbents with reduced mass transfer limitations for enhancing the bed service time. In this sense, the accessibility to the micropores, which are responsible for most of the adsorption capacity of an activated carbon, can be enhanced by the presence of mesopores [14,15], but the use of porous carbon fibers will reduce the mass transfer due to the better accessibility to the pores.

A wide diversity of carbonaceous materials has been used as precursors for activated carbon. In this chapter, the use of Alcell lignin as precursor of carbon fibers

has been proposed. Lignin is the second most abundant polymer in biomass after cellulose and it is the main co-product in the papermaking industry. The use of lignin along with the electrospinning technique allows the preparation of continuous fibers with considerably smaller diameters (micro- and submicro-scale) at room temperature, directly in a single step.

This study details the removal of phenol by adsorption on biomass-based activated carbon fibers in batch and column operation. The scope of this work is also related to validate the use of batch adsorption experiments for determining the adsorption parameters that can later be used to accurately describe the behavior of a fixed-bed adsorber. Thus, batch adsorption experiments were used to determine the phenol uptake, adsorption equilibrium as well as the kinetic parameters, which were later employed to calculate the breakthrough profiles for a fixed-bed adsorption column. A numerical solution to the phenol molar balance in the fixed-bed and carbon fiber, where a heterogeneous diffusion coefficient in the pores related to the amount of adsorbed phenol is considered has been checked for the description of the breakthrough profiles. The modeled breakthrough profiles along with the service parameters of rapid small scale column tests were confronted with those experimentally obtained at laboratory, which allowed us to clarify how batch adsorption data should be worked out for achieving a successful description of the behavior of a given adsorbent in fixed-bed adsorption.

5.2. Materials and methods.

5.2.1. Preparation of activated carbon fibers.

Alcell lignin provided by Repap Technologies Inc. (Canada) was used as the raw material. This abundant and economic residue constitutes an excellent and underutilized carbon precursor. Lignin fibers were prepared by electrospinning method using a co-axial configuration [16-20] and ethanol as solvent. Lignin fibers have been prepared in two ways in order to study the effect that phosphoric acid produces on the preparation of the fibers and in the phenol adsorption process: (i) carbonization of pure lignin fibers (CF) and (ii) chemical activation with H_3PO_4 (PCF).

For the preparation of pure lignin fibers, a solution of lignin and ethanol (in a weight ratio of 1/1) was necessary to obtain proper viscosity of the solution prior to

spinning. In the case of phosphorus-containing lignin fibers, the solution was prepared by mixing H_3PO_4 (85%)/Lignin/Ethanol with an impregnation ratio of 0.3/1/1. Both solutions were stirred overnight at 200 rpm and 60 ºC before spinning. In the electrospinning system, the ethanol and lignin solution flow rates were 0.1 and 1 $mL \cdot h^{-1}$, respectively for the preparation of lignin fibers. In case of phosphorus-lignin solution, the flow rates needed were 0.3 $mL \cdot h^{-1}$ for ethanol and 3 $mL \cdot h^{-1}$ for H_3PO_4/lignin solution. The applied electrical potential differences was 14 kV (collector potential at -7 kV and the tips at +7 kV) and 22 kV (collector at -11 kV and tip at +11 kV), respectively for the production of lignin fibers or phosphorus containing lignin fibers. The tip-to-collector distance was 25 cm.

Next to the electrospinning step, a thermal stabilization step is carried out to prevent the fusion of the fibers during carbonization. The thermal stabilization step was carried out from room temperature up to 200 ºC in a tubular furnace with an air flow of 50 $cm^3 \cdot min^{-1}$. In the case of the lignin fibers, a slow heat treatment it necessary to avoid the fusion of the fibers, being necessary a heating rate of 0.08 $ºC \cdot min^{-1}$ and keeping the final temperature for 60h. In previous chapters have been studied that the presence of phosphoric acid in the lignin fibers allows a faster stabilization step, due to the cross linking reactions being improved in its presence and by the generation of phosphates esters. By this way, a heating rate of 0.8 $ºC \cdot min^{-1}$ is used in the case of phosphorus-containing lignin fibers, and keeping the final temperature of 200 ºC for 1 h. Stabilized fibers were carbonized in the same tubular furnace up to 900 ºC with a continuous flow of N_2 (150 cm^3 STP$\cdot min^{-1}$) with a heating rate of 10 $ºC \cdot min^{-1}$, in order to obtain lignin-based carbon fibers with and without phosphorus (PCFs and CFs, respectively). Phosphorus carbon fibers (PCFs) were washed with distilled water at 60 ºC to neutral (or constant) pH and negative phosphate analysis in the eluate to remove the remaining phosphoric acid after the carbonization stage.

5.2.2. Characterization of activated carbon fibers.

The porous texture was characterized by N_2 adsorption-desorption at -196 ºC, and by CO_2 adsorption at 0 ºC performed in ASAP 2020 equipment (Micromeritics). Samples were previously outgassed at room temperature for at least 8 hours. From the N_2 isotherm, the apparent surface area (A_{BET}) was determined applying the BET equation [21]. The micropore volume (V_t) and the external surface area (A_t) were

calculated using the t-method [22] using a non-porous carbon black as standard. The narrow mesopore volume (V_{mes}) was determined by the difference between the adsorbed volume of N_2 at a relative pressure of 0.995 and the micropore volume (V_t). From the CO_2 adsorption data, the narrow micropore volume (V_{DR}) and apparent surface area (A_{DR}) were calculated using the Dubinin-Radushkevich equation [23]. Mercury porosimetry measurements were also carried out in an AUTOPORE IV instrument (Micromeritics).

The surface chemistry of the samples was analyzed by X-ray photoelectron spectroscopy (5700C model Physical Electronics) with Mg kα radiation (1253.6 eV). The maximum of the C1s peak was set to 284.5 eV and used as reference for shifting the whole spectrum. Temperature-programmed desorption (TPD) profiles were obtained in a customized quartz fixed-bed reactor placed inside an electrical furnace and coupled to a non-dispersive infrared (NDIR) gas analyzers (Siemens ULTRAMAT 22) in order to quantify CO, CO_2, (calibration error < 1%). In these experiments, c.a. 100 mg of the sample was heated from room temperature to 1000 °C at a heating rate of 10 °C·min^{-1} in nitrogen (purity 99.999%, Air Liquide) flow (200 cm^3 STP·min^{-1}).

The size, shape and texture of the carbon fibers were analyzed by scanning electron microscopy (SEM) in a JSM 6490LV JEOL instrument.

5.2.3. Adsorption equipment and procedures.

5.2.3.1. Equilibrium adsorption.

Phenol (C_6H_6O (99.5%) Sigma-Aldrich, molecular weight: 94.11 g·mol^{-1}, melting point: 40.5 ºC, solubility (20ºC): 83 g·L^{-1}, pKa: 10) solutions were prepared with distilled water at different initial concentrations (1 – 75 mg·L^{-1}). The equilibrium tests were carried out in the installation shown in Figure 5.1. Doses of 100 mg of carbon fibers were put inside a thermostatized glass column, with an internal diameter of 7 mm. The carbon fibers were packed between two slices of inert quartz wool inside the column. The ability of the phenol adsorption to be adsorbed on the quartz fibers was discarded by a previous blank experiment. To get the phenol adsorption isotherm, different initial phenol concentrations (from 2.5 to 75 mg·L^{-1}) were pumped downflow through the column at a constant flow rate of 5 mL·min^{-1}. Once the column is saturated to the initial concentration, a more concentrated solution is pumped through the column,

by this way and calculating the adsorption capacity of each equilibrium (or initial) concentration, it is possible to obtain the phenol adsorption isotherm for each carbon and temperature, which varies between 15 and 35 ºC

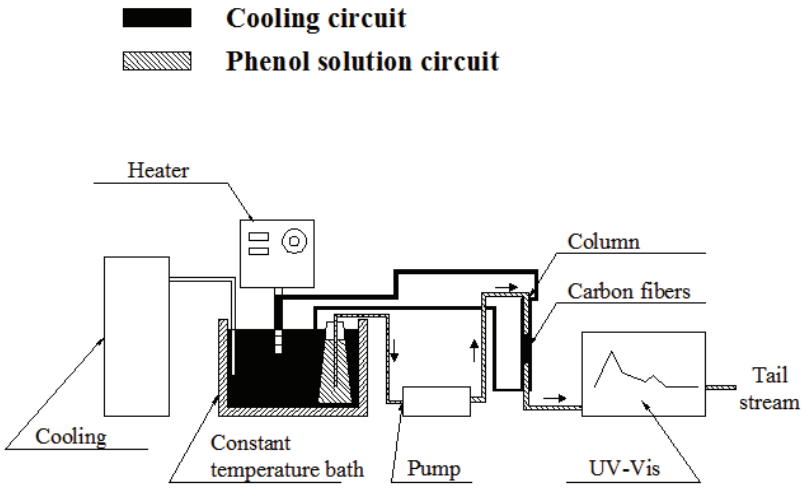

Figure 5.1. Installation used for equilibrium and column adsorption experiments

The adsorbate concentrations were determined, in continuous, by UV spectroscopy ((λ_{max}: 268 nm) with an UV-Visible (VARIANT) spectrophotometer.

The experimental data for phenol adsorption at the equilibrium were fit using the adsorption isotherm model of Langmuir:

$$q_e = \frac{q_L \cdot K_L \cdot C_e}{1 + K_L \cdot C_e} \quad (1)$$

C_e is the equilibrium concentration (mg·L^{-1}), q_e is the capacity at the equilibrium (mg·g^{-1}), K_L is the equilibrium constant (L·mg^{-1}), usually related to the enthalpy of adsorption, and q_L is the equilibrium concentration of the adsorbate (mg·g^{-1}) on the solid phase corresponding to a complete coverage (adsorption capacity for a monolayer). To obtain the K_L and q_L values we have used the Langmuir isotherm as two linear forms:

$$\frac{C_e}{q_e} = \frac{1}{K_L \cdot q_L} + \frac{C_e}{q_L} \quad (2)$$

$$\frac{1}{q_e} = \frac{1}{q_L} + \frac{1}{K_L \cdot q_L \cdot C_e} \quad (3)$$

By using Eq. 3, q_L was calculated from the slope of the linear plot of C_e/q_e vs C_e. K_L was calculated from the slope of $1/q_e$ vs. $1/C_e$ plots from Eq. 4. Only values of the slopes of the straight lines have been used with the purpose of eluding possible errors associated to the extrapolations to the origin of coordinates.

5.2.3.2. Kinetic adsorption.

For the kinetic tests, 220 mL of phenol solutions and an initial concentration of 25 mg·L^{-1} were put in contact with a 50 mg of activated carbon fibers. These experiments were carried out in the installation shown in Figure 5.2, where the initial concentration solution is pumped, at 5 mL·min^{-1}, through the UV- Vis (to obtain the concentration at each time) previously to pass through the column where the adsorption process occurs. The outside flow is guided towards the tank where it is mixed with the initial concentration, by this way the concentration is decreased at each time. To obtain a proper mixing of the solution, an agitation at 500 rpm is used. The temperatures for the experiments varied between 15 ºC and 35 ºC.

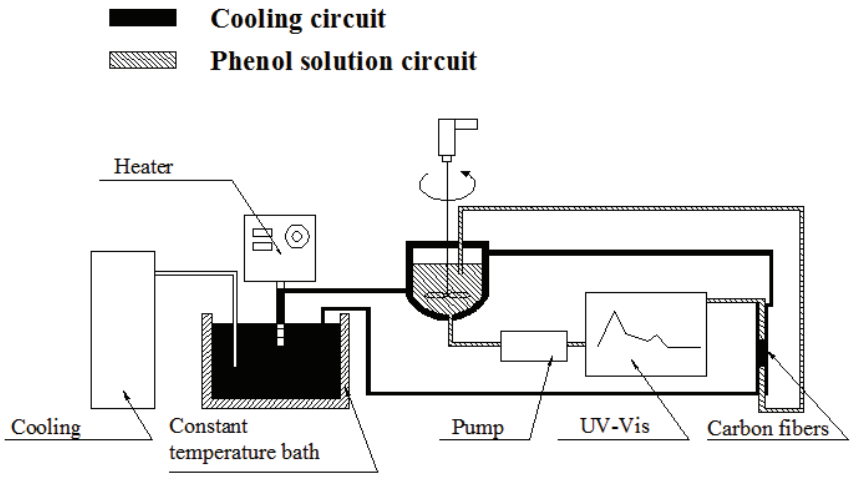

Figure 5.2. Installation used for kinetics experiments.

The adsorbed amount of phenol, q_t, in the kinetic tests was calculated as:

$$q_t = \frac{C_0 - C_t}{w} \quad (4)$$

where C_0 (mg·L^{-1}) and C_t (mg·L^{-1}) represents the initial and adsorbate concentration in the aqueous phase at time t (min), respectively, and w is the adsorbent dose (g·L^{-1}).

The kinetic experimental results have been fitted by a hyperbolic empirical equation previously used by our research group [24] for smoothing the experimental curves, which will be helpful in avoiding noise during subsequent treatment of the experimental data:

$$q_{\mathrm{t}} = \frac{a \cdot q_{\mathrm{m}} \cdot t^{m}}{1 + \mathrm{a} \cdot t^{m}} \tag{5}$$

where a, q_{m} and m are empirical parameters related to the kinetic curve shape. q_{m} represents the asymptotic q_{t} value in the function at the set experimental conditions. Therefore, q_{t} tended to q_{m} at the maximum contact time in the kinetic test.

5.2.3.2.1. Effective diffusion coefficients.

The relationship between heterogeneous diffusion coefficient (D_e) and surface coverage has been reflected by using the Vermeulen equation [25]

$$\frac{q_{\mathrm{t}}}{q_{\mathrm{e}}} = \left[1 - \exp\left(\frac{-D_{\mathrm{e}}\pi^{2}t}{R_{\mathrm{f}}^{2}}\right)\right]^{0.5} \tag{6}$$

$$D_{\mathrm{e}} = \frac{-R_{\mathrm{f}}^{2}}{\pi^{2}t}\mathrm{Ln}\left[1 - \left(\frac{q_{\mathrm{t}}}{q_{\mathrm{e}}}\right)^{2}\right] \tag{7}$$

where R_f is the radius of the carbon fiber.

The hyperbolic Eq (5) has been used for the estimation of q_{t}. Eq (5) and (7) have been employed for establishing the relationship between the diffusion coefficient and the surface coverage [26], i.e. the adsorbed amount of phenol. First, D_{e} for each t is estimated from (7), then, the obtained data were fitted to an exponential empirical equation:

$$D_{\mathrm{e}} = b \cdot \exp\left(\frac{c}{t + d}\right) \tag{8}$$

b, c, and d are empirical parameters. The hyperbolic Eq (5) can be combined with (8) in order to obtain an expression which relates the diffusion coefficient with q_{t}:

$$D_e = b \cdot \exp\left(\frac{c}{\left[\left(\frac{q_t}{a}\right)/(q_e - q_t)\right]^{1/m} + d}\right) \quad (9)$$

The fitting of D_e vs q_t was conducted using higher contact times to avoid the underestimation of D_e at low contact times, where the wetting process of the initially dry micropores hinders the mass transfer of the adsorbate through the fiber.

5.2.3.3. Column adsorption.

Column adsorption experiments were carried out in the same installation used for equilibrium test (Figure 5.1). Phenol solution was pumped downflow through the column at controlled flow rate using a peristaltic pump. The breakthrough curves were obtained by continuous monitoring of the effluent concentrations by UV spectrometry.

Before the column test was started, water (5 mL·min^{-1}) was fed to the column for 20 minutes in order to remove the trapped air and to wet the activated carbon fibers porosity. To minimize axial dispersion effects, the bed-length to fiber diameter ratio (L_b/R_f) was larger than 20 for all experiments [27]. Two different sets of experiments were carried out to separate the effects from the concentration, temperature, flow rate and bed length changes. First, a design of experiment (DOE) was used for minimizing the number of experiments required to study the influence of the temperature and the concentration, as showed in Figure 5.3, while the solution flow and the activated carbon amount were set at 5 mL·min^{-1} and 200 mg, respectively.

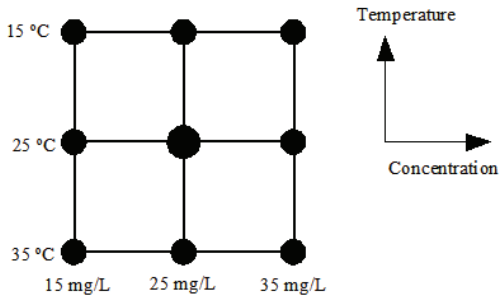

Figure 5.3. DOE of experiments for column adsorption studies

Second, tests were conducted to study the influence of the flow rate (3, 5 and 7 $mL \cdot min^{-1}$) and the bed length (170, 200 and 230 mg of activated carbon) on the adsorption kinetics at the experimental conditions of the central point of the design of experiments (DOE), i.e. 25 $mg \cdot L^{-1}$ and 25 ºC.

Regeneration process has been studied from columns saturated in the central point of the DEO. For these studies, a pure water flow rate of 5 $mL \cdot min^{-1}$ is pumped down the column and 25 ºC was set as desorption temperature. At the end desorption step, the temperature was increased up to 80 ºC at different heating rates.

5.3. Mass balance analysis.

5.3.1. Physical assumptions.

The use of two mass transfer resistance models for adsorption is generally accepted as the best choice for describing the adsorption process in activated carbons [26,28]. A model that considers external-film and diffusion mass-transfers beside axial dispersion along the bed length has been used in this chapter to calculate the breakthrough profiles under varying operation conditions. The following assumptions are made for the sake of providing an adequate description of the operation of the column:

- Gradients in the concentration profiles of the adsorbate due to radial flow are accepted as negligible. They are excluded by a suitable design of the column (R_b>20 R_f).
- The process operates under isothermal conditions, being ensured by thermostatizing the column using a recirculated water bath.
- The activated carbon fibers are treated as cylindrical and homogeneous in size and density.
- The axial velocity, v_z ($m \cdot s^{-1}$), is supposed to be constant and the occurrence of preferential paths is not considered.
- Mass transport between the bulk phase and the solid fiber is described by the external-film mass-transfer coefficient, k_f ($m \cdot s^{-1}$) [29].
- Intraparticle mass transfer mainly controlled by surface diffusion, represented by an effective diffusion coefficient D_e (m^2/s).

5.3.2. Fluid phase to external surface mass balance.

After assuming the aforementioned hypothesis, a generalized differential equation for the mass balance of the solute which flows through a fixed bed adsorber can be drawn:

$$\frac{\partial C_b}{\partial t} = -v_z \cdot \frac{\partial C_b}{\partial z} + D_z \cdot \frac{\partial^2 C_b}{\partial z^2} - k_f \cdot \frac{2}{R_p} \cdot \frac{(1-\varepsilon_b)}{\varepsilon_b} \cdot (C_b - C_f) \quad (10)$$

in this equation C_b is the bulk adsorbate concentration in the water flowing through the bed, C_f is the concentration in the fiber external surface, and D_z is the axial dispersion coefficient. The terms of Eq. (10) account the phenomenon for the transient, convective, axial dispersion and external mass transfer across the boundary layer between the bulk and the external surface of the adsorbent, respectively.

The initial conditions and the boundary conditions at the both ends of the bed are:

t=0; z=0; C_f=0; C_b=0

t=0; z>0; C_f=0

t>0; z=0; $D_z \cdot \frac{\partial C_b}{\partial z} = \frac{v_z}{\varepsilon_b} \cdot (C_b - C_i)$

t>0; z=L_b; $\frac{\partial C_b}{\partial z} = 0$

where L_b is the length of the fixed bed.

The external mass transfer coefficient as well as the axial dispersion coefficient was calculated using the following correlation [30].

$$k_f = \frac{D_l \cdot \left(2 + 0.644 \cdot Re^{1/2} \cdot Sc^{1/3}\right) \cdot \left(1 + 1.5 \cdot (1-\varepsilon_b)\right)}{2 \cdot R_f} \quad (11)$$

being Re and Sc the Reynolds and Schmidt numbers, and D_l the molecular diffusivity for the solute (i.e., phenol in water $1 \cdot 10^{-10}$ $m^2 \cdot s^{-1}$).

$$Re = \frac{2 \cdot R_b \cdot v_z \cdot \rho_l}{\mu_l \cdot \varepsilon_b} \quad (12)$$

$$Sc = \frac{\mu_l}{D_l \cdot \rho_l} \tag{13}$$

$$D_z = D_l = \frac{1.326 \cdot 10^{-4}}{\mu_l^{1.14} \cdot V_b^{0.589}} \tag{14}$$

where ρ_l (1000 kg·m^{-3}) and μ_l (0.00089 kg·m^{-1}·s^{-1}) are the density and viscosity of the fluid through the column (for Eq (14) μ_l = 0.89 cP), and V_b (108 cm^3·mol^{-1}) is the molar volume of the solute at its normal boiling point. V_b has been calculated using the estimation formula proposed by Treybal [31].

5.3.3. Mass balance within the fibers.

Since diffusion is considered to be predominant in the mass transfer through the micropore system of the activated carbon [28,32], the mass balance within a differential radial section of an adsorbent fibers can be described by the following equation:

$$\varepsilon_p \cdot \frac{\partial q_r}{\partial t} = -\frac{1}{r^2} \cdot \frac{\partial (r^2 \cdot N_s)}{\partial r} \tag{15}$$

where ε_p is the particle porosity, q_r the adsorbed concentration at the radial r position in the fiber.

The diffusion molar flux N_s can be expressed according to Fick's law:

$$N_S = -\left(D_e \cdot \frac{\partial q_r}{\partial r}\right) \tag{16}$$

As for the estimation of the effective diffusion coefficient, D_e, it has been detailed in the 5.2.3.2.1. section. Finally, the required initial and boundary conditions are:

t=0; $q_r = 0$

t>0; r=0; $\frac{\partial q_r}{\partial r} = 0$

t>0; r=R_f; $Ns = k_f \cdot (C_b - C_p)$

In the approach proposed in this work, the surface concentrations profiles along the radius of the particle are averaged by means of the assumption of parabolic

concentration profiles of the solute within the pores. This approximation has been found to be trustworthy when comparing these profiles with those obtained from the rigorous approach [33]. As a consequence of the parabolic concentration profile approximation, the mass balance equation can be simplified as follows:

$$Ns = 5 \cdot \frac{D_e}{R_f} \cdot \left(q|_{Cp} - \bar{q}\right) \tag{17}$$

$$\frac{\partial \bar{q}}{\partial t} = -\frac{15 \cdot D_e}{R_f^2} \cdot \left(q|_{Cp} - \bar{q}\right) \tag{18}$$

where $\bar{q}$ represents the mean concentration of solute adsorbed in the adsorbent particle and $q|_{Cf}$ stands for the adsorbed concentration at the solid external surface which is in equilibrium with C_f. Last, the boundary condition at the external surface of the particle requires that the diffusion flow entering must be equal to the molar transfer rate through the liquid film around the particle:

$$Ns = \frac{5 \cdot D_e}{R_f} \cdot (q|_{Cf} - \bar{q}) = k_f \cdot (C_b - C_f) \tag{19}$$

This equation allows establishing the C_f value. This is possible because the adsorbed concentration $q|_{Cf}$ may be related to the fluid phase concentration C_f in that same location, at $r=R_f$, by an adequate adsorption equilibrium isotherm.

5.4. Results and Discussion

5.4.1. Preparation and characterization of activated carbon fibres.

Table 5.1 summarizes the preparation yields, surface properties as well as the surface chemistry of the activated carbon fibers. Similar yields are obtained in the preparation of CF and PCF, being the stabilization yield higher for PCF due to the faster stabilization step, the presence of phosphorus, the less time required for the stabilization treatment and the mayor oxygen gain during the process. Little difference has been found in the carbonization yield. PCF has lower carbonization yield because of the higher development of the porosity.

High values of surface area are obtained, which constitute valuable features in an adsorption capacity. A high development of microporosity ($V_t \approx V_{DR}$) are obtained, the narrow microporosity is predominant in the CF, whereas for the PCF a widening of the

microporosity is produced due to the chemical activation with H_3PO_4. In spite of being microporous activated carbon fibers, the solute diffusion is favored by the small size of the fibers and the easy access to the pores. As it can be seen in Table 5.1, the carbon used in this work presented surface phosphorus groups. The generation of surface phosphorus groups during H_3PO_4-activation of biomass have been long proven by our research group, while their striking influence in the surface acidity, kinetic activity and oxidation resistance of the resulting activated carbons have been reported in the past [34,35].

Table 5.1. Physico-chemical properties of the activated carbon fibers

Sample	CF	PCF
Preparation yields		
Stabilization yield (%)	73.2	88.2
Carbonization yield (%)	36.9	32.9
Porous structure		
A_{BET} ($m^2 \cdot g^{-1}$)	851	1210
At ($m^2 \cdot g^{-1}$)	8	14
Vt ($cm^3 \cdot g^{-1}$)	0.33	0.47
Vmeso ($cm^3 \cdot g^{-1}$)	0.01	0.01
Vp ($cm^3 \cdot g^{-1}$)	0.34	0.48
A_{DR}^{CO2} ($m^2 \cdot g^{-1}$)	1002	1007
V_{DR}^{CO2} ($cm^3 \cdot g^{-1}$)	0.40	0.41
Surface composition (XPS)		
C (%wt)	95.9	90.5
O (%wt)	4.1	7.3
P (%wt)	--	2.2
TPD Experiments		
CO ($mg \cdot g^{-1}$)	68.3	98.5
CO_2 ($mg \cdot g^{-1}$)	12.7	15.4
R_f (μm)	0.5±0.03	1.1±0.05
ρ_f ($kg \cdot m^3$)	415	491

Figure 5.4 shows a micrograph of the CF and PCF. From these and similar micrographs, fibers sizes were estimated, the particle density (ρ_f) of the fibers measured by Hg porosimetry, both have been used as input parameters for the mass balance equations.

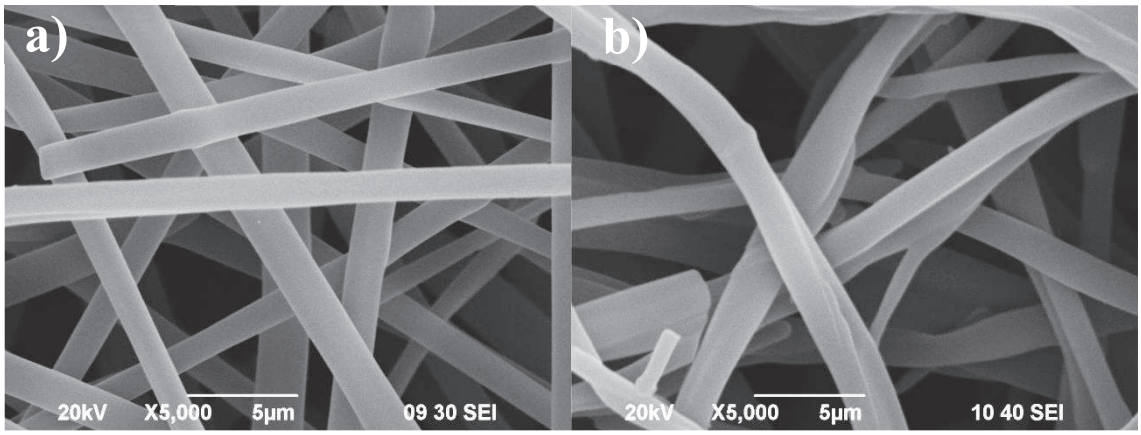

Figure 5.4. SEM micrographs of a) CF and b) PCF

5.4.2. Adsorption equilibrium.

The equilibrium adsorption isotherms of phenol solutions at 15, 25 and 35 ºC on both activated carbon fibers are shown in Figure 5.5. The isotherms resulted as type L of Giles classification [36]. The observed uptakes for an equilibrium phenol concentration of 75 $mg \cdot L^{-1}$ are close to 250 and 200 mg of phenol per gram of adsorbent, respectively for CF and PCF. These values are higher than those reported for P-containing activated carbons [6] or activated carbons prepared by physical activation with CO_2 [37], which shown uptakes of 130 and 40 $mg \cdot g^{-1}$ respectively. At higher phenol concentrations, lateral interaction between adsorbed species and/or multilayer adsorption may enhance the adsorbed amount by the activated carbon. The increase on adsorption temperature produces a decrease in the phenol adsorbed amount, which suggests the exothermic nature of the adsorption process. The values of K_L, q_L and R^2 (determination coefficient) are shown in Table 5.2.

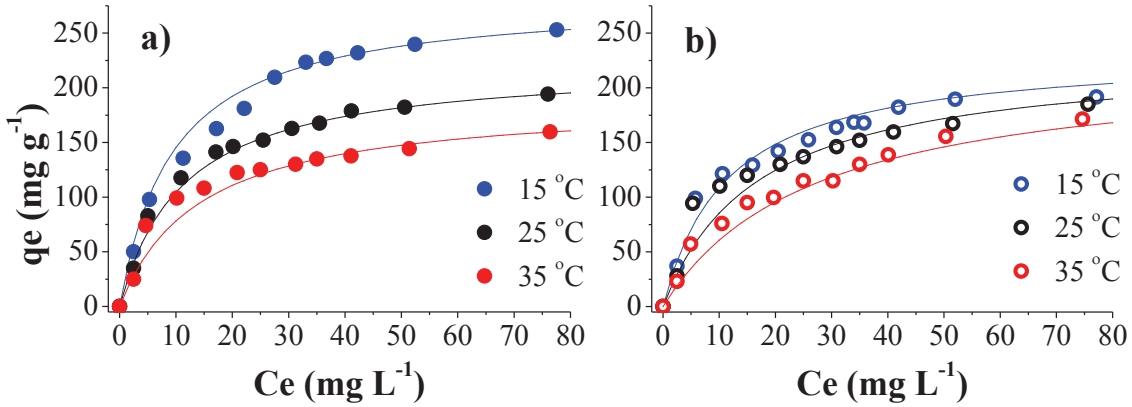

Figure 5.5. Phenol adsorption isotherm on a) CF and b) PCF at different temperatures. (C_0 = 0-75 mg·L^{-1}). Experimental data (dots) and Langmuir fits (curves).

In spite of having PCF the highest surface area, higher phenol adsorption capacities are found for CF. As was said before, the utilization of H_3PO_4 for preparing activated carbons produce activated carbons with acid character (due to the P retain in the carbon surface). There are some works [6,38] where the phenol adsorption is relate to the surface area and porosity, although the surface chemistry of the adsorbent plays a crucial role on the adsorption of different compounds, where the hydrophobicity and basic oxygen groups, as CF presents, are beneficial for phenol adsorption.

The free energy (ΔG), enthalpy (ΔH) and entropy (ΔS) changes were calculated by the following equations: the free energy change related to the equilibrium constant (Eq . 20), the Van't Hoff's (Eq. 21) for the enthalpy change, and the Gibbs-Helmholtz's (Eq. 22) to estimate the entropy change. The values obtained are showed in Table 5.2.

$$\Delta G = -RT \ln K_L \tag{20}$$

$$\frac{\partial \ln K_L}{\partial T} = \frac{\Delta H}{R \cdot T^2} \Rightarrow \ln K_L = \ln K_{L0} - \frac{\Delta H}{R \cdot T} \tag{21}$$

$$\Delta S = \frac{\Delta H - \Delta G}{T} \tag{22}$$

in these equations, R is the gas constant (8.31 J·mol^{-1}·K^{-1}), T is the absolute temperature (K), and K_{L0} is the pre-exponential factor, i.e., the value of K_L when T tends to infinite. The negative values of ΔG from Eq. (20) indicate the spontaneity of the adsorption process. The average molar values of ΔG are quite influenced by the temperature.

Table 5.2. Parameters obtained from the equilibrium / thermodynamics study.

Sample		**CF**			**PCF**	
Temperature (ºC)	**15**	**25**	**35**	**15**	**25**	**35**
Langmuir isotherm parameters						
q_L **(mg·g^{-1})**	283.3	222.9	189.2	221.1	229.9	214.0
K_L **(L·mg^{-1})**	0.106	0.088	0.071	0.092	0.059	0.034
R^2	0.997	0.996	0.994	0.996	0.996	0.995
Thermodynamic parameters						
AG (kJ·mol^{-1})	-22.0	-22.4	-22.5	-21.7	-21.4	-20.7
AS (J·K^{-1}·mol^{-1})	25.0	25.3	25.0	-41.5	-41.3	-41.5
AH (kJ·mol^{-1})		-14.8			-36.3	
K_{L0} **(L·mg^{-1})**		20.5			0.0023	
R^2		0.998			0.997	

The low negative value of the enthalpy from the slope in the linear regression of Eq. (21) confirms the exothermic nature of the adsorption process. Positive values of the adsorption entropy changes for CF adsorbent are coherent with a decrease of the freedom of the molecules in the fluid phase when they are adsorbed. Negative values, for PCF, of adsorption entropy indicate changes in the adsorbent surface when phenol is adsorbed.

5.4.3. Kinetic study.

The kinetic results obtained at three temperatures are shown in Figure 5.6. It is clear that the adsorption yield decreases with increasing temperature, being higher the phenol adsorption capacities for CF due to the basic surface character. It should be noted that the fast adsorption rate is observed on both activated carbon fibers, getting the equilibrium in 30 or 50 minutes for CF and PCF, respectively. For PCF the equilibrium is reached at lower times than for CF. The wide microporosity, produced during the activation step by H_3PO_4, favors liquid phase adsorption and higher diffusion coefficients are found for phenol adsorption on PCF (see Figure 5.7). The small carbon fibers sizes and the pores accessibility, favors the phenol diffusion into the pores to be adsorbed, which is an important advantage of carbon fibers in adsorption studies [11].

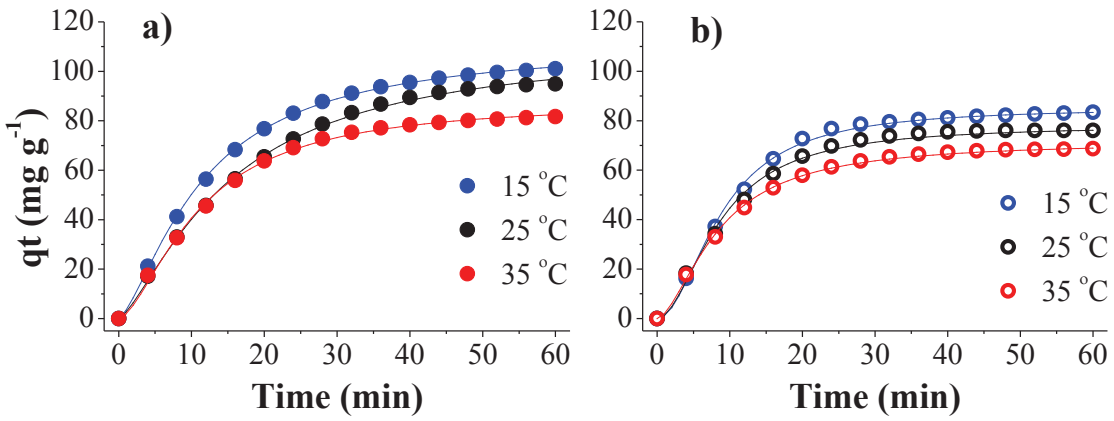

Figure 5.6. Kinetic curves of phenol adsorption on a) CF and b) PCF at different temperatures. (C_0 = 25 mg·L^{-1}; W = 50 mg). Experimental data (dots) and hyperbolic fittings (curves).

Table 5.3 compiles the fitting coefficients for kinetics studies. The hyperbolic equation proposed correctly fits the experimental kinetics data. The empirical kinetic parameter q_m (related to the equilibrium capacity when the concentration C_t tends to infite) is very similar to the equilibrium capacity q_e calculated by Langmuir equation at C_t equilibrium concentration. These values are in accordance with the above explained, i.e. higher adsorption capacities values for lower temperatures and higher values for CF regarding to PCF.

Table 5.3. Parameters obtained from the kinetic studies.

	CF			PCF		
Temperature (ºC)	15	25	35	15	25	35
Hyperbolic equation						
a **(s^{-1})**	0.030	0.024	0.022	0.014	0.018	0.029
q_m **(mg g^{-1})**	111	109	88	86	78	72
m	1.43	1.38	1.59	1.96	1.87	1.66
R^2	0.9907	0.9910	0.9887			
Heterogeneous diffusion coefficient						
b **x 10^{18} (m^2 s^{-1})**	2.0	2.4	2.3	3.5	4.1	3.7
c **(s)**	53461	48947	52280	112747	97720	95764
d **(s)**	25208	31023	24701	29564	26858	26507
R^2	0.999	0.999	0.998	0.998	0.999	0.997

Figure 5.7 presents the relationship between the effective diffusion coefficient and the adsorbed amount of phenol (i.e. phenol surface coverage) for a given initial concentration (25 mg·L^{-1}) and different temperatures. As expected the calculated curves corroborate that an increase in the temperature of the kinetic adsorption experiment are

answered by an overall increase in the value of the diffusion coefficients. As for the dependence of diffusion with the adsorbed amount of phenol, D_e values decrease with the surface coverage (or time) due to the depletion of the available free adsorption sites that are necessary to allocate the adsorbed phenol molecules that are diffusing over the surface. This decrease of the diffusion coefficient can also be explained in terms of the wide pore structure distribution of the pore network and the heterogeneity of the surface chemistry of the activated carbon, which will render not only different energies of interaction between the adsorbate and the adsorbent depending on the surface coverage of phenol over the carbon surface, but also a different mobility of the adsorbed phenol molecule on the pore network. Thus, as the adsorption phenomenon proceeds (long times), phenol will be adsorbed first in the more energetically favorable and accessible adsorption sites at a fast rate. When the most favored sites are fully covered by phenol moleucles, the mass transport becomes progressively controlled by a slower diffusion of the phenol into the less energetically favorable and isolated adsorption sites. Higher diffusion coefficients were found when phenol is adsorbed on PCF, the wide porosity and the high fibers sizes (1.1 μm) favors the phenol rate adsorption on the carbon. Diffusion coefficients are found to be almost constant for all the surface coverage, decreasing slightly when the equilibrium is reached ($q_t/q_e \approx 1$). These constant diffusion coefficients will be explain by the adsorbate used for the adsorption. The ultra-fine activated carbon fibers and the accessibility of the pores, improve phenol adsorption process, because the phenol molecule has to move less distance until reaching the adsorption center.

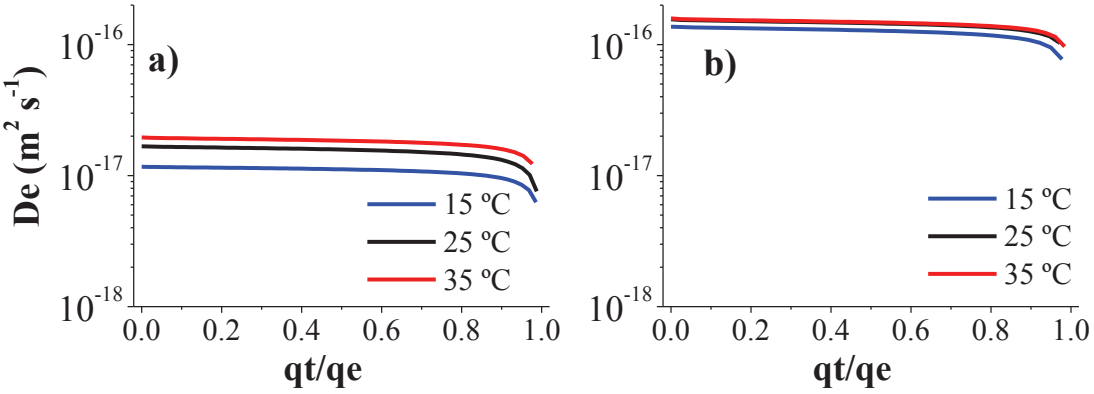

Figure 5.7. Diffusivity coefficients of phenol adsorption on a) CF and b) PCF at different temperatures.

5.4.4. Column adsorption studies.

It is important to note that the kinetic and equilibrium adsorption parameters obtained in discontinuous system, i.e. adsorption isotherm constants and the effective diffusion coefficient, have been used for solving the mass balance equations that allow the prediction of the breakthrough profile. Note that the solution of these equations allows the determination of the time for the breakthrough appearance or bed service time (BST), which is stablished as the time at what the outlet concentration reach the $C/C_i = 0.05$ value, and the shape of the breakthrough profile, which is related to the height of the mass transfer zone (H_{MTZ}). These are actually critical parameters for determining the operation and the dynamic response of an activated carbon when used as adsorbent for an adsorption bed that cannot be directly determined from batch adsorption experiments. In simple terms, the breakthrough time is proportional to the capacity of the adsorbent, while inversely related to the H_{MTZ} value. For a given inlet concentration, the adsorption capacity of the adsorbent can be determined if its adsorption isotherm is established. Contrariwise, the height of mass transfer zone does not keep a direct relationship to any specific kinetic parameter, and it results from the interaction between the hydrodynamics of the experimental set-up and the surface properties (surface chemistry, pore structure) of the adsorbent [39]. Since breakthrough time and therefore bed service time are dependent on both H_{MTZ} and adsorption capacity, and there is no direct relationship between H_{MTZ} and the kinetic and thermodynamic batch adsorption parameters, the numerical solving of the mass balance equations detailed here is proposed for predicting them.

The validity of some of the assumptions made in section 5.3.1 have been checked by analyzing the dimensionless numbers that dictate the dominating processes during the operation of the fixed bed adsorber. Table 5.4 compiles the experimental values of both adsorbents and the bed that have been used for this purpose, along with the values of the mentioned dimensionless numbers concerned. High values of bed porosities (ε_b) are found, being 0.784 and 0.817 for CF and PCF respectively. The Reynolds values (Re) between 10 and 27 indicate that a laminar flow regime is governing in the fixed bed, and that liquid flow through the column is mainly produced by convection, hence the Schmidt number (Sc) was lower than 0.15 for all the column experiments, indicating the low viscosity and high difussivity. Values of the Biot

number (Bi) and the mass transfer coefficient (k_f) are also high, pointing out the absence of limited mass transfer through the stationary layer of liquid around the particles of the adsorbent.

Table 5.4. Operation variables for the adsorption column process.

	T (ºC)	W (mg)	Q (mL·min^{-1})	C_i (mg·L^{-1})	L_b (cm)	Re	Sc	Bi	k_f (m·s^{-1})
CF	15	200	5	15.3	5.8	18.2	0.05	601	53
	15	200	5	25.7	5.8	16.8	0.05	733	53
	15	200	5	34.9	5.8	16.1	0.025	1672	106
	25	200	5	14.7	5.8	19.6	0.05	766	53
	25	200	5	25.4	5.8	19.6	0.033	1365	80
	25	200	5	34.1	5.8	19.8	0.11	456	24
	25	200	2.8	23.3	5.8	10.5	0.10	442	27
	25	200	7	23.3	5.8	27.3	0.02	2208	133
	25	170	5	23.2	4.9	17.5	0.067	663	40
	25	230	5	24.0	6.7	17.5	0.067	669	40
	35	200	5	12.9	5.8	17.4	0.1	459	27
	35	200	5	25.7	5.8	17.4	0.1	543	27
	35	200	5	34.9	5.8	17.4	0.1	595	27
PCF	15	200	5	15.9	5.8	18.5	0.03	974	35
	15	200	5	25.8	5.8	18.5	0.01	3818	116
	15	200	5	35.6	5.8	18.5	0.02	2167	58
	25	200	5	14.3	5.8	18.5	0.1	385	12
	25	200	5	25.3	5.8	19.0	0.033	1324	35
	25	200	5	37.1	5.8	19.0	0.033	1486	35
	25	200	2.8	23.3	5.8	13.0	0.033	1292	35
	25	200	7	24.0	5.8	26.0	0.02	2173	58
	25	170	5	23.2	4.9	18.6	0.02	2153	58
	25	230	5	24.0	6.6	18.6	0.033	1307	35
	35	200	5	14.8	5.8	18.5	0.1	495	12
	35	200	5	24.4	5.8	18.5	0.05	1068	23
	35	200	5	34.9	5.8	18.5	0.02	3433	70

Figures 5.8 and 5.9 show the breakthrough profiles obtained for the phenol adsorption in the activated carbon fixed-bed under different operating conditions for CF and PCF. All the experimental breakthrough curves follow the typical S-shaped curve for column operation with favorable adsorption isotherms [33]. In all the curves, the experimental data are identified by symbols, whereas the breakthrough curves obtained

from the solution of the numerical model with heterogeneous diffusion coefficient proposed in this work have been represented by continuous lines. The profiles are reported in terms of time for easing the comparison among results obtained using different experimental conditions (flow rate, inlet concentration, temperature…).

It can be observed in Figures 5.8 and 5.9 how the thermodynamic and kinetic parameters obtained and then introduced in the numerical solution proposed in this work for the mass balance to the fixed-bed adsorber can satisfactorily explain the experimental curves when the heterogeneous effective diffusion coefficient approach is considered.

5.4.4.1. Effect of inlet concentration and temperature.

Figure 5.8 shows the breakthrough curves for the phenol adsorption at different temperatures and concentrations for both activated carbon fibers (Figure 5.8; variation of inlet concentration on CF a) 15 ºC, b) 25 ºC) c) 35 ºC and PCF: d)15 ºC, e) 25 ºC and f) 35 ºC), in all cases the inlet concentration was kept at 15, 25 or 35 $mg \cdot L^{-1}$, the flow rate at 5 $mL \cdot min^{-1}$ and a bed of 200 mg of activated carbon fibers were used. It can be seen that the breakthrough time ($C/C_i \approx 0.05$) decreased when temperature increases at each inlet concentration, while the saturation times ($C/C_i \approx 0.99$) were higher for those runs performed at lower temperature, and the height of the mass transfer zone decreased a 40 and 15 %, respectively for CF and PCF, when raising the temperature from 15 to 35º C. These modifications are reflecting the higher values for the diffusion coefficients and the lower phenol adsorption capacities at higher temperatures that were already found in the batch study.

The effect of the inlet concentration of phenol on the breakthrough profiles has also been analyzed and featured in Figure 5.8. Again, the expected behavior is found when concentration decreases, finding a great increase in the breakthrough time, a lower adsorption capacity and similar value of H_{MTZ} at each temperature.

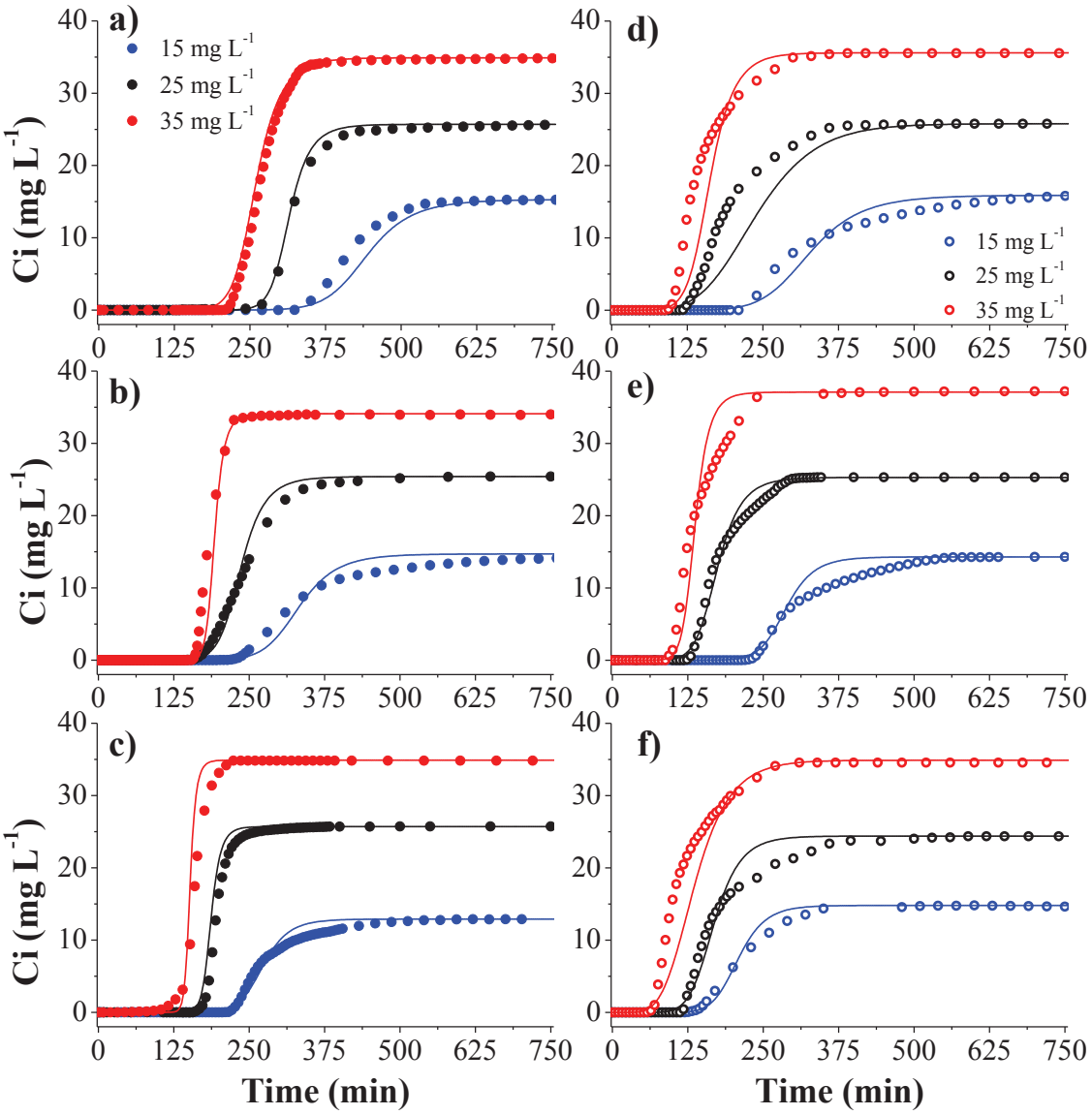

Figure 5.8. Breakthrough curves at different temperatures and inlet concentration. CF; a) 15 ºC, b) 25 ºC, c) 35 ºC and PCF; d) 15 ºC, e) 25 ºC, f) 35 ºC. (W: 200 mg, Ci: 15-35 mg·L^{-1}, Q: 5 mL·min^{-1})

5.4.4.2. Effect of amount of activated carbon fibers and flow rate.

The effect of axial dispersion was analyzed by carrying out experiments at 25 ºC, phenol inlet concentration of 25 mg·L^{-1}, flow rate of 5 mL·min^{-1} and different bed lengths (4.9-6.7 cm). As observed in Figure 5.9, the breakthrough time is affected by the amount of activated carbon (Figure 5.9 a) and c)) for CF and PCF, repectively). The behavior of the breakthrough profile at different lengths, which shows a similar shape no matter the chosen bed length, leads to the conclusion that it does not exist any back mixing or axial dispersion problem in the column. This is confirmed by the absence of any relevant difference when the mass balance in 5.3.2. was solved without

including the axial dispersion term. Therefore, and under the operating conditions selected for this work, the mass balance to the small column can be solved without considering axial dispersion and external mass transfer control, and consequently the numerical solution can be simplified reflecting these conclusions.

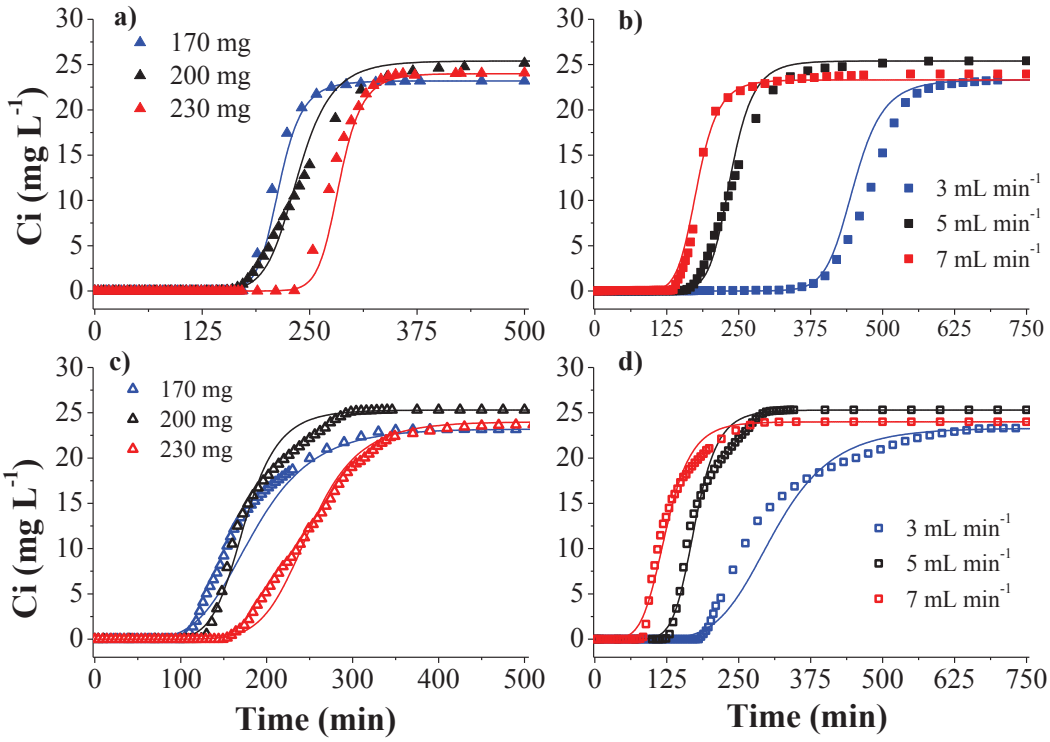

Figure 5.9. Breakthrough curves at different amount of carbon fibers and flow rate. CF; a) amount of carbon fibers, b) flow rate and PCF; c) amount of carbon fibers d) flow rate. (For a) and c): Ci: 25 mg·L^{-1}, Q: 5 mL·min^{-1}, T: 25 ºC; b) and d) Ci: 25 mg·L^{-1}, W: 200 mg, T: 25 ºC)

The experiments displayed in Figure 5.9 b) and d) were conducted at variable flow rates to establish the possible influence of mass transfer in the film of stationary liquid that surrounds the particle. The rest of the experimental conditions were those used for the central point, i.e. 25 ºC, 25 mg·L^{-1} of phenol at the column inlet and 200 mg of activated carbon. It was found that the variation of the flow rate has a negligible impact on the shape of the breakthrough curves, confirming the absence of external mass transfer control, as predicted from the Biot numbers in Table 5.4. This finding was further corroborated by simply solving the mass balance to the fixed bed and the carbon fiber proposed in 5.3.2. and 5.3.3. sections while removing the consideration of external mass transfer (thus, $C_f = C_b$). The obtained profile was identical to that obtained when the mass balance was solved upon consideration of external mass transfer in the liquid film.

5.4.4.3. Design parameters and models comparison.

There are only few samples in the literature about using the adsorption parameters obtained from the batch studies in order to estimate the fixed bed behavior [26,32] of an adsorbent. In this study, the numerical solution of the mass balances have been employed for the calculus of the breakthrough profiles using the adsorption and the kinetic parameters determined in a discontinous study. The resulting breakthrough profiles for each model have been shown along with the experimental data in Figures 5.8 and 5.9. Furthermore, Table 5.5 and 5.6 compiles the experimental and the estimated design parameters beside the conditions used in the given experiment for CF and PCF respectively.

It can be seen that the phenol adsorptivities calculated using the mass balance procedure (q_{cal}; $C/C_i \approx 1$) are very close to those obtained from the experimental breakthrough profiles (q_{exp}; $C/C_i \approx 0.99$). Similarly, H_{MTZ} and BST are accurately predicted for all the tested experimental conditions. Furthermore, the high values of r^2 indicate that the proposed model can reproduce fairly well not only BST and H_{MTZ}, but also most of the experimental breakthrough profile.

Table 5.5. Experimental and design parameters for breakthrough curves on CF

T (ºC)	*W* (mg)	*Q* (mL min^{-1})	C_i (mg L^{-1})	*EXPERIMENTAL*			*MASS BALANCE*			
				q_{exp} (mg g^{-1})	*BST* (min)	H_{MTZ} (cm)	q_{cal} (mg g^{-1})	*BST* (min)	H_{MTZ} (cm)	R^2
15	200	5	15.3	162	312	1.74	172	350	1.34	0.981
15	200	5	25.6	211	248	2.00	204	270	2.03	0.988
15	200	5	34.8	238	223	1.18	230	210	1.27	0.993
25	200	5	14.7	136	241	2.17	125	253	1.53	0.985
25	200	5	25.4	161	177	1.88	152	187	1.39	0.990
25	200	5	33.9	165	164	0.85	166	172	0.69	0.979
25	200	3	23.3	167	337	1.93	159	383	1.01	0.989
25	200	7	24.0	162	144	1.59	152	133	1.67	0.994
25	170	5	23.2	145	157	1.31	148	178	0.89	0.992
25	230	5	24.0	145	274	0.62	150	250	0.91	0.991
35	200	5	12.9	94	225	1.42	89	219	1.48	0.990
35	200	5	25.7	128	175	0.94	121	166	0.93	0.992
35	200	5	34.9	138	128	0.79	133	139	0.78	0.991

Table 5.6. Experimental and design parameters for breakthrough curves on PCF

T (ºC)	*W* (mg)	*Q* (mL min^{-1})	C_i (mg L^{-1})	*EXPERIMENTAL*			*MASS BALANCE*			
				q_{exp} (mg g^{-1})	*BST* (min)	H_{MTZ} (cm)	q_{cal} (mg g^{-1})	*BST* (min)	H_{MTZ} (cm)	R^2
15	200	5	15.9	140	231	2.33	134	227	1.98	0.981
15	200	5	25.8	163	129	2.30	160	130	2.86	0.980
15	200	5	35.6	140	104	2.13	147	113	1.98	0.990
25	200	5	14.3	112	239	1.54	104	193	2.02	0.985
25	200	5	25.3	117	134	1.70	113	125	1.87	0.995
25	200	5	37.0	136	101	2.12	129	108	1.4	0.994
25	200	3	25.3	105	196	2.23	113	196	2.41	0.992
25	200	7	24.0	110	87	2.09	106	72	2.74	0.996
25	170	5	23.2	115	120	2.01	113	121	2.10	0.989
25	230	5	24.0	120	180	1.80	122	185	1.98	0.991
35	200	5	14.8	99	188	1.84	78	153	1.72	0.992
35	200	5	24.4	119	120	2.03	105	116	2.02	0.989
35	200	5	34.9	111	72	2.64	124	75	2.86	0.987

5.4.4.4. Regeneration studies.

A very important aspect to study in adsorption processes is the possibility of regenerating the adsorbent to be used in successive adsorptions cycles. For this purpose, phenol regeneration studies have been carried out on the two adsorbents used and their textural properties have been analyzed by N_2 adsorption at -196 ºC. A desorption temperature of 25 °C and a flow rate of water of 5 mL·min^{-1} were set as regeneration parameters.

Figure 5.10 presents the cycles of phenol adsorption-regeneration-adsorption on CF(a) and PCF (b). In both cases the amount of phenol after adsorption (first (1st) or second one (2nd)) is the same, referring with the adsorption capacity of the adsorbents. During regeneration steps, different amount of phenol are removed from CF and PCF. For CF, only 15.4 % of phenol is removed during the regeneration while for PCF the phenol desorbed increase to 53.0 %. This difference will be explained for the porosity of the adsorbents and for the surface chemistry. In section 5.4.2. was discussed the variation of phenol adsorption capacity on CF and PCF, being higher the phenol adsorption capacity for CF. This indicates more attraction of phenol molecules with the surface of CF, making it more difficult the regeneration of CF carbon fibers. Also, CF presents narrower microporosity than PCF, being the adsorption forces higher in the

case of CF. To obtain a complete regeneration of activated carbon, advanced regeneration processes, such as increasing desorption temperature or phenol electro-oxidation [40,41], may be necessary.

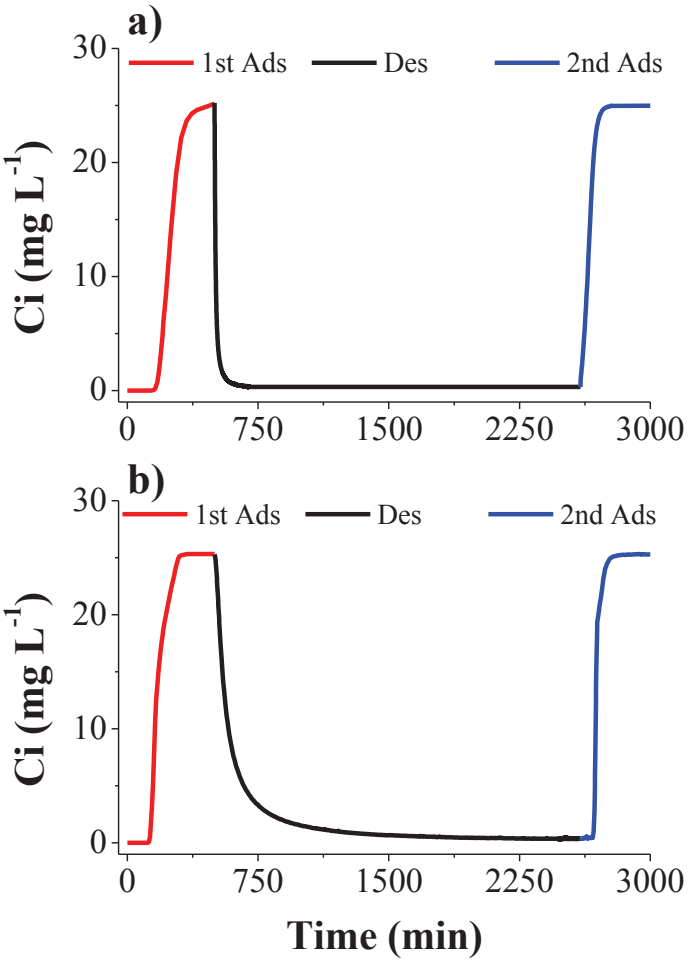

Figure 5.10. Cycles of Adsorption-desorption-adsorption on: a) CF and b) PCF.

Figure 5.11 shows the adsorption isotherm of N_2 at -196 0 ºC in different stages of the phenol adsorption-regeneration process. CF and PCF are referred to the fresh activated carbon, -S is added when the samples are saturated with phenol and when the carbon fibers are regenerated –R is added after the initial nomenclature.

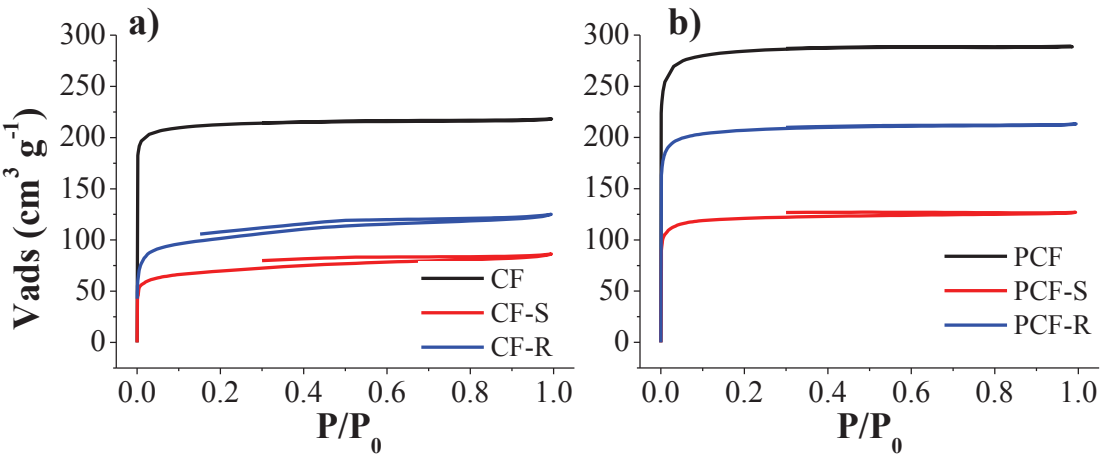

Figure 5.11. N_2 adsorption-desorption isotherms of fresh, saturated (-S) and regenerated (-R) activated carbon fibers. a) CF and b) PCF.

A decrease in the gas volume adsorbed is shown when the samples are saturated with phenol, due to the phenol occluded in the porosity. When the sample regenerated is analyzed, an increase on the volume adsorbed is produced but it does not recover the same volume that the fresh samples, indicating that phenol are presented in the porous structure after regeneration.

It is possible to calculate the area of the phenol molecules adsorbed and regenerated. Knowing the amount of phenol adsorbed, or desorbed, per gram of activated carbon fibers and the area of a phenol molecule (0.47 x 0.43 nm), the area occupied by phenol molecules will be calculated by the following equation, which is multiplied by 2 because of the consideration of both sides of phenol molecule:

$$A_P = 2 \cdot \frac{q_p \cdot N_A \cdot \alpha_p}{Mw_p} \qquad (23)$$

where A_p is the area occupied by phenol molecules ($m^2 \cdot g^{-1}$), q_p is the amount of adsorbed or desorbed phenol per gram of carbon fibers ($g_p \cdot g^{-1}$) for each carbon fibers, Mw_p is the molecular weight of phenol (94.11 $g \cdot mol^{-1}$), N_A is the Avogadro number and α_p is the area of one phenol molecule ($2.451 \cdot 10^{-19}$ $m^2 \cdot molecule^{-1}$).

By this way, it is possible to calculate the free surface area (A_f $m^2 \cdot g^{-1}$) present in the carbon fibers in each cycle. On one hand, for saturated samples, A_f will be calculated

subtracting A_p to the surface area calculated by the BET method for fresh carbon fibers. On the other hand, the area desorbed for phenol during the regeneration will be added to the A_f, corresponding to the saturated samples, to calculate the free surface area after regeneration. This free surface should be similar to the one calculated by the BET method in each stage.

Table 5.7 shows the parameters calculated from the regeneration process. If the A_f is compared with A_{BET} in each case, we will see that for CF fibers, the free area calculated matches with the A_{BET} in each cycle. On the contrary, for PCF fibers only A_f matchs with A_{BET} after regeneration.

Table 5.7. Parameters calculated from the regeneration process.

	q_p	A_p	A_f	A_{BET}
CF	---	---	---	850
CF-S	0.162	505	345	300
CF-R	0.025	78	423	389
PCF	---	---	---	1145
PCF-S	0.117	367	778	484
PCF-R	0.062	195	972	834

Regeneration at higher temperatures (80 ºC) has been studied after regeneration at adsorption temperature (25 ºC). The influence of the water heating rate (1.5, 2.5 and 4 ºC min^{-1}) is shown in Figure 5.12. Higher outlet phenol concentration have been obtained for CF, what can be associated to the higher residual phenol content on the carbon fibers after regeneration at 25 ºC. The lower heating rate the higher amount of phenol regenerated (area below the profile), this behavior is due to the longer desorption time at higher temperatures.

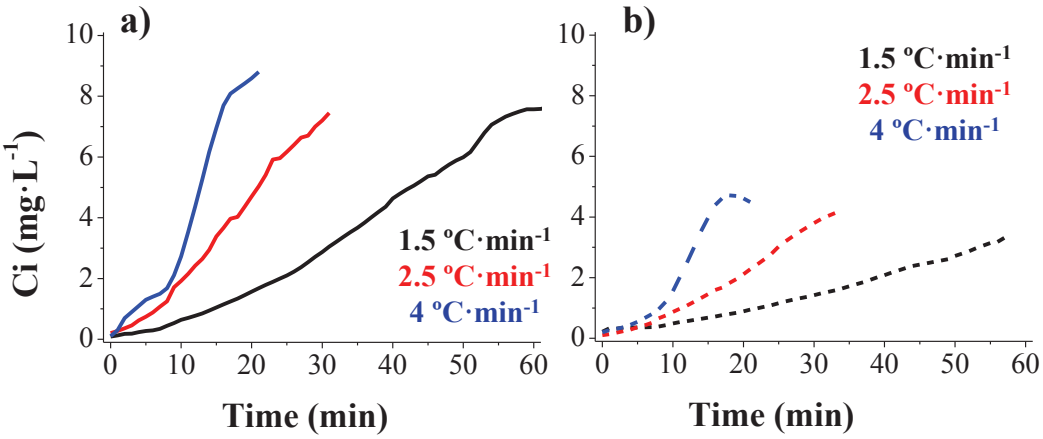

Figure 5.2. Effect of the water heating rate until 80 ºC in regeneration process.

5.5. Conclusions

Activated carbon fibers have been prepared by electrospinning of Alcell lignin. The effect of the addition to the initial solution H_3PO_4 has been studied on the porosity, chemical composition and phenol adsorption. Submicron diameter carbon fibers have been obtained (from 0.4 to 3 μm) with high development of the microporosity, getting high surfaces areas of 850 and 1150 $m^2 \cdot g^{-1}$ and different basic-acid properties. Adsorption of phenol in the range concentrations from 0.3 to 75 $mg \cdot L^{-1}$ and temperatures from 15 to 35º C has been studied using discontinuous batch experiments. The adsorption isotherms are well described using the Langmuir model, obtaining adsorption capacities of 250 and 200 $mg \cdot g^{-1}$, being the highest phenol adsorption capacity for CF. Kinetic studies in discontinuous experiments have been used for the estimation of effective diffusion coefficients. An empirical equation has been drawn to relate the heterogeneous diffusion coefficient with the surface coverage of phenol. The effectiveness of the prepared carbon fibers for phenol removal has also been studied using rapid small-scale column experiments. The activated carbon showed high bed service times and reduced heights of the mass transfer zone thanks to the favorable adsorption of phenol on its surface. The effects of operational variables (temperature, flow rates, fixed-bed length and inlet concentration) have been analyzed using a design of experiments.

The most important finding in this study was the possibility of accurately modeling the breakthrough behavior of the fixed-bed adsorber by using the kinetic and

thermodynamic parameters obtained from the discontinuous experiments. Using the adequate experimental and boundary conditions, mathematical tools, model considerations and a diffusion coefficient related to the surface coverage of the pollutant, it is possible to attain from simple batch experiments a precise knowledge of the performance of a given adsorbent in column adsorption, which allows an accurate prediction of the breakthrough profile, BST and H_{MTZ} than the adsorbent would show if it is used in lab-scale column tests.

5.6. References

[1] R.C. Bansal, J.B. Donnet, F. Stoeckli. Active carbon. New York: Marcel Dekker; 1988 [Chapter 2].

[2] H. Jankowska, A. Swiatkowski, J. Choma. Active carbon. Chinchester: Ellis Horwood; 1991.

[3] R.W. Coughlin, R.S. Erza, R.N. Tan RN. J Colloid Interface Sci 28 (1968) 386–96.

[4] O.P. Mahajan, C. Moreno-Castilla, P.L. Walker Jr. Sep Sci Technol 15 (1980)1733–52.

[5] J.S. Mattson, H.B. Mark Jr, M.D. Malbin, W.J. Weber, J.C. Crittenden. J Colloid Sci. 31 (1969) 116–130.

[6] E. Gonzalez-Serrano, T. Cordero, J. Rodriguez-Mirasol, L. Cotoruelo, J.J. Rodríguez. Water Research. 38 (2004) 3043–3050.

[7] L.M. Cotoruelo, M.D. Marqués, F.J. Díaz, J. Rodríguez-Mirasol, T. Cordero. Chem Eng Journal. 184 (2012) 176-183.

[8] J.C. Crittenden, J.K. Berrigan, D.W. Hand. J. Water Pollut. Control Fed. 58 (4) (1986) 312–319.

[9] J.C. Crittenden, J.K. Berrigan, D.W. Hand, B. Lykins. J. Environ. Eng.113 (2) (1987) 243–259.

[10] L. Cummings, R.S. Summers. J. Am. Water Works Assn. 86(6) (1994) 88-97.

[11] C. Moreno-Castilla, C. Carbon. 42 (1) (2004) 83-94.

[12] P. Hou, F.S.Cannon, N.R. Brown, T. Byrne, X. Gu, C.N. Delgado. Carbon, 53 (2013) 197-207.

[13] J.J.M. Órfao, A.I.M. Silva, J.C.V. Pereira, S.A. Barata, I.M. Fonseca, P.C.C. Faria, M.F.R. Pereira. J. Colloid Interface Sci. 296 (2006) 480-489.

[14] C.H. Hsieh T. and Hsisheng. Carbon 38(6) (2000) 863–869.

[15] A.M. Redding, F.S. Cannon. Water Res. 56 (2014) 214-224.

[16] M. Lallave, J. Bedia, R. Ruiz-Rosas, J. Rodríguez-Mirasol, T. Cordero, J.C. Otero, M. Marquez, A. Barrero, I.G. Loscertales. Adv. Mater. 19 (2007) 4292–4296.

[17] R. Ruiz-Rosas, J. Bedia, M. Lallave, I.G. Loscertales, A. Barrero, J. Rodríguez-Mirasol, T. Cordero. Carbon. 48(3) (2010) 696-705.

[18] R. Berenguer, F.J. García-Mateos, R. Ruiz-Rosas, D. Cazorla-Amorós, E. Moralón, J. Rodríguez-Mirasol, T. Cordero. Green Chem. 18 (2016) 1506-1515.

[19] R. Berenguer, J. Fornells, F.J. García-Mateos, M.O. Guerrero-Pérez, J. Rodríguez-Mirasol,T. Cordero, Novel Synthesis Method of porous VPO catalysts with fibrousstructure by Electrospinning, Catalysis Today 277 (2016) 266–273.

[20] F.J. García-Mateos, T. Cordero-Lanzac, R. Berenguer, E. Morallón, D. Cazorla-Amorós, J. Rodríguez-Mirasol, T. Cordero. Appl. Catal. B Environ. 211 (2017) 18-30.

[21] S. Brunauer, P.H. Emmett, E. Teller. J Amer Chem Soc. 60 (1938) 309-319.

[22] B.C. Lippens, J.H. de Boer. J Catal. 4 (1965) 319-323.

[23] M.M. Dubinin, E.D. Zaverina, L.V. Radushkevich. J. Phys. Chem. (URSS) 21 (1947) 1351-1362.

[24] L.M. Cotoruelo, M.D. Marqués, A. Leiva, J. Rodríguez-Mirasol, T.Cordero. Adsorption. 17 (2011) 539-550

[25] T. Vermeulen. Ind. Eng. Chem. 45 (8) (1953) 1664-1670.

[26] F.J. García-Mateos, R. Ruiz-Rosas, M.D. Marqués, L.M. Cotoruelo, J. Rodríguez-Mirasol, T. Cordero. Chem Eng Journal. 279 (2015) 18-30.

[27] N.S. Raghavan, D.M. Ruthven. AIChE J. 29 (6) (1983) 922-925.

[28] H. Moon, W.K. Lee. J. Colloid Interface Sci. 96 (1983) 162–171.

[29] A.P. Mathews, J.R. Weber, J. Walter. AIChE. Symp. Ser. 73 (166) (1977) 91–98

[30] V. GnielinskiV. Verf. Tech 12 (6) (1978), 363-366.

[31] R.E. Treybal. 1988. Operaciones de trasnsferencia de masa (2nd ed). 858p. Ed. Mc Graw Hill. ISBN 968-6046-34-8

[32] A.I. Liapis, D.W.T. Ripping. Chem. Eng. Sci. 33 (5) (1978), 593-600.

[33] R.T. Yang. 1987. Gas separation by adsorption processes. Butterworths, BostonUK Imperial College, 1997

[34] J.M. Rosas, R. Ruiz-Rosas, J. Rodríguez-Mirasol, T. Cordero. Carbon 50 (4) (2012) 1523-1537.

[35] J. Bedia, J.M. Rosas, J. Márquez, J. Rodríguez-Mirasol, T. Cordero. Carbon 47 (1) (2009) 286-294.

[36] C.H. Giles, T.H. MacEwan, S.N. Nakhwa, D. Smith. J. Chem. Soc. (1960) 3973-3993.

[37] N. Tancredi, N. Medero, F. Möller, J. Píriz, C. Plada, T. Cordero. J. Colloid Interface Sci. 279 (2004) 157-163

[38] C. Moreno-Castilla, J. Rivera-Utrilla, M.V. López-Ramón, F.Carrasco-Marín. Carbon. 35 (1995) 845-51.

[39] D.M. Ruthven. 1984. Principles of adsorption and adsorption processes. 464p. Jhon Wiley & Sons.

[40] R. Berenguer, J.P. Marco-Lozar, C. Quijada, D. Cazorla-Amorós, E. Morallón. Carbon. 48(10) (2010) 2734-2745.

[41] R. Berenguer, J.P. Marco-Lozar, C. Quijada, D. Cazorla-Amorós, E. Morallón. Energy and Fuels. 24(6) (2010) 3366-3372.

Chapter 6

Isopropanol decomposition on basic and acid carbon fibers catalysts

6.0. Abstract

Different carbon fibers catalysts have been prepared by electropinning of Alcell lignin in absence or presence of H_3PO_4 as chemical activating agent. Carbonization at different temperatures between 500 and 1600 ºC allows preparing carbon fibers with a high variety of porosity and chemical surface properties. Diverse oxygen surface groups are presented in the carbon catalysts surface. Specifically, for carbon fibers catalysts prepared with H_3PO_4, phosphorus groups are presented in different oxidation states as C-O-P, C-P-O and C-P groups. The isopropanol decomposition has been used as catalytic test to study the acid or basic character of the carbon fibers prepared. Carbon fibers without phosphorus groups show acetone, from 400 to 600 ºC, as the main product of the isopropanol decomposition, suggesting the basic character of these catalysts. On the contrary, phosphorus-containing carbon fibers show high acid character, producing selectivity to propylene of 100 % at temperatures between 250 and 350 ºC. The influence of oxygen has been studied on the most active phosphorus-carbon catalyst. In this case, higher conversion values are obtained at the same temperatures than those used in the isopropanol decomposition with helium. At conversion below 20 %, acetone is produced in the presence of oxygen due to the oxidative dehydrogenation and 100 % of propylene is produced at higher conversion values.

6.1. Introduction

Alcohol decomposition by dehydrogenation or dehydration is an important process for the production of different compounds of high interest for pharmaceutical and chemistry industry [1,2]. The textural properties, as porosity and specially, the surface chemistry, are the responsible to the activity and selectivity of the catalyst.

Alcohol decomposition has been studied on a large variety of catalysts, as materials based on noble metals [3], oxides of transition metals [4,5], zeolites [6,7] and amorphous phosphates [8], among other [9,10]. However, carbonaceous materials are receiving high attention [10,11] due to the fact that they have a number of unquestionable advantages, such as high surface area and high thermal and chemistry stability, and these carbon materials can be obtaining from different lignocelullosic residues [12,13]

In this sense, isopropanol decomposition is used as catalyst test to characterize the acid or basic catalyst properties, where the aldehydes and ketone are formed on

basic catalyst surface and the dehydration product, as olefins and ethers, are produced on acid catalyst.

The use of low size fibers as a catalyst can avoid problems arising from the transfer of matter, which is essential when optimizing the reaction conditions. Typically, the diffusive problems are solved using smaller particle size, which leads to an increase in the high pressure drops and a decrease in the porosity of the bed. Fibers as catalyst are easy to handle, may be packed or constructed in the best form to fit the particular use and show very small resistance to diffusion and lower pressure drop [14].

In this chapter, Alcell lignin, which is the second most abundant polymer in nature, has been used for the preparation of carbon fibers by electrospinning. The influence of the carbonization temperature and the impregnation of the initial solution with H_3PO_4 has been studied in order to obtain different carbon fibers catalyst with a large variety of porous and chemical properties to be used for isopropanol decomposition.

6.2. Materials and methods.

6.2.1. Preparation of carbon fibers catalyst.

Carbon fibers catalysts have been prepared by electrospinning technique. Alcell lignin was used as raw material for the preparation of the carbon fibers. Alcell fibers with and without H_3PO_4 have been synthetized.

For the preparation of pure lignin fibers, a solution of lignin and ethanol, in a weight ratio of 1/1, was prepared before spinning. For phosphorus-containing lignin fibers two different impregnation ratios of H_3PO_4 have been used. The solution was prepared by mixing H_3PO_4 (85%)/Lignin/Ethanol with a weight impregnation ratio of 0.1/1/1 and 0.3/1/1. All solutions were stirred overnight at 200 rpm and 60 ºC before spinning. In the case of pure lignin fibers and fibers prepared with the lowest impregnation ratio (0.1), a flow rate of 1 $mL \cdot min^{-1}$ was pumped through the inner needle and 0.1 $mL \cdot min^{-1}$ of ethanol, used as a solvent, was pumped through the external one. For phosphorus-containing lignin fibers with an impregnation ratio of 0.3, a flow rate of 3 mL·min-^{1} and 0.3 $mL \cdot min^{-1}$ was needed through the internal and external needle, respectively.

The applied electrical potential differences was 14 kV (collector potential at -7 kV and the tips at +7 kV) for pure lignin fibers and for H_3PO_4 lignin fibers with lower impregnation ratio and 22 kV (collector at -11 kV and tip at +11 kV), for the production of phosphorus containing lignin fibers with high impregnation ratio. The tip-to-collector distance was 25 cm.

Lignin and phosphorus-containing lignin fibers were stabilized under oxidizing atmosphere (50 $cm^3 \cdot min^{-1}$ of air). The stabilization was carried out from room temperature to 200 ºC. On the one hand, for pure Alcell lignin fibers, the heating rate in the stabilization step was 0.08 $ºC \cdot min^{-1}$ and the final temperature was kept for 80 h. On the other hand, for phosphorus-containing lignin fibers (both impregnation ratio) the stabilization step were carried out at 0.8 $ºC \cdot min^{-1}$ and the final temperature was kept for 1 hour. As explained in Chapter 4, the impregnation with H_3PO_4 favors alcell lignin stabilization, doing faster this step without fusion fibers.

Stabilized fibers were carbonized in a tubular furnace at 500 ºC and 900 ºC under a continuous flow of N_2 (150 cm^3 STP$\cdot min^{-1}$) with a heating rate of 10 $ºC \cdot min^{-1}$ Phosphorus carbon fibers (PCFs) were washed with distilled water at 60 ºC. The carbon fibers prepared at 900 ºC were also thermally treated (TT) at 1200 and 1600 ºC. The nomenclature used in this chapter is CF and PCF for pure and phosphorus-containing carbon fibers, respectively. For PCF, the impregnation ratio, 01 or 03, was added at the end of the name. The carbonization temperature and the thermal treatment temperature are also added at the end of the name. For example, the sample PCF01-900-TT1200, makes reference to a phosphorus carbon fiber with an impregnation ratio of 0.1, obtained at 900 ºC and followed by a thermal treatment at 1200 ºC.

6.2.2. Characterization of carbon fibers catalyst.

The porous structure of the samples was characterized by N_2 adsorption-desorption at -196 ºC, and by CO_2 adsorption at 0 ºC performed in ASAP 2020 apparatus (Micromeritics). Samples were outgassed at room temperature for at least 8 hours. From the N_2 isotherm, the apparent surface area (A_{BET}) was determined applying the BET equation [15]. The micropore volume (V_t) and the external surface area (A_t) were calculated using the t-method [16] using a non-porous carbon black as standard and the micropore surface. From the CO_2 adsorption data, the narrow micropore volume

(V_{DR}^{CO2}) and apparent surface area (A_{DR}^{CO2}) were calculated using the Dubinin-Radushkevich equation [17].

Elemental analysis of the carbon fibers was carried out in a Leco CHNS-932 system, being the oxygen content calculated by difference. The surface chemistry of the sample was analyzed by X-ray photoelectron spectroscopy (5700C model Physical Electronics) with Mg kα radiation (1253.6 eV). The maximum of the C1s peak was set to 284.5 eV and used as reference for shifting the whole spectrum.

Temperature-programmed desorption (TPD) analyses were obtained in a customized quartz fixed-bed reactor placed inside an electrical furnace and coupled to a mass spectrometer (Pfeiffer Omnistar GSD-301) and to non-dispersive infrared (NDIR) gas analyzers (Siemens ULTRAMAT 22) in order to quantify CO and CO_2, (calibration error < 1%). In these experiments, c.a. 50 mg of the carbon fibers was heated from room temperature to 1000 °C at a heating rate of 10 °C·min^{-1} in nitrogen (purity 99.999%, Air Liquide) flow (200 cm^3 STP·min^{-1}).

The total acidity of the catalyst prepared with H_3PO_4 has been determined by chemisorbed pyridine at 120 ºC. The analysis was performed using about 15 mg of catalyst. The inlet partial pressure of pyridine was 0.02 atm. After saturation of the carbon catalyst, desorption is carried out at the adsorption temperature in helium flow.

Non-isothermal thermogravimetric analysis were performed in a CI Electronis MK2 balance under air flow (150 cm^3·min^{-1}) from room temperature to 900 ºC at a heating rate of 10 ºC·min^{-1}, with a carbon weight of about 15 mg.

The size, shape and texture of the carbon fibers were analyzed by scanning electron microscopy (SEM) in a JSM 6490LV JEOL instrument.

6.2.3. Isopropanol catalytic conversion

The catalytic activity of the carbon fibers was studied by decomposition of isopropanol in the gas phase at atmospheric pressure in a fixed bed microreactor (i.d. 4 mm) placed inside a vertical furnace with temperature control, under different operating conditions. In a typical experiment 60 mg of catalyst was used. Isopropanol was fed to the system in a controlled way by using a syringe pump (Cole-Parmer® 74900-00-05 model). The reaction was carried out in inert atmosphere in the

temperature range of 200-700 ºC (depending on the carbon fibers to obtain a conversion of 100 %). To avoid condensation of any compound, all the lines were heated up to 120 ºC. The standard conditions were an isopropanol partial pressure of 0.0185 atm and a space time of 0.055 $g \cdot s \cdot \mu mol^{-1}$ (GHSV = 42 $m^3 gas \cdot kg^{-3} catalyst \cdot h^{-1}$). For PCF03 catalyst, isopropanol decomposition was also studied under oxidizing atmosphere (air flow of 150 $cm^3 \cdot min^{-1}$).

The isopropanol and products concentrations in the outlet gas stream were analyzed by gas chromatography (490 micro-GC equipped with PPQ, MolSieve 5A and Wac columns, Agilent). The conversion was defined as the molar ratio of isopropanol converted to isopropanol fed to the reactor. The selectivity was defined as the molar concentration of a given product to that of the total products formed. The carbon balance was reached with an error lower than 5%.

6.3. Results and Discussion

6.3.1. Preparation carbon fibres catalyst.

Table 6.1. shows the carbon fibers preparation yields. The stabilization yields increase with the amount of H_3PO_4 on the Alcell fibers. This step consists of an oxidative treatment in order to increase the glass transition temperature and avoid the fiber fusion in carbonization step. The stabilization yields vary from 88 to 77 %, respectively for lignin fibers with and without H_3PO_4. The presence of H_3PO_4 produces higher stabilization yields because H_3PO_4 eludes the gasification of the material in the presence of oxygen with temperature. Weight-loss during the stabilization step has been assigned to condensation and dehydration reaction involved in the cross-linking reactions and to the evaporation of occluded ethanol [18]. In general, carbonization yields decrease with carbonization temperature due to the volatile material removed, the dehydration of the precursor and the possible activation of the samples. In this sense, previous studies revealed that the high oxygen content in the stabilized Alcell fibers could act as activating agent during carbonization step, producing a development of the porosity [18,19].Carbon fibers catalysts prepared by chemical activation with H_3PO_4 present higher carbonization yields, due to the restriction of the formation of tar during the activation process, increasing the final solid weight [20]. In spite of being prepared by H_3PO_4, PCF03-900 presents the lowest carbonization yield because of the high activation of this carbon fibers catalyst. These fibers present high oxygen content after

the stabilization step (≈30 wt% by XPS). This oxygen can act as a further activating agent [18,19], decreasing the carbonization yield. These yields, which vary between 70 to 30 %, are similar to other yields obtained in the preparation of activated carbon or activated carbon fibers using other biomass precursors [21-25]. High thermal treatments yields show the carbon material retained after the treatments. These values correspond to the decomposition of the oxygen surface groups present in the samples. Preparation of carbon materials by chemical activation with H_3PO_4 produces an increase on the oxygen surface group due to the presence of C-O-P and C-P-O surface groups, for this reason, the lowest thermal treatment yields are obtained for these samples. Total yields vary from 61 to 21 % and it is referred to the weight of carbon fibers with respect to the initial weight of lignin.

Table 6.1. Preparation yields of carbon fibers catalyst

Carbon catalyst	Stabilization Yield (%)	Carbonization Yield (%)	TT 1200 Yield (%)	TT 1600 Yield (%)	Total Yield %
CF-500	77.20	54.5	--	--	42.1
CF-900		41.9	--	--	32.4
CF-900-TT1200		--	93.3	--	30.2
CF-900-TT1600		--	--	87.5	28.3
PCF01-500	88.24	68.3	--	--	60.3
PCF01-900		55.2	--	--	48.7
PCF01-900-TT1200		--	92.7	--	45.2
PCF01-900-TT1600		--	--	82.5	40.2
PCF03-500	86.49	70.6	--	--	61.0
PCF03-900		32.3	--	--	28.0
PCF03-900-TT1200		--	84.8	--	23.7
PCF03-900-TT1600		--	--	75.0	21.0

6.3.2. Porous structure.

Figure 6.1. presents the N_2 adsorption-desorption isotherms at -196 ºC as well as the CO_2 adsorption isotherms at 0 ºC. All N_2 adsorption-desorption isotherms show type I isotherm characteristic of solids with a development of the microporosity. The increase of the volume adsorbed at relative pressures between 0.385 and 0.9 is negligible, which indicates the low contribution of mesoporosity. The increase of carbonization temperature produces higher N_2 volumes adsorbed, reaching the maximum adsorbed volume for the sample prepared at 900 ºC. Thermal treatments at

1200 and 1600 ºC produce a decrease of the N_2 adsorbed, due to the contraction of the porous structure during the thermal treatment steps. Similar behaviors have been obtained for CO_2 adsorption isotherms. An increase of the N_2 adsorbed on the carbon fibers prepared with H_3PO_4 due to the activation produced and the widening of the posority, being this different higher for carbon fibers prepared at higher impregnation ratios.

Textural parameters derived from N_2 and CO_2 adsorption isotherms are shown in Table 6.2. As it is said before, the maximum development of the porosity for all the series of samples is produced when the samples are carbonized at 900 ºC. In the case of CF series, BET surface areas between 154 and 850 $m^2 \cdot g^{-1}$ are obtained. When apparent surfaces areas calculated from N_2 (A_{BET}) and CO_2 adsorption (A_{DR}) are compared, higher A_{DR} values (from 458 to 1000 $m^2 \cdot g^{-1}$) are observed, what suggests the presence of narrow microporosity, specially for the sample CF-900-TT1600, in which the thermal treatment at 1600 ºC produces an enormous decrease of the N_2 adsorbed, while the CO_2 adsorbed volume continues being high. Similar behaviors are found for carbons materials prepared at higher temperature from Kraft lignin [26], where the porosity contraction is due to the graphitizaton and order of the carbon structure.

For phosphorus-containing carbon fibers catalysts, the higher the impregnation ratio is, the higher the surface are is produced. It is well known the development of the porous structure that H_3PO_4 produces on the carbon precursor material [27]. The increase of the H_3PO_4 ratio produces a slight increase on the external surface area (At) due to the widening of the porosity. This widening is observed when the surfaces areas A_{BET} and A_{DR} are compared. In the case of PCF01 series, similar values of areas obtaining from N_2 and CO_2 are found. On the contrary, lower A_{DR} (from CO_2 adsorption) are obtained for PCF03 series, indicating, again, the widening of the porosity. For PCF01 series, BET surface areas from 400 to 800 $m^2 \cdot g^{-1}$ are achieved, and areas from 750 to 1150 $m^2 \cdot g^{-1}$ are presented in the PCF03 series. When H_3PO_4 is present in the preparation of carbon fibers, thermal treatments at 1600 ºC do not produce as much pores contraction as it is produced in the absence of H_3PO_4, this fact could be associated to the presence of phosphorus surface groups, which probably reduces the contraction and condensation of porous structure at 1600 ºC.

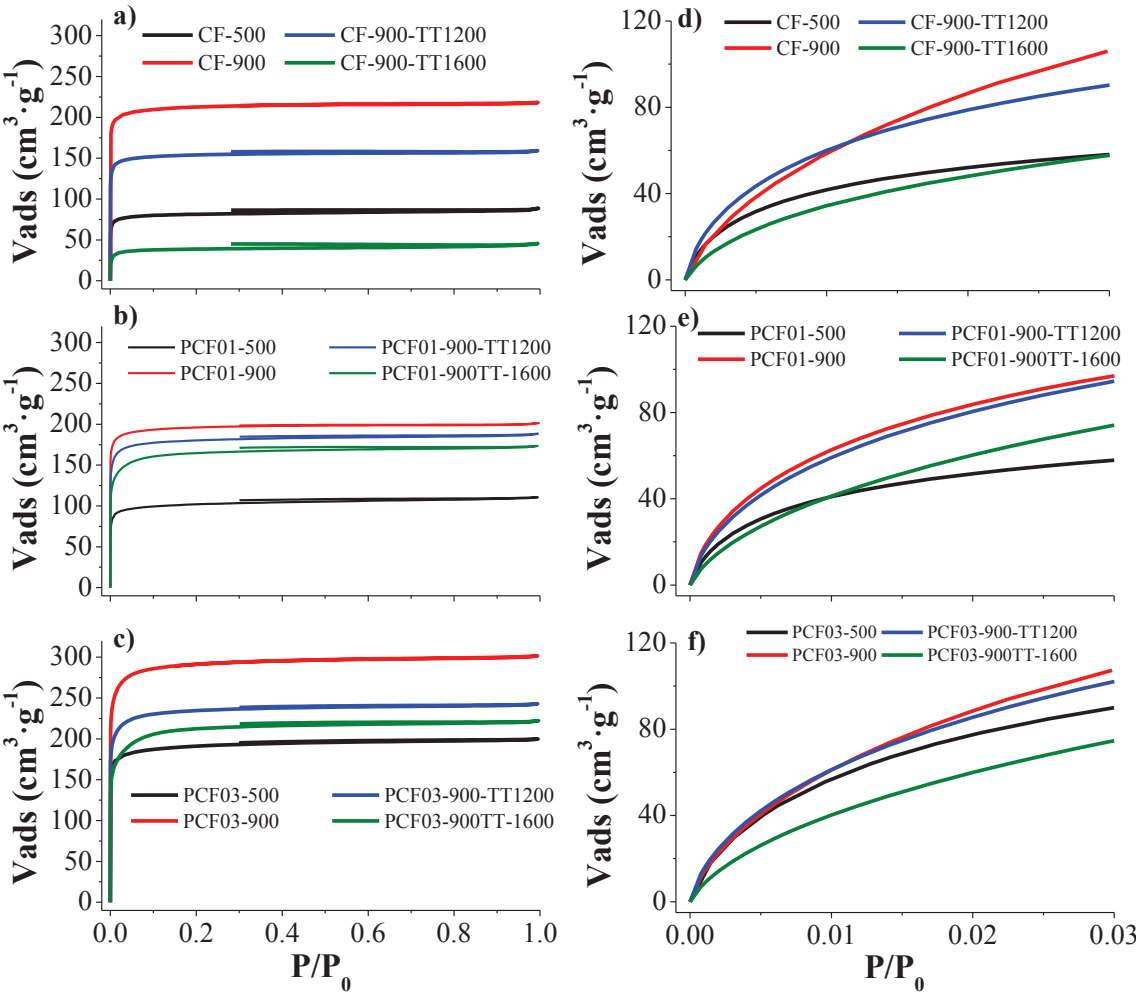

Figure 6.1. N_2 adsorption-desorption isotherms at -196 ºC of the different carbon fibers series of (a) CF, b) PCF01 and c) PCF03); and CO_2 adsorption isotherms at 0 ºC of the series (d) CF, e) PCF01 and f) PCF03).

6.3.3. Chemical characterization.

Table 6.3. shows the chemical surface composition calculated by XPS and chemical composition obtained by elemental analysis (in dry basis and mineral mater free). In all the samples, the main element of the carbon fibers catalysts is carbon. Oxygen and phosphorus are presented on the samples in lower concentrations. When the temperature is increased, the removal of oxygen surface groups is produced. On the one hand, an increase in the final preparation temperature produces an increase of the carbon content. On the other hand, a decrease of oxygen content is produced when the final temperature is increased. The phosphorus concentration varies between 3.0 to 0.2 %. Until 1200 ºC, similar values of P are found. However, when the temperature increases to 1600 ºC, a decrease in the phosphorus content is observed, probably due to the volatilization of phosphorus at temperatures as high as 1400 ºC.

Table 6.2. Structural parameters from N_2 and CO_2 adsorption isotherms.

	N_2 Isotherm				CO_2 Isotherm	
Carbon catalyst	A_{BET} ($m^2 \cdot g^{-1}$)	A_t ($m^2 \cdot g^{-1}$)	V_t ($cm^3 \cdot g^{-1}$)	V_{tot} ($cm^3 \cdot g^{-1}$)	A_{DR} ($m^2 \cdot g^{-1}$)	V_{DR} ($cm^3 \cdot g^{-1}$)
CF-500	328	11	0.12	0.14	458	0.18
CF-900	851	7	0.33	0.34	1002	0.40
CF-900-TT1200	628	5	0.24	0.25	739	0.30
CF-900-TT1600	154	7	0.06	0.07	517	0.21
PCF01-500	406	17	0.15	0.17	465	0.19
PCF01-900	796	5	0.30	0.31	798	0.32
PCF01-900-TT1200	728	11	0.28	0.29	788	0.32
PCF01-900-TT1600	648	13	0.25	0.27	674	0.27
PCF03-500	749	14	0.29	0.31	794	0.32
PCF03-900	1155	16	0.45	0.47	950	0.38
PCF03-900-TT1200	938	13	0.36	0.38	870	0.35
PCF03-900-TT1600	823	15	0.33	0.34	686	0.27

Table 6.2. Chemical composition calculated by XPS; elemental analysis and CO-CO_2 evolved from TPD experiments.

	Chemical composition XPS (%wt)				Elemental Analysis (%wt)			CO-CO_2 DTP ($\mu mol \cdot g^{-1}$)	
Carbon catalyst	**C**	**O**	**P**	**N**	**C**	**H**	**O***	**CO**	**CO_2**
CF-500	84.3	15.1	--	0.6	74.4	2.2	23.4	4046	761
CF-900	95.9	4.1	--	0.0	92.0	1.7	6.3	1582	259
CF-900-TT1200	97.5	2.0	--	0.5	95.8	0.2	4.1	718	274
CF-900-TT1600	98.0	1.9	--	0.1	98.5	0.1	1.4	167	87
PCF01-500	79.4	17.9	1.9	0.8	73.5	2.0	24.5	2744	580
PCF01-900	82.9	14.0	2.4	0.7	78.8	1.3	19.9	2428	230
PCF01-900-TT1200	91.4	5.4	2.8	0.4	85.0	0.2	14.8	1433	305
PCF01-900-TT1600	97.6	1.9	0.5	0.0	96.6	0.0	3.4	210	82
PCF03-500	86.0	12.3	1.0	0.7	76.7	2.4	20.9	2329	525
PCF03-900	90.5	7.3	2.2	0.0	81.4	1.5	17.2	5125	399
PCF03-900-TT1200	89.6	6.9	3.1	0.4	85.2	0.4	14.3	1102	231
PCF03-900-TT1600	97.9	1.8	0.2	0.1	97.2	0.0	2.8	241	84

O* calculated by difference

Figure 6.2. shows the XPS region spectra for all carbon fibers catalysts (some intensities have been magnified in order to compare different samples). C1s spectrum of carbon fibers catalysts present a main contribution at 284.5 eV related to C=C/C-C groups and lower contribution of C-OH and C-O-C groups at 286.0 eV. O1s spectrum of the different carbon series shows a main peak at 532.6 eV, which is characteristic of single bonded oxygen in C-OH, C-O-C and C-O-P linkages [28], the last one for samples prepared with H_3PO_4. Also, a contribution in the binding energy of 530.9 eV is observed in the samples, these bonds are characteristic of C=O and P=O groups. Furthermore, a displacement to lower binding energies is observed when the final temperature increases. Carbon fibers catalysts prepared with H_3PO_4 have higher oxygen content due to the presence of surface C-O-P and C-P-O groups that have been generated during the activation step in presence of phosphoric acid.

Similar behavior is found for P2p spectra. Samples prepared at the lowest temperature, PCF01-500 and PCF03-500, present a main peak centered in 134 eV, which is characteristic of the most phosphorus oxidized species (C-O-PO_3, $(CO)_3PO$ and $(CO)_2PO$) [28,29]. It can also be observed a peak at 133.2 eV, with lower contribution, which can be associated to the presence of C-PO_3 and C_2PO_2 groups [29]. When the carbonization temperature is increased to 900 ºC, a displacement toward lower binding energies is observed in both samples. A reduction of the contribution of oxidized groups (C-O-P) is produced and an increase of the less oxidized phosphorus groups is obtained (C-P-O). When the preparation temperature increase to 1200 or 1600 ºC, the phosphorus groups in the samples are the most reduced one, presenting high contribution of C_3PO [29-31]and C_3P groups [30] (between 132 and 131 eV, respectively). Similar behavior has been previously described for activated carbons prepared with H_3PO_4 under inert and oxidative atmosphere treatments [28].

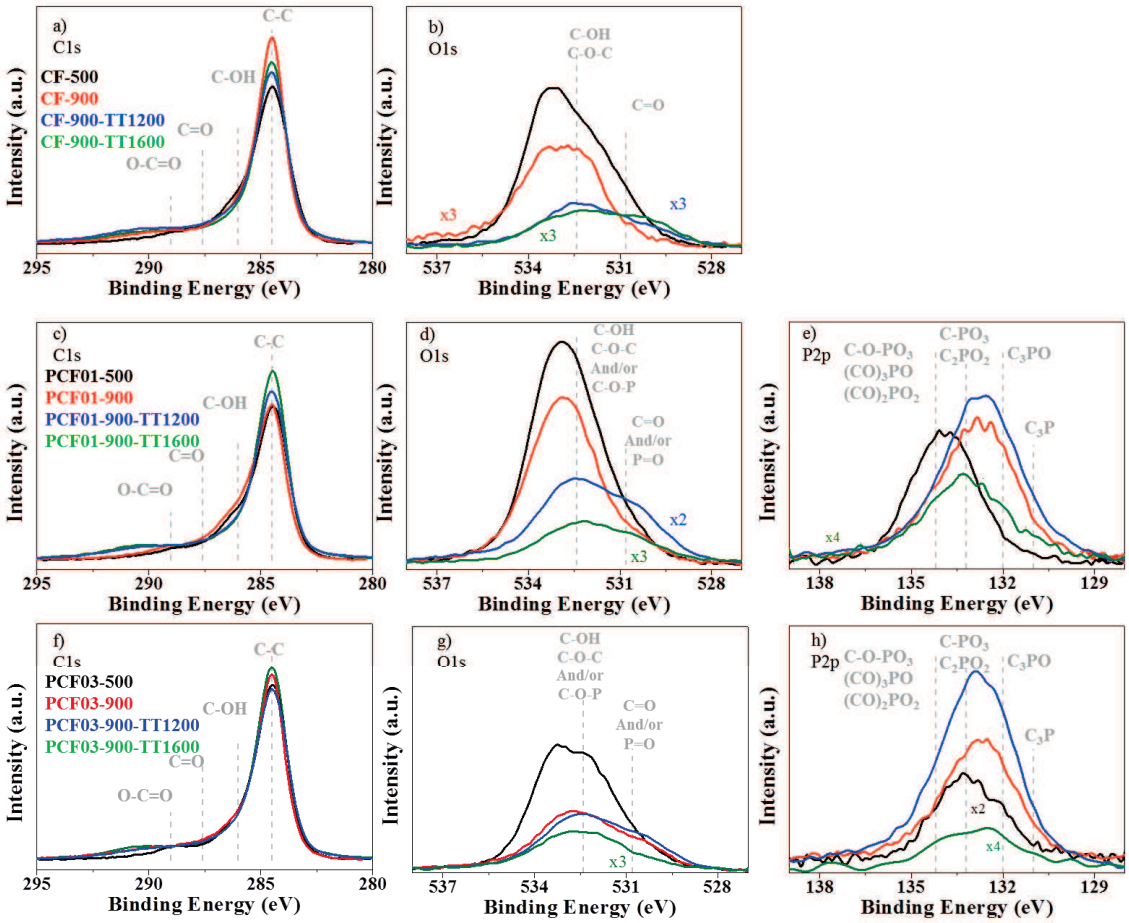

Figure 6.2. C1s, O1s and P2p XPS spectra for the different carbon fibers catalysts series.

Figure 6.3. presents the evolution of CO and CO_2 profiles during TPD experiments for all the carbon fibers catalysts. According to literature, carbon-oxygen groups of acidic character, such as carboxylic and lactonic, evolve as CO_2 upon thermal decomposition, whereas non acidic, such as carbonyl, ether, quinone and phenol, evolve as CO. Anydride surface groups evolve as both CO and CO_2 [32,33].

For carbon fibers catalysts prepared at 500 ºC, the CO desorbed during TPD experiments appears at temperatures between 500 and 700 ºC probably in the form of anhydride, phenol and ether groups [32,34,35]. An increase in the CO desorbed with the increase of the carbonization temperature is observed in phosphorus-containing carbon (Figure 6.3 b and c). This tendency can be explained by the higher amount of surface P complexes that decomposes as CO (and CO_2), as indicated by XPS. At carbonization temperatures of 500 ºC, a new contribution of CO desorbed is appreciated from 650 to 720 ºC, which corresponds to the most oxidized phosphorus groups (C-O-PO_3, $(CO)_3PO$

and $(CO)_2PO$). When the carbonization temperature increases up to 900 ºC, it can be observed an increase in the CO evolution at high temperatures (860 ºC), which could be related to more stable phosphorus groups (C-PO_3 and C_2PO_2). Lower CO evolutions are present when the samples are carbonized at 1200 ºC, in this case the CO evolution can be referred to the decomposition of C_3PO groups. Finally, no CO profile signal is obtained when the samples are prepared at 1600 ºC, indicating that the oxygen surface groups that remain in the surface are mainly due to C-P type.

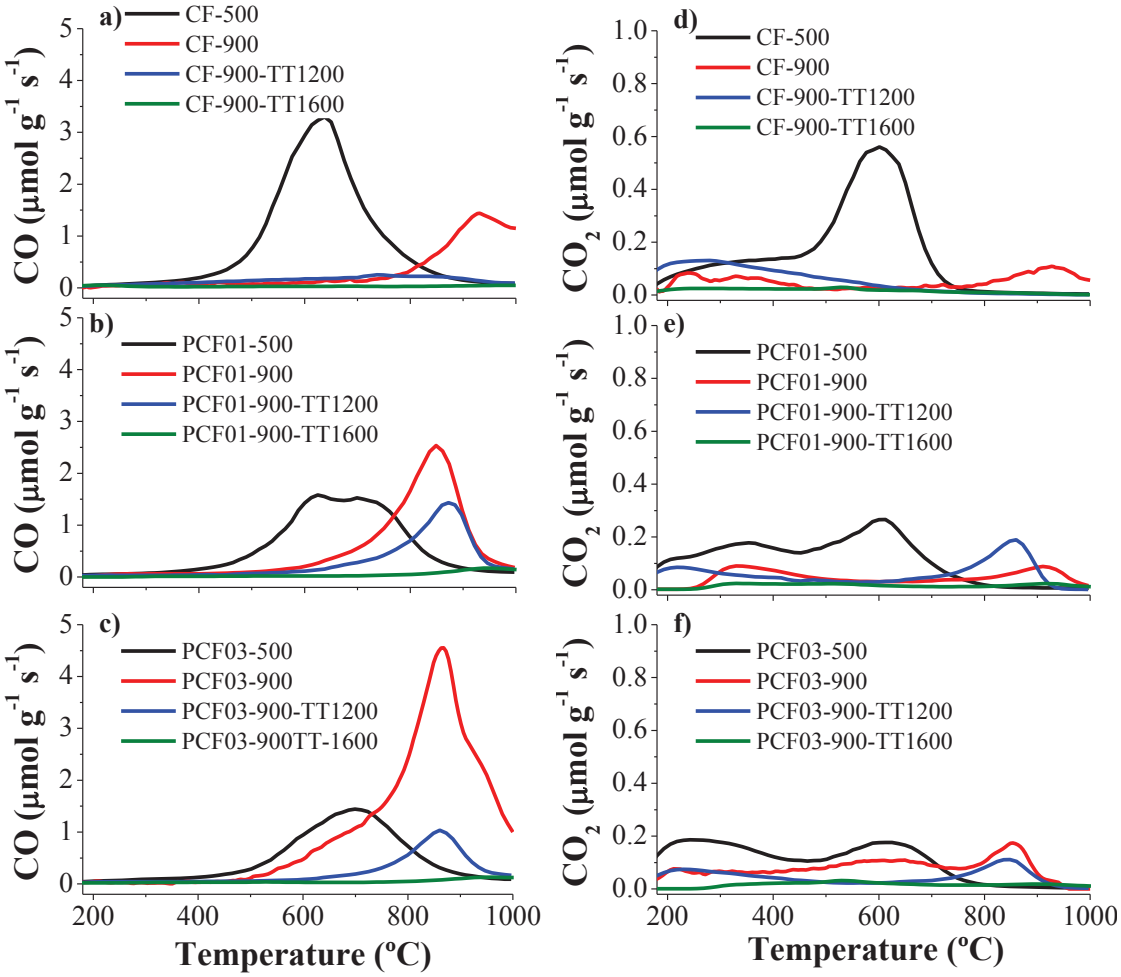

Figure 6.3. Amounts of CO and CO_2 evolved with temperature during the TPD experiment for the different carbon series of CF (a and d), PCF01 (b and e) and PCF03 (c and f).

CO_2 profiles show lower desorbed amounts compared to those for CO ones, indicating a lower presence of carboxyl, lactonic and anhydride groups on the surface of the different carbon catalysts. For the phosphorus-containing carbon fibers catalysts, it is noteworthy the evolution of CO_2 at around 850 ◦C that seems to be related to the

evolution of CO at this temperature [29]. Evolution of CO_2 at this high temperature may be associated to secondary reactions between CO and oxygen surface complexes [36].

The amounts of CO and CO_2 evolved during the TPD experiments obtained by the integration of the areas under the TPD curves are summarized in Table 6.2.

Figure 6.4. represents the adsorption-desorption kinetics of pyridine on the carbonaceous catalyst used. The first part of the curve indicates the total amount of pyridine adsorbed, which is related to the catalyst total surface area. The amounts of pyridine retained after the desorption process (amount adsorbed irreversibly or chemisorbed) are very similar, being between 0.8 and 2.2 $mmol_{Py} \cdot g^{-1}$. The highest amount of pyridine chemisorbed is obtained for catalyst prepared at 1200 ºC. The final amount of pyridine maintains a relationship with the final amount of phosphorus on the carbon fibers surface.

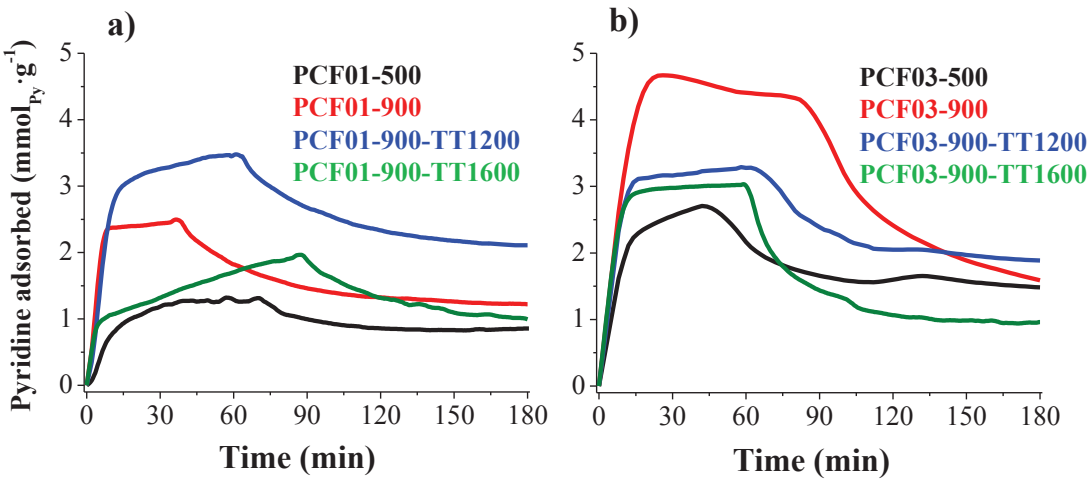

Figure 6.4. Kinetic adsorption-desorption of pyridine on: a) PCF01 and b) PCF03 catalyst.

The loss weight profiles under air atmosphere of CF, PCF01 and PCF03 series are shown in Figure 6.5. A high oxidation resistance and acidity are well-known required properties of carbon materials for their potential use as catalysts and catalyst supports in several reactions [27,30, 37-42]. In particular, since the presence of O_2 in the reaction atmosphere is generally necessary to enhance the conversions, inhibit the catalyst deactivation and reach steady-state conditions [40].

In spite of the high surface area of the carbon catalyst, an increase in the oxidation resistance is observed when the carbonization temperature arises, varying

from 400 ºC (for CF-500) to 560 ºC (for CF-900-TT1600). The increase in the carbonization temperature produce carbon fibers with high grade of order, then, the presence of certain carbon ordered structures [43] and the lack of superficial defects (Figure 6.6) can be the responsible of the high starting oxidation temperatures of the carbon fibers catalysts.

Phosphorus-containing carbon fibers catalysts present higher oxidation resistances than pure carbon fibers ones. According to previous works, activated carbons without phosphorus start to oxidize significantly below 400 ºC [44,45]. The high oxidation resistance of phosphoric acid activated carbons has been previously reported for activated carbon derived from hemp fibers, lignin and olive stone and was related to the presence of phosphorus groups on the carbon surface. It was reported that the phosphorus complexes could act as a physical barrier and/or block the active carbon sites for the oxidation reaction. But most recently, our research group, based on TGA, XPS and DTP results [45], suggested that oxidation of the most reduced phosphorus groups, C-P, to most oxygenated phosphorus groups, mainly C-O-PO_3, avoids the carbon oxidation and thus retards the gasification of the carbon support

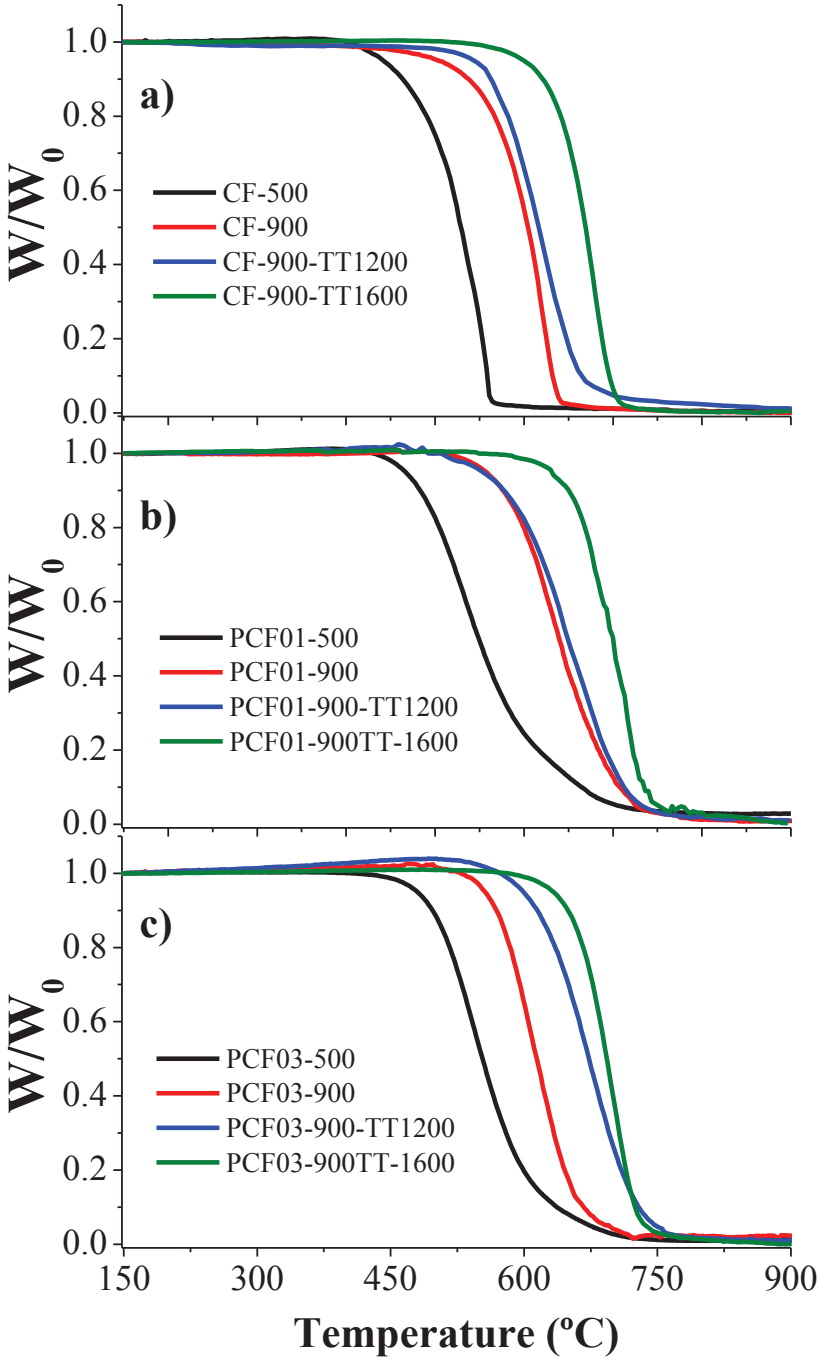

Figure 6.5. Non isothermal loss weight profiles of the different carbon catalysts series of a) CF, b) PCF01 and c) PCF03.

Figure 6.6. shows the morphology of the carbon fibers catalysts series. Similar diameters are found for CF and PCF01 samples, probably due to the use of the same flow rate in the electrospinning step. The diameters suffer a reduction when carbonization temperatures are higher than 500 ºC, obtaining diameters values between 0.5 and 2 μm. PCF03 carbon catalysts present higher fiber diameters because of the

higher flow rate used in the electrospinning. For CF carbon fibers, when the carbonization temperature is as high as 1200 or 1600 ºC, the fibers start to fuse, mainly in the contact point of the fibers.

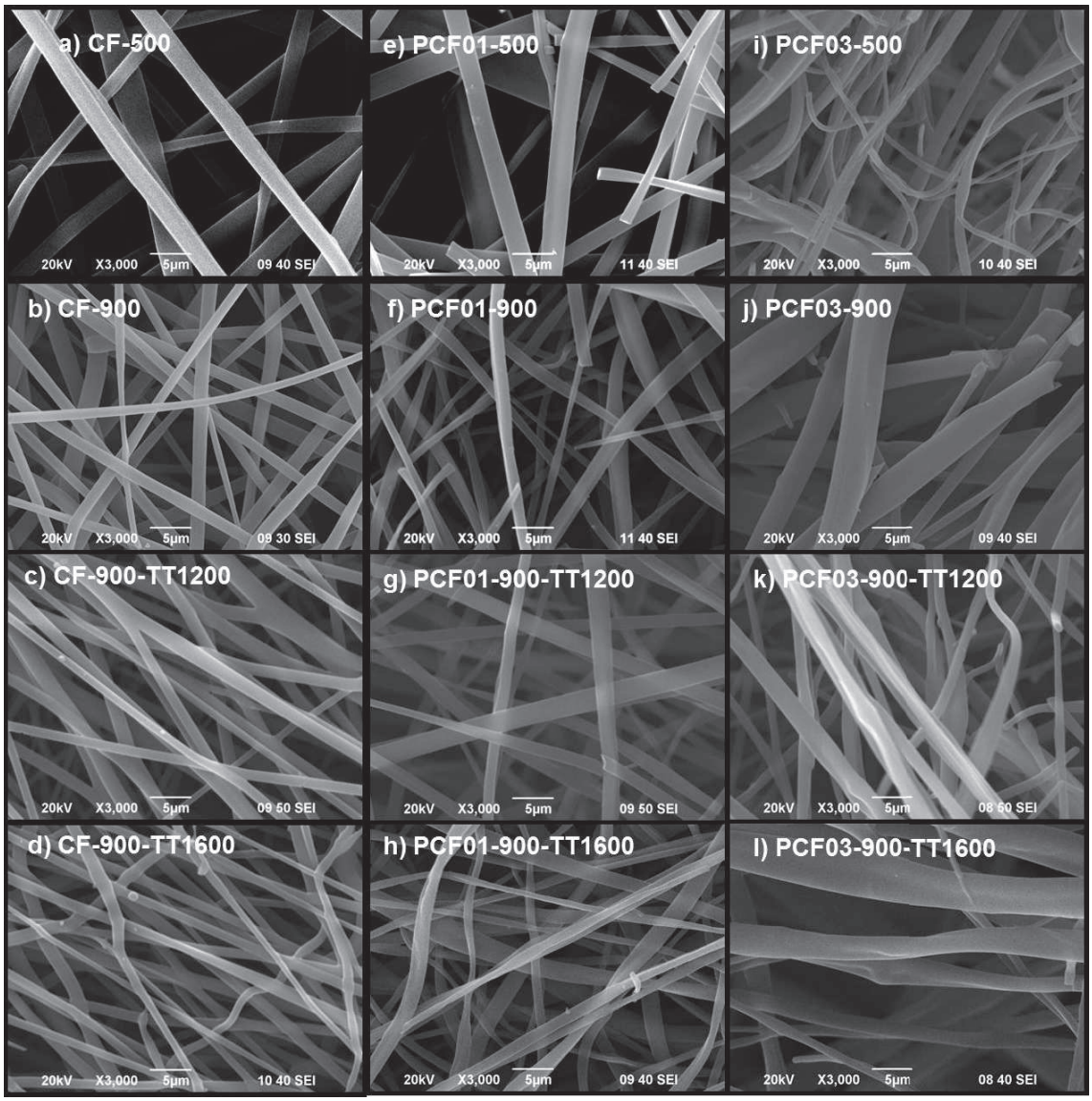

Figure 6.6. SEM micrographs of carbon fibers catalysts. CF series (a-d), PCF01 series (e-h) and PCF03 series (i-l).

6.3.4. Isopropanol decomposition

The steady state conversions of isopropanol on the carbon fibers catalysts are shown in Figure 6.7. Conversion on carbon fibers has been represented different symbols and continuous line, for selectivity on carbon fibers catalysts, solid and hollow dots have used to represent, selectivity to propylene and acetone, respectively. Carbon

catalysts have been compared with a commercial γ-Al_2O_3 to analyze the acid properties. Isopropanol conversions of γ-Al_2O_3 catalyst are represented by * symbol and red dashed line in Figure 6.7a-c. In order to represent the selectivity of γ-Al_2O_3, dashed and continuous red lines have been used to represent the selectivity to propylene and acetone, respectively. For the sake of comparison, isopropanol gas phase decomposition is also included, being isopropanol conversion represented by * symbol and black dashed line in Figure 6.7 a-c, and the selectivity to propylene and acetone, (Figure 6.7. d-f), by dashed and continuous lines, respectively.

As expected, an increase in the isopropanol conversion increases with the reaction temperatures. Carbon fibers catalysts prepared with H_3PO_4 show higher steady state conversion than the corresponding carbon fibers prepared in absence of H_3PO_4.

The differences in the surface chemistry of the carbon fibers catalysts are clearly observed analyzing the selectivity of the isopropanol decomposition in a helium flow. For CF carbon fibers catalysts, besides to a low amount of propylene as dehydration product, acetone is obtained as the only isopropanol dehydrogenation product. The selectivity is similar for all CF carbon catalysts, yielding mainly acetone. As could be seen in Figure 6.7.a), carbon catalysts prepared at 500, 1200 and 1600 ºC require high temperatures to produce isopropanol conversion in some extent. High selectivity to acetone is obtained until 600 ºC of reaction temperature. When reaction temperature is higher than 600 ºC an increase of the propylene selectivity is observed, which will be due to the contribution of the decomposition of isopropanol in the gas phase, which yield to propylene at higher temperatures.

Steady state isopropanol conversions for acid catalysts (PCF01 and PCF03) are shown in Figure 6.7.b) and c). In the case of the acid catalysts prepared at 500, 900 and 1200 ºC, isopropanol decomposition reaction yields only propylene at reaction temperatures lower than 500 and 350 ºC for PCF01 and PCF03, respectively. This is a consequence of the acidity of the surface of these carbons. In this line, other lignocellulosic residues were already activated with phosphoric acid and showed high activity in the alcohol decomposition [30,41]. This high activity was associated to the presence of –OH groups derived from phosphates and polyphosphate esters, formed during the activation step, which can act as Brönsted acid sites [30,41]. An increase in the reaction temperature is necessary to produce a complete isopropanol conversion on

phosphorus-carbon catalysts prepared at 1600 ºC. In spite of the removal of all oxygen surface groups and the low P content of these fibers (see Table 6.2), the selectivity yields mainly to propylene, indicating the presence of certain acid groups of low strength, probably related to some P groups. Only an increase in the selectivity to acetone is produced when the isopropanol decomposition gas phase is also taking place. The analysis of the chemical surface composition by XPS reveals that most phosphorus groups are removed during the thermal treatment. Although XPS technique is a superficial technique, these catalyst presents selectivity to propylene, which will suggest the presence of P content on carbon catalyst prepared at 1600 ºC.

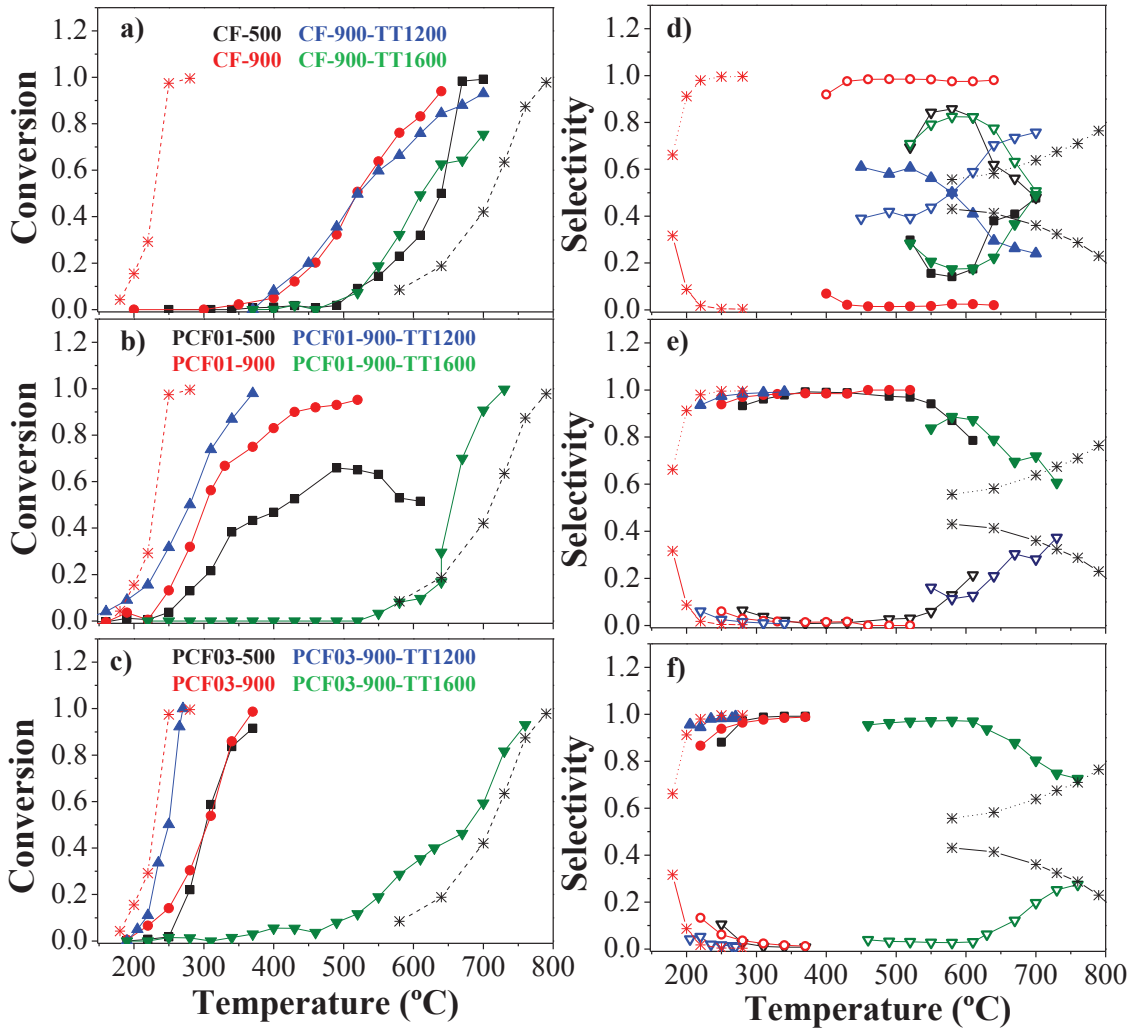

Figure 6.7. Steady state conversion of isopropanol for the carbon series of CF a), PCF01 b) and PCF03 c), and selectivity (CF d), PCF01 e), PCF03 f)).

If it is analyzed each PCF series, the activity of these materials are referred to the amount of P in the surface. By this way, the sample prepared at 1200 ºC, with higher P content, is the most active. Samples prepared with higher impregnation ratio (PCF03) are the most actives, showing a total conversion (for PCF03-(500-1200)) at 350 ºC. Comparing the phosphorus carbon catalyst with the commercial acid catalyst γ-Al_2O_3, only a difference of 20 ºC is observed to obtain the same conversion, indicating the high acid character of these catalysts.

The influence of the presence of oxygen (21 vol.%) in the isopropanol decomposition has been analyzed on the PCF03 series. The steady state conversions and selectivities of PCF03 catalyst series for helium flow (Figure 6.8. a) and b)) and air flow (Figure 6.8. c) and d)) are compared in Figure 6.8. . The presence of oxygen produces higher reaction rates and a change in the products distribution for these acid carbon catalysts. When air is used, acid carbon catalysts produce acetone by oxidative dehydrogenation of isopropanol and propylene by dehydration of the alcohol, by the presence of oxygen. These results are in accordance with those published in the litterature, where these authors indicated that the carbon surface active sites were reduced by alcohol and regenerated by the oxygen, and the presence of air in the reactant mixture cleaned some of carbon surface sites, increasing the dehydrogenation activity and decreasing the dehydration [46,47].

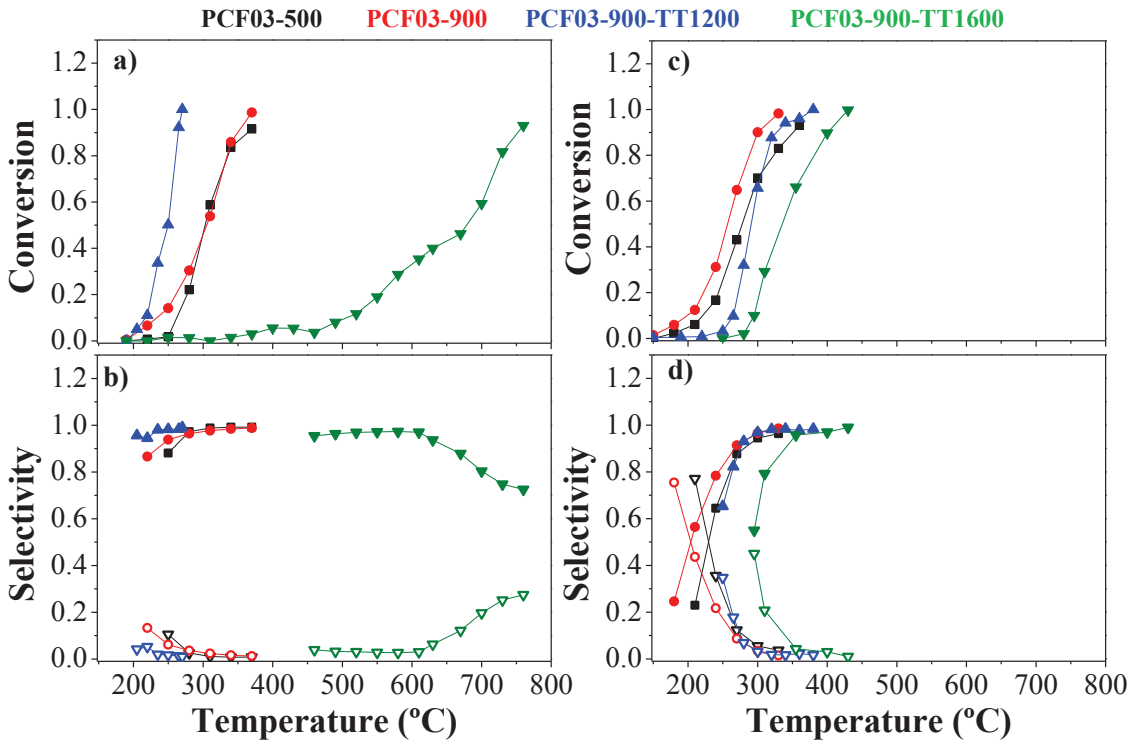

Figure 6.8. Steady state conversion and selectivity of isopropanol on the PCF03 carbon fibers catalysts series in: helium a) and b), respectively; and in presence of oxygen. c) and d), respectively.

Isopropanol decomposition will be assumed to follow a first-order kinetic, which is described by the following equation:

$$ln\left(\frac{1}{1-X}\right) = k \cdot P_{oIPA} \cdot \frac{W}{F_{oIPA}}$$

where k is the apparent rate constant, W is the catalyst weight, F_{oIPA} is the reactant molar flow rate, P_{oIPA} is the reactant partial pressure and X is the conversion. The activation energy is derived from the Arrhenius equation. The values of the kinetic parameters (ko is the preexponential factor and Ea is the activation energy) for all the carbon fibers catalysts are summarized in Table 6.3. The Arrhenius plots for all the carbon catalysts under inert atmosphere and, also for PCF03 series in air flow, are shown in Figure 6.9. Values from 46 to 250 kJ/mol have been obtained, which are in the same range than those previously obtained for carbon based acid catalysts prepared from biomass by phosphoric acid activation for the dehydration of isopropanol [30,41]. As it was aforementioned, the preparation of these carbon fibers catalyst results in

catalysts with a high range on surface chemistry oxygen groups, this fact could be the responsible of the differences in the activation energy values obtained.

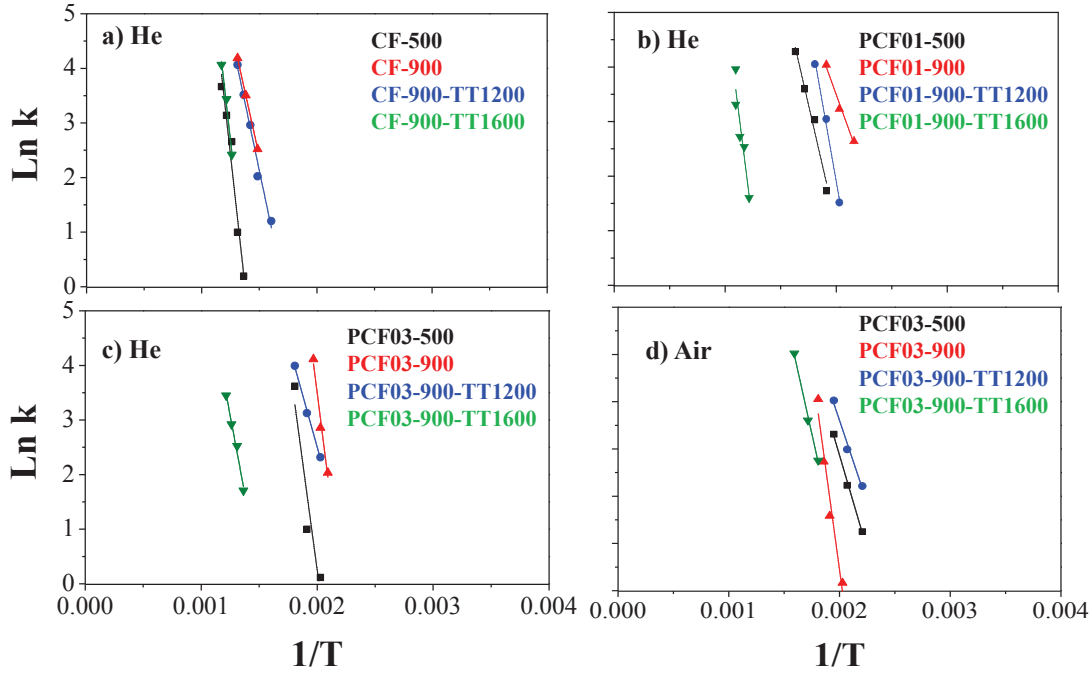

Figure 6.9. Arrhenius plot for isopropanol decomposition on the carbon catalysts series: a) CF, b)PCF01, c) PCF03 and d) PCF03 in Air

Table 6.3. Apparent kinetic parameters for isopropanol decomposition of the different carbon catalyst series under helium gas (CF, PCF01 and PCF03) and air gas (PCF03).

Carbon Catalyst	Gas	E_a (kJ/mol)	$\ln k_o$
CF-500	He	158.2	26.2
CF-900	He	83.1	17.1
CF-900-TT1200	He	79.0	16.6
CF-900-TT1600	He	154.0	25.9
PCF01-500	He	73.5	18.8
PCF01-900	He	96.1	25.0
PCF01-900-TT1200	He	46.8	14.8
PCF01-900-TT1600	He	111.2	18.0
PCF03-500	He	131	31.7
PCF03-900	He	63.2	17.7
PCF03-900-TT1200	He	139.5	37.0
PCF03-900-TT1600	He	94.2	17.3
PCF03-500	Air	66.3	18.8
PCF03-900	Air	58.1	17.6
PCF03-900-TT1200	Air	143.1	18.8
PCF03-900-TT1600	Air	253.0	56.4

6.4. Conclusions

Carbon fibers catalysts have been prepared by electrospinning of Alcell lignin. The use of H_3PO_4 in the initial solution along with the variation of the carbonization temperature have allowed the preparation of different carbon catalysts with a wide range of porosity and surface chemistry properties. Carbon fibers catalysts prepared in the absence of phosphoric acid present basic character in the isopropanol decomposition reaction, yielding mainly acetone as the reaction product. Carbon fibers catalysts prepared with H_3PO_4 show acid character, producing as main product propylene. These acid carbon fibers catalysts show high activity to isopropanol conversion to propylene. Comparing the most active carbon fibers, PCF03-900-TT1200, with the result obtaining for isopropanol decomposition on a commercial γ-Al_2O_3 acid catalyst only a difference of 20 ºC is necessary to obtain the same isopropanol conversion. The presence of oxygen in the inlet gas produces higher reaction rates and changes of the product distribution in carbon fibers prepared with H_3PO_4, producing acetone by oxidative dehydrogenation and propylene by dehydration.

6.5. References

[1] R.M. Rioux, M.A. Vannice. J Catal 216 (2003) 362-376.

[2] U.K. Singh, M.A. Vannice. Appl Catal A: Gen 213 (2001) 213, 1-24.

[3] G.J. Millar, M.L. Nelson, P.J.R. Uwins. J Catal 196 (1997) 143-156.

[4] N.E. Quaranta, J. Soria, V.C. Corberán, J.L.G. Fierro. J Catal 171 (1997) 1-13.

[5] M.J.L. Gines, E. Iglesia. J Catal. 176 (1998) 155-172.

[6] L.G.A. van de Water, .C. van der Waal, J.C. Jansen, T. Maschmeyer. J. Catal 223 (2004) 170-178.

[7] F.S. Ramos, A.M. Duarte de Farias, L.E.P. Borges, J.L. Monteiro, M.A. Fraga, E.F. Sousa-Aguilar, L.G. Appel. Catal Today 101 (2005) 39-44.

[8] S. Delsarte, P. Grange. Appl Catal A: Gen 259 (2004) 269-279.

[9] M.I. Kaki, M.A. Hasan, L. Pasuputely. Langmuir 17 (2001) 4025-4034.

[10] S. Delsarte, M. Florea, F. Maugé, P. Grange. Catal Today 116 (2006) 216-225.

[11] G. Szymansky, Rychlicki. Carbon 29 (1991) 489-498.

[12] J. Rodríguez-Mirasol, J. Bedia, T. Cordero, J.J. Rodríguez. Sep Sci & Tech 40 (2005) 3113-3135.

[13] E. González-Serrano, T. Cordero, J. Rodríguez-Mirasol, J.J. Rodríguez. Ind Eng Chem Res 36 (1997) 4832-4838.

[14] Y. Matatov-Meytal, V. Barelko, I. Yuranov, M. Sheintuch. Appl. Catal. B 27 (2000).

[15] S. Brunauer, P.H. Emmett, E. Teller. J Amer Chem Soc. 60 (1938) 309-319.

[16] B.C. Lippens, J.H. de Boer. J Catal. 4 (1965) 319-323.

[17] M.M. Dubinin, E.D. Zaverina, L.V. Radushkevich. J. Phys. Chem. (URSS) 21 (1947) 1351-1362.

[18] M. Lallave, J. Bedia, R. Ruiz-Rosas, J. Rodríguez-Mirasol, T. Cordero, J.C. Otero, M. Marquez, A. Barrero, I.G. Loscertales. Adv. Mater. 19 (2007) 4292–4296.

[19] R. Ruiz-Rosas, J. Bedia, M. Lallave, I.G. Loscertales, A. Barrero, J. Rodríguez-Mirasol, T. Cordero. Carbon. 48(3) (2010) 696-705.

[20] M. Jagtoyen, F. Derbyshire. Carbon. 36 (7-8) (1998) 1085-1097.

[21] P.T. Williams, A.R. Reed. J. Anal Apl Pyrolysis. 70 (2003) 563-577.

[22] P.T. Williams, A.R. Reed. J Anal Appl Pyrolysis 71 (2004) 971-986.

[23] A.M. Puziy, O.I. Poddubnaya, A. Martínez-Alonso, F. Suárez-García, J.M.D. Tascón. Carbon 43 (2005) 2857-2868.

[24] F.J. García-Mateos, R. Ruiz-Rosas, M.D. Marqués, L.M. Cotoruelo, J. Rodríguez-Mirasol, T. Cordero. Chem Eng Journal. 279 (2015) 18-30.

[25] J.M. Rosas, J. Bedia, J. Rodríguez-Mirasol, T. Cordero. Fuel. 88 (1) (2009) 19-26.

[26] J. Rodríguez-Mirasol, T. Cordero, J.J. Rodríguez. Carbon 34 (1996) 43-52.

[27] J.M. Rosas, J. Bedia, J. Rodríguez-Mirasol, T. Cordero. Ind. Eng. Chem. Res. 47 (2008) 1288-1296.

[28] M.J. Valero-Romero, F.J. García-Mateos, J. Rodríguez-Mirasol, T. Cordero. Fuel Processing Technology 157 (2017) 116–126.

[29] X. Wu, L.R. Radovic, Carbon 44 (2006) 141.

[30] J. Bedia, R. Ruiz-Rosas, J. Rodríguez-Mirasol, T. Cordero. J. Catal. 271 (2010) 33.

[31] J.F. Moulder, W.F. Stickle, P.E. Sobol, K.D. Bombemn. Physical Electronics Inc., Eden Prairie, (1995) 4872-4875.

[32] J.L. Figueiredo, M.F.R.Pereira, M.M.A Freitas, J.J.M. Órfao. Carbon 37 (9) (1999) 1379–1389.

[33] U. Zielke, K.J. Huttinger, W.P. Hoffman. Carbon 34 (1996) 983-998.

[34] C. Moreno-Castilla, F. Carrasco-Marín, F.J. Maldonado-Hódar, J. Rivera-Utrilla. Carbon 36(1-2) (1998):145-51.

[35] B. Marchon, J. Carrazza, H. Heinemann, G.A. Somorjai. Carbon 26(4) (1988):507-14.

[36] P.J. Hall, J.M. Calo, Energy Fuels 3 (1989) 370.

[37] A. Linares-Solano, D. Cazorla-Amorós. Handbook of Advanced Ceramics (Ed.: S. Somiya) Academic Press: Elsevier Inc., (2013) 155-169.

[38] Y. Matatov-Meytal, M. Sheintuch. Appl. Catal. A Gen. 231 (2002) 1-16.

[39] J. Bedia, R. Ruiz-Rosas, J. Rodríguez-Mirasol, T. Cordero. AIChE 56 (2010) 1557-1568.

[40] J. Bedia, R. Barrionuevo, J. Rodríguez-Mirasol, T. Cordero. Appl. Catal. B: Env. 103 (2011) 302-310.

[41] J. Bedia, J.M. Rosas, D. Vera, J. Rodríguez-Mirasol, T. Cordero. Catal. Today 158 (2010) 89-96.

[42] J. Bedia, J.M. Rosas, J. Márquez, J. Rodríguez-Mirasol, T. Cordero. Carbon 47 (2009) 286-294.

[43] J.F. Vivo-Vilches, E. Bailón-Garcí,. A.F. Pérez-Cadenas, F. Carrasco-Marín, F.J. Maldonado-Hódar. Carbon 68 (2014)520-530.

[44] F. Rodríguez-Reinoso. Carbon- 36(3) (1998)159-75

[45] J.M. Rosas, R. Ruiz-Rosas, J. Rodríguez-Mirasol, T. Cordero. Carbon 50 (2012)1523-1537.

[46] G.C. Grunewald, R.S. Drago, J. Am. Chem. Soc. 113 (1991) 1636.

[47] F. Carrasco-Marín, A. Mueden, C. Moreno-Castilla, J. Phys. Chem. B 102 (1998) 9239.

Chapter 7

Lignin-derived Pt supported carbon (submicron)fiber electrocatalysts for alcohol electro-oxidation

7.0. Abstract

Lignin fibers, with and without phosphorus, and loaded with platinum have been prepared in a single step by electrospinning of lignin/ethanol/phosphoric acid/platinum acetylacetonate precursor solutions. Thermochemical treatments have been carried out to obtain lignin-based carbon fiber electrocatalysts. The electrospun lignin fibers were thermostabilized in air and carbonized at 900 ºC. The effect of phosphorus and platinum content on the porous structure, the surface chemistry and the oxidation/electro-oxidation resistance have been studied. Phosphorus-containing carbon fibers develop a higher surface area (c.a. 1200 $m^2 \cdot g^{-1}$), exhibit a lower Pt particle size (2.1 nm) and a better particle distribution than their counterpart without phosphorus (c.a. 750 $m^2 \cdot g^{-1}$ of surface area and 9.6 nm Pt particle size). It has been proved that phosphorus improves the oxidation and electro-oxidation resistance of the fibers, avoiding their oxidation during the preparation thermal stages and is responsible of the generation of a microporous material with an unusual wide operational potential window (1.9 V). An important Pt-P synergy has been observed in the oxygen transfer during the oxidation and electro-oxidation of the fibers. The obtained carbon fibers can act directly as electrodes without any binder or conductivity promoter. The fibers with platinum have shown outstanding catalyst performance in the electro-oxidation of methanol and ethanol.

7.1. Introduction

Fibers and composites have become one of the most studied materials due to their physical and chemical properties. Particularly, carbon fibrous materials have been widely studied because of the large spectrum of applications that they present [1]. Carbon fibers are usually obtained from polyacrylonitrile (PAN), pitch or rayon [2,3] and they exhibit outstanding mechanical properties [3]. On the other hand, renewable source of carbon, such as, lignin, has been proposed as carbon-fiber precursor as well [4,5]. Lignin is the second most abundant polymer in biomass after cellulose and it is the main co-product in the papermaking industry. However, the limited market of the lignin makes it an attractive raw material for “waste-refinery” or “bio-refinery” [6].

Lignin contains aromatic and phenolic groups that make it suitable as carbon precursor. Many applications have been proposed to exploit its potential, in this way,

lignin has been used to produce porous carbon materials of great interest in many applications as adsorbent [7,8], catalyst [9], or catalysts support [10]. Although Kraft lignin is more abundant than organosolv lignin, organosolv one is being more studied for these applications as natural carbon fiber source because of its low content in inorganic materials that makes it more environmentally friendly [11,12].

Carbonaceous materials, in many different conformations and structures (activated carbons, carbon black, carbon nanotubes, carbide-derived carbons, graphene sheets, etc) have been studied in electrochemical applications [13–15]. On the other hand, platinum supported-carbon electrodes are receiving a growing interest because they are used as electrocatalysts in proton exchange membrane fuel cells (PEMFCs) and direct methanol fuel cells (DMFCs) [16–20]. The core part of these fuel cells is the preparation of the electrodes in which the platinum-based electrocatalysts are the most efficient.

Carbonaceous materials, in many different conformations and structures (activated carbons, carbon black, carbon nanotubes, carbon aerogels, carbide-derived carbons, graphene sheets, etc) have been studied in electrochemical applications. On the other hand, platinum supported-carbon electrodes are receiving a growing interest because they are used as electrocatalysts in proton exchange membrane fuel cells (PEMFCs) and direct methanol fuel cells (DMFCs) [13–17]. The core part of these fuel cells is the preparation of the electrodes in which the platinum-based electrocatalysts are the most efficient.

Porous carbon materials have been considered as electrocatalyst supports for its properties. However, Pt supported carbon catalysts undergo from decreasing its performance during operation, being corrosion of the carbon supports one of the main reasons. The surface chemistry of carbon materials is important for their use as catalysts support and a key factor for improving their properties. In order to deposit metal catalysts on carbon materials uniformly and efficiently, surface chemistry modification is adopted as an effective method to change interfacial properties and improve the interaction between metal catalysts and carbon materials [21]. Then, the incorporation of N or P heteroatom surface groups is widely studied because these groups also enhance the electrochemical properties [22–24]. In particular, P-groups have been demonstrated to be an effective inhibitor of the carbon electro-oxidation, improving the

electrocatalyst performance [24]. Nevertheless, the main drawback of commonly used powdered carbon supports is that a polymeric material must be added for binding the carbon grains and for obtaining a good current yield of carbon electrode. The binder (a non-conducting solid) could degrade the carbon electrode properties, and lead to the pore blockage and the decrease of the electrode conductivity.

Carbon fibers have many advantages over other carbon conformations, and show good flexibility, density, high surface area and, in some cases, excellent electrical conductivity [25]. In fact, as a continuous material, the conductivity of the fiber is much higher than that of particles obtained from the same precursor [13]. These properties make carbon fibers one of the best carbon conformations for electrochemical applications. Several promising results have been obtained with carbon fibrous materials as electrodes in interesting applications like energy storage [26], or solar cells [27]. Despite carbon fibers can be prepared by different ways, electrospinning method allows for easily obtaining a binderless carbon electrode from a precursor solution [13]. In addition to the good structural characteristics, it is possible to obtain a uniform dispersion of a metal all over the fibers by this method in a single step, yielding, after a thermal stabilization and carbonization, a final carbon fiber-based electrocatalyst with very well dispersed metallic particles of reduced diameter [28], which increases the metallic active surface of the catalyst.

In this chapter, a simple way for obtaining carbon fibers with relatively low content but very well distributed platinum nanoparticles to be used as electrocatalysts is presented. The conductivity of the lignin-based carbon fibers, prepared by co-electrospinning of lignin solution at room temperature without any additives apart from the platinum salt and phosphoric acid, enables the preparation of flexible electrode to work without any binder or conductivity promoter. The use of this kind of binderless electrodes with low platinum loading is a novel contribution from an application point of view. The porous texture, surface chemistry and oxidation/electrooxidation resistance of different carbon fibers catalysts (with and without platinum and phosphorus) has been analyzed. The obtained materials have been tested as electrocatalysts in methanol and ethanol electro-oxidation, paying attention to the above mentioned main advantages of these catalysts (i.e., low platinum loading, flexible electrodes and no binder is used), which are recognized as desirable properties of electrocatalysts for methanol and ethanol electrooxidation [29–33]. The use of low-Pt loading electrocatalyst for DMFCs

and the obtaining of energy (via electro-oxidation) from ethanol, which can be obtained from lignocellulosic sources (bio-ethanol), are interesting strategies towards a more sustainable and efficient production of energy.

7.2. Materials and methods.

7.2.1. Electrode preparation

Lignin fibers were prepared by electrospinning method using Alcell® lignin as precursor in a co-axial configuration [34] and ethanol as solvent. The best electrospinning behavior was obtained when the weight ratio (lignin:ethanol) was 1:1. In the case of phosphorus-containing lignin fibers, the solution was prepared by mixing lignin:ethanol:H_3PO_4 (85%) with a weight impregnation ratio of 1:1:0.3 respectively. The solution was stirred over night at 200 rpm and 60 ºC before spinning. In order to compare, lignin fibers and phosphorus-containing lignin fibers were prepared with different platinum concentrations to study the effect of metal. Different platinum acetylacetonate concentrations were added to the initial solutions in order to obtain, in one step, lignin fibers and phosphorus-containing lignin fibers with platinum nanoparticles. The weight ratios (Platinum acetylacetonate:Lignin) used, in both cases, to obtain a spinnable solution was 0.006:1 and 0.03:1 to prepare lignin fibers with low and high platinum concentrations (about 1 wt% and >5 wt% respectively). Platinum chloride is typically used as precursor to deposit platinum particles [35], however, the organic salt shows advantages against the inorganic. Acetylacetonate anion can add some carbon chain to the support in the thermal treatment, and acetone evaporation can improve the porous structure of the fiber due to its size.

In the electrospinning system, a typical Taylor cone is formed in the needle due to the electrical field generated between the tip and the collector [28,34]. For lignin fibers, the applied electrical potential difference was 14 kV (the collector was at -7 kV and the tips at +7kV), however, phosphorus-lignin fibers need an electrical voltage of 22 kV (collector at -11 kV and tip at +11 kV) to form the Taylor cone due to the electrostatic interactions caused by the phosphoric acid. Ethanol was pumped through the external needle as solvent to avoid the solidification of the cone. The ethanol and lignin solution flow rates were 0.1 and 1 mL h^{-1}, respectively, for the preparation of lignin fibers. In case of the initial lignin solution containing phosphoric acid, the flow

rates needed were 0.3 mL h^{-1} for ethanol and 3 mL h^{-1} for lignin/H_3PO_4 solution. The tip-to-collector distance was 25 cm.

Lignin fibers were thermostabilized in air from room temperature up to 200 ºC with a heating rate of 0.08 ºC min^{-1} followed by 100 h of isothermal treatment in a tubular furnace with an air flow of 50 cm^3 STP min^{-1}, whereas for phosphorus-containing fibers the thermostabilization temperature (also 200 ºC) was reached at 0.8 ºC min^{-1}, and maintained for 1h. Stabilized fibers were carbonized in the same tubular furnace up to 900 ºC with a continuous flow of N_2 (150 cm^3 STP min^{-1}) and a heating rate of 10 ºC min^{-1}, in order to obtain lignin-based carbon fibers with and without phosphorus (PCFs and CFs respectively) and with different platinum concentrations: with no platinum (PCF and CF), with low platinum concentration (PCFLPt and CFLPt) and with high platinum concentration (PCFHPt and CFHPt). Phosphorus-containing lignin-based carbon fibers (PCFs) were washed with distilled water at 60 ºC to neutral (or constant) pH and negative phosphate analysis in the eluate to remove the remaining phosphoric acid after the carbonization stage.

7.2.2. Characterization of activated carbon electrode.

The porous texture was characterized by N_2 adsorption-desorption at -196 ºC and by CO_2 adsorption at 0 ºC, using a Micromeritics ASAP2020 apparatus. Samples were previously outgassed for 8 h at 150ºC under vacuum. From the N_2 adsorption/desorption isotherm, the specific surface area (A_{BET}) was calculated using the BET equation. The micropore volume (V_t) and the external surface area (A_t) were determined using the t-method. The mesopore volume (V_{mes}) was calculated as the difference between total pore volume (at relative pressure of 0.995) and micropore volume [36]. Finally, the narrow micropore volume (V_{DR}) and the narrow micropore surface area (A_{DR}) were estimated by applying the Dubinin-Radushkevich equation to the CO_2 adsorption isotherm [37]. Pore size distribution was determined from N_2 adsorption isotherm by 2D-NLDFT heterogeneous surface model [38].

The surface chemistry of CFs and PCFs was studied by X-ray photoelectron spectroscopy (XPS), the analyses were carried out in a 5700 C model Physical Electronics apparatus with MgKα radiation (1253.6 eV). The C1s peak position was located at 284.5 eV [9] and used as reference to locate the other peaks, and the fitting of the XPS peaks was done by least squares using Gaussian-Lorentzian peak shapes.

The oxygen surface groups were also analyzed by temperature-programmed desorption (TPD). TPD experiments were carried out in a customized quartz fixed-bed reactor placed inside an electrical furnace and coupled to a non-dispersive infrared (NDIR) gas analyzer Siemens ULTRAMAT 22. A carbon fiber sample of 100 mg was heated from room temperature to 930 ºC at a heating rate of 10 ºC min^{-1} in a 200 cm^3 (STP)/min N_2 (99.999 %) flow.

Scanning electron microscopy (SEM), using a JSM 6490LV JEOL microscope working at 25 kV, and transmission electron microscopy (TEM), in a Phillips CM200 microscope at an accelerating voltage of 200 kV, were used to study the fibers morphology. Platinum particle sizes were estimated with an image analyzer software. Energy dispersive X-ray spectroscopy (EDAX) was used to analyze the composition and elements distribution on the carbon electrodes.

The oxidation of the carbon fibers was evaluated by thermogravimetric (TG) analysis in a CI Electronics MK2 balance under 150 cm^3 (STP) min^{-1} air flow from room temperature up to 900 ºC with a heating rate of 10 ºC min^{-1} using about 10 mg of carbon fiber.

7.2.3. Electrochemical characterization

The electrochemical characterization was carried out in a standard three electrode cell using a Pt wire as counter electrode and an Ag/AgCl/KCl 3M electrode as the reference one. The working electrode was prepared by contacting a round piece (ca. 0.1 mg) of the carbon fibers with the tip of a glassy carbon rod (3 mm diameter), used as current collector. Thus, the nominal Pt loading in the tested electrodes is as low as 0.014 and 0.071 mg_{Pt} cm^{-2} (for the CFs with lower and higher Pt content, respectively). The electric contact between the CFs and the collector was better attained by using a drop of Nafion solution (5 wt% Nafion® perfluorinated resin solution, Aldrich). Therefore, neither any binder nor any conductivity promoter were used for the utilization of the carbon fibers as electrodes. A 0.5 M H_2SO_4 aqueous solution was used as supporting electrolyte. N_2 (99.999 %) was bubbled in the cell before the analysis to eliminate dissolved oxygen in the electrolyte.

The electrochemical properties of the fibers were studied by cyclic voltammetry, with a scan rate of 10 mV s^{-1}. Particularly, in order to study the electrochemical stability

of the different CFs, the electrode potential was stepwise shifted by 0.1 V: (i) firstly, from the open circuit potential (OCP) to negative values until the observation of the hydrogen evolution reaction (HER). The onset potential for the HER was indicative of the lower limit potential (LLP) of the electrodes; and (ii) secondly, from the LLP to positive potentials above the OCP, until the observation of anodic currents accompanied with an increase in the intensity of faradic processes in the subsequent cycles. Since these processes are inherent to electro-active oxygen surface groups, both facts occurring together are considered an evidence of carbon electro-oxidation. The onset potential of these anodic currents were then indicative of the upper limit potential (ULP) of the electrodes.

The different lignin-based carbon fiber electrodes were tested as electrocatalysts for the methanol and ethanol oxidation reactions (MOR and EOR, respectively). The experiments were carried out in a similar three electrode cell under the presence of 1.5 M alcohol solution. To ensure reproducibility, the electrodes were first electrochemically stabilized by cyclic voltammetry in the absence of alcohols under an operational potential window of -0.2 to 0.9 V or -0.2 to 1.2 V (vs. Ag/AgCl/KCl 3M), for CFs without or with P, respectively. Next, the electrode was immersed at 0.0 V (controlled potential) in a second cell containing the supporting electrolyte and 1.5 M alcohol solution. After current stabilization, the electrode potential was scanned at 10 mV s^{-1} up to 0.9 V (or 1.2 V in the case of P-containing CFs) and repeatedly cycled between -0.2 to 0.9 V (or 1.2 V) until a stable voltammogram was achieved (the reported steady voltammograms were usually registered at the 10^{th} cycle).

After the voltammetric characterization some electrodes were subsequently submitted to chronoamperometric measurements at different potentials. Different electrode potential was increased from 0.0 V to 0.5, 0.6 or 0.7 V. All the electrochemical measurements experiments were performed using a Biologic VSP 300 potentiostat.

7.3. Result and discussion

7.3.1. Carbon electrodes preparation

Table 7.1 reports the stabilization and carbonization yields of the different carbon fibers prepared in this work. During the stabilization stage, the polymeric lignin

chains suffer cross-linking reaction and the fibers surface takes oxygen producing carbonyl, carboxyl, anhydride and ester surface groups [34,39]. Some oxygen groups can leave the structure as evolved CO and CO_2. Surface phosphorus groups are more capable of taking oxygen, forming different surface carbon-oxygen-phosphorus complexes (mainly C-O-PO_3 and C-PO_3) [40]. In the carbonization stage up to 900ºC, volatile carbon compounds leave the solid and oxidation reactions take place with the retained oxygen during the stabilization process [28], forming complex and condensed carbon structures in the final product. Phosphoric acid acts as activating agent, anchoring on the fibers surface different phosphorus groups and generating a developed porous texture in the final carbon fibers.

Lignin-based carbon fibers (CFs) and phosphorus-containing lignin-based carbon fibers (PCFs) preparation present different yields (Table 7.1). Likewise, these materials show different behavior during the stabilization and carbonization steps when platinum is present in their composition. The stabilization yields of CFs are lower than those of PCFs, which would be attributed to the effect of P. In the presence of Pt, the stabilization yields of CFs decrease, and the higher the amount of metal in the lignin fibers, the lower the yield is observed. This could be related to the high activity of a well-known oxidation catalyst like Pt [41]. However, independently of the Pt content, the PCFs show similar stabilization yields as can be observed in Table 7.1. This result indicates that phosphorus prevents the oxidation of the fibers surface during the stabilization stage, even in the presence of platinum.

In addition, the presence of phosphorus-carbon groups allows a 10-60 times faster stabilization process. As lignin presents a glass transition temperature (Tg) far below the carbonization temperature, as-spun fibers need to be stabilized to avoid softening and fibers melting. Air oxidation is an easy and cheap process of stabilization [28,39] due to the increase of the Tg through oxygen cross-linking reactions and oxygen groups formation. Slow heating rates are needed in the air stabilization process to ensure a temperature lower than the Tg. The presence of H_3PO_4 in the as-spun fibers increases the amount of oxygen surface content. Therefore, the cross-linking reactions and the formation of oxygen groups (with and without Pt) are favored in this case. This way, the stabilization of P-containing lignin fibers can be carried out at faster heating rate and less time without fibers melting in the carbonization step.

Table 7.1. Stabilization and Carbonization yields.

Sample	Stabilization yield (wt%)	Carbonization yield (wt%)	Overall yield (wt%)
CF	73.2	36.9	27.0
CFLPt	62.8	37.2	23.4
CFHPt	44.5	22.3	9.9
PCF	88.2	32.9	29.0
PCFLPt	87.5	33.4	29.2
PCFHPt	85.1	35.0	29.8

When stabilized fibers were heat-treated up to 900 ºC in N_2 atmosphere, the carbonization yields (referred to the stabilized fibers) are similar for all the experiments (about 35%), except for CFHPt (Table 7.1). This low carbonization yield corresponds to the lowest stabilization yield obtained in the first thermal treatment. Hence, it is possible to conclude that CFHPt takes a huge amount of oxygen in the stabilization stage (due to the high percentage of metal in its surface), which is partially removed during the carbonization stage as CO_2 and CO.

Comparison of the overall yields (loss of oxidation products and volatile carbon compounds) of the fibers (Table 7.1) indicates that CF and PCF present similar yields (about 30 wt%). However, the presence of Pt in CFs produces a very different behavior as said above: the high oxygen content of the fibers after stabilization treatment in CFLPt and CFHPt, and the absence of an oxidation inhibitor (as phosphorus) favor carbon gasification during the subsequent carbonization process, producing a development of mesoporosity as will be discussed in the next section. On the contrary, the presence of P inhibits the carbon oxidation even in the presence of Pt, thus, quite similar and higher overall yields are obtained for the production of Pt-supported carbon fibers (PCFLPt and PCFHPt).

7.3.2. Physicochemical characterization

Figure 7.1 shows the N_2 adsorption-desorption isotherms at -196ºC for the different carbon fibers with or without phosphorus and with or without platinum. Textural parameters derived from these isotherms are displayed in Table 7.2. CFs exhibit between 750 and 850 $m^2\ g^{-1}$ BET surface area, while PCFs can develop more than 1100 $m^2\ g^{-1}$ BET surface area. These results indicate that H_3PO_4 produces an additional development of porosity in phosphorus-containing fibers. However, these

fibers do not develop wide mesopores, as the impregnation ratio used for the chemical activation (g H_3PO_4/g precursor) is lower than 1 (0.3 in this case) [9,42]. This different behavior can also be appreciated by comparing the isotherms of CF and PCF (Figure 7.1a and 7.1c), which show that PCF is able to adsorb more nitrogen at lower relative pressures than the phosphorus-free counterpart (CF).

The effect of platinum on the porous texture of CFs is shown in Figure 7.1a. While CF exhibits a type I isotherm (characteristic of microporous materials), CFLPt and CFHPt present a type IV isotherm, with a hysteresis loop beyond 0.4 relative pressures, typical of materials with wide mesopores. In the absence of P, platinum produces a development of mesoporosity in the carbon fibers, being more appreciable as Pt content increases. This result may be attributed to the aforementioned high oxygen content after the fiber stabilization [34] and the Pt-promoted gasification of some carbon material during the thermal processes, which reduces the overall yield (Table 7.1). Pore size distribution (Figure 7.1b) shows a reduction of the microporosity, shifting the maximum of the micropore size distribution to slightly higher values upon increasing the amount of Pt in CFs. Moreover, CFLPt and CFHPt develop new pores bigger than 20 Å as result of the greater surface oxidation of these carbon fibers.

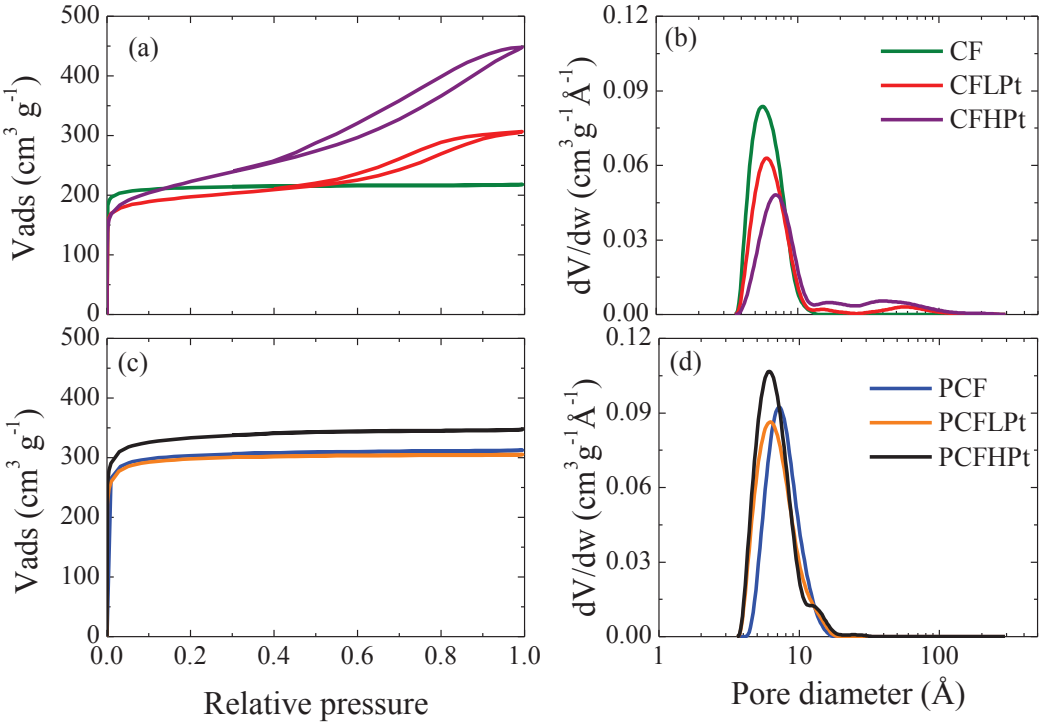

Figure 7.1. N_2 adsorption-desorption isotherms at -196˚C of (a) CFs and (c) PCFs. Pore size distribution of (b) CFs and (d) PCFs.

By contrast, PFCs show type I isotherms (Figure 7.1c), typical of microporous solids (this type of isotherm are usually obtained with a low amount of phosphoric acid [42]). This result evidences that Pt does not induce the mesoporosity generation in PCFs although they withhold more oxygen in the stabilization process than CFs. PCF and PCFLPt present practically overlapped isotherms, which suggests the total inhibition of the Pt-catalyzed gasification reaction. However, the increase in BET surface area in PCFHPt indicates that this higher amount of platinum allows some gasification, developing higher pore volume on the carbon surface (Table 7.2). Figure 7.1d displays the pore size distribution of these P-containing carbon fibers. A smaller micropore size is shown by carbon fibers with platinum, which means that in this case the oxidation of the carbon surface generates narrower microporosity.

Table 7.2. Porous textural parameters of the carbon fibers.

Sample	N_2 isotherm				CO_2 isotherm	
	A_{BET} (m^2/g)	A_t (m^2/g)	V_t (cm^3/g)	V_{mes} (cm^3/g)	A_{DR} (m^2/g)	V_{DR} (cm^3/g)
CF	851	8	0.33	0.01	1002	0.40
CFLPt	747	161	0.23	0.24	729	0.30
CFHPt	786	383	0.18	0.51	618	0.25
PCF	1210	14	0.47	0.01	1017	0.41
PCFLPt	1159	11	0.46	0.01	1007	0.40
PCFHPt	1289	29	0.51	0.02	1158	0.46

As it is possible to observe in Table 7.2, CFs show a more accused increase in external surface area and mesopore volume than PCFs upon increasing the amount of platinum. This suggests that the presence of phosphorus plays a key role in the porosity development of the fibers during the thermal stages. Comparing the parameters obtained from CO_2 isotherms (Table 7.2), PCFs exhibit values of narrow micropore area (A_{DR}) and narrow micropore volume (V_{DR}) quite similar to the results obtained from N_2 isotherms (A_{BET} and V_t). On the other hand, for CFs, only CF presents higher narrow micropore area and volume calculated from CO_2 isotherm than BET surface area and micropore volume ($V_{t)}$ determined from N_2 isotherm, which indicates that CF presents a large proportion of pores of size below about 0.5 nm. Therefore, the presence of phosphorus avoids the mesopores development by oxidation but generates wider microporosity than P-free lignin-based carbon fibers.

Table 7.3 reports the elemental surface mass concentration obtained by XPS. As explained before, PCFs are more capable of taking oxygen than CFs due to the presence of phosphorus surface groups (e.g. C-O-PO_3 like groups), so oxygen mass surface concentration is higher in phosphorus-containing fibers (PCFs). Similar results have been observed for other carbonaceous materials activated with H_3PO_4 [24,43,44]. The decrease in oxygen mass surface concentration in CFs with the increase of the platinum content can be assigned to the gasification reaction that occurs during the carbonization stage, where oxygen is removed as CO or CO_2. According to XPS analyses, it is easy to control the amount of phosphorus in the final carbon fibers (Table 7.3).

Table 7.3. Mass Surface concentration obtained by XPS quantitative analysis and CO and CO_2 evolved from TPD analyses.

Sample	XPS				TPD	
	C (wt%)	O (wt%)	P (wt%)	Pt (wt%)	CO (mg/g)	CO_2 (mg/g)
CF	95.9	4.1	-	-	68.3	12.7
CFLPt	95.1	3.9	-	1.0	41.8	19.9
CFHPt	90.4	2.5	-	7.1	97.2	14.3
PCF	90.5	7.3	2.2	-	98.5	15.4
PCFLPt	87.6	7.8	2.3	2.3	202.1	28.1
PCFHPt	75.0	11.4	2.4	11.2	152.7	44.5

Figure 7.2 displays the Pt4f and O1s spectra for the different carbon fibers (spectra are normalized to have a better visual comparison). The Pt4f region of the spectra presents a doublet corresponding to $Pt4f_{7/2}$ and $Pt4f_{5/2}$ respectively [45]. The separation between peaks, due to spin orbital splitting, is a quantized value of 3.33 eV. The Pt4f peak can be deconvoluted into two contributions. The $Pt4f_{7/2}$ peak at around 71.5 eV can be attributed to Pt^0, while the Pt $4f_{7/2}$ peak located at around 73.0 eV is related to Pt^{2+} [45]. PCFs do not show significant modifications in the platinum species ratio (about 65 wt% of Pt^0), whereas the amount of metallic platinum increases when increasing the total platinum mass in CFs. Interestingly, the amount of Pt^{2+} is higher for PCFs.

O1s spectra show a well-defined maximum located at 532.2 eV that can be attributed to C-O single bond. In comparison with CFs, PCFs exhibit a higher intensity of the hump corresponding to combined platinum (Pt-O) at 529.8 eV, due to the higher presence of Pt^{2+}-oxygen species.

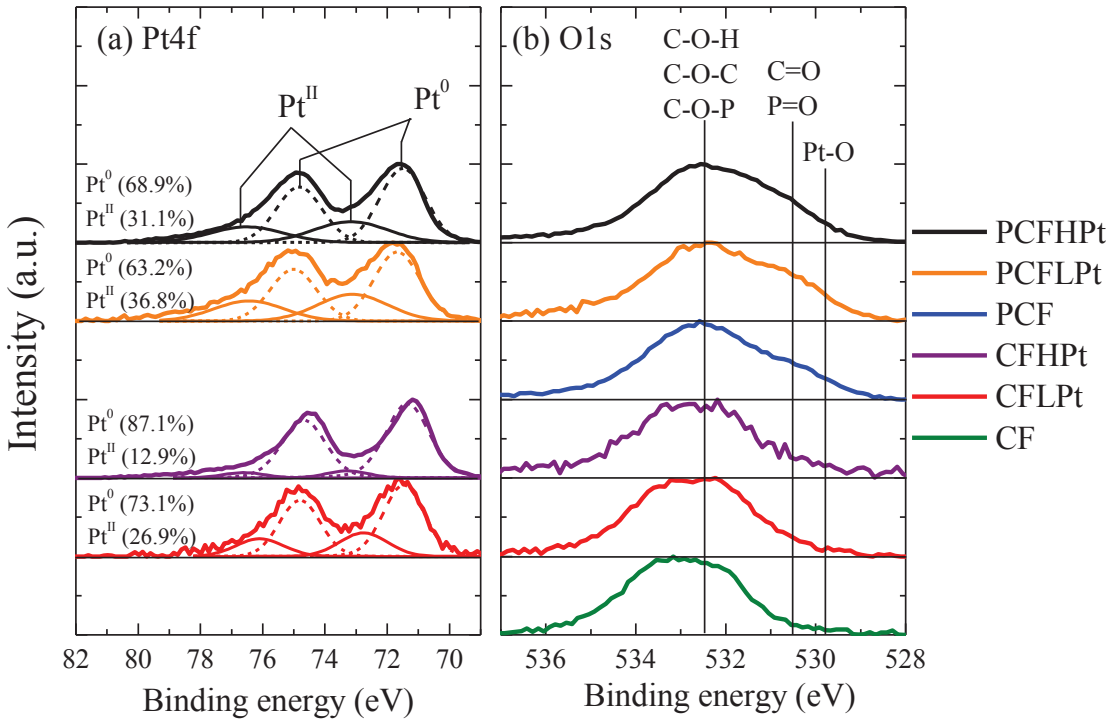

Figure 7.2. (a) Pt 4f and (b) O 1s XPS spectra for the carbonized fibers with and without phosphorus.

Figure 7.3 shows the variation of carbon, oxygen, phosphorus and platinum species concentration during the preparation of the final CFHPt and PCFHPt electrodes: just after being electrospun (as-spun), after stabilization stage in air and after carbonization stage at 900 ºC. The loss of volatile compounds and oxygen groups explains the increase in carbon concentration and the decrease in oxygen in the carbonization stage (Figures 7.3a and 7.3b). Pt^{2+} concentration is similar in the two first stages (as-spun and after stabilization), being the platinum ratio (Pt^{2+}/Pt^{0}) c.a. 60/40 in both, CFHPt and PCFHPt.

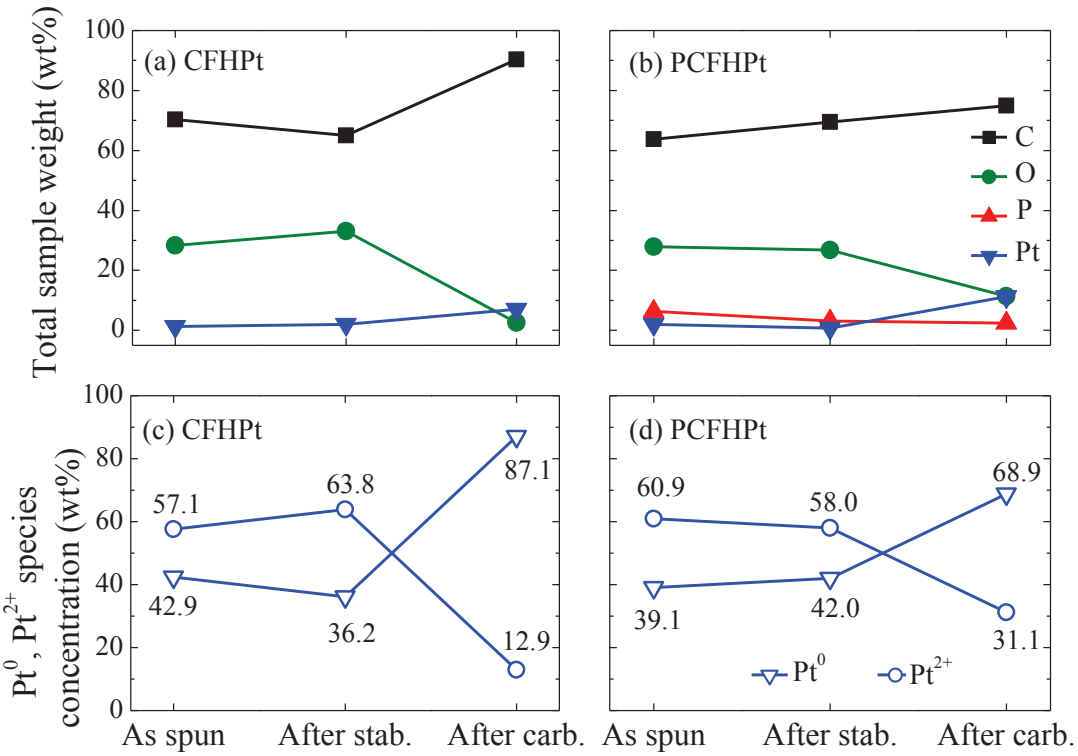

Figure 7.3. C, O, P and Pt mass surface concentration obtained by XPS quantitative analysis for as-spun, stabilized and carbonized (a) CFHPt and (b) PCFHPt, and evolution of Pt^0 and Pt^{II} species concentration in (c) CFHPt and (d) PCFHPt.

As shown in Figure 7.3c, the platinum ratio after carbonization stage is 13/87 (Pt^{2+}/Pt^0) for CFHPt, involving an important increase in the metallic species. The suggested oxygen transfer between platinum and carbon may explain this result. Thus, Pt^{2+} is reduced to the metallic form, and carbon takes the oxygen, which leads to carbon gasification and to the development of mesopores in CFHPt. This carbon gasification during the carbonization stage also explains the important oxygen mass surface concentration drop (Figure 7.3a) in comparison to that of PCFHPt. On the other hand, PCFHPt exhibits a change of the platinum ratio from 60/40 to 30/70 approximately (Figure 7.3d) during the carbonization stage. Therefore, part of platinum reduces its oxidation state but carbon does not undergo a significant oxidation reaction, since this carbon fiber does not develop mesopores. This result suggests that the presence of phosphorus changes the mechanism of the carbon oxidation reaction [43]. In this case, surface phosphorus groups take the oxygen that Pt^{2+} loses, allowing the metal reduction and inhibiting the carbon oxidation. For this reason, oxygen represents more than 11 wt% (Figure 7.3b) of the final PCFHPt, which remains most of it combined with phosphorus, forming stable phosphate anions (C-O-P-O- and C-P-O-). The higher

platinum ratio (Pt^{2+}/Pt^{0}) in P-containing carbon fiber is probably due to a strong interaction between Pt2+ and these P-anions.

TPD analysis was used to identify the oxygen surface groups of the carbon fibers. Table 7.3 reports the amount of CO and CO_2 evolved from TPD of the carbon fibers up to a final temperature of 930 ºC. Oxygen surface groups with acid character such as carboxylic and lactonic evolve as CO_2 upon thermal desorption. Carbonyl, ether, phenolic and quinone carbon-oxygen surface groups evolve as CO at higher temperature, while anhydride evolves as both CO and CO_2 [46]. As can be seen in Table 7.3, the amount of desorbed CO is higher than the amount of CO_2, what means that carbon-oxygen groups of acid character are minority on the carbon fibers surface. According to previous research, this fact usually happens when the carbonization temperature is higher than 600 ºC [47].

An increase in the evolution of oxygen (mainly as CO) has been observed in PCFs (Table 7.3) at higher temperatures than 800 ºC, which has been previously assigned to the decomposition of stable C-O-P-O surface groups to produce C-P-O [42,48]. The CO_2 evolution observed in these fibers at these high temperatures could be due to CO-evolved secondary reactions with other surface oxygen groups [49], in part catalyzed by the presence of platinum in PCFLPt and PCFHPt.

Phosphorus groups of carbonaceous materials provide the fibers with a regular and non-defect surface with small platinum nanoparticles, as shown in SEM and TEM micrographs (Figure 7.4). General fiber morphology is shown in Figure 7.4a and 7.4b where SEM micrographs are represented. Melting of fibers is avoided due to the thermostabilization treatment applied to the as-spun material [39]. Non-interconnected fibers are displayed in Figure 7.4a and 7.4b, corresponding to CFHPt and PCFHPt respectively, in spite of the faster thermostabilization process of PCFs. The fibers diameter obtained by this preparation method is between 600 nm and 1 μm for CFs, whereas fiber sizes from 600 nm to 3 μm are observed when phosphoric acid is added to the spinnable solution (PCFs).

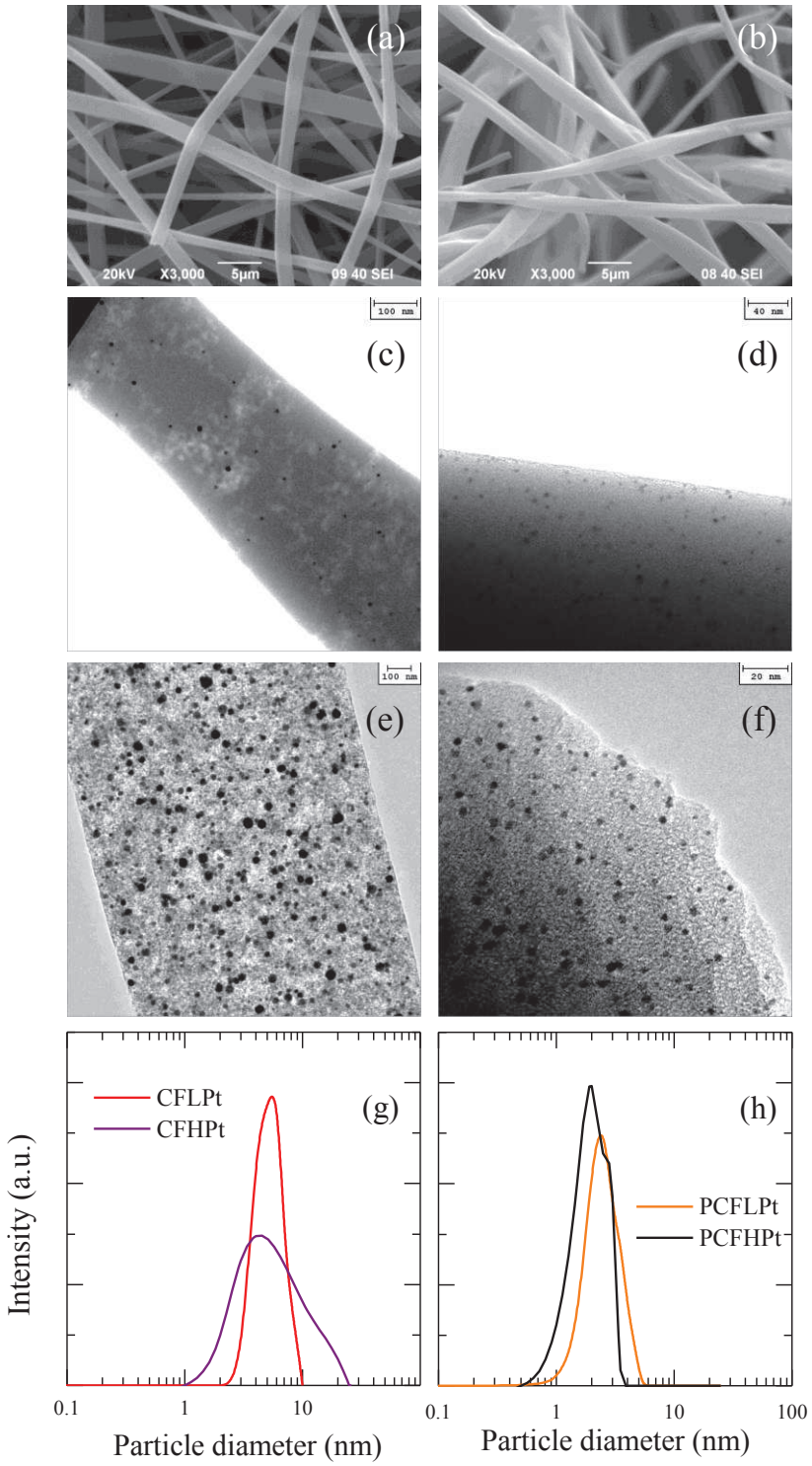

Figure 7.4. SEM and TEM images of carbon fibers electrocatalysts. SEM microgrhaps of (a) CFHPt and (b) PCFHPt; TEM images of (c) CFLPt, (d) CFHPt, (e) PCFLPt and (f) PCFHPt; Pt particle size distribution of (g) CFLPt, CFHPt, (h) PCFLPt and PCFHPt

Electrospinning method allows for obtaining a good distribution of platinum nanoparticles in the fibers as all TEM images show (Figure 7.4c-f) and it was previously reported [28,50]. Phosphorus-containing fibers present a smaller Pt particle size (see bar length) than those of the homologues fibers without phosphorus. The larger particle size of Pt on CFHPt (Figure 7.4e) could be related to the formation of mesopores and the decrease in the carbonization yields (Figure 7.1a and Table 7.1). This way, the Pt-promoted gasification of the carbon surface during the thermal stages facilitates the migration and sintering of platinum particle, reducing the metallic specific area. On the other hand, the inhibition of carbon oxidation in PCFs and the interaction of Pt^{2+} with P-anions, observed by XPS analysis, restrict this Pt migration, yielding smaller and well-dispersed Pt particles. This improvement of Pt dispersion has been previously observed in P-containing carbonaceous materials [51].

As shown in Figure 7.4g and 7.4h, the particle size distributions of CFs are wider than those for PCFs. The average particle size, which has been estimated from the particle size distribution, is similar for PCFLPt and PCFHPt (2.8 and 2.1 nm respectively). On the other hand, the increase in the surface oxidation of CFs (developing mesopores) leads to higher Pt particle sizes (5.6 nm for CFLPt and 9.6 nm for CFHPt).

Figure 7.4e shows an apparent higher Pt concentration than the one determined by XPS analysis (Table 7.3). TEM images allow for observing the total amount of platinum in the studied region, while XPS analysis only determines the surface concentration (around 20 Å deep). The total concentration of platinum in carbon fibers can also be calculated by a mass balance of platinum in the fibers, attending to the overall yield in thermal stages and considering no platinum losses during thermal processes. On one hand, similar Pt concentrations are obtained from XPS and from mass balance in CFs, indicating the uniform distribution of Pt in the carbon fibers. On the other hand, higher Pt content is shown in PCFs from XPS analysis when these values are compared with that calculated in the bulk. This result suggests that Pt is meanly located in the most external fiber surface in these cases. This phenomenon can be related to the P-groups behavior during the thermal stage, which could retain the metal in the external surface of the fibers.

EDAX analysis of all carbon electrodes is shown in Figure 7.5. Once again, by this analysis, we demonstrated that the electrospinning technique is unique for obtain materials with well dispersion of elements, which are included at the beginning of the preparation steps (as Pt and P).

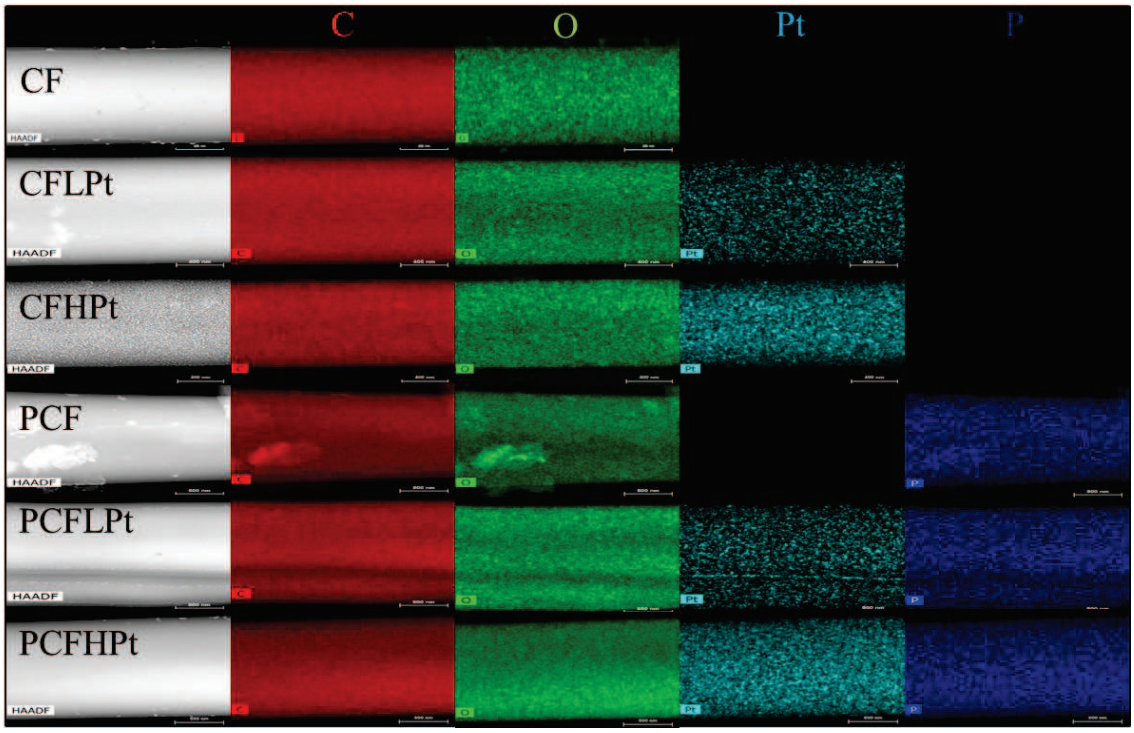

Figure 7.5. EDAX analysis of carbon electrodes.

Carbon fibers were submitted to TG analyses in air atmosphere for comparing the fiber behavior and the platinum activity with and without phosphorus (Figure 7.6). Platinum-free fibers show similar behavior than the ones previously reported for activated carbons with H_3PO_4 [43,44]. Phosphorus makes fibers more resistant to oxidation, and platinum tends to decrease the temperature at which oxidation reaction begins (about 50 ºC and 100 ºC for low and high Pt content respectively).

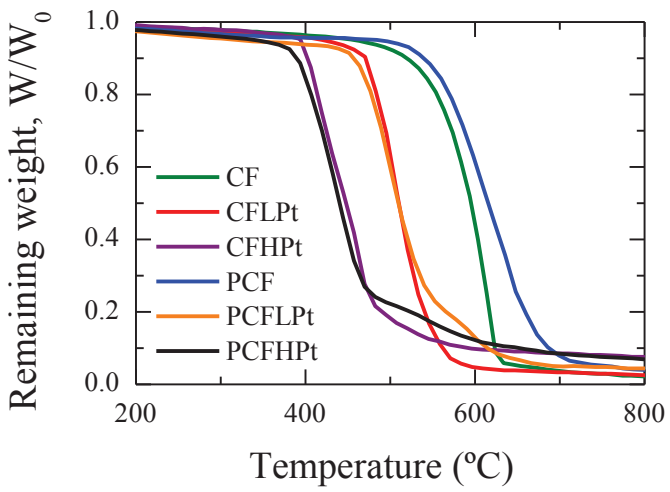

Figure 7.6. Non isothermal oxidation profiles of CFs and PCFs

As previously discussed, phosphorus makes carbon resistant to oxidation in poor-oxygen atmosphere (carbonization conditions) in spite of platinum presence, (see the carbonization yields in Table 7.1). Nevertheless, an opposite behavior is observed in oxygen-rich atmosphere (combustion conditions). The promotion of the onset combustion temperature of PCFLPt and PCFHPt (versus their counterparts) suggests that phosphorus enhances the platinum activity as it acts as oxygen donor. However, TG analysis proved that carbon-phosphorus surface groups are very stable and it is necessary to submit the fiber to higher combustion temperature to oxidize the entire carbon surface. Comparing the 3 pairs of TG curves, PCFs need higher temperature than the corresponding CFs (with the same platinum composition) to burn-off all the carbon. These stable phosphorus groups present a maximum in TPD curves at high temperatures, corresponding to C-O-P surface groups decomposition, as reported in previous researches [40,48,52].

7.3.3. Electrochemical characterization

The electrochemical characterization was carried out in a three electrode cell by using the obtained lignin-based CFs and PCFs as electrodes without any conductivity promoter and binder. Figure 7.7 displays the voltammograms, within the stability potential window, in acid electrolyte of the different lignin-based carbon fibers prepared in this work. The anodic current rise at higher positive potentials has been related to the electro-oxidation of carbon and/or the oxygen evolution reaction (OER); whereas the

increase in the cathodic current at negative potentials mainly seems to correspond with the hydrogen evolution reaction (HER). This HER is highly reversible on Pt, so that the anodic peaks in the potential region between -0.2 V and 0.0 V observed for Pt-containing samples are due to the oxidation of the generated H_2 on this electrocatalyst. Accordingly, the observation of these peaks suggests that the Pt nanoparticles in the different lignin-based CFs and PCFs are accessible to the electrolyte and electro-active.

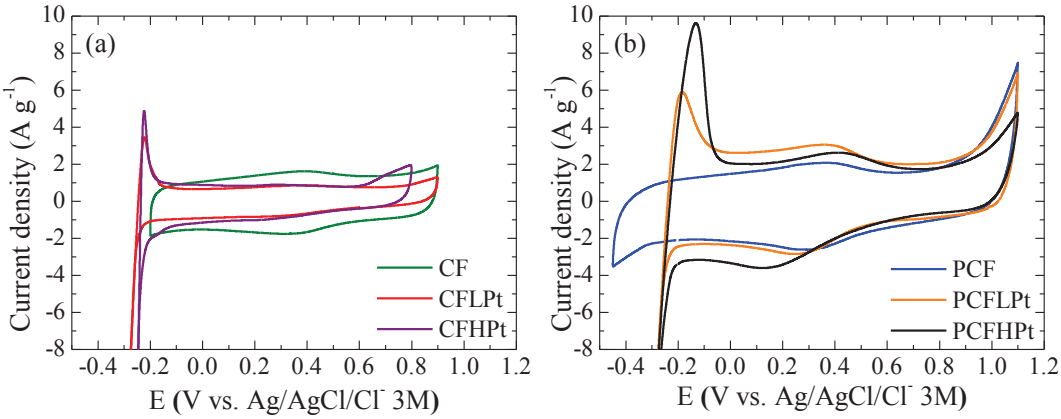

Figure 7.7. Cyclic voltammograms up to different upper limit potentials (1st cycle) of (a) CFs and (b) PCFs electrodes with variable Pt content in the absence of methanol. 0.5 M H_2SO_4; v =: 10 mV·s^{-1}.

The presence of phosphorus in the fibers (Figure 7.7b) yields carbon electrodes with a larger double-layer charge, which can be related to their larger surface area and/or volume of wider micropores (Table 7.2) accessible to the electrolyte ions. On the other hand, the voltammograms of the different electrodes also contain a more or less reversible broad peak centered at around 0.4 V. This peak is attributed to faradic processes involving quinone-like oxygen groups on carbon surfaces [53] and it is more intense in PCFs electrodes, in agreement with their higher content in CO-evolving groups (Table 7.3).

Regarding the electrochemical stability, in the absence of P (Figure 7.7a), the electrode without Pt (CF) started to suffer from electro-oxidation [54] above ca. 0.9 V (vs. Ag/AgCl/Cl-(3M)). This oxidation potential can be considered slightly high when compared to conventional activated carbons [24], and may be associated to the suitable structure of carbon electrodes prepared from lignin [13]. On the other hand, the electro-oxidation resistance of the fibers was further enhanced with the incorporation of P (PCF), with an onset potential from 1.1 V (Figure 7.7b). This inhibition of carbon

electro-oxidation in PCFs is in agreement with the higher oxidation resistance observed in O_2 atmosphere (Figure 7.6), and can be uniquely assigned to the slower oxidation of carbon mediated by phosphorus surface functionalities [24].

As it can be observed in Figure 7.7a, the introduction of Pt on CFs without P remarkably decreases their electro-oxidation onset potential down to ca. 0.75 and 0.6 V for the fibers with low and high Pt content, respectively. This is due to the well-known electrocatalytic activity of Pt for carbon oxidation and oxygen evolution reaction [55]. However, in the presence of P (Figure 7.7b), this effect decreases independently of the studied Pt content. This result indicates that P surface groups could protect carbon against electro-oxidation, even when it is acting as electrocatalyst support, and that Pt electrocatalysts activity for oxygen evolution reaction is strongly decreased.

In the region of lower potentials, Pt causes a decrease in the overpotential and an increase in the cathodic current density for the HER (Figure 7.7a and 7.7b). In particular, the onset potential for HER in the carbon fibers without P is shifted from -0.30 (CF) to -0.15 V for the high Pt concentration (CFHPt). Nevertheless, the P surface groups were found to affect also the HER. In this sense, from the comparison of Figure 7.7a with 7.7b it can be clearly deduced that the HER overpotential for the fibers with P and variable Pt content (Figure 7.7b) are at least 0.1 V higher than that of the corresponding electrodes without P (Figure 7.7a). This indicates that P surface groups are also affecting the activity of Pt species although this effect is much less relevant than at positive potentials [56]. These results are extremely interesting and reflect the effect of P on the Pt reducibility as observed by XPS. Upon positive polarization P-functional groups remain oxidized or can be fully oxidized what favors the interaction with Pt^{2+} species which will not be reduced and will have a low activity towards oxidation reaction either of the support or the electrolyte. On the other hand, at negative potentials P-groups can be reduced (especially in presence of a catalyst like Pt) what will remove the impediment for further Pt^{2+} species reduction which will contribute to the reaction occurring at these negative potential conditions.

The conductivity and stability shown by the different lignin-based carbon fibers make these electrodes auspicious electrocatalysts for electro-oxidizing several compounds in aqueous solution. In such a way, the electrocatalytic behavior of these electrodes has been studied for the methanol and ethanol oxidation reactions (MOR and

EOR, respectively), which are well-known important processes in fuel cells for energy conversion [57,58]. Figures 7.8a and 7.8b display the voltammetric response of the CF electrodes without (Figure 7.8a) and with P (Figure 7.8b) and variable Pt content in the presence of methanol. Independently of the presence of P, the electrodes without Pt (samples CF and PCF) showed a CV profile quite similar to those obtained in an electrolyte solution free of methanol. And the same result was found in the case of ethanol (Figure not shown). This indicates that without Pt, the lignin-based carbon fibers electrodes present no electro-activity for MOR or EOR.

By contrast, the electrodes exhibited an outstanding alcohol electro-oxidation performance when Pt was introduced in the carbon fibers. In the absence of P (Figure 7.8a), both CFLPt and CFHPt electrodes display two defined anodic peaks, in the forward and reverse scans, respectively, characteristic of methanol oxidation on Pt via the so-called ‘‘dual-path’’ mechanism [59]. The oxidation process in the forward scan has been assigned to “the active intermediate reaction path”, in which adsorbed methanol and intermediates are oxidized directly by O-containing species on Pt to form CO_2. In the reverse scan, the anodic peak is related to the “poisoning intermediate reaction path”, i.e. the removal of the incompletely oxidized carbonaceous species formed in the forward scan, mostly in the form of CO bonded to Pt. Nevertheless, it has been recently proposed that the origin of this second oxidation peak is the methanol oxidation on platinum oxides (Pt−Ox) [60]. In the case of CFLPt, the peak currents of the forward and reverse peaks were found at 0.65 and 0.57 V, respectively; whereas they appeared at 0.71 and 0.59 V increasing the amount of Pt (CFHPt).

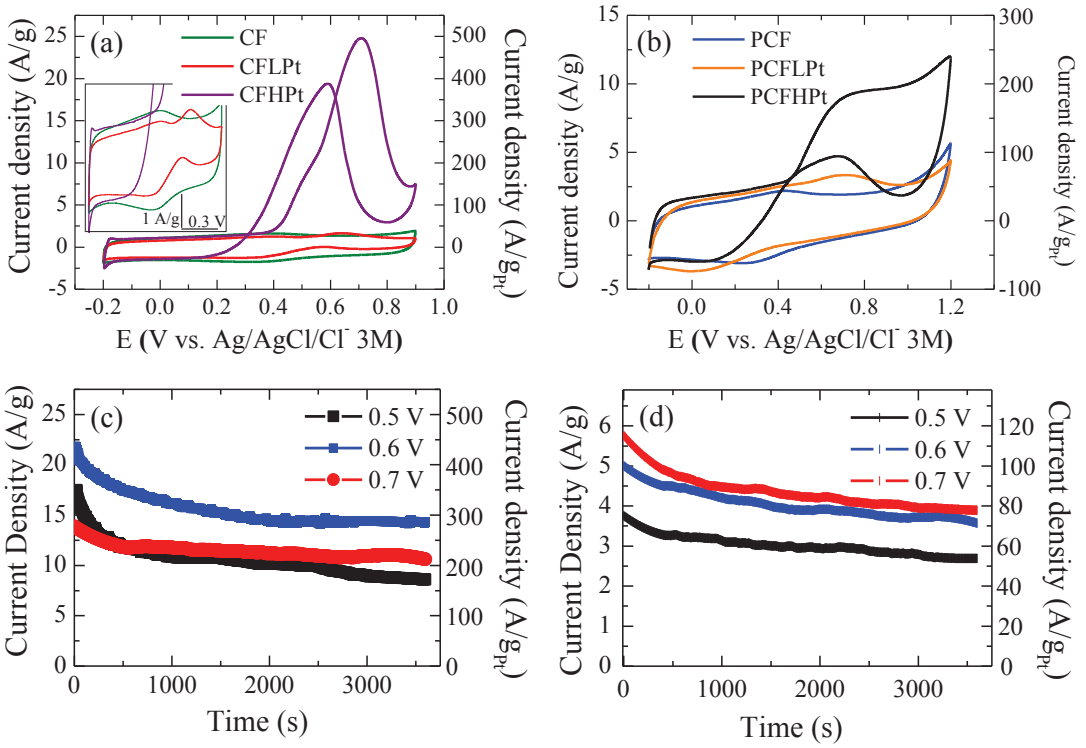

Figure 7.8. Steady cyclic voltammograms of (a) CFs and (b) PCFs electrodes with variable Pt content in the presence of methanol (v = 10 mV/s). Chronoamperometric measurements for methanol electro-oxidation at different potentials on (c) CFHPt and (d) PCFHPt. Electrolyte 0.5 M H_2SO_4 + 1.5 M methanol.

The effect of Pt content on methanol oxidation was particularly remarkable when comparing the oxidation onset potentials and current densities of both electrodes. As it can be observed in Figure 7.8a, the fibers with lower Pt content (CFLPt) start to oxidize methanol at ca. 0.35 V, producing a maximum current density in the forward scan (I_f) close to 1.7 A g^{-1}. On the other hand, for CFHPt electrode the oxidation onset potential is ca. 0.25 V and the reaction produces a prominent anodic peak with I_f up to 25 A g^{-1}. Considering the content of Pt electrocatalyst (active phase) on the electrodes (nominal Pt contents), and after correction of the double-layer charge, the values of I_f can be calculated as 75 and 495 A g_{Pt}^{-1} for CFLPt and CFHPt, respectively

Regarding the mentioned "dual-path'' mechanism, the ratio of the forward (I_f) to the reverse (I_b) anodic peak current densities, I_f/I_b, can be used to describe the catalyst tolerance to carbonaceous species accumulation [61]. The electrocatalytic response and, therefore, the I_f/I_b ratio for the different electrodes was remarkably stable upon cycling (see Figure 7.9). For the CFLPt and CFHPt electrodes, the calculated I_f/I_b values are

0.60 and 1.20, respectively. This last high I_f/I_b ratio indicates excellent oxidation of methanol to CO_2 during the anodic scan and poor accumulation of intermediates on the Pt surface [61].

With respect to the role of P, Figure 7.8b shows that Pt-containing PCFs electrodes present also a good electro-activity for methanol electro-oxidation. However, their performance is significantly lower when compared to that of the corresponding electrodes without P (Figure 7.8a). This seems to be consequence of the Pt interaction with P-functional groups that results in different degree of Pt reducibility as has been previously discussed. The PCFLPt starts to oxidize methanol at ca. 0.4 V and the forward oxidation reaches a maximum of 3.3 A g^{-1} at 0.71 V. Particularly, and probably due to the large double-layer currents, the reverse oxidation peak is poorly defined in this case. This response was greatly improved when a higher Pt content was introduced in the fibers. Thus, PCFHPt oxidized methanol from ca. 0.35 V, entailing considerably broader forward and reverse oxidation peaks. The forward peak presents a less-defined maximum at 0.79 V with a current density of 9.5 A g^{-1}. Interestingly, PCFHPt electrode can effectively electro-oxidize methanol at higher potentials, between 0.9-1.1 V, where, unlike in the case of CFs without P, neither carbon nor electrolyte electro-oxidation reactions occur (Fig. 7.7b). In the reverse scan, the maximum is observed at 0.67 V and the current density reaches 4.7 A g^{-1}. Expressed in terms of Pt mass, the values of I_f can be calculated as 130 and 170 A g_{Pt}^{-1} for PCFLPt and PCFHPt, respectively, and the I_f/I_b ratio for the PCFHPt electrode is 1.1, which again reflects a good activity towards complete methanol oxidation during the anodic scan.

The electro-oxidation of methanol was further studied at constant electrode potential. Figures 7.8c and 7.8d display the chronoamperometric response of CFHPt and PCFHPt electrodes at various potentials in the presence of methanol. Among the electrodes with or without P, CFHPt and PCFHPt electrodes have been chosen for this study because of their higher activity for methanol oxidation. As it can be observed, independently of the applied potential, both electrodes show high oxidation currents that slightly decrease with time. Nevertheless, a 70-75 % of the initial current is retained by both electrodes in the first hour of experiment. This current decay has been generally observed in several electrocatalysts and has been related to a blockage of the surface by some organic residue and/or other deactivation mechanisms [62]. Particularly, the oxidation currents provided by the electrode without P are 3-5 times higher, what is in

agreement with the voltammetric characterization. On the other hand, the influence of the applied potential on the oxidation currents seems to be different for both electrodes. Thus, in the case of CFHPt electrode (Figure 7.8c), a remarkably higher maximum current is obtained when working at 0.6 V, while it gradually increases with the electrode potential for the PCFHPt electrode (Figure 7.8d).

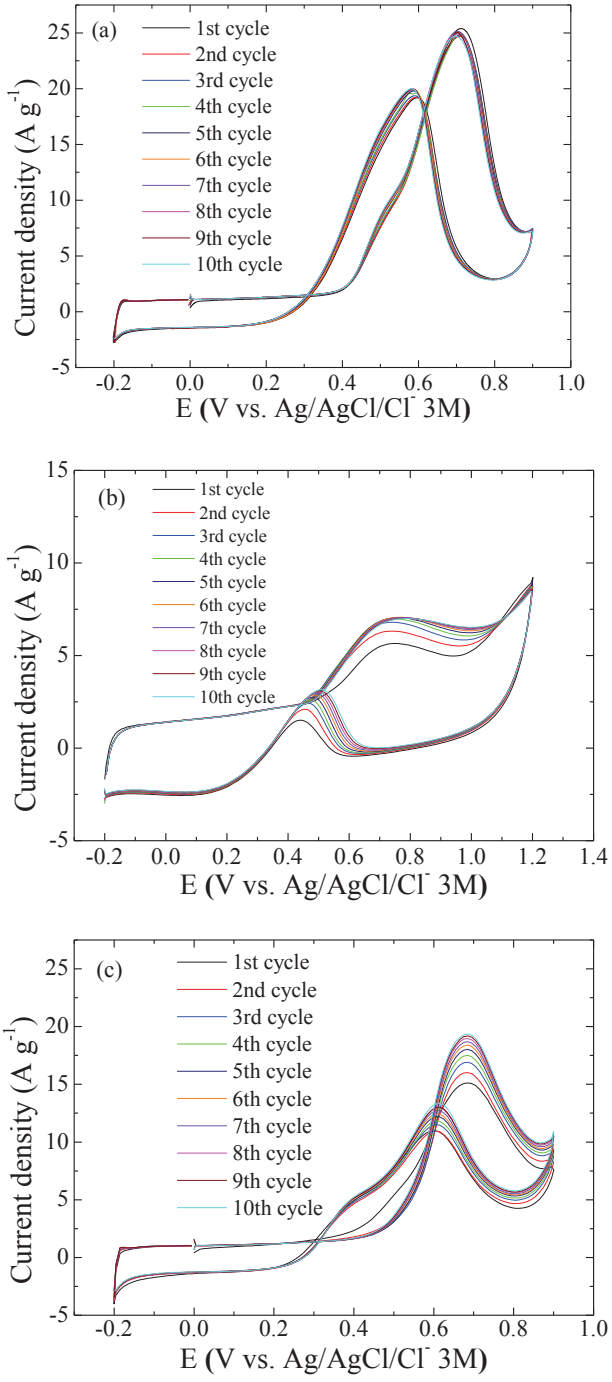

Figure 7.9. Cyclic voltammograms (1st to 10th cycles) of (a) CFHPt and (b) PCFHPt in 0.5 M H_2SO_4 + 1.5 M methanol, and of (c) CFHPt in 0.5 M H_2SO_4 + 1.5 M ethanol. v = 10 mV s^{-1}

Finally, the electro-activity of the reported lignin-based carbon fibers was tested for ethanol electro-oxidation. Fig. 7.10a compares the voltammetric response of a CFHPt electrode in the presence or absence of ethanol. The onset for ethanol oxidation is observed at ca. 0.25 V and, as in the case of methanol, the voltammogram shows two clear oxidation peaks in the forward and reverse scans, respectively. In the forward scan the current reaches a maximum of 19.4 A g^{-1} (I_f = 370 A g_{Pt}^{-1}) at 0.69 V, whereas it reaches 13.4 A g^{-1} (I_b = 290 A g_{Pt}^{-1}) at 0.61 V in the reverse scan. This electrode exhibits, then, an I_f/I_b = 1.26 for ethanol oxidation. Again, the high oxidation currents as well as the high I_f/I_b ratio are indicative of an excellent electrocatalytic performance.

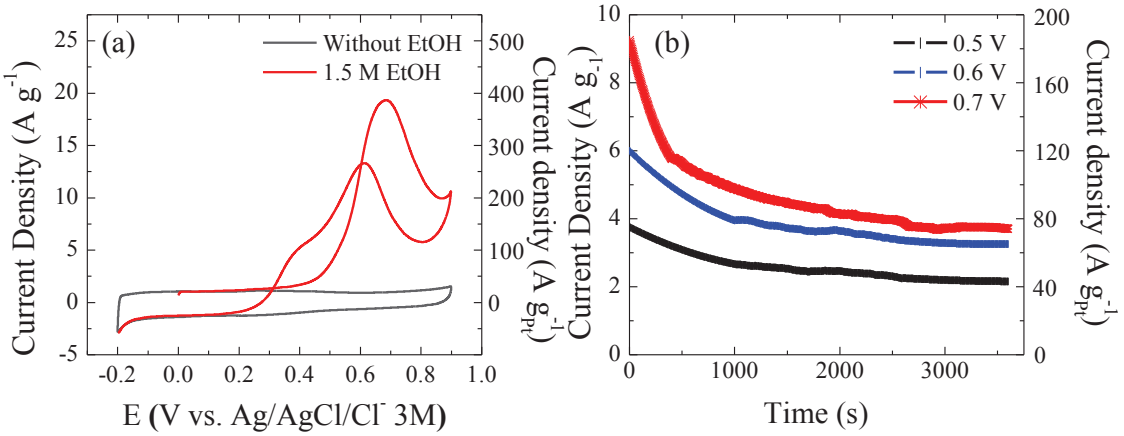

Figure 7.10. (a) Steady cyclic voltammograms of CFHPt electrode in the presence or absence of EtOH (v = 10 mV·s^{-1}). (b) Chronoamperometric measurements for EtOH electro-oxidation at different potentials on CFHPt electrode. Electrolyte 0.5 M H_2SO_4 + 1.5 M EtOH.

Under potentiostatic conditions (Fig. 7.10b), the CFHPt electrode exhibits high oxidation currents that increase with the electrode potential. These ethanol oxidation currents gradually decay with time, so that a 40-60 % of the initial current is obtained after 1h-experiments. The activity loss increases with the electrode potential and is larger than in the case of methanol. Nevertheless, the observed steady currents range high from 40 to 80 A g_{Pt}^{-1}.

Although any comparison with vast literature is difficult (because of the multiple different preparation methods and characterization conditions and protocols used by other authors) [29,57,63,64], we have tried to compare our results with some data in the literature (Table 7.4). Regarding the values of current density (A g_{Pt}^{-1}), it is noteworthy that the CFHPt electrodes studied in the present work exhibit an outstanding

performance for methanol and ethanol oxidation: low onset potential, and high specific oxidation currents and I_f/I_b ratios as well as stable catalytic response. Probably, the excellent platinum distribution and high dispersion are the main factors that explain this good activity. On the other hand, the presence of P decreases the catalytic performance of these electrodes, but they increase the electro-oxidation resistance of the carbon support. Moreover, regarding the Pt (active phase) morphology after MOR and EOR, TEM images (not shown) reveal that both nanoparticle size and dispersion are quite similar to those exhibited by the initial carbon electrodes (with and without P). Thereby, no particle migration or sintering is observed during the alcohol electro-oxidation, which confirms the great stability of these Pt-containing carbon fibers as electrocatalysts. All these features make the reported lignin-based carbon fibers, which have been prepared by an advantageous procedure, promising low-Pt content electrodes for fuel cell technology. This is an important result since suitable low-Pt content catalysts are necessary for the up-coming large scale commercialization of different types of fuel cells [57].

Table 7.4. Comparison of CFHPt sample activity with data in the literature

j ($A\ g_{Pt}^{-1}$)	Nominal Metal Content (wt%)	Alcohol concentration (M)	Electrolyte	Reference
Methanol oxidation				
495	Pt (5)	1.5	0.5M H_2SO_4	CFHPt (this work)
300	PtRu (20)	2	0.5M H_2SO_4	[65]
260	PtRu (30)	2	0.5M H_2SO_4	[66]
215	Pt (5)	1	1M H_2SO_4	[67]
91	Pt (20)	1	1M H_2SO_4	[67]
73	Pt (20)	1	1M H_2SO_4	[67]
86	Pt (electrodeposited)	0.1	0.5M H_2SO_4	[68]
275	Pt (20)	0.1	0.5M H_2SO_4	[69]
Ethanol oxidation				
370	Pt (5)	1.5	0.5M H_2SO_4	CFHPt (this work)
125	Pt (40)	1	0.1M $HClO_4$	[70]
180	Pt (20)	1	0.5M H_2SO_4	[71]

7.4. Conclusions

Lignin fiber, with and without phosphorus surface groups and platinum nanoparticles, were synthesized in a single step by electrospinning lignin/ethanol/phosphoric acid/platinum acetylacetonate precursor solutions. The different lignin fibers thus obtained were stabilized in air atmosphere and carbonized at 900ºC in nitrogen atmosphere in order to obtain lignin-based carbon fiber electrocatalysts. Phosphorus groups allow a 10 times faster heating rate (0.08 ºC min^{-1} versus 0.8 ºC min^{-1} with phosphorus) and a decrease of the isothermal stabilization step 100 times (100 h and 1 h) to avoiding fibers melting. Phosphorus-containing carbon fibers obtained are microporous solids that can develop an apparent surface area of 1141 m^2 g^{-1}, whereas lignin-based carbon fibers without phosphorus present wide mesoporosity and apparent surface areas lower than 780 m^2 g^{-1}. Phosphorus groups allow the preparation of catalysts with very well dispersed metallic nanoparticles (about 2 nm) while without phosphorus larger Pt particle sizes are obtained. Better oxidation and electrooxidation resistance have been shown by carbon fibers with phosphorus. The obtained Pt-containing carbon fibers can be directly used as electrodes with no binder or conductivity promoter, showing a remarkable electrocatalytic response in the methanol and ethanol electro-oxidation reactions. Cyclic voltammograms displays two defined anodic peaks for these electrocatalysts and, in both reactions, they exhibit relatively low onset potential, high specific oxidation currents and a stable catalytic response.

7.5. References

[1] R. Sahay, P.S. Kumar, R. Sridhar, J. Sundaramurthy, J. Venugopal, S.G. Mhaisalkar, et al., Electrospun composite nanofibers and their multifaceted applications. J. Mater. Chem. 22 (2012) 12953.

[2] M. Zhang, A.A. Ogale. Carbon. 69 (2014) 626–629.

[3] E. Frank, L.M. Steudle, D. Ingildeev, J.M. Spörl, M.R. Buchmeiser Angew. Chem. Int. Ed. 53 (2014) 5262–5298.

[4] P.T. Williams, A.R. Reed. Biomass and Bioenergy. 30 (2006) 144–152.

[5] J.F. Kadla, S. Kubo, R.A. Venditti, R.D. Gilbert, A.L. Compere, W. Griffith. Carbon. 40 (2002) 2913–2920.

[6] J.M. Rosas, R. Berenguer, M.J. Valero-Romero, J. Rodríguez-Mirasol, T. Cordero. Front. Mater. 1 (2014) 29.

[7] L.M. Cotoruelo, M.D. Marqués, A. Leiva, J. Rodríguez-Mirasol, T. Cordero. Adsorption. 17 (2011) 539–550.

[8] L.M. Cotoruelo, M.D. Marqués, J. Rodríguez-Mirasol, J.J. Rodríguez, T. Cordero. J. Colloid Interface Sci. 332 (2009) 39–45.

[9] J. Bedia, R. Barrionuevo, J. Rodríguez-Mirasol, T. Cordero. Appl. Catal. B Environ. 103 (2011) 302–310.

[10] J. Bedia, J.M. Rosas, J. Rodríguez-Mirasol, T. Cordero. Appl. Catal. B Environ. 94 (2010) 8–18.

[11] M. Funaoka. Macromol. Symp. 201 (2003) 213–221.

[12] D. Yawalata, L. Paszner. Holzforschung. 58 (2005) 1–6.

[13] R. Berenguer, F.J. García-Mateos, R. Ruiz-Rosas, D. Cazorla-Amorós, E. Morallón, J. Rodríguez-Mirasol, T. Cordero. Green Chem. 18 (2016) 1506–1515.

[14] R.R. Salunkhe, S.H. Hsu, K.C.W. Wu, Y. Yamauchi. ChemSusChem. 7 (2014) 1551–1556.

[15] R.R. Salunkhe, C. Young, J. Tang, T. Takei, Y. Ide, N. Kobayashi, et al. Chem. Commun. 52 (2016) 4764–4767.

[16] W. Zhou, Z. Zhou, S. Song, W. Li, G. Sun, P. Tsiakaras, et al. Appl. Catal. B Environ. 46 (2003) 273–285.

[17] A.M. Zainoodin, S.K. Kamarudin, M.S. Masdar, W.R.W. Daud, A.B. Mohamad, J. Sahari. Appl. Energy. 113 (2014) 946–954.

[18] M. Sevilla, C. Sanchís, T. Valdés-Soh, E. Morallón, A.B. Fuertes. J. Phys. Chem. C. 111 (2007) 9749–9756.

[19] M. Sevilla, C. Sanchís, T. Valdés-Solís, E. Morallón, A.B. Fuertes. Carbon. 46 (2008) 931–939.

[20] J.M. Sieben, A. Ansón-Casaos, M.T. Martínez, E. Morallón. J. Power Sources. 242 (2013) 7–14.

[21] J. Tang, J. Liu, N.L. Torad, T. Kimura, Y. Yamauchi. Nano Today. 9 (2014) 305–323.

[22] D. Hulicova-Jurcakova, M. Seredych, G.Q. Lu, N.K.A.C. Kodiweera, P.E. Stallworth, S. Greenbaum, et al. Carbon. 47 (2009) 1576–1584.

[23] D. Hulicova-Jurcakova, M. Kodama, S. Shiraishi, H. Hatori, Z.H. Zhu, G.Q. Lu. Adv. Funct. Mater. 19 (2009) 1800–1809.

[24] R. Berenguer, R. Ruiz-Rosas, A. Gallardo, D. Cazorla-Amorós, E. Morallón, H. Nishihara, et al. Carbon. 95 (2015) 681–689.

[25] X. Xu, J. Zhou, L. Jiang, G. Lubineau, S.A. Payne. Carbon. 80 (2014) 91–102.

[26] N. Diez, P. Díaz, P. Álvarez, Z. González, M. Granda, C. Blanco, et al. Mater. Lett. 136 (2014) 214–217.

[27] D. Sebastián, V. Baglio, M. Girolamo, R. Moliner, M.J. Lázaro, A.S. Aricò. J. Power Sources. 250 (2014) 242–249.

[28] R. Ruiz-Rosas, J. Bedia, M. Lallave, I.G. Loscertales, A. Barrero, J. Rodríguez-Mirasol, T. Cordero. Carbon. 48 (2010) 696–705.

[29] M.A.F. Akhairi, S.K. Kamarudin Int. J. Hydrogen Energy. 41 (2016) 4214–4228.

[30] Y. Lu, S. Du, R. Steinberger-Wilckens. Appl. Catal. B Environ. 199 (2016) 292–314.

[31] J.W. Hong, Y. Kim, Y. Kwon, S.W. Han. Chem. Asian J. 11 (2016) 2224.

[32] L. Li, L. Hu, J. Li, Z. Wei. Nano Res. 8 (2015) 418–440.

[33] J.N. Tiwari, R.N. Tiwari, G. Singh, K.S. Kim. Nano Energy. 2 (2013) 553–578.

[34] M. Lallave, J. Bedia, R. Ruiz-Rosas, J. Rodríguez-Mirasol, T. Cordero, J.C. Otero, et al. Adv. Mater. 19 (2007) 4292–4296.

[35] E. Leal da Silva, M.R. Ortega Vega, P. dos Santos Correa, A. Cuña, N. Tancredi, C. de Fraga Malfatti. Int. J. Hydrogen Energy. 39 (2014) 14760–14767.

[36] K. Kaneko, C. Ishii, T. Rybolt. Stud. Surf. Sci. Catal. 87 (1994) 583–592.

[37] M.M. Dubinin, E.D. Zaverina, L.D. Radushkevich J. Phys. Chem. [URSS]. 21 (1947) 1351–1362.

[38] J. Jagiello, J.P. Olivier. Carbon. 55 (2013) 70–80.

[39] J.L. Braun, K.M. Holtman, J.F. Kadla. Carbon. 43 (2005) 385–394.

[40] J. Bedia, J.M. Rosas, J. Márquez, J. Rodríguez-Mirasol, T. Cordero. Carbon. 47 (2009) 286–294.

[41] M. Jeguirim, K. Villani, J.F. Brilhac, J.A. Martens. Appl. Catal. B Environ. 96 (2010) 34–40.

[42] J.M. Rosas, J. Bedia, J. Rodríguez-Mirasol, T. Cordero. Fuel. 88 (2009) 19–26.

[43] J.M. Rosas, R. Ruiz-Rosas, J. Rodríguez-Mirasol, T. Cordero. Carbon. 50 (2012) 1523–1537.

[44] M.J. Valero-Romero, F.J. García-Mateos, J. Rodríguez-Mirasol, T. Cordero. Fuel Process. Technol. 157 (2017) 116–126.

[45] J.F. Moulder, W.F. Stickle, P.E. Sobol, K.D. Bomben, Handbook of X-ray Photoelectron Spectroscopy, 1995.

[46] M. Calzado, M.J. Valero-Romero, P. Garriga, A. Chica, M.O. Guerrero-Pérez, J. Rodríguez-Mirasol, T. Cordero. Catal. Today. (2014) 4–11.

[47] E. Gonzalez-Serrano, T. Cordero, J. Rodriguez-Mirasol, L. Cotoruelo, J.J. Rodriguez. Water Res. 38 (2004) 3043–3050.

[48] X. Wu, L.R. Radovic. Carbon. 44 (2006) 141–151.

[49] J. Bedia, J.M. Rosas, D. Vera, J. Rodríguez-Mirasol, T. Cordero. Catal. Today. 158 (2010) 89–96.

[50] R. Ruiz-Rosas, J.M. Rosas, I.G. Loscertales, J. Rodríguez-Mirasol, T. Cordero. Appl. Catal. B Environ. 156–157 (2014) 15–24.

[51] Z. Liu, Q. Shi, F. Peng, H. Wang, R. Zhang, H. Yu. Electrochem. Commun. 16 (2012) 73–76.

[52] J.M. Rosas, J. Bedia, J. Rodríguez-Mirasol, T. Cordero. Ind. Eng. Chem. Res. 47 (2008) 1288–1296.

[53] M.J. Bleda-Martínez, J.A. Maciá-Agulló, D. Lozano-Castelló, E. Morallón, D. Cazorla-Amorós, A. Linares-Solano. Carbon. 43 (2005) 2677–2684.

[54] R. Berenguer, H. Nishihara, H. Itoi, T. Ishii, E. Morallón, D. Cazorla-Amorós, et al. Carbon. 54 (2013) 94–104.

[55] Y. Shao, G. Yin, Y. Gao. J. Power Sources. 171 (2007) 558–566.

[56] C. Huang, T. Sun, D. Hulicova-Jurcakova. ChemSusChem. 6 (2013) 2330–2339.

[57] X. Zhao, M. Yin, L. Ma, L. Liang, C. Liu, J. Liao, et al. Energy Environ. Sci. 4 (2011) 2736.

[58] S.P.S. Badwal, S. Giddey, A. Kulkarni, J. Goel, S. Basu. Appl. Energy. 145 (2015) 80–103.

[59] T. Iwasita, Methanol and CO electrooxidation (Ch. 41), in: Handb. Fuel Cells Fundam. Technol. Appl. Eds. W. Vielstich, A. Lamm, H. A. Gasteiger. Vol 2 Electrocatal., John Wiley & Sons, Ltd, 2003.

[60] D.Y. Chung, K.J. Lee, Y.E. Sung. J. Phys. Chem. C. 120 (2016) 9028–9035.

[61] Z. Liu, X.Y. Ling, X. Su, J.Y. Lee. J. Phys. Chem. B. 108 (2004) 8234–8240.

[62] M. Ohanian, C.F. Zinola. J. Power Sources. 168 (2007) 307–322.

[63] B. Braunchweig, D. Hibbitts, M. Neurock, A. Wieckowski. Catal. Today. 202 (2013) 197–209.

[64] H. Liu, C. Song, L. Zhang, J. Zhang, H. Wang, D.P. Wilkinson. J. Power Sources. 155 (2006) 95–110.

[65] W.H. Lizcano-Valbuena, V.A. Paganin, E.R. Gonzalez. Electrochim. Acta. 47 (2002) 3715–3722.

[66] B. Yang, Q. Lu, Y. Wang, L. Zhuang, J. Lu, P. Liu, et al. Chem. Mater. (2003) 3552–3557.

[67] V. Raghuveer, A. Manthiram. Electrochem. Solid State Lett. 7 (2004) A336–A339.

[68] S. Domínguez-Domínguez, J. Arias-Pardilla, Á. Berenguer-Murcia, E. Morallón, D. Cazorla-Amorós. J. Appl. Electrochem. 38 (2008) 259–268.

[69] M. Sevilla, C. Salinas Martínez-de Lecea, T. Valdés-Solís, E. Morallón, A.B. Fuertes. Phys. Chem. Chem. Phys. 10 (2008) 1433–1442.

[70] S. Beyhan, C. Coutanceau, J.M. Léger, T.W. Napporn, F. Kadirgan. Int. J. Hydrogen Energy. 38 (2013) 6830–6841.

[71] Y. Li, L. Han, B. An, Y. Wang, L. Wang, X. Yin, et al. J. Mater. Sci. Mater. Electron. 27 (2016) 6208–6215.

Chapter 8

Biomass-derived binderless fibrous carbon electrodes for ultrafast energy storage

8.0. Abstract

The possibility to store energy efficiently and sustainably at little cost is crucial to prevent climate change and exhaustion of natural resources. In this chapter it is demonstrated that interconnected and porous carbon fibers easily obtained from lignin exhibit ultrafast charge-discharge and excellent energy density and cyclability performance, to be used as binderless and flexible electrodes in supercapacitors. Carbn fibers have been prepared by electrospining of alcell liginin. Varying the parameters of the stabilization step, lignin fibers with different degrees of interconnection have been prepared. The stabilized fibers have been carbonized at 900 ºC, obtaining carbon fibers with excellent electrical conductivities and surfaces areas that varies from 800 to 1300 $m^2 \cdot g^{-1}$.

8.1. Introduction

Electrochemical capacitors, usually referred to as supercapacitors, are electrochemical devices for electrical energy storage and harvesting applications that can complement or replace batteries when high power delivery or uptake and/or long cycling stability are required. Additionally, these devices improve efficiencies in supply systems (such as internal combustion engines, renewable energy systems, batteries and fuel cells) by storing energy when in excess or not needed. Thus, they are considered as one of the most powerful technologies that will provide a more efficient and sustainable utilization of energy on a short-term and real scenario of increasing energy costs and threatening climate change [1-5].

In spite of such relevance, the widespread utilization of supercapacitors has not been achieved due to a high cost to performance ratio. Among different electrode candidates, the last decade has witnessed a very intense research in the capacitance and storage performance of different nanostructured carbons, like graphene, CNTs, fullerenes, CNFs, onions, templated carbons, etc [1-5]. Nevertheless, apart from the significant progress on fundamental aspects, the complex and expensive manufacture as well as the complicated handling and electrode processing of these carbon materials make uncertain their feasible application. Accordingly, while novel electrode materials and chemistries are being developed to improve the storage performance, further research on simpler and cheaper manufacture and processing is demanded.

Activated carbons (AC) derived from biomass and polymers have been identified as the currently most viable materials for supercapacitors, from both economic and sustainability points of view [1]. To attain the specifications for widespread commercialization, various issues need to be solved, being the most important to produce AC with a high accessible surface area and a sufficiently high electrical conductivity. On the one hand, biomass and natural polymers show a heterogeneous structure and contain impurities that complicate their processing to produce adequate conductive carbon electrodes. On the other hand, the derived ACs are conventionally obtained as powder or granular materials. Both the particle-like morphology and porosity strongly increase their inter- and intra-particle electrical resistances [5], respectively, what makes necessary their processing into electrode pastes (by using auxiliary binders and conductivity promoters). This generates many electric point contacts that decrease their mechanical and chemical stability [6]. Hence the development of binderless porous carbons by a direct route would improve the conductivity and stability of carbon electrodes, and at the same time, it would reduce the time, complexity and the environmental and economic impacts of the overall manufacture. In addition, the possibility of using biomass precursors for the preparation of these electrodes could suppose a unique opportunity for their valorization into high added-value products.

In this chapter, we report a sustainable and inexpensive approach to process one of the most abundant polymers in nature, lignin [7], into binderless flexible carbon electrodes with ultrafast response and overall high-performance for energy storage in supercapacitors. The approach involves the preparation of interconnected and porous carbon fibers (CFs), with submicron diameter and high surface area and conductivity. Particularly, we demonstrate that these materials can be simply but uniquely accomplished by electrospinning and subsequent thermal conversion of a proper lignin into CFs, with an easy control of their connectivity and porosity degree.

The preparation of the biomass-derived fibrous carbon electrodes firstly entails the electrospinning of Alcell®-lignin/ethanol solutions, at ambient temperature and pressure, into submicron-diameter lignin fibers [8,9]. Electrospinning is a simple and powerful technique for fiber production [10], whereas the chemical and structural properties of lignin make it a unique precursor for the attainment of carbon materials [11,12]. Furthermore, Alcell lignin can be dissolved in ethanol [13] and it is the only

variety of this polymer that, up to now, has been electrospun at room temperature, directly without any modification treatment and without any added binder polymer [14,15]. Interestingly, its pulping (organosolv) process uses ethanol as both delignifying agent and solvent, and exhibits higher pulp yields and it is more environmentally friendly than the production of Kraft lignin, the other more-produced lignin today [7,8]. Since lignin is a worldwide by-product of pulp and paper industries and will be generated, together with ethanol, what in future may result in wood-to-ethanol bio-refineries [7], the hereby reported preparation procedure, the resulting electrode materials and their use for energy storage are considered a model example of biomass valorisation, green chemistry and sustainability. In fact, the valorization of lignin into new and highly valuable products is essential for the replacement of petroleum-derived counterparts in multiple applications [7-10].

8.2. Materials and methods.

8.2.1. Preparation of lignin-based CFs

Lignin fibers were prepared by electrospinning of Alcell® lignin-ethanol solutions by using a co-axial configuration [8,9]. The spinnable solution had a lignin concentration of 45 wt% and a viscosity of 370 cP. The flow rates were 1 $mL \cdot h^{-1}$ for the lignin solution (inner spinneret) and 0.1 $mL \cdot h^{-1}$ for pure ethanol (outer spinneret). The tip-to-collector distance was 30 cm and the electrical potential difference was 12 kV (the collector was at -6 kV and the tips at +6 kV). The lignin was kindly provided by Repap Technologies Inc. (Canada), while ethanol absolute (p.a. Merck) was used as solvent. The composition of the used lignin was determined by CHNS/O elemental analysis (PerkinElmer® 2400C Instruments) as: 65.9 wt% C; 6.3 wt% H; 0.2 wt% N; 0.00 wt% S; and 27.6 wt% O, while the ash content was 0.00 wt%. Thermostabilization and carbonization treatments were carried out in a horizontal tubular furnace. The thermostabilization was performed under air atmosphere (150 $cm^3(STP) \cdot min^{-1}$) and different heating rates up to 200 ºC, and keeping this final temperature for 36 h. After electrospinning, the lignin submicrofibers were thermally air-stabilized and carbonized under various conditions to generate carbon submicrofibers with different connectivity and porosity. The connectivity of fibers, i.e. the production of individual (loose) or interconnected CFs, was controlled by using a suitable heating rate during stabilization. At 0.08 $ºC \cdot min^{-1}$, the heating rate is slow enough to stabilize lignin and prevent its softening during subsequent carbonization [16], rendering loose CFs (sample CF-L in

Figure 8.1a,b). By contrast, thermostabilization of lignin fibers at 0.16 ºC·min^{-1} resulted in their partial softening and interconnection at contact points between fibers during carbonization (sample CF-I in Fig. 8.1c,d).

The stabilized materials were carbonized at 10 ºC·min^{-1} up to 900 ºC under inert (N_2) or 1 v% O_2 in N_2 atmospheres (150 cm^3(STP)·min^{-1}), CF-IA for the last one.

8.2.2. Physico-chemical characterization

SEM and TEM images were obtained by a JEOL JSM-6490LV microscope (at 25 kV voltage) and a Philips CM200 microscope (at an accelerating voltage of 200 kV), respectively. The histogram of fiber diameters was constructed from SEM images after the analysis of more than 120 cases for each different CF. The textural properties were characterized by N_2 adsorption-desorption at -196 ºC in a Micromeritics ASAP2020, after outgassed for 8 h at 150 ºC under vacuum. From the N_2 adsorption/desorption isotherms, the apparent surface area (A_{BET}) was calculated by applying the BET equation, and the micropore volume (V_t) by using the t-method. Pore size distribution has been calculated from the N_2 adsorption isotherms considering the proposed 2D-NLDFT Heterogeneous surface model [17], and by applying the Solution of Adsorption Integral Equation Using Splines (SAIEUS, available online at http://www.nldft.com/) Software. For thermogravimetric analysis (TG), a CI Electronics MK2 balance and samples of 10 mg were used.

The amount of oxygen surface groups was determined as CO and CO_2 desorbed from the samples in temperature-programmed desorption (TPD) analyses. These analyses were carried out up to 940 ºC (10 ºC·min^{-1}) in He flow (100 cm^3·STP min^{-1}) in a differential scanning calorimetry−thermogravimetric analysis (DSC−TGA) equipment (TA Instruments, SDT 2960 Simultaneous) coupled to a mass spectrometer (Thermostar, Balzers, GSD 300 T3). The amounts of CO and CO_2 desorbed from the samples were monitored following the 28 and 44 m/z signals, which were previously calibrated by non-isothermal decomposition of calcium oxalate monohydrate (99.999%). XPS data were registered by a 5700C model Physical Electronics apparatus with Mg Kα radiation (1253.6 eV). Raman spectra were recorded with a RENISHAW micro-Raman system using an Ar^+ laser at 514 nm as the excitation source with a spectral resolution of 2 cm^{-1}. The fitting of both the XPS and Raman spectra was done by least squares using Gaussian–Lorentzian peak shapes. The X-ray diffractograms

were obtained in a PANalytical diffractometer (X´Pert PRO) using a CuKα_1 radiation (1.5406 Å). The profile intensities were measured step by step (0.0167° in 2θ) for a whole time of 3000 s. In order to determine the exact angular position of the (002) peak, 10 wt% Si (Aldrich 99.999%) was used as an internal standard. For the application of Scherrer equation, the instrumental broadening contribution was determined by using LaB_6 as crystalline standard.

8.2.3. Electrochemical characterization

The electrochemical measurements have been performed in 1M H_2SO_4 using an Autolab PGSTAT302 potentiostat equipped with FRA module for the Electrochemical Impedance Spectroscopy (EIS), Cyclic voltammetry (CV) and Galvanostatic charge-discharge (GCD) measurements in three electrode cell and an Arbin SCTS Instruments for the galvanostatic charge-discharge experiments and durability tests in two electrode cell. A T-shaped Teflon Swagelock system equipped with gold collectors and Ag/AgCl 3M KCl reference electrode has been used for the assessing the cell performance while registering separately the potential of each electrode. Round-shaped CF pieces were cut in a surface of 0.196 cm^2, the working and counter electrodes being constructed by stacking three round pieces together (total weight between 1.00-1.20 mg) over the gold collectors at each side of the cell, achieving a surface loading in the range of 5-6 $mg \cdot cm^{-2}$. A round piece of Nylon membrane (pore size: 0.45 μm, 7 mm diameter) was used as separator. The electrodes were dried at 80ºC under vacuum for 2 h before determining their weight, and afterwards soaked in the electrolyte for 1 h prior the cell construction and the electrochemical measurements.

The electrochemical behavior of the binderless electrodes have been analyzed using cyclic voltammetry (CV) at scan rates between 10 and 8000 mV s^{-1}, with capacitance being measured from the area enclosed by the CV. They have been plotted in terms of diferential gravimetric capacitance by dividing the measured intensity between the scan rate and the weight of single electrode (three-electrode cell) or the sum of both electrodes (two-electrode cell). Gravimetric capacitances have been determined from the charge enclosed by the CV curves and dividing the resulting value by the potential window and the weight of single (3E-cell) or both electrodes (2E-cell).

Galvanostatic charge-discharge experiments (GCD) at different specific currents have been utilized for the determination of the capacitance and the rate performance of

the materials in the role of positive and negative electrodes. The gravimetric capacitance (C_g, F g^{-1}) of the electrodes have been determined from the discharge process using the following expression:

$$C_g = \frac{I \cdot t}{w \cdot (\Delta V - IR_{drop})}$$

where *I* stands for the current (A), *w* is the weight of the electrode (g), *t* is the discharge time (s) and ΔV (V) is the potential window the electrode has been submitted to after discounting the ohmic drop (IR_{drop}). Similarly, the capacitance of the supercapacitor cells have been measured using the same equation, but considering the weight of the two electrodes as *w*. The specific energy (Eg, Wh kg^{-1}) is obtained from the integration of the discharge curve:

$$E_g = \left(\int_0^{Q_{dis}} V(t) \cdot dQ\right)/w = \left(\int_0^{t_{dis}} V(t) \cdot d(I \cdot t)\right)/w = I \cdot \left(\int_0^{t_{dis}} V(t) \cdot d(t)\right)/w$$

in this equation, *w* is the weight of both electrodes (kg), and the time, *t*, is in expressed in hours. The specific power (P_g, kW kg^{-1}) reported in the Ragone plots has been determined by dividing the specific energy by the discharge time expressed in hours. The cell resistance has been determined at different specific currents from the ohmic drop registered at the beginning of the discharge of the cell and the corresponding current intensity value. Coulombic and Energy efficiencies (C_{eff} and E_{eff}, respectively) of the GCD measurements are defined as the ratio between the discharge time and charge time in the former case, and the charge energy and discharge energy for the latter one. The electrical resistances present in the 2-electrode cells have been analyzed using the Nyquist plots obtained from Electrochemical Impedance Spectroscopy (EIS) technique at 50 mV. For these measurements, the frequency ranged from 100 kHz to 10 mHz, with and amplitude of the sine wave of 10 mV.

In order to assess the durability of the carbon films as supercapacitors, two-electrode cells have been built using a Teflon Swagelock fitting equipped with stainless steel collectors and submitted to 4 set of 25000 cycles at 1.3 V and 5 $A \cdot g^{-1}$ that were conducted with relaxing time of 3-9 hours between them. The cyclibility test was then followed by a floating test at 1.3 V for 24 hours. The durability of the cell, defined as

the retained capacitance, power and energy, was evaluated during the cyclability test and after the floating test.

8.3. Result and discussion.

8.3.1. Characterization of lignin-based CFs

It is well known that the thermostabilization step and, therefore, the fabrication of lignin-based CFs is a very slow process [18]. This causes a large energy consumption. In addition, many exhausts evolve during the stabilization and carbonization of lignin precursors [9,18]. These specifications are inherent to the low glass transition temperature of any lignin source and their high oxygen content. In fact, the slow thermostabilization step is also common of most CF precursors, like PAN, pitches, cellulose, etc. [16], whereas the evolution of H_2, H_2O, CO, CO_2, light hydrocarbons and waste products (tar and other condensable volatiles) is unavoidable when biomass precursors are used. Although the acceleration of lignin fibers thermostabilization is the aim of intense research, most approaches involve the modification or purification of lignin, the use of thermal pre-treatments or the utilization of polymers and/or chemicals [19-25]. As a result, additional steps, reagents and energy consumption are involved and by-products could be generated. In this sense, the hereby proposed method for the preparation of interconnected lignin-based CFs reduces the duration of the conventional air thermostabilization process to the half by raising the heating rate, just without any modification of the conventional procedure or any added compound or step. Thanks to be working slightly over the glass transition temperature of the material, interconnection of fibers is also achieved without additives and the activation and functionalization with oxygen surface groups occur simultaneously to thermal processing, without post-treatments. Table 8.1 collects the yields of thermostabilization and carbonization treatments. Stabilization yields not only account for the condensation and decarboxylation reactions that results in weight losses; they also consider the removal of adsorbed ethanol on the surface of the lignin fibers, which represents around 15% of their initial weight, thus leaving a weight loss accountable to lignin oxidation of only ~10%. The carbonization yields were found to be slightly lower than the direct carbonization of the same alcell lignin upon similar conditions (40.3% wt.). This can be explained considering that the high amount of oxygen groups introduced during the stabilization treatment will be later released as CO and CO_2, thus removing part of the carbon that otherwise would remain in the carbonized product.

Nevertheless, the preparation yield is high considering the development of surface area achieved after the carbonization step (which could be seen as a combined carbonization/activation treatment). In fact, for obtaining a similar textural development in the activation of a non-porous carbon fibers from biomass precursors or even from phenolic resins, a burn-off higher than 20% would be necessary [26-28], resulting in a worse use (lower yield when carbonization and activation are both considered) of the raw material. The overall yields (involving stabilization and carbonization treatments) for the production of the reported lignin-based CFS range between 26-30 %, similar to those achieved in biomass based activated carbons [29] and in agreement also with those of CFs obtained from other organosolv-based lignins [13,30]. Hence, not only the described production of lignin fibers by electrospinning of ethanol solutions, but also their thermal processing into interconnected CFs can be considered an environmentally improved route to this type of materials.

Table 8.1. Specific surface area (A_{BET}); Volume of micropores (V_t); CO and CO_2 evolved from TPD experiments; mass surface composition; and yields of thermostabilization and carbonization treatments and that of the overall production.

Sample	S_{BET} m^2/g	Vt cm^3/g	TPD (mmol/g)		XPS (wt%)		Yields (wt%)		
			CO	CO_2	C(1s)	O(1s)	Stab.	Carb.	Overall
CF-L	834	0.33	0.6	0.5	95.9	4.1	77.0	39.1	30.1
CF-I	780	0.27	1.0	0.4	95.8	4.2	73.2	38.0	27.8
CF-IA	1315	0.44	3.5	0.5	95.4	4.6	74.1	34.5	25.6

Both the loose and interconnected CFs exhibited quite similar diameters, mainly in the range of 400 nm to 1.5 μm (Figure 8.1g) and are essentially microporous, as deduced from their characteristic type-I N_2 isotherms (Figure 8.2a). From these data, the specific surface area (Table 8.1) and the pore size distribution (Figure 8.2b) were calculated (see experimental section). These materials display a high surface area of ca. 800 $m^2\ g^{-1}$ and pores in the range 0.4 - 1.3 nm, prevailing those of 0.6 - 0.8 nm. Such microporosity develops directly during carbonization, without any additional activation process, and seems to be related to the high oxygen content in lignin [8,9,18]. These pores of less than 2 nm-size have been found optimum for double layer charging, whereas the porous structure of CFs favors the accessibility and diffusion of ions [31], well-known properties beneficial for energy storage in supercapacitors [1-5].

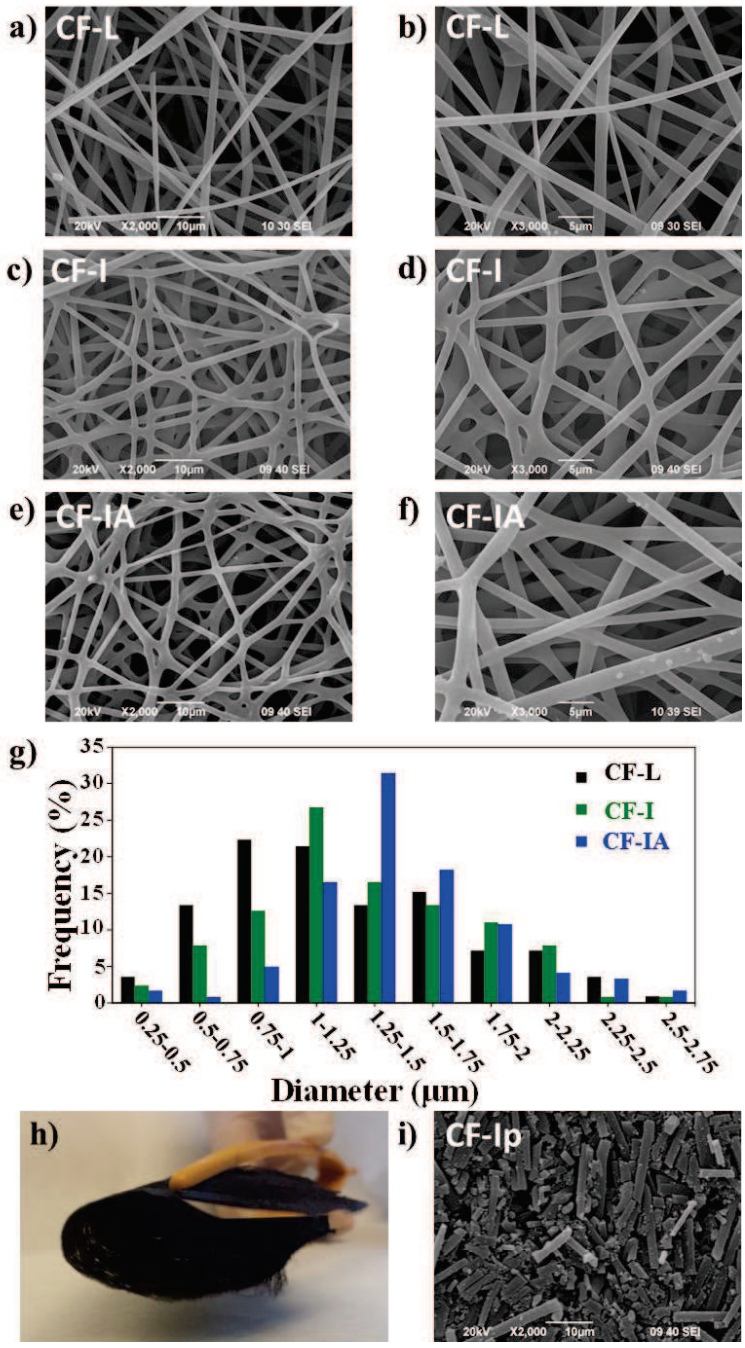

Figure 8.1. SEM images, covering different areas, of loose (a,b), interconnected (c,d) and interconnected + partially gasified (e,f) lignin-based CFs; (g) histogram of fiber diameters from SEM images; (h) photograph of a binderless CF-IA electrode; (i) SEM of a pasted CF-IA electrode.

On the other hand, the microporosity of the interconnected CFs was further developed (Figure 8.2a), again without additional steps, by partial gasification during carbonization in the presence of 1 v% O_2 (5 % burn-off) (CF-IA sample). This was possible because of the high oxidation resistance of CFs obtained from lignin [8,9], again a unique feature of this precursor. Such a high oxidation resistance was confirmed by thermogravimetric analysis (Figure 8.2c), illustrating that these CFs start to react in

air at very high temperatures (from 550 ºC). The resulting interconnected CFs (sample CF-IA in Figure. 8.1e,f) displayed similar diameters (Figure 8.1g), but a higher surface area of 1300 $m^2 \cdot g^{-1}$ (Table 8.1), the presence of some wider micropores (d = 1.2-1.7 nm) (Figure 8.2b) and a larger concentration of oxygen surface groups (Table 8.1). Particularly, these groups mainly consisted in phenol- and quinone-like functionalities, as evidenced by their evolution as CO between 600-900 ºC during TPD experiments [32] or their clear contributions at 286.1 and 289.7 eV, respectively, in XPS spectra (Figure 8.2d), which can actively contribute to charge storage by pseudocapacitive reactions [1-5,32]. Thus, while the high carbonization temperatures applied for the obtainment of sufficiently conducting carbons usually restrains their functionalization (≤ 1.0 mmol $CO \cdot g^{-1}$ for CF-L and CF-I), the hereby reported O_2-activation allows to obtain not only a higher surface area but also an electro-active surface chemistry (3.5 mmol $CO \cdot g^{-1}$ for CF-IA), directly without any post-treatment. In addition, by interconnection the materials became flexible (Figure 8.1h), the prerequisite to achieve stretchable and bendable energy storage devices [33]. This is in agreement with the enhanced mechanical behavior caused by inter-fiber bonding of lignin-based carbon fibers prepared by electrospinning [34].

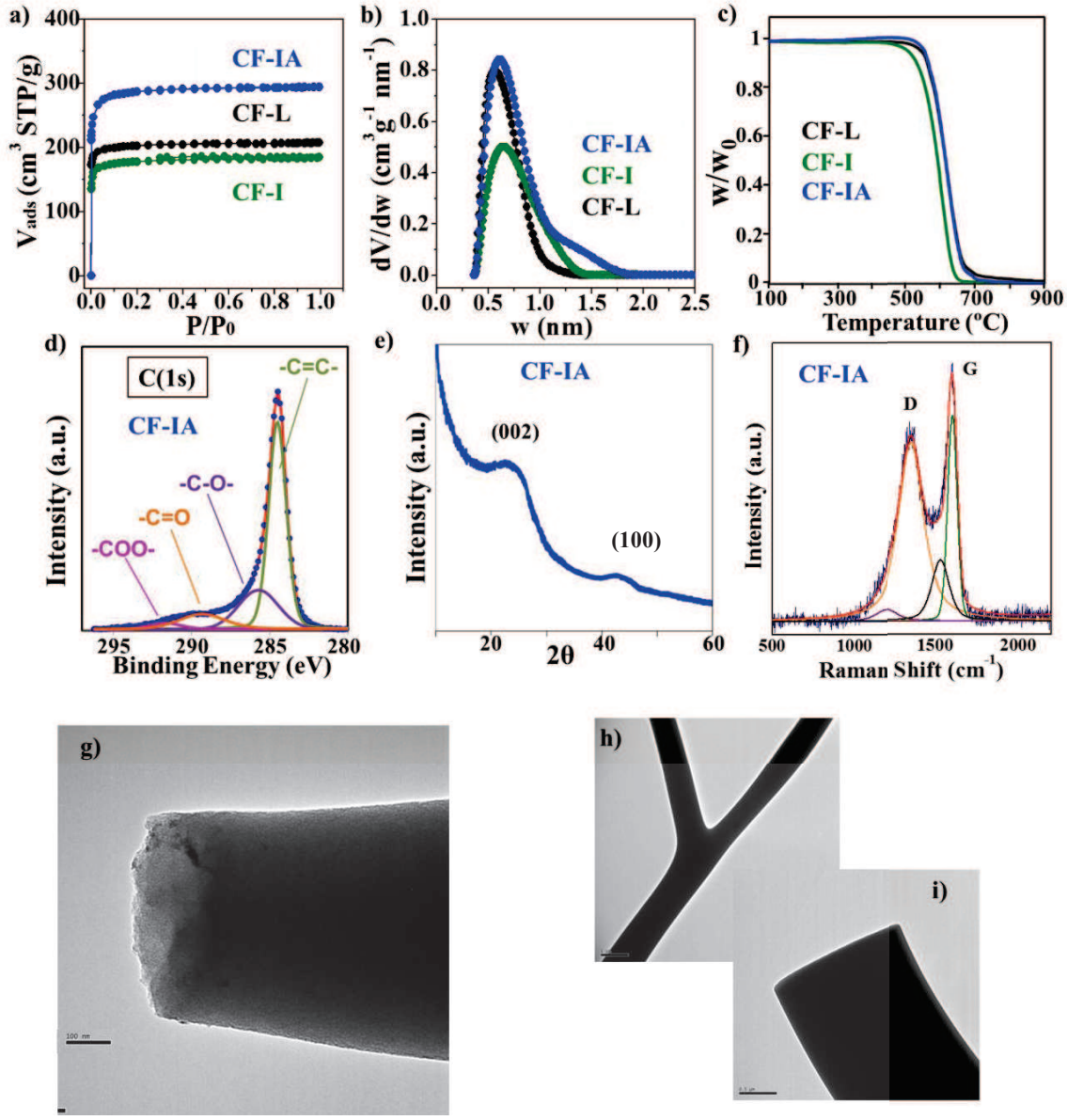

Figure 8.2. (a) N_2 adsorption isotherms, (b) pore-size distributions and (c) thermogravimetric analysis of the studied lignin-based CFs. (d) C(1s) XPS deconvoluted spectrum, (e) X-ray diffractogram, (f) deconvoluted first-order Raman spectrum, and (g-i) TEM images (scale bars are 1 μm (g) 0.5 μm (h) and 100 nm (i)) of CF-IA fibers.

The structural features of the obtained lignin-based CFs were also analyzed. These properties have been widely related to their electron conductivity, but they were found practically independent of the different connectivity and porosity of the studied fibers. For instance, the XRD Raman and TEM characterization of the most porous CFs (CF-IA) is shown in Figures 8.2e-i. The X-ray diffractogram and the Raman spectrum reflect some common features characteristic of disordered porous carbons. The observed broad (002) and (100) diffraction peaks (Figure 8.2e), centered at around

2θ = 25° and 43°, points out the lower crystallinity of the CFs compared to that of the graphite [35,36]. By using the Scherrer equation [35], the mean size of the ordered (crystalline) domains in the perpendicular (Lc) and parallel (La) directions of graphene layers were estimated to be 18 and 33 Å, respectively. On the other hand, the strong D band (at 1355 cm^{-1}) in the Raman spectrum is indicative of the presence of structural defects, and the weaker ones at 1170 and 1515 cm^{-1}, have been ascribed to oxygen surface groups and interstitial defects, respectively (Figure 8.2f) [8,9,37,38].

However, TEM reveals that the studied lignin-based CFs exhibit an apparently smooth surface with no macro-/microscopic defects (Figure 8.2g), even at the connecting points (Figure 8.2h) or ending regions (Figure 8.2i). Moreover, although they cannot be compared with those of graphitic or graphitized carbons, the calculated mean crystal dimensions are among the largest of porous carbons prepared at temperatures in the range 700-1000 ºC [39-41]. These values and the position of the (002) peak (2θ = 25.08 º), with an interlayer spacing of d002 = 3.548 Å, being close to that obtained after carbonization of kraft lignin at temperatures as high as 2000 ºC [37,38], suggest the existence of an incipient graphitic structure. This can also be deduced from the position of G band in Raman spectrum (1595 cm^{-1}), approaching that of graphite [35-37].

8.3.2. Electrochemical characterization of lignin-based CFs

The electrochemical behavior of the as-prepared lignin-based CFs was studied in a three-electrode cell in sulfuric acid electrolyte (Figure 8.3).

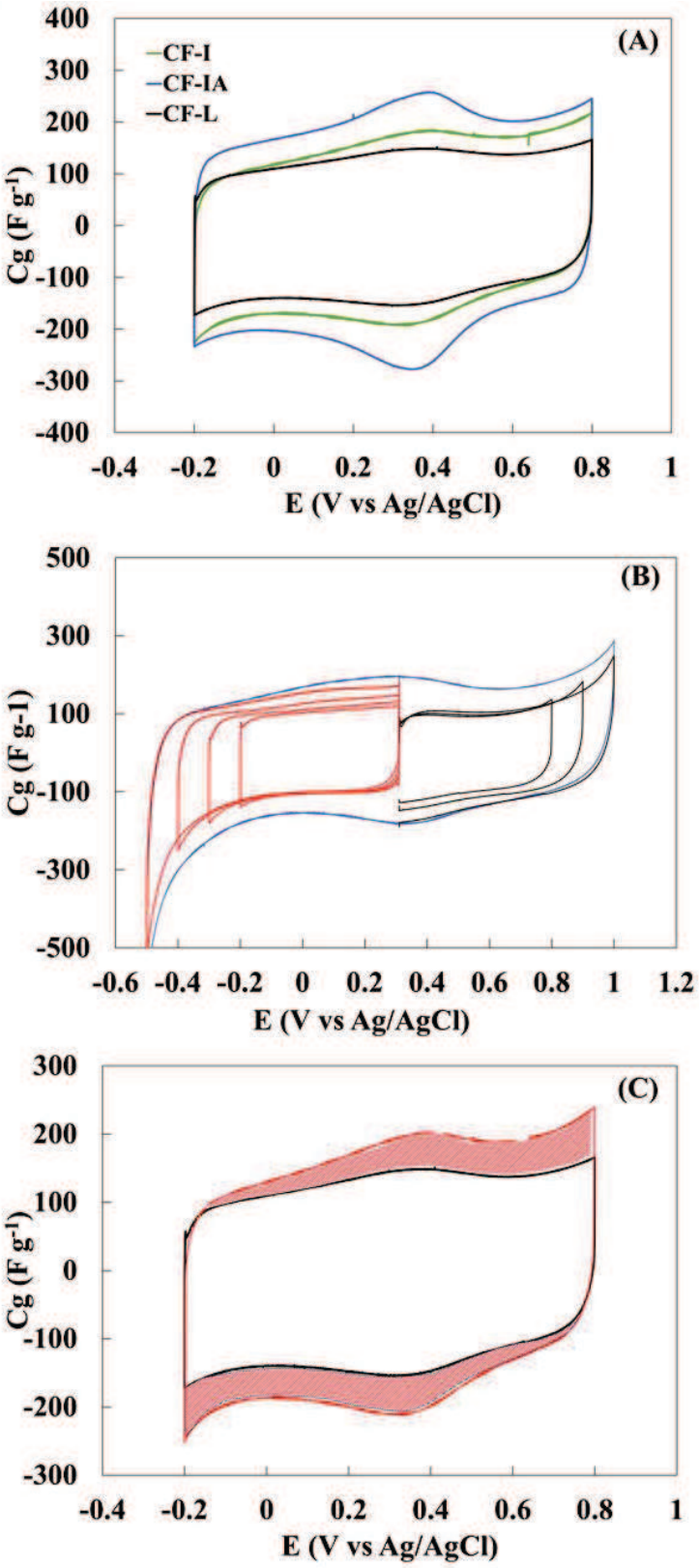

Figure 8.3. (a) Steady-state CVs of CF-L, CF-I and CF-IA binderless electrodes; (b) 4th scan CVs of CF-L electrodes upon step-wise opening of the potential window on the positive and negative sides; (c) CV of CF-L electrode before and after repetitively cycling up to an expanded potential window of 1.0 V. NOTE: All data were obtained in a three-electrode cell, scan rate 10 mV·s^{-1}.

Cyclic voltammetry (CV) revealed the ideal rectangular shape of a pure electric double-layer capacitor (EDLC) [1-5], no matter the connectivity of the CFs (Figure 8.3a). In addition, the different CFs displayed a pseudocapacitive contribution at around 0.4 V, related to the electrochemical reaction of quinone-like oxygen functionalities [32]. The significance of this contribution was found proportional to the concentration of these oxygen groups, which can be related to the amount of CO evolved during TPD experiments (Table 8.1). The formation of such kind of CO-evolving groups is known to occur upon oxygen (ambient conditions) exposure of a carbon surface prepared at high temperatures [42]. From the charge enclosed by the CVs (Figure 8.3a), gravimetric capacitance values of 134, 153 and 201 $F \cdot g^{-1}$ were obtained for CF-L, CF-I and CF-IA electrodes, respectively. These values seem to be proportional to the combination of their specific surface area and concentration of electroactive CO-evolving groups (Table 8.1). The stability of the carbon electrodes was studied by step-wise opening of the voltammetric potential window, from the open circuit potential (around 0.3 V) to both negative and positive sides (Figure 8.3b). The large cathodic current observed below -0.4 V, corresponding to protons electro-reduction, was probably indicative of the negative stability potential of CF-L. In the case of CF-I and CF-IA this current was shifted towards lower (more negative) potentials. On the positive side, CF-L also started to show anodic currents at lower overpotentials than CF-I and CF-IA. This material was able to reach 1.0 V without apparent voltammetric changes (Figure 8.3b). However, after continuous cycling up to this potential a considerable development of pseudocapacitance was observed when compared to a previous CV registered in a narrower potential window (see Figure 8.3c). This increase in pseudocapacitance may be attributed to the electrochemical oxidation of carbon surface upon positive polarization in acid media, which produces the generation of electroactive CO-type evolving groups [43-45]. As a consequence, we concluded that the potential safety limits determined for the three studied materials were at least -0.4 and 0.9 V (vs. Ag/AgCl/Cl-sat.), and that supercapacitor cells constructed using them as binderless electrodes could be operated safely up to 1.3 V. Such a high electrochemical stability is in agreement with the high resistance of the lignin-based CFs to air oxidation (Figure 8.2c), and may be related to their characteristic structure and spatial arrangement of the graphitic crystallites and undefective surface (see Figure 8.2e-i and the corresponding discussion); as well as the binderless conformation

of the electrodes, avoiding the stability problems conventionally derived from the use of additives.

The practical application of the lignin-based CFs as electrodes for supercapacitors was investigated in symmetric two-electrode cells, which were constructed by using the as-prepared materials as binderless electrodes, without using any kind of additives or conditioning treatments. The advantages of using interconnected CFs as binderless electrodes can be observed in Figure 8.4a, where the response of binderless CF-I is compared with that of binderless CF-L and also that obtained for CF-I processed in the conventional form of an electrode paste (sample CF-Ip in Figure 8.1i), adding Teflon and a carbon black as binder and conductivity promoter, respectively. At low scan rate (100 $mV \cdot s^{-1}$), the three materials render a quite similar electrochemical (CV) response. However, at faster scan rates, for example at 1 $V \cdot s^{-1}$, the carbon paste CF-Ip shows a sluggish response, while the binderless CF-I electrode is able to keep the characteristic rectangular-shape CV of EDLCs better than the CF-L. This difference must be undoubtedly related to differences in fibers connectivity (loose vs interconnected), a feature that is correlated to the conductivity of the electrode [34]. In particular, when the scan rate is raised from 10 to 1000 $mV \cdot s^{-1}$ the capacitance retention for the binderless CF-I electrode (62 %) is higher than that of CF-L (36 %) and three times higher than for the pasted one (17 % for CF-Ip), highlighting the beneficial utilization of CF-I directly as binderless electrodes.

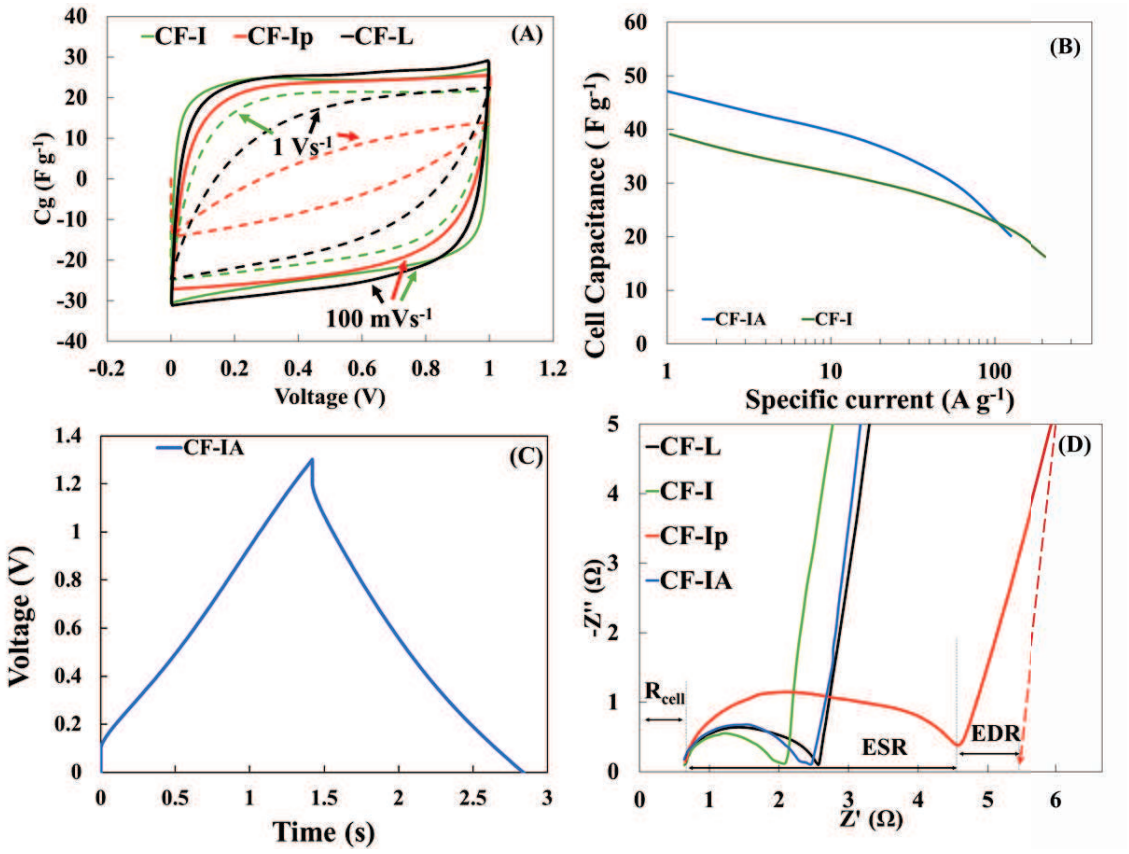

Figure 8.4. a) Steady-state CVs from symmetric two-electrode cells of binderless CF-L and binderless and pasted CF-I (composition of the carbon paste: 90/5/5 = CF/Teflon/acetylene black). b) Rate performance for the binderless CF-I and CF-IA cells. c) GCD profiles of the binderless CF-IA cell at 32 $A \cdot g^{-1}$ (cut-off voltage: 1.3 V). d) Nyquist plots of freshly constructed two-electrode cells with different electrodes (applied voltage: 50 mV, sine amplitude: 10 mV; frequency ranges: 100 kHz-0.1 Hz).

Capacitance retention for the CF-I supercapacitor cell is higher than those found for seamless carbon forms like activated carbon monoliths [46]. Only advanced porous carbon materials, such as hierarchical porous carbons [47,48] or electrospun PAN-based CO_2-activated carbon binderless electrodes [49-51] can match the outstanding performance of CF-I binderless electrode, though they required the use of more expensive and less environmental carbon precursors or their preparation is burdened by complicated and energy-demanding procedures.

Under galvanostatic charge-discharge (GCD) conditions, the different electrodes display the triangular-shape response characteristic of the charge and discharge processes in EDLCs (Figure 8.5). Table 8.2 compiles a collection of properties for the analysed supercapacitor cells. First, their cell capacitance was found practically

independent of the cut-off voltage, slightly increasing up to a maximum value of 1.3 V (Figure 8.5 and Table 8.2). As expected, cell capacitances values at low specific currents are similar between the CF-L and CF-I electrodes, being 35 % higher when carbonized in the presence of oxygen (CF-IA). After a 64-fold increase of the specific current, the capacitance severely dropped for the unconnected electrode (CF-L). Surprisingly, the interconnected binderless electrode obtained after smooth air activation showed a boosted capacitance while preserving a low ohmic drop (CF-IA, Figure 8.5 and Table 8.2).

Table 8.2. Cell gravimetric capacitance (C_g), coulombic (C_{eff}) and energy (E_{eff}:) efficiencies, and resistance (R_{cell}) of two-electrode cells constructed with the lignin-based CFs.

		1 A g^{-1}			64 A g^{-1}			
Electrode	**Voltage V**	**C_g F g^{-1}**	**E_{eff} %**	**C_{eff} %**	**C_g F g^{-1}**	**E_{eff} %**	**C_{eff} %**	**R_{cell} Ω**
LCF-L	1.0	32	89.1	99.3	19	75.4	99.5	3.19
	1.3	34	86.5	98.9	18	69.2	98.0	
LCF-I	1.0	32	90.2	99.3	27	75.9	99.4	2.12
	1.3	34	86.9	98.9	27	71.1	98.3	
LCF-IA	1.0	45	90.6	99.3	35	71.2	99.8	2.36
	1.3	47	84.8	98.9	29	69.8	99.9	

It can be seen that, although all the electrodes exhibited very low IR drops at 1 A·g^{-1}, differences between the cells arises as the applied current increases, with CF-I and CF-IA (ohmic drops of 0.186 and 0.207 V) outperforming the results from the CF-L (0.282 V). The cell resistances were calculated from these values, going down from 3.19 to 2.12 ohms after the interconnection of the carbon fibers. As observed in the table, most of the stored charge was effectively recovered during discharge of the cells, with coulombic efficiencies ranging between 99.0 and 99.5 % in the case of the interconnected electrodes, even when the voltage was increased up to 1.3 V. The energy efficiency of the cells, which is usually an underestimated parameter of supercapacitors, was also measured. It reaches values close to 90 % when working at 1.0 V. When the cut-off voltage was further increased up to 1.3 V, the larger contribution of redox reactions to capacitance leaded to a small decrease (around 3-5 %) in the energy efficiency for all the electrodes, being slightly larger for the electrode with the larger amount of surface functionalities (5.6 % for CF-IA). Upon raising the applied current intensity from 1 to 64 A·g^{-1}, the increasing energy losses due to Joule effect made the energy efficiencies to decay. Nevertheless, the interconnection of fibers seemed to

lower these energy losses when working at higher specific currents, at least for 1.3 V operating voltage.

Owing to their better response, the rate performance of CF-I and CF-IA cells was then analyzed upon a wide range of specific currents (Figure 8.4b). Considering the maximum cell capacitances and the overall high-enough coulombic and energy efficiencies obtained when working at 1.3 V (Table 8.2), this was selected as the operational voltage for both cells. Because of their higher surface area and content of electroactive oxygen groups, the interconnected and more activated CFs (CF-IA) exhibited the highest capacitance, while those without additional activation (CF-I) showed the best rate performance. For CF-IA, a cell capacitance of 48.0 $F \cdot g^{-1}$ is achieved at the lowest tested specific current. Interestingly, the cell retains 42% of the capacitance when the applied current was raised from 0.25 to an ultrahigh specific current density of 128 $A \cdot g^{-1}$. A comparable storage rate performance, with a lower capacitance but a better capacitance retention (58%), has been also found for the CF-I. In particular, under an extremely demanding specific current of 32 $A \cdot g^{-1}$, the cell with CF-IA can be charged and discharged in less than 1.5 s while keeping a high capacitance of 34.1 $F \cdot g^{-1}$ and showing only 103 mV of ohmic drop (Figure 8.4c).

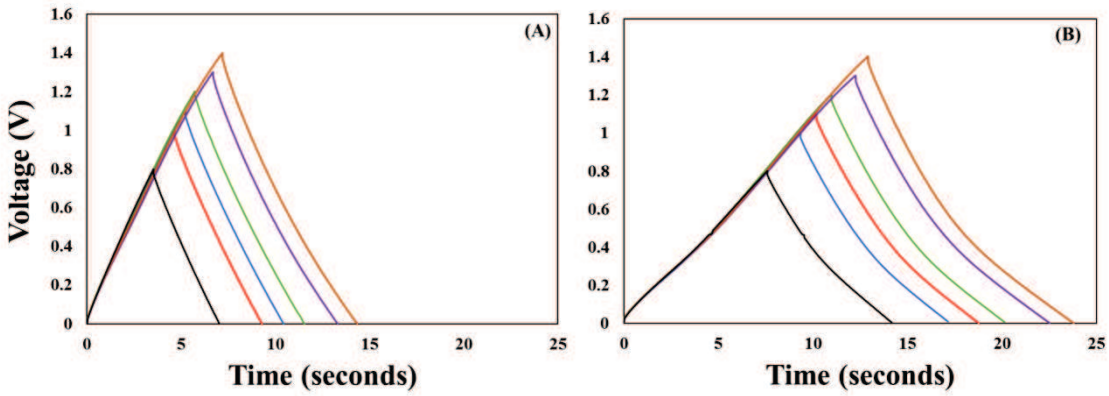

Figure 8.5. Comparison between GCD profiles for the CF-I (A) and CF-IA (B) electrodes at 5 $A \cdot g^{-1}$, upon increasing the cut-off voltage from 0.8 to 1.4V

Moreover, these electrodes show other valuable features for their use in symmetric supercapacitors. On the one hand, both the negative and positive electrodes display quite similar capacitances, causing only a slightly uneven operational potential window (values of ΔV+ and ΔV- of 0.69 and 0.61 V, Figure 8.6). On the other hand, the potential limits of each electrode reached during the charge of the cell were nearly

constant, no matter the used specific current (Figure 8.6). This stability of the potential windows allows to safely operate this cell at 1.3V under a wide range of current loads, a very interesting feature for systems that require or provide variable source of power.

The observed ultrafast response of the lignin-based interconnected CFs and their superior rate performance is supported by electrochemical impedance spectroscopy (EIS) measurements (Figure 8.4d). The low and fairly similar R_{cell} values (first intercept on the Z'axis) in Nyquist plots (around 0.64-0.70 Ω at 100 kHz) observed in all cases reflects the high conductivity of the whole cell, including that of the electrode materials [21], what may be associated to the suitable properties of lignin to produce ordered carbon structures [37]. However, clear differences in the semicircle diameters (and the Equivalent Series Resistance (ESR)) were found for the different electrode materials, which are indicative of a remarkable influence of their distinct continuity, connectivity and porosity, or amount of functional groups [52]. The huge increase of resistivity observed for the CF-I electrode when prepared as a paste highlights the benefits of using binderless materials to obtain higher conductivities. In addition, ca. 40 % reduction in resistance is achieved when the topology of the carbon electrode is changed from loose (CF-L) to a well-interconnected network of CFs (CF-I). This is attributed to the increased network connectivity in the interconnected CFs, providing a greater number of pathways for charge transport [34]. Furthermore, the results also indicate that an extra activation of the interconnected CFs (CF-IA) increases their electrical resistance, probably connected to the presence of a larger amount of electron-withdrawing surface oxygen groups and porosity-derived structural defects [9]. Nevertheless, in spite of their narrow porosity, all the electrodes showed a low Equivalent Distributed Resistance (EDR) [52], reflecting the low electrolyte resistance within the highly accessible pore system of CFs [53], especially, in those with ultrafine diameter prepared by electrospinning [54].

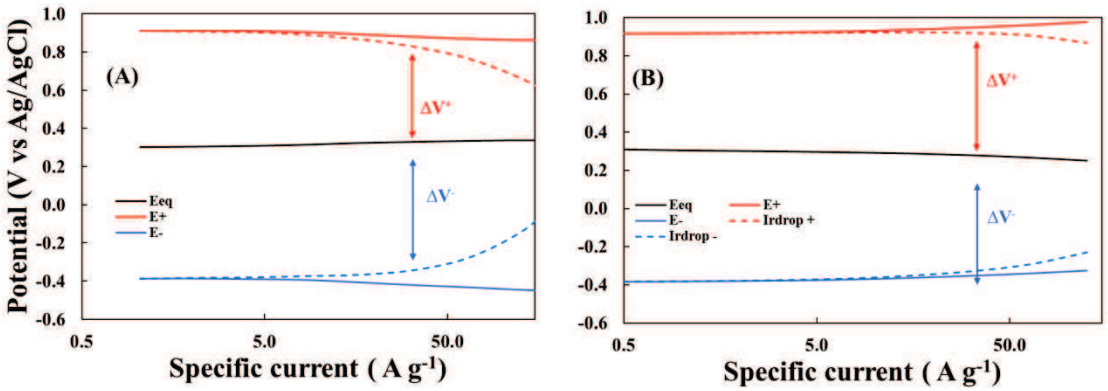

Figure 8.6. Equilibrium potential of the electrodes, potential limits and the respective IRdrop values reached by each electrode during GCD experiments for (A) LCF-IA and (b) LCF-I cells working at 1.3V under different specific currents.

The exceptional performance of the lignin-based fibrous carbon materials was finally highlighted in terms of specific energy and power of the supercapacitor cells in a Ragone plot (Figure 8.7a). For comparison purposes, the plot collects also the performance results, among the best reported, of other supercapacitor devices constructed with flexible [55,56] and electrospun-based [54,57-63] carbon materials. In terms of energy density, the most activated CFs (CF-IA) outperform the other tested lignin-based materials in a broad range of power densities, with a maximum energy density close to 10 $Wh \cdot kg^{-1}$ and near 5 $Wh \cdot kg^{-1}$ when discharged for 1 s (power of 18 $kW \cdot kg^{-1}$). Nevertheless, the maximum deliverable power density is observed for the less porous CFs (CF-I), showing a maximum power of 61 $kW \cdot kg^{-1}$ while storing an energy of 2.0 $Wh \cdot kg^{-1}$ that would be delivered in less than 0.2 s in those conditions. By contrast, the loose CFs (CF-L) and, in much more extent, the pasted discontinuous ones (CF-Ip) show a marked performance decay at high demanding power densities. Hence, the ultrafast responses of CF-I and CF-IA electrode materials are uniquely attributed to their excellent conductivity and the interconnection and long-range continuity of the fine electrospun CFs, attained through the control of their stabilization process and by using them as binderless electrodes, respectively. As it is also deduced from the Ragone plot, the energy and power characteristics of the cells made with both kinds of interconnected lignin-based CFs are similar to the best results found for supercapacitors based in electrospun electrodes reported in the literature [57,59,63], but without requiring the use of porogens or porosity development treatments. Furthermore, the ultrafast energy delivery exhibited by the reported CFs exceeds by far that of activated

carbons and approaches the performance of the top-engineered nanocarbons [1-5], just by using an abundant and biorenewable precursor and a simple preparation procedure.

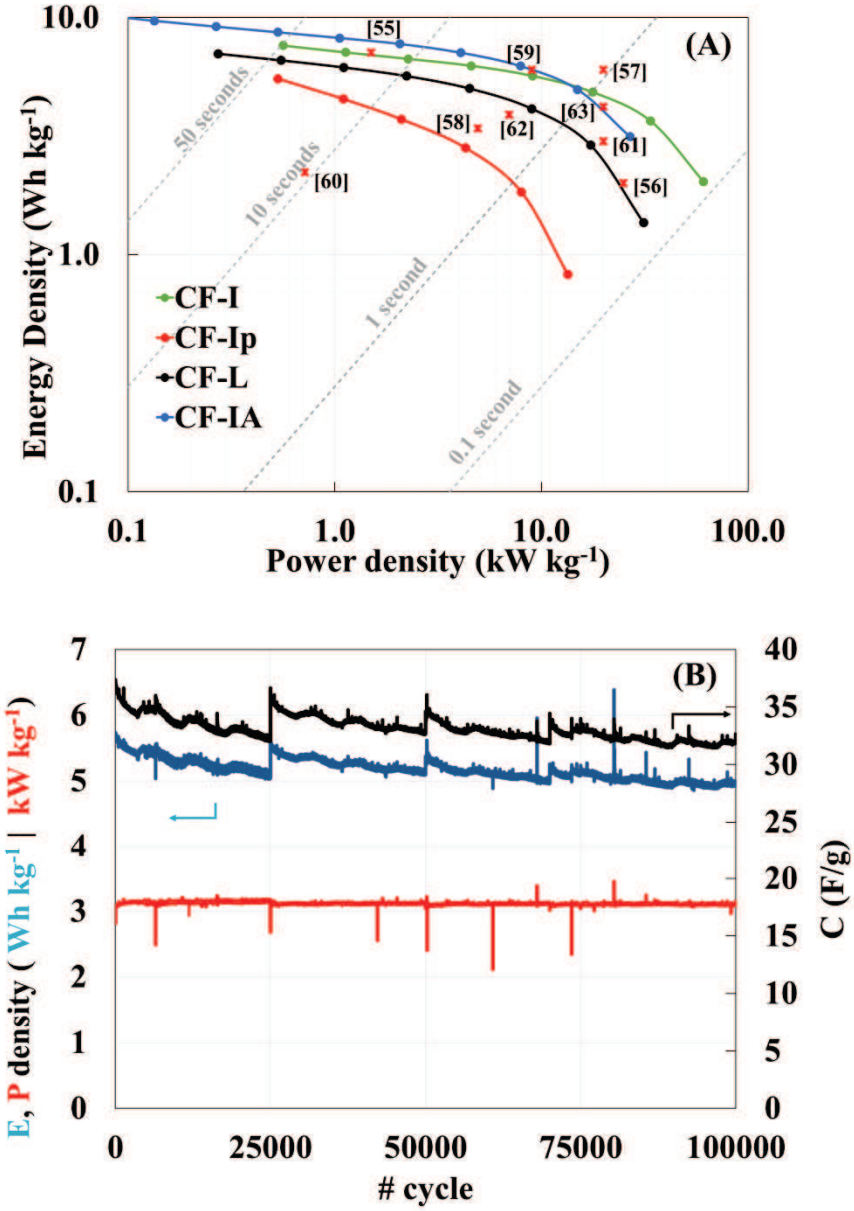

Figure 8.7. a) Ragone plots for the studied materials. Literature values from other electrospun-based or flexible supercapacitors are also referred. b) Durability test of the LCF-I cell carried out at 5 A g^{-1}. A resting time of 1 h was imposed each 25000 cycles. (a, b) Operating voltage = 1.3 V.

Another important aspect from a practical point of view is the stability of supercapacitors upon charge-discharge cycling. The cycle life of the lignin-based interconnected CFs was evaluated upon 100000 GCD cycles at 5 A·g^{-1} and 1.3 V voltage. As it can be observed in Figure 8.7b, the cell can practically retain 100 % of its

power and around 90 % of total capacitance and energy, with this slight fading being stabilized after the first 50000 cycles. An additional test consisting of a holding voltage ("floating" accelerated test [64]) at 1.3 V during 24 h was conducted after the cycling one. GCD profiles recorded after the cycling and holding test show small changes in the resistivity and the capacitance of the cell (Figure 8.8a), resulting in a reduced impact in its energy and power (Figure 8.8b).

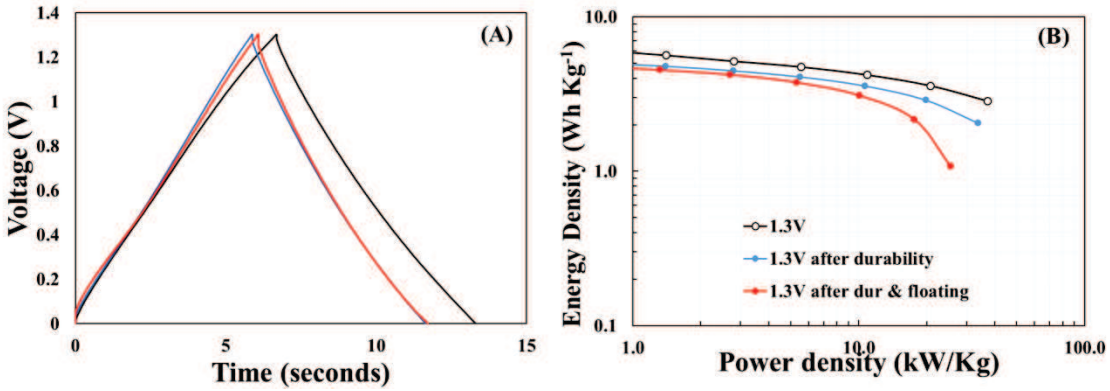

Figure 8.8. (A) GCD profiles and (B) Ragone plots of LCF-I before (black line) and after the cycling (blue line) and floating (red line) tests.

8.4. Conclusions

We have demonstrated that an abundant and renewable precursor like lignin can be inexpensively and sustainably processed into interconnected and porous CFs, of submicron diameter, which exhibit an ultrafast storage performance when used as electrode materials for supercapacitor devices. The electrodes are simply prepared by electrospinning of Alcell®-lignin/ethanol solutions and subsequent thermal conversion into CFs, with an easy control of their connectivity and activation degree. Supercapacitor cells can be easily mounted using the CFs as flexible binderless electrodes, showing power and energy densities of up to 61 $kW \cdot kg^{-1}$ and 10 $Wh \cdot kg^{-1}$, respectively, which are comparable or superior to the up-to-now top engineered structures, and can retain 100 % and more than 90 % of initial power and energy densities, respectively, after 100000 charge-discharge cycles at 5 $A \cdot g^{-1}$.

8.5. References

[1] Y. Zhai, Y. Dou, D. Zhao, P. F. Fulvio, R. T. Mayes and S. Dai, Adv. Mater., 23 (2011) 4828.

[2] S. L. Candelaria, Y. Shao, W. Zhou, X. Li, J. Xiao, J. -G. Zhang, Y. Wang, J. Liu, J. Li and G. Cao, Nano Energy, 1 (2012) 195.

[3] T. Chen and L. Dai, Mater. Today, 16 (2013) 273.

[4] H. Nishihara and T. Kyotani, Adv. Mater., 24 (2012) 4473.

[5] M. Inagaki, H. Konno and O. Tanaike. J. Power Sources, 195 (2010) 7880.

[6] S. Shiraishi, Boletín del Grupo Español del Carbón, ISSN-e 2172-6094, 2013, 28, 18.

[7] A. J. Ragauskas, G. T. Beckham, M. J. Biddy, R. Chandra, F. Chen, M. F. Davis, B. H. Davison, R. A. Dixon, P. Gilna, M. Keller, P. Langan, A. K. Naskar, J. N. Saddler, T. J. Tschaplinski, G. A. Tuskan and C. E. Wyman, Science, 344 (2014) 1246843

[8] M. Lallave, J. Bedia, R. Ruiz-Rosas, J. Rodríguez-Mirasol, T. Cordero, J. C. Otero, M. Márquez, A. Barrero and I. G. Loscertales, Adv. Mater., 19 (2007) 4292.

[9] R. Ruiz-Rosas, J. Bedia, M. Lallave, I. G. Loscertales, A. Barrero, J. Rodríguez-Mirasol and T. Cordero, Carbon, 48 (2010) 696.

[10] A. Greiner and J. H. Wendorff, Angew. Chem. Int. Ed. 46 (2007) 5670.

[11] J. M. Rosas, R. Berenguer, M. J. Valero-Romero, J. Rodríguez-Mirasol and T. Cordero, Front. Mater., 1:29 (2014) 1

[12] W. -J. Liu, H. Jiang and H.-Q. Yu, Green Chem., 2015, doi: 10.1039/C5GC01054C.

[13] Y. Ni and Q. Hu, J. Appl. Polym. Sci., 57 (1995) 1441.

[14] D. A. Baker and T. G. Rials, J. Appl. Polym. Sci. 130 (2013) 713.

[15] E. Frank, L. M. Steudle, D. Ingildeev, J. M. Spörl and M. R. Buchmeiser, Angew. Chem. Int. Ed., 53 (2014) 5262.

[16] J. L. Braun, K. M. Holtman and J. F. Kadla, Carbon, 43 (2005) 385.

[17] J. Jagiello and J.P. Oliver. Carbon. 55 (2013) 70

[18] J.-W. Jeon, L. Zhang, J. L. Lutkenhaus, D. D. Laskar, J. P. Lemmon, D. Choi, M. I. Nandasiri, A. Hashmi, J. Xu, R. K. Motkuri, C. A. Fernandez, J. Liu, M. P. Tucker, P. B. McGrail, B. Yang and S. K. Nune, ChemSusChem, 8 (2015) 428.

[19] E. Sjöholm, G. Gellerstedt, R. Drougge and I. Brida, WO 2012/112108A1.

[20] E. Sjöholm, G. Gellerstedt, R. Drougge and I. Norberg, WO 2013/112100A1.

[21] S. Kubo and J. F. Kadla J. Polym. Environ., 13 (2005) 97.

[22] S. Hu and Y.-L. Hsieh, J. Mater. Chem. A, 1 (2013) 11279.

[23] I. Dallmeyer, L. T. Lin, Y. Li, F. Ko and J. F. Kadla, Macromol. Mater. Eng., 298 (2013) 1.

[24] W. Qin and J. F. Kadla, J. Appl. Polym. Sci., 126 (2012) E203.

[25] J. Lin, S. Kubo, T. Yamada, K. Koda and Y. Uraki, BioResources, 7 (2010) 5634.

[26] A. Oya, S. Yoshida, J. Alcaniz-Monge and A. Linares-Solano, Carbon, 34 (1996) 53.

[27] P. T. Williams and A. R. Reed, Biomass Bioenerg., 30 (2006) 144.

[28] W. M. Qiao, M. Huda, Y. Song, S.-H. Yoon, Y. Korai, I. Mochida, O. Katou, H. Hayashi and K. Kawamoto, Energy Fuels, 19 (2005) 2576.

[29] H. Marsh and F. R. Reinoso, Activated Carbon, Elsevier, 2006.

[30] S. Kubo,,Y. Uraki and Y. Sano. Carbon. 36 (1996) 1119.

[31] A. Linares-Solano and D. Cazorla-Amorós, Activated Carbon Fibers. In Handbook of Advanced Ceramics, Ed. S. Somiya, Academic Press: Elsevier Inc.; 2013. p. 155.

[32] M. J. Bleda-Martínez, J. A. Maciá-Agulló, D. Lozano-Castelló, E. Morallón, D. Cazorla-Amorós and A. Linares-Solano, Carbon, 43 (2005) 2677.

[33] K. Xye and B. Wei, Adv. Mater., 16 (2014) 3592.

[34] I. Dallmeyer, L. T. Lin, Y. Li, F. Ko and J. F. Kadla, Macromol. Mater. Eng., 299 (2014) 540.

[35] M. A. Short and P. L., Jr. Walker, Carbon, 1 (1963) 3.

[36] D. D. L. Chung, J. Mater. Sci., 37 (2002) 1475.

[37] J. Rodríguez-Mirasol, T. Cordero and J. J. Rodríguez, Carbon, 34 (1996) 43

[38] A. Sadezky, H. Muckenhuber, H. Grothe, R. Niessner and U. Poschl. Carbon, 43 (2005) 1731.

[39] M. M. Dubinin, Thermal treatment and microporous structure of carbonaceous adsorbents. Proceedings of the fifth Conference on Carbon. Y. Zhou Ed., Pergamon Press Inc. 1962.

[40] Z. Ryu, H. Rong, J. Zheng, M. Wang and B. Zhang, Carbon, 40 (2002) 1131.

[41] X. Ma, H. Yang, L. Yu, Y. Chen and Y. Li Materials 7 (2014) 4431.

[42] T. J. Bandosz, in Carbon Materials for Catalysis, eds. P. Serp and J. L. Figueiredo, John Wiley & Sons, Inc., 2008, pp. 45–92.

[43] R. Berenguer, J. P. Marco-Lozar, C. Quijada, D. Cazorla-Amorós, E. Morallón, Carbon 47 (2009) 1018.

[44] R. Berenguer, H. Nishihara, H. Itoi, T. Ishii, E. Morallón, D. Cazorla-Amorós and T. Kyotani, Carbon, 54 (2013) 94.

[45] Z. Tabti, R. Berenguer, R. Ruiz-Rosas, C. Quijada, E. Morallón, D. Cazorla-Amorós. Electrochemistry 81 (2013) 833.

[46] V. Ruiz, C. Blanco, R. Santamaría, J. M. Ramos-Fernández, M. Martínez-Escandell, A. Sepúlveda-Escribano and F. Rodríguez-Reinoso, Carbon, 47 (2009) 195.

[47] D.-W. Wang, F. Li, M. Liu, G. Q. Lu and H.-M. Cheng, Angew. Chem. Int. Ed., 47 (2008) 373.

[48] A. Berenguer-Murcia, R. Ruiz-Rosas, J. García-Aguilar, K. Nueangnoraj, H. Nishihara, E. Morallón, T. Kyotani, D. Cazorla-Amorós. Phys Chem. Chem. Phys. 15(25) (2013), 10331-10334.

[49] Y. Gao, V. Presser, L. Zhang, J. J. Niu, J. K. McDonough, C. R. Pérez, H. Lin, H. Fong and Y. Gogotsi, J. Power Sources, 201 (2012) 368.

[50] C. Kim, J. Power Sources, 142 (2005) 382.

[51] E. J. Ra, E. Raymundo-Piñero, Y. H. Lee and F. Béguin, Carbon, 47 (2009) 2984.

[52] R. Kötz and M. Carlen, Electrochim. Acta, 45 (2000) 2483.

[53] M. J. Bleda-Martínez, D. Lozano-Castelló, D. Cazorla-Amorós and E. Morallón, Energy Fuels, 24 (2014) 3378.

[54] M. Inagaki, Y. Yang and F. Kang, Adv. Mater., 24 (2012) 2547.

[55] W. Liu, X. Yan, J. Lang, C. Peng and Q. Xue, J. Mater. Chem., 22 (2012) 17245

[56] S. H. Aboutalebi, R. Jalili, D. Esrafilzadeh, M. Salari, Z. Gholamvand, S. Aminorroaya Yamini, K. Konstantinov, R. L. Shepherd, J. Chen, S. E. Moulton, P. C. Innis, A. I. Minett, J. M. Razal and G. G. Wallace, ACS Nano, 8 (2014) 2456.

[57] E. J. Ra, E. Raymundo-Piñero, Y. H. Lee and F. Béguin, Carbon, 47 (2009) 2984.

[58] A. Kurniawan, L. K. Ong, F. Kurniawan, C. X. Lin, F. E. Soetaredjo, X. S. Zhao and S. Ismadji, RSC Adv., 4 (2014) 34739.

[59] C. Ma, Y. Li, J. Shi, Y. Song and L. Liu, Chem. Eng. J., 249 (2014) 216.

[60] C. Lai, Z. Zhou, L. Zhang, X. Wang, Q. Zhou, Y. Zhao, Y. Wang, X.-F. Wu, Z. Zhu and H. Fong, J. Power Sources, 247 (2014) 134.

[61] T. Le, Y. Yang, Z. Huang and F. Kang, J. Power Sources, 278 (2015) 683.

[62] T. Wang, D. Song, H. Zhao, J. Chen, C. Zhao, L. Chen, W. Chen, J. Zhou and E. Xie, J. Power Sources, 274 (2015) 709.

[63] C. Tran and V. Kalra, J. Power Sources, 235 (2013) 289.

[64] D. Weingarth, A. Foelske-Schmitz and R. Kötz, J. Power Sources, 225 (2013) 84.

GENERAL CONCLUSIONS AND FUTURE WORK

The preparation of carbon fibers from Alcell lignin has been studied by electrospinning technique. Porous carbon fibers are relevant materials for many functional applications of industrial and technological interest. Specially, they receive great attention in catalysis, adsorption, gas storage and/or separation processes, electrochemical devices for energy storage and conversion, etc. Regarding the obtainment of advanced properties, the preparation of carbon fibers by a simple and versatile technique, such as the electrospinning, entails an advantageous and promising approach. It solves the most important problems associated to conventional melt-extrusion, since it allows the preparation of continuous fibers with considerably smaller diameters (micro- and submicro-scale) at room temperature, directly in a single step without the aid of blending polymeric additives and/or chemical treatments.

The addition of H_3PO_4 to the initial solution has allowed the preparation of carbon fibers with a large variety of porosity and chemical properties. In addition, H_3PO_4 allows the preparation of carbon fibers by other routes and reducing the preparation time by 60 times with respect to pure carbon fibers (from Alcell lignin without phosphoric acid). In Chapter 3, the possible routes of carbon fibers preparation from Alcell lignin have been describedAlso, H_3PO_4 allows the stabilization step in inert atmosphere, and phosphorus-containing stabilized fibers will, also, be activated in presence of low concentration of oxygen. Carbon fibers with high surface area values, from 850 to 2000 $m^2 \cdot g^{-1}$, have been obtained with different chemical properties. Due to the easy stabilization of the H_3PO_4 lignin fibers, a more complete study on the stabilization of this type of fibers has been studied in Chapter 4. The variation in stabilization parameters, such as temperature, time and heating rates, has been studied. The stabilization of Alcell fibers without the presence of H_3PO_4 needs to be carried out at low heating rate (0.08 $ºC \cdot min^{-1}$). On the contrary, we have observed that for phosphorus-Alcell fibers, heating rates up to 3 $ºC \cdot min^{-1}$ could be used without fibers fusion. Moreover, the stabilization of phosphorus-Alcell fibers at 100 ºC and in inert atmosphere (150 ºC) is possible thanks to the incorporation of H_3PO_4. Here, we propose a stabilization mechanism of H_3PO_4-lignin fibers, demonstrated that the phosphoric acid favors the cross-linking reactions in the Alcell lignin structure.

Due to the excellent properties of the carbon fibers obtained, their uses in various applications, as adsorption, catalyst, electro-catalyst and energy storage, have been checked. In Chapter 5, the phenol adsorption on carbon fibers has been carried out. Due to the small sizes of the carbon fibers the diffusion and the decrease of high pressures are favored on these materials. High phenol adsorption capacities have been found (from 200 to 250 $mg \cdot g^{-1}$ at 75 $mg \cdot L^{-1}$ and 25 ºC). The breakthrough profiles have benn successfully described by a mathematical model by using adsorption parameters obtained from the equilibrium and kinetic studies in batch. The isopropanol decomposition in gas phase on carbon fibers catalyst has been studied in Chapter 6 in order to check the acid-basic properties of the carbon catalysts. The preparation of carbon fibers without phosphoric acid and with different H_3PO_4 impregnation ratios at different carbonization temperatures (from 500 to 1600 ºC) produces carbon fibers catalysts with different porosities and chemical properties. On the one hand, carbon fibers prepared without phosphoric acid presents basic character, obtaining high acetone selectivity. On the other hand, phosphorus-containing carbon catalyst yields to propylene, presenting acid character.

The preparation of carbon fibers with different Pt content has been studied in Chapter 7. The incorporation of Pt salt precursor in the initial conductive solution, allows the preparation of lignin fibers with Pt in one step. After carbonization, a well dispersion and particle size distribution are obtained. Due to the excellent dispersion and the Pt size (from 2 to 9 nm), these electro-catalysts show a good performance in the ethanol and methanol electro-oxidation, which allows the use of lower Pt content on the catalyst for fuel cells. Finally, the use of carbon fibers from lignin obtaining by electrospinning in energy storage application is show in Chapter 8. In this chapter it is demonstrated that interconnected and porous carbon fibers easily obtained from lignin exhibit ultrafast charge-discharge, excellent power energy density (61 $kW \cdot kg^{-1}$ and 10 $Wh \cdot kg^{-1}$, respectively) and cyclability performance to be used as binderless and flexible electrodes in supercapacitors.

But there is still more work to finish and to do.

- ✓ Taking into account the possibility of carbonizing the phosphorus-lignin fibers in the presence of low oxygen concentrations and the high surface area obtained by this way (up to 2200 $m^2 \cdot g^{-1}$), these fibers will be tested for adsorption and energy storage.
- ✓ The preparation of carbon fibers at high temperatures (1600 ºC) produces carbon fibers with excellent electric conductivities for electrochemical applications. Some initial results, suggest that the power and energy density increase with the carbonization temperatures.
- ✓ Carbon fibers catalyst prepared with H_3PO_4, which present acid properties, have to be checked in the gas phase ethanol and methanol decomposition for the production of ethylene and diethyl ether.
- ✓ Pt-carbon electrocatalysts used for alcohol electro-oxidation will be checked in the oxygen reduction reaction (ORR). The well dispersed and particle size distribution suggests that the use on ORR will be appropriated.
- ✓ To improve the preparation of carbon fibers catalyst with metal content, the use of a tri-axial electrospinning configuration will be studied. By this way, it is possible the preparation of submicro-carbon tubes with metal in their content, and also, the preparation of carbon tubes with different metals in both sides (internal and external) of the tubes.

RESUMEN

En la presente Tesis Doctoral se estudia la preparación de fibras de carbono activadas por electrospinning de lignina Alcell y su aplicación en diversas aplicaciones de Ingeniería Química como son la adsorción de compuestos en fase acuosa, descomposición catalítica de isopropanol, electro-catálisis directa de metanol para celdas de combustible y aplicaciones de almacenamiento de energía.

La memoria de la Tesis Doctoral se ha dividido en 9 capítulos. El ***Capítulo 1*** corresponde a la introducción. En este capítulo se ha dado una visión general de los métodos de preparación y tipos de fibras de carbono, nombrando los posibles precursores para la preparación de las mismas y haciendo hincapié en la técnica de electrohilado. La técnica de electrohilado permite la preparación de filamentos de reducido tamaño de diámetro utilizando disoluciones conductoras. Los parámetros que mayor efecto tienen sobre las propiedades de las fibras finales son la viscosidad de la disolución, el potencial aplicado y los caudales utilizados. Variando estos parámetros podemos conseguir una estabilidad en el equipo de electrospinning la cual es crucial para el correcto hilado de las fibras.

En el ***Capítulo 2*** se describe la metodología experimental utilizada en el desarrollo de la Tesis Doctoral. Se describe la parte experimental para la preparación fibras de lignina Alcell mediante electrospinning, donde se muestran las concentraciones utilizadas para la preparación de la disolución conductora, así como los parámetros del equipo de electrospinning que se han utilizado para su preparación. Posteriormente se muestran las instalaciones donde se han llevado a cabo los tratamientos térmicos necesarios para la preparación de fibras de carbono, diferenciando la etapa de estabilización, carbonización y lavado. Una vez preparadas las fibras de carbono se procede a su caracterización para obtener un mayor conocimiento de sus propiedades. De esta forma, la caracterización de la estructura porosa se ha llevado a cabo mediante adsorción física de gases, diferenciando entre adsorción-desorción de N_2 a -196 ºC y adsorción de CO_2 a 0 ºC. Mediante espectroscopia fotoelectrónica de Rayos X (XPS), análisis elemental, difracción de Rayos X (DRX) y desorción térmica programada (DTP) se ha caracterizado la química superficial de los materiales carbonosos preparados. El comportamiento térmico de los materiales se ha analizado mediante Calorimetría Diferencial de Barrido (DSC), que mide el flujo de calor que

tiene lugar en la muestra durante el tratamiento térmico. La pérdida de peso con el aumento de la temperatura en presencia de atmósfera oxidante se ha analizado mediante análisis termogravimétrico en termobalanza. Finalmente, la morfología superficial de los materiales se ha caracterizado mediante microscopia electrónica de barrido y transmisión (SEM y TEM). Además de la descripción de la metodología experimental utilizada para la preparación y caracterización de los materiales, en el segundo capítulo se han descrito las instalaciones y equipos utilizados para llevar a cabo la adsorción de fenol, descomposición de isopropanol en fase gas, electro-oxidación de metanol para reacciones electrocatalíticas en pilas de combustible y el almacenamiento de energía en sistemas de supercondensadores.

Comenzando la parte de los resultados más relevante obtenidos en la Tesis Doctoral, en el ***Capítulo 3*** se muestran los resultados de la preparación de una gran variedad y novedad de fibras de carbono. El presente capítulo propone un nuevo método de preparación de fibras de carbono mediante electrohilado de mezclas de lignina/H_3PO_4, en el que se obtienen materiales fibrilares, en una sola etapa. Se pretende optimizar el proceso de estabilización y se realizará el estudio de las propiedades físico-químicas de las fibras de carbono resultantes.

Se han preparado fibras de carbono mediante electrospinning de lignina con y sin presencia de ácido fosfórico. Para la preparación de las fibras de lignina sin ácido fosfórico se ha utilizado una relación másica de lignina/etanol de 1/1, mientras que la preparación de fibras con H_3PO_4 conlleva la preparación de una disolución en concentración másica de H_3PO_4/lignina/etanol de 0.3/1/1. Los caudales utilizados en la fase de electrospinning han variado entre 0.1 y 0.3 $mL \cdot h^{-1}$ para el etanol como disolvente y entre 1 y 3 $mL \cdot h^{-1}$ para la disolución de lignina. Los potenciales utilizados han variado entre 12 y 24 kV.

Un paso crucial en la preparación de fibras de carbono es la etapa de estabilización. En esta etapa, las fibras de lignina sufren una termoestabilización oxidativa en presencia de oxígeno para aumentar la temperatura de transición vítrea de la lignina y evitar que ésta funda en la posterior etapa de carbonización. En el caso de fibras de lignina sin ácido fosfórico es necesario realizar un tratamiento oxidativo con velocidades de calentamiento muy bajas (0.08 $ºC \cdot min^{-1}$) hasta 200 ºC y manteniendo esta temperatura final durante 80 horas, lo que hace que el proceso de preparación de

este tipo de fibras de carbono sea un proceso largo, y por lo tanto, caro. Estudios iniciales en la estabilización de fibras de lignina con presencia de H_3PO_4 muestran la posibilidad de estabilizar estos materiales a mayores velocidades de calentamiento, del orden entre 1-3 ºC·min^{-1}, hasta alcanzar 200 ºC y manteniendo la temperatura final durante 1 hora sin producir la fusión de las fibras en la etapa de carbonización, lo que se traduce en una reducción del tiempo de preparación de 60 veces. Además, la incorporación de ácido fosfórico, incluso, permite la estabilización de fibras de lignina en atmósfera inerte. La carbonización a 900 ºC de las fibras estabilizadas produce fibras de carbono activadas con excelentes propiedades porosas y químicas que son de mucho interés para diversas aplicaciones.

La caracterización porosa de las fibras de carbono muestra un mayor desarrollo de la porosidad cuando la disolución inicial se ha impregnado con ácido fosfórico. Además, las fibras de carbono preparadas con ácido fosfórico muestran un mayor contenido en grupos oxigenados superficiales, características muy importantes para el uso de estos materiales en diversas aplicaciones. En la parte de resultados y discusión se muestra la versatilidad las fibras de carbono preparadas para ser usadas como adsorbentes para la eliminación de contaminantes en agua, como catalizadores ácidos y como electrodos carbonosos en aplicaciones electroquímicas.

En el siguiente capítulo, ***Capítulo 4***, se realiza un estudio más profundo sobre las variables del proceso de estabilización de las fibras de lignina preparadas a partir de mezclas de ácido fosfórico, lignina y etanol. En este capítulo, las fibras de lignina con presencia de ácido fosfórico se han estabilizado bajo una amplia variedad de condiciones. Se ha estudiado el efecto de la velocidad de calentamiento, tiempo, temperatura y atmósfera de la etapa de estabilización y el posterior efecto que estos parámetros producen al carbonizar las fibras estabilizadas. La estabilización de las fibras de lignina con ácido fosfórico se ha llevado a cabo a una velocidad de calentamiento de 1 ºC·min^{-1} a las temperaturas de 100, 150, 200 y 250 ºC. La temperatura final de estabilización se ha mantenido durante 1 o 6 horas. También se ha estudiado el efecto de la variación de la velocidad de calentamiento en la etapa de estabilización, utilizando velocidades de calentamiento que se ha variado entre 1 y 4 ºC·min^{-1} desde temperatura ambiente hasta 150 ºC, temperatura que se ha mantenido constante durante 1 hora. Se ha observado la posibilidad de estabilizar las fibras de lignina preparadas a partir de mezclas de lignina, ácido fosfórico y etanol sin presentar

síntomas de fusión a temperaturas comprendidas entre 100 y 250 ºC, utilizando tiempos de estabilización relativamente cortos entre 1 y 6 horas, y además es posible realizar el proceso de estabilización aumentando la velocidad de calentamiento. Todo hace indicar que la impregnación del ácido fosfórico con la lignina, produce en ésta reacciones de cross-linking que favorecen la unión entre la molécula de la lignina, mejorando de este modo la estabilización de estos materiales. La formación de grupos superficiales de tipo éteres fosfatos acelera la reacción de cross-linking.

Se han obtenido fibras de carbono son superficie específicas de hasta 1700 $m^2 \cdot g^{-1}$, obteniendo el mayor desarrollo de para porosidad para las fibras estabilizadas a 200 ºC durante 6 horas. Un aumento en la temperatura de estabilización produce un aumento del contenido de oxígeno en las fibras estabilizas, favoreciendo, en la etapa de carbonización, el desarrollo de la porosidad en las fibras carbonosas finales, las cuales presentan una alta variedad de grupos oxigenados superficiales debidos a la incorporación del ácido fosfórico. Este efecto se ve levemente magnificado cuando el tiempo de estabilización se prolonga hasta 6 h. La variación de la velocidad de calentamiento en la etapa de estabilización no tiene efecto sobre las propiedades texturales y químicas de los materiales carbonosos finales. Aun así, es posible la estabilización de fibras de lignina con ácido fosfórico a velocidades de calentamiento tan elevadas como 3 $ºC \cdot min^{-1}$ sin que se produzca fusión en la etapa de carbonización.

La adsorción de fenol en fase líquida sobre dos tipos de fibras de carbono se ha estudiado en el ***Capítulo 5***. El fenol es un compuesto orgánico aromático que posee un anillo bencénico en su estructura el cual le proporciona una alta estabilidad y reactividad química. La capacidad de producción anual mundial de fenol ha sido de 10 millones de toneladas en 2015. La industria siderúrgica, conjuntamente con la petrolífera, son las mayores generadores de estos residuos fenólicos. En la industria siderúrgica, las aguas de coquería y la de alto horno son las que presentan mayor toxicidad. El fenol y sus derivados, incluso a bajas concentraciones, proporciona al agua un olor y sabor característico. La toxicidad de los fenoles en estos efluentes se debe tanto a su carácter nocivo, como al elevado consumo de oxígeno durante su degradación. Estos compuestos se caracterizan por ser muy poco biodegradables; el tiempo de vida media de descomposición está entre 2 y 72 días. Otro aspecto a tener en cuenta en relación con la elevada toxicidad del fenol es la irritabilidad que causa en ojos, membranas mucosas y piel, producción de convulsiones por simple absorción,

afección al hígado, sistema nervioso y a los riñones, y su absorción por la piel, que puede llegar a ser mortal.

En este capítulo se han preparado dos tipos de fibras de carbono activadas. Se han preparado fibras de carbono a partir de mezclas de lignina/etanol y mezclas de ácido fosfórico/lignina/etanol en concentraciones másicas de 1/1 y 0.3/1/1, respectivamente mediante la técnica de elctrospinning. Por un lado, para el hilado de las fibras de lignina sin ácido fosfórico se han usado caudales de disolución de lignina/etanol de 1 $mL \cdot h^{-1}$y un caudal de etanol como disolvente por la aguja exterior de 0.1 $mL \cdot h^{-1}$, con aplicación de una diferencia de potencial de 12 kV. Por otro lado, para el hilado de las fibras de lignina impregnadas con ácido fosfórico, se ha utilizado un caudal de disolución y de disolvente de 3 y 0.3 $mL \cdot h^{-1}$, respectivamente aplicando una diferencia de potencial de 24 kV. Las fibras de lignina sin H_3PO_4 se han estabilizado en un horno tubular hasta 200 ºC durante 80 horas con una velocidad de calentamiento de 0.08 $ºC \cdot min^{-1}$, mientras que las fibras de lignina con presencia de ácido fosfórico se han estabilizado a 0.8 $ºC \cdot min^{-1}$ a 200 ºC durante 1 hora. Finalmente, la carbonización de las fibras estabilizadas se ha llevado a cabo en un horno tubular desde temperatura ambiente hasta 900 ºC en presencia de atmósfera inerte. Las fibras preparadas con ácido fosfórico se han lavado con agua destilada a 60 ºC para eliminar el agente activante que queda ocluido en los poros hasta pH constante. La estructura porosa de las fibras de carbono activo preparadas se han caracterizado mediante adsorción - desorción de N_2 a -196 ºC y adsorción de CO_2 a 0 ºC, obteniendo fibras de carbono con superficies específicas de 850 y 1150 $m^2 \cdot g^{-1}$. La caracterización de la química superficial se ha realizado mediante espectroscopia fotoelectrónica de Rayos X (XPS) y desorción térmica programada (DTP) y la morfología superficial se ha caracterizado mediante microscopia electrónica de barrido (SEM).

La adsorción de fenol sobre las fibras de carbono activo se ha realizado a temperaturas de 15, 25 y 35 ºC. Para el estudio termodinámico se ha utilizado la instalación que se muestra en la Figura 2.4. (Capítulo 2), con concentraciones de fenol que varían desde 5 hasta 75 $mg \cdot L^{-1}$ y usando una masa de fibras de carbono activo de 100 mg. Para obtener la isoterma de adsorción de fenol, inicialmente el carbón se satura con la concentración más baja de fenol, obteniendo de esta forma una curva de ruptura de la cual podemos calcular su capacidad de adsorción a la concentración de equilibrio correspondiente. Una vez saturado el carbón, se aumenta la concentración de entrada o

equilibrio para obtener el siguiente punto de la isoterma, continuando así hasta la disolución más concentrada para obtener todos los puntos de la isoterma de adsorción de fenol. Los parámetros experimentales se han explicado satisfactoriamente mediante el modelo propuesto por Langmuir, y el estudio termodinámico arroja valores de entalpía negativos, indicando la exotermicidad del proceso de adsorción. Las isotermas de adsorción de fenol muestran altas capacidades de adsorción de fenol sobre las fibras de carbono, las cuales están comprendidas entre 200 y 250 $mg \cdot g^{-1}$ para una concentración de equilibrio de 75 $mg \cdot L^{-1}$. El estudio cinético se ha llevado a cabo en la instalación presente en la Figura 2.5 (Capítulo 2). Para este estudio, la concentración inicial de fenol ha sido de 25 $mg \cdot L^{-1}$ y se ha usado una agitación de 500 rpm. Se han utilizado 50 mg de fibras de carbono y un caudal de impulsión de 5 $mL \cdot min^{-1}$. Los datos experimentales obtenidos en el proceso de adsorción se han explicado mediante una ecuación hiperbólica de carácter empírico. Se han obtenido altas velocidades de adsorción de fenol sobre las fibras de carbono, llegando al equilibrio en tiempos no superiores a 1 hora. Usando la ecuación propuesta por Vermeulen se han calculado los coeficientes efectivos de difusión de fenol sobre las fibras de carbón, obteniendo valores bajos de dicho coeficiente el cuál es prácticamente constante para todo el grado de recubrimiento.

Para completar el estudio de adsorción de fenol sobre las fibras de carbón, se ha realizado el estudio de la adsorción de fenol en continuo para la obtención de las curvas de ruptura. Para estos estudios se ha utilizado la instalación mostrada en la Figura 2.4 (Capítulo 2). Las temperaturas de adsorción han variado entre 15 y 35 ºC y se ha analizado el efecto de la concentración inicial, la cual varía entre 15 y 35 $mg \cdot L^{-1}$. También se ha estudiado el efecto de la variación del caudal y masa de carbón activo, variando entre 3 y 7 $mL \cdot min^{-1}$ y 170 y 230 mg, respectivamente. Finalmente se ha realizado un estudio de regeneración a 25 ºC de las fibras de carbón activo saturadas, con un caudal de agua de 5 $mL \cdot min^{-1}$. En los estudios en dinámico, se han obtenido mayores capacidades de adsorción a mayores concentraciones iniciales y menores temperaturas de adsorción, indicando que se favorece el proceso de adsorción propuesto por Langmuir y que el proceso de adsorción es exotérmico. El aumento de la temperatura de adsorción produce una disminución del tiempo de ruptura y una disminución de la altura de transferencia de masas, por otro lado, el aumento de la concentración inicial únicamente produce una disminución del tiempo de ruptura La

variación de masa y caudal prácticamente no tiene efecto sobre la capacidad de adsorción de los adsorbentes, aunque si se ve afectado el tiempo de ruptura y la altura de la zona de transferencia de masas.

Uno de los objetivos de este trabajo ha sido la obtención del modelo matemático que consiga describir el sistema de adsorción en continuo a partir de los resultados obtenidos en el estudio termodinámico y cinético. Para ello, el primer paso ha sido analizar el proceso de adsorción en sí con los fenómenos de transferencia que implica y las posibles resistencias que aparecen a esta transferencia de materia. Así mismo, se han evaluado todos los parámetros que afectan al proceso, ya sea mediante correlaciones encontradas en bibliografía o a partir de los resultados experimentales obtenidos en el laboratorio. Finalmente, los resultados obtenidos de este modelo matemático han permitido el cálculo de curvas de ruptura que satisfacen el comportamiento experimental observado en el laboratorio.

El ***Capítulo 6*** está dedicado a la descomposición de isopropanol en fase gaseosa. La descomposición de isopropanol se ha estudiado principalmente para caracterizar las propiedades ácido-básicas de los catalizadores. La mayoría de los autores concluyen que el isopropanol se deshidrata sobre los sitios ácidos del catalizador para producir propileno y, sobre los sitios básicos se deshidrogena para producir acetona. La gran variedad de grupos superficiales oxigenados presentes en los carbones activos hacen que estos materiales posean buenas propiedades catalíticas. Las ventajas de la utilización de carbón activo en catálisis heterogénea son varias. En primer lugar, la estructura del carbón es resistente a medios ácidos y básicos, siendo esta estable a elevadas temperaturas. Existe la posibilidad de controlar la estructura porosa y la química superficial de los catalizadores, pudiendo prepararse una larga variedad de estos, y además el coste de estos materiales es menor que el de otros soportes como son la alúmina o la sílice. El uso de fibras como catalizadores y/o soporte de catalizadores puede reducir los problemas derivados de la transferencia de masa y problemas de difusión, así como producir menores pérdidas de carga en los reactores.

En este capítulo se han preparado varios catalizadores en forma fibrilar a partir de electrospinning de lignina Alcell estudiando la influencia del ácido fosfórico en las propiedades finales de los mismos. Se han preparado disoluciones de lignina Alcell/etanol en relaciones másicas de 1/1. Para la preparación de las disoluciones

conductoras impregnadas con ácido fosfórico se han utilizado concentraciones másicas de H_3PO_4/lignina/etanol de n/1/1, siendo n = 0.1 o 0.3 dependiendo de la relación de impregnación utilizada. Para el hilado de las fibras en el equipo de electrospinning, se han utilizado caudales de disolución de lignina/etanol y H_3PO_4/lignina/etanol con la menor concentración de H_3PO_4 de 1 $mL \cdot h^{-1}$ y un caudal de disolvente por la aguja externa de 0.1 $mL \cdot h^{-1}$. Para el hilado de la disolución impregnada con mayor relación de impregnación de ácido fosfórico, se ha utilizado un caudal por la aguja interna de 3 $mL \cdot h^{-1}$ y 0.3 $mL \cdot h^{-1}$ de etanol como disolvente por la aguja externa. La diferencia de potencial para la preparación de estas fibras de lignina ha variado entre 12 y 24 kV. El proceso de estabilización se ha llevado a cabo en un horno tubular bajo atmósfera de aire. Para las fibras de lignina que contienen ácido fosfórico se ha usado una velocidad de calentamiento de 0.8 $ºC \cdot min^{-1}$ desde temperatura ambiente hasta 200 ºC, temperatura que se ha mantenido durante 1 hora. Por otra parte, para la estabilización de las fibras de lignina sin H_3PO_4 una velocidad de estabilización más baja es necesario, siendo de 0.08 $ºC \cdot min^{-1}$ hasta 200 ºC, temperatura que se ha mantenido 80 horas. Las fibras estabilizadas se han carbonizado en un horno tubular en presencia de atmósfera de N_2 (150 cm^3 $STP \cdot min^{-1}$) a 500 y 900 ºC, usando una velocidad de calentamiento de 10 $ºC \cdot min^{-1}$. Las fibras de carbono preparadas con ácido fosfórico se han lavado con agua destilada a 60 ºC hasta conseguir pH constante. Además, se han preparado otros catalizadores en forma de fibras a temperaturas de 1200 y 1600 ºC. Para ello, se ha realizado un tratamiento térmico sobre todas las fibras preparadas a 900 ºC en un horno tubular hasta 1200 o 1600 ºC, con una velocidad de calentamiento de 5 $ºC \cdot min^{-1}$.

Los catalizadores preparados se han caracterizado mediante adsorción física de gases, donde se ha observado que el mayor desarrollo de la estructura porosa se ha producido para los catalizadores preparados a 900 ºC. Los tratamientos térmicos a elevadas temperaturas producen una contracción de la porosidad, siendo esta mayor para las fibras de carbono preparadas sin ácido fosfórico. Mediante espectroscopia fotoelectrónica de Rayos X (XPS) se ha analizado su composición química superficial, presentando distinta distribución en los porcentajes de carbono, oxígeno y fósforo. Se observa un aumento de los grupos superficiales más reducidos al aumentar la temperatura de preparación de los catalizadores, que han podido comprobarse, también, con el análisis de desorción térmica programada (DTP).

La resistencia a la oxidación de estos catalizadores se ha estudiado mediante termogravimétria en presencia de oxígeno. Esta es una propiedad muy importante que deben poseer los catalizadores, ya que dependiendo la reacción a llevar a cabo se necesitarán elevadas temperaturas de reacción y, en algunos casos, atmósferas oxidantes. Los catalizadores carbonosos preparados presentan elevada resistencia a la oxidación. Las fibras de carbón preparadas en ausencia de ácido fosfórico comienzan a quemarse sobre los 400 ºC cuando han sido carbonizadas a 500 ºC. Un aumento en la temperatura de preparación produce un aumento de la resistencia a la oxidación, así, las fibras preparadas entre 900 y 1600 ºC comienzan a quemarse a temperaturas comprendidas entre 500 y 560 ºC. Es conocido que los materiales carbonosos preparados por impregnación de ácido fosfórico aumentan la resistencia a la oxidación de los materiales. Se ha comprobado que las fibras de carbón preparadas con ácido fosfórico presentan mayor resistencia a la oxidación, aumentando la temperatura a la cuál comienza a quemarse 20 ºC con respecto las fibras de carbón preparadas sin H_3PO_4.

Los resultados obtenidos de la descomposición de alcoholes, en líneas generales, muestran selectividad a acetona para los materiales que se han preparado en ausencia de ácido fosfórico, por lo que estos catalizadores presentan propiedades básicas. La actividad de los materiales ha variado en función de la temperatura de carbonización, siendo las fibras preparadas a 900 ºC las que presentan más actividad. Es conocido, que los materiales preparados con ácido fosfórico poseen características ácidas. La selectividad de las fibras de carbono preparadas a partir de disoluciones de lignina con ácido fosfórico tiende a producir propileno, con selectividades del 100 %. El aumento de la relación de impregnación con H_3PO_4 aumenta la actividad catalítica de la descomposición de isopropanol, siendo, para ambos casos, el catalizador preparado a 1200 ºC el más activo. Se ha encontrado una relación entre la actividad y el contenido de fósforo en la muestra, siendo las fibras más activas las que mayor porcentaje en fósforo poseen. Para evaluar la actividad de los catalizadores, se han comparado con un catalizador ácido comercial, γ-Al_2O_3, obteniéndose, para las fibras de carbono preparadas con relación de impregnación 0.3, comportamientos muy parecidos. Únicamente un aumento de 20 ºC en la temperatura de reacción ha sido necesario para conseguir la misma actividad que el catalizador comercial. Por último, se ha estudiado la influencia del oxígeno en la descomposición de isopropanol sobre las fibras que

presentan un carácter más ácido, obteniéndose principalmente selectividades a propileno por deshidratación del alcohol, pero también han aparecido selectividades a acetona debido a la deshidrogenación.

En los dos capítulos restantes de la Tesis Doctoral se han evaluado las propiedades de las fibras de carbono en aplicaciones electroquímicas. En el ***Capítulo 7*** se muestra la preparación de elctro-catalizadores carbonoso con Pt para su aplicación en pilas de combustible de metanol directo. Las pilas de combustible tienen un funcionamiento similar al de las baterías y tienen la capacidad de transformar la energía química en eléctrica, siendo su principal ventaja la alta densidad de energía que pueden proporcionar. Una celda de combustible, está constituida básicamente por: i) un ánodo o electrodo negativo donde ocurre la reacción de oxidación del combustible, ii) un cátodo en el que se lleva a cabo la reducción del oxidante y iii) un electrolito que permite la transferencia de los iones entre los compartimentos anódico y catódico, cerrando así el circuito eléctrico de la celda.

Se han preparado fibras de lignina con y sin grupos superficiales de fosforo y con nanopartículas de Pt en una única etapa mediante la técnica de electrospinning. Las diferentes fibras de lignina obtenidas se han estabilizado en atmósfera de aire y se carbonizaron a 900 ºC en atmósfera de nitrógeno para obtener electrocatalizadores de fibra de carbono a partir de lignina. Las fibras de carbono que contienen fósforo obtenidas son sólidos microporosos que pueden desarrollar una superficie aparente de 1141 $m^2 \cdot g^{-1}$, mientras que las fibras de carbono a base de lignina sin fósforo presentan una mesoporosidad amplia y áreas superficiales aparentes menores que 780 $m^2 \cdot g^{-1}$. Los grupos de fósforo permiten la preparación de materiales con nanopartículas metálicas muy bien dispersas (alrededor de 2 nm), mientras que sin el fósforo se obtienen mayores tamaños de partícula de Pt. Las fibras de carbono con fósforo han demostrado una mejor resistencia a la oxidación y electro-oxidación. Las fibras de carbono que contienen Pt pueden usarse directamente con los electrodos sin ningún tipo de aglomerante o promotor de la conductividad, mostrando una notable respuesta electro-catalítica en las reacciones de electro-oxidación con metanol y etanol.

El ***Capítulo 8*** se ha dedicado al uso de las fibras de carbón para almacenamiento de energía. El término de supercondensador o condensador electroquímico hace referencia a los sistemas de almacenamiento de energía compuestos por dos electrodos

de elevada porosidad separados por una membrana porosa y en contacto con un electrolito. Los materiales más utilizados para estos dispositivos son los carbones activos. El uso de las fibras de carbón como electrodos posee la ventaja de que no es necesario añadir ningún aglomerante, el cual reduce la porosidad de los electrodos, ni ningún promotor de la conductividad. Estos electrodos carbonosos presentan excelentes propiedades en supercondensadores con elevadas velocidad de carga y descarga.

En este trabajo se ha demostrado que un precursor abundante y renovable como la lignina puede ser procesado de manera barata y sostenible para la preparación de fibras de carbono interconectadas y porosas, obteniéndose tamaños de diámetro sub-micrométrico, que presentan elevado rendimiento de almacenamiento de energía y una alta velocidad de carga y descarga cuando se utilizan como materiales de electrodo para dispositivos como supercondensadores. Los electrodos se han preparado mediante electrospinning de disoluciones de Lignina Alcell® / etanol y su posterior conversión térmica para obtener las fibras de carbón. Se ha podido controlar el grado de su conectividad y su grado de activación. Los supercondensadores se pueden montar fácilmente utilizando las fibras de carbono como electrodos flexibles sin aglutinante, mostrando densidades de energía y potencia de hasta 61 $kW \cdot kg^{-1}$ y 10 $Wh \cdot kg^{-1}$, respectivamente, valores que son comparables o superiores a los valores obtenidos hoy en día para electrodos carbonosos preparados a partir de residuos lignocelulósicos. Además, tras 100000 ciclos de carga y descarga a densidades de corriente de 5 $A \cdot g^{-1}$ pueden retener el 100% de su potencia y más del 90% de la densidad de energía.

Finalmente, en el último capítulo se muestran las conclusiones generales así la continuación con posibles trabajos futuros.

CURRICULUM

This work is a compendium of the following publications:

F.J. García-Mateos, R. Berenguer, M.J. Valero Romero, J. Rodríguez-Mirasol, T. Cordero. "Phosphorus functionalization for the rapid preparation of highly nanoporous submicron-diameter carbon fibers by electrospinning of lignin solution". Submitted.

R. Berenguer, J. Rodríguez-Mirasol, T. Cordero, F.J. García-Mateos. 2016. Materiales carbonosos con propiedades avanzadas. España. ES2531462

F.J. García-Mateos, R. Berenguer, J. Rodríguez-Mirasol, T. Cordero. "Influence of H_3PO_4 on the stabilization and activation of lignin fibers prepared by electrospinning. Optimization of thermo-stabilization conditions". Submitted.

F.J. García-Mateos, H. Martín, J. Rodríguez-Mirasol, T. Cordero. "Modeling the dynamic adsorption of phenol on activated carbon fibers by electrospinning of Alcell lignin using batch parameters". Submitted.

F.J. García-Mateos, J. Rodríguez-Mirasol, T. Cordero. "Isopropanol decompositon on acid and basic carbon fibers catalysts". Submitted.

F.J. García-Mateos, T. Cordero-Lanzac, R. Berenguer, E. Morallón, D. Cazorla-Amorós, J. Rodríguez-Miraso1, T. Cordero. "Lignin-derived Pt supported carbon (submicron)fiber electrocatalysts for alcohol electro-oxidation". Applied Catalysis B: Environmental, 211 (2017) 18-30.

R. Berenguer, F.J. García-Mateos, R. Ruiz-Rosas, E. Morallón, D. Cazorla-Amorós, J. Rodríguez-Miraso1, T. Cordero. "Biomass-derived binderless fibrous carbon electrodes for ultrafast energy storage". Green Chemistry, 18 (2016) 1506.

This work has also generated the following congress and workshop contribution:

F.J. García-Mateos, R. Berenguer, T. Cordero-Lanzac, J. Rodríguez-Mirasol, T. Cordero. "Innovative single step preparation method of Pt-supported carbon fibers electrodes from lignin by electrospinning". The Annual World Conference on Carbon. Penn State (USA). Julio 2016. Poster.

F.J. García-Mateos, R. Berenguer, J. Rodríguez-mirasol, T. Cordero. "Rapid production of high-value submicron-diameter carbon fibers by electrospinning of lignin". The Annual World Conference on Carbon. Penn State (USA). Julio 2016. Poster.

F.J. García-Mateos, T. Cordero-Lanzac, R. Berenguer, E. Morallón, D. Cazorla-Amorós, J. Rodríguez-Miraso1, T. Cordero. "Nuevo método de preparación en un solo paso de electrodos de Pt soportado sobre fibras de carbono a partir de lignina y la técnica de electrohilado". Reunión del Grupo de electroquímica. Julio 2016. Alicante. Oral.

F.J. García-Mateos, R. Berenguer, M.J. Valero Romero, J. Rodríguez-Mirasol, T. Cordero. "Preparación de fibras de carbono funcionalizadas de tamaño submicrométrico mediante electrospinning de soluciones de lignina". Congreso nacional de materiales. Junio 2016. Gijón.

R. Berenguer, F.J. García-Mateos, R. Ruiz-Rosas, E. Morallón, D. Cazorla-Amorós, J. Rodríguez-mirasol, T. Cordero. "Electrodos de materiales carbonosos con estructura fibrilar y de elevada potencia, obtenidos a partir de lignina. Aplicación en el almacenamiento de energía". XIII Reunión del GEC, Alicante, Octubre 2015. Oral.

F.J. García-Mateos, R. Berenguer, J. Rodríguez-mirasol, T. Cordero. "Efecto del H_3PO_4 en la preparación de fibras de carbono a partir de lignina. Mejoras en el proceso de estabilización y propiedades finales". XIII Reunión del GEC, Alicante, Octubre 2015. Oral.

T. Cordero-Lanzac, F.J. García-Mateos, R. Berenguer, J. Rodríguez-Mirasol, T. Cordero. "Preparación de electrodos de fibras de carbono con nanopartículas de Pt a partir de Lignina". XXXV Bienal RSEQ, A Coruña, Julio 2015. Oral.

F.J. García-Mateos, R. Berenguer, T. Cordero-Lanzac, J. Rodríguez-Mirasol, T. Cordero. "Development of value-added lignin-based carbon fibrous materials prepared by electrospinning". 1st International Workshop on Biorefinery of Lignocellulosic Materials (IWBLCM), Junio 2015, Córdoba. Oral.

R. Berenguer, F.J. García-Mateos, J. Rodríguez-Mirasol, T. Cordero. "Electrospinning of P-containing lignin solution for the preparation of carbon fibers with enhanced surface area and oxidation resistance". The Annual World Conference on Carbon. Julio 2014. Jeju (Corea). Póster.

R. Berenguer, F.J. García-Mateos, J. Rodríguez-Mirasol, T. Cordero. "Novel lignin-based fibrous carbon materials". II International Congress of Chemical Engineering of ANQUE, Julio 2014. Madrid. Póster.

R. Berenguer, F.J. García-Mateos, T. Cordero, J. Rodríguez-Mirasol. "Efecto de compuestos de fósforo sobre la estabilización y activación de fibras de lignina preparadas por electrohilado". XII Reunión del Grupo Español del Carbón. Octubre 2013. Madrid. Póster.

Other publications by the autor:

M.J. Valero-Romero, F.J. García-Mateos, J. Rodríguez-Mirasol, T. Cordero, Role of surface phosphorus complexes on the oxidation of porous carbons, Fuel Processing Technology 157 (2017) 116–126.

E.M.Calvo-Muñoz, F.J. García-Mateos, J.M. Rosas, J. Rodrígez-Mirasol, T. Cordero. Biomass waste carbon materials as adsorbent for CO2 capture under post-combustion conditions. Front. Mater. 3 (2016) 23.

R. Berenguer, J. Fornells, F.J. García-Mateos, M.O. Guerrero-Pérez, J. Rodríguez-Mirasol, T. Cordero. Novel synthesis of porosus VPO catalysts with fibrous structure by electrospinning. Catalysis Today. 277 (2016) 266-273.

M. Namane, F.J. García-Mateos, B. Sithole, D. Rramjugernath, J. Rodríguez-Mirasol, T. Cordero. Characteristics of lignin precipitated with organic acids as a source for valorization og carbon products. Cellulose Chemistry and Technology. 50(3-4) (2016) 355-360.

F.J. García-Mateos, R. Ruiz-Rosas, M.D. Marqués, L.M. Cotoruelo, J. Rodríguez-Mirasol, T. Cordero. Removal of paracetamol on biomass-derived activated carbon: Modeling the fixed bed breakthrough curves using batch adsorption experiments. Chem Eng Journal. 279 (2015) 18-30.

Estancias de investigación

Estancia en el Instituto de Materiales de la Universidad de Alicante bajo la supervisión de los profesores Emilia Morallón y Diego Cazorla, para evaluar las propiedades electroquímicas de materiales carbonosos. Desde 3 de Octubre de 2016 hasta 11 de Noviembre de 2016.

Programa de Doctorado:
Química Avanzada. Preparación y Caracterización de Materiales

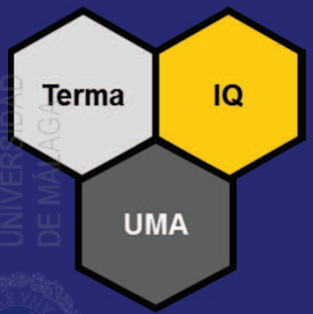

Tecnología de Residuos y Medioambiente
Universidad de Málaga